

This item was submitted to Loughborough University as a PhD thesis by the author and is made available in the Institutional Repository (<https://dspace.lboro.ac.uk/>) under the following Creative Commons Licence conditions.



For the full text of this licence, please go to:
<http://creativecommons.org/licenses/by-nc-nd/2.5/>

BLDSC no:- DX 175931

LOUGHBOROUGH
UNIVERSITY OF TECHNOLOGY
LIBRARY

AUTHOR/FILING TITLE

GAO, F.

ACCESSION/COPY NO.

040073774

VOL. NO.

CLASS MARK

- 1 JUL 1994

LOAN COPY

0400737744



BADMINTON PRESS
18 THE HALFCROFT
SYSTON
LEICESTER LE17 8LD
ENGLAND
TEL: 0533 602917

**STRUCTURE OF 2-D CARBON/CARBON
COMPOSITES AND ITS DEPENDENCE ON
PROCESSING**

By

Fengge Gao

BSc., MSc.

A Doctoral Thesis

Submitted in partial fulfilment of the requirement

for the award of

Doctor of Philosophy

of the Loughborough University of Technology

January 1993

© Fengge Gao 1993

ABSTRACT

Carbon fibre reinforced carbon (C/C) composites are advanced materials which exhibit good performance in high temperature inert environments. These materials are generally produced from carbon fibre reinforced polymers (CFRP) by carbonisation and a long series of densification treatments using chemical vapour deposition (CVD) or polymer impregnation. The carbonisation of CFRP results in a highly porous structure with low strength and stiffness so that the aim of the densification is to fill the voids to improve mechanical properties. It is however known that an understanding of void structure in the composites and its relation to raw materials, processing conditions and mechanical properties is important.

In this study, a novel method to characterise voids in the 2-D C/C composites was developed. This characterisation was based on qualitative investigation of a large number of composites produced from PAN, pitch and rayon fibre cloths using SEM and polarised light microscopy. Four types of void in 2-D composites, namely planar cracks, bundle cracks, inter-fibre pores and inter-fibre cracks, were classified, according to their position, size and orientation. With this characterisation, quantitative information on void structure could be obtained from two dimensional sections of the composites by computerised image analysis. This method then provided useful data in understanding the structure of the composites, the mechanism of the densification and the mechanical properties of the composites.

It was found that the void structure of the materials studied could be described by two models according to their densification behaviour. Both models were three-dimensional ink-bottle domains connected by thin capillaries. For the PAN fibre based composites, the planar cracks acted as thin capillaries and the bundle cracks as globes, whereas for the rayon and pitch fibre reinforced composites, the thin capillaries were mostly the inter-fibre pores and cracks. The investigation of multiple CVD, multiple resin impregnation and various combined processes involving both CVD and resin impregnation resulted in recommendations for the optimisation of the densification routes at two industrial concerns.

Failure behaviour of the composites subjected to tensile, flexural and delamination tests indicated that surface properties of the carbon fibres present played an important role in determining the mechanical properties of the composites. An understanding of the influence of void structure on the mechanical properties of the composites was achieved by correlation of voidage and appropriate strengths.

Pre-densification processing influences certain types of voids in the composites. A higher moulding pressure and a slower heating rate during carbonisation within the conditions applied would produce a lower porosity carbonised preform.

ACKNOWLEDGEMENTS

I am grateful to my supervisor Professor J. W. Patrick for his guidance and encouragement throughout this study.

I am greatly indebted to Dr. Alan Walker for his guidance in this project and constructive criticism in the writing of this thesis. Our friendly arguments on many aspects of the project were always impressive.

My thanks go to Mr. Douglas Hays and many other colleagues in the Carbon Research Group for their assistance in my experiments, also Dr. R.H. Bradley in the Institute of Surface And Technology for providing me with X-ray photoelectron spectroscopy data.

I offer my gratitude and sincere thanks to my wife, Xiaohong, for her enduring encouragement and taking care of all home affairs during my writing.

I am grateful to the Committee of Vice-Chancellors And Principals of The Universities of The United Kingdom for offering me an ORS Award during 1990 to 1992 and the Committee of The European Communities, New Metals And Chemicals Ltd. and Sintec Keramik GmbH for the financial support of this project through the BRITE programme.

CONTENTS

1. INTRODUCTION	1
2. LITERATURE REVIEW	4
<u>2.1 STRENGTH OF C/C COMPOSITES</u>	4
2.1.1 FUNDAMENTAL NATURE OF CARBON	4
2.1.1.1 Bonding in Carbon Materials	4
2.1.1.2 Structure of Carbon	6
2.1.1.3 Stress Analysis of The Graphite Structure	8
2.1.2 STRENGTH OF CARBON	13
2.1.2.1 Theoretical Maximum Values for Mechanical Properties of Carbon Materials	13
2.1.2.2 Effects of Flaws on The Strength of Brittle Materials	14
2.1.2.3 Shear Resistance of Carbon Materials	17
2.1.2.4 Carbon Fibres for High Performance Materials	20
2.1.3 CARBON FIBRE REINFORCEMENT OF COMPOSITES	25
2.1.3.1 General Rules of Fibre Reinforcement	25
2.1.3.2 Multidirectional Reinforcement	33
2.1.3.3 Additional Factors Influencing Strength And Stiffness	36
<u>2.2 FABRICATION OF C/C COMPOSITES</u>	40
2.2.1 GENERAL PROCESS	40
2.2.2 GREEN FABRICATION	41
2.2.3 DENSIFICATION PROCESSING	43
2.2.3.1 Chemical Vapour Deposition	43
2.2.3.2 Liquid Impregnation	45
<u>2.3 OUTLINE OF RESEARCH</u>	50
3. EXPERIMENTAL METHODS	51
<u>3.1 MATERIALS STUDIED</u>	51
3.1.1 RAW MATERIALS AND PROCESSING CONDITIONS	51
3.1.2 MATERIALS EXAMINED	52

<u>3.2 MEASUREMENTS OF THE MECHANICAL PROPERTIES</u>	54
3.2.1 FLEXURAL STRENGTH AND MODULUS MEASUREMENT	56
3.2.2 INTERLAMINAR SHEAR STRENGTH MEASUREMENT	56
3.2.3 DIAMETRAL COMPRESSION TEST	57
3.2.4 TRANSVERSE COMPRESSION STRENGTH MEASUREMENT	57
3.2.5 LONGITUDINAL TENSILE STRENGTH MEASUREMENT	57
<u>3.3 DETERMINATION OF DENSITY, VOLUME POROSITY AND FIBRE VOLUME FRACTION</u>	59
3.3.1 BULK DENSITY AND POROSITY	59
3.3.2 TRUE RELATIVE DENSITY AND TOTAL AND CLOSED POROSITY	59
3.3.3 FIBRE VOLUME FRACTION	60
3.3.4 OPEN VOLUME POROSITY DISTRIBUTION	61
<u>3.4 CHARACTERISATION OF THE COMPOSITE STRUCTURE</u>	62
3.4.1 PREPARATION OF SAMPLES FOR MICROSCOPY	62
3.4.2 POLARISED LIGHT MICROSCOPY	62
3.4.3 SCANNING ELECTRON MICROSCOPY	63
3.4.4 DEVELOPMENT OF IMAGE ANALYSIS TECHNIQUE TO CHARACTERISE PORE STRUCTURE IN THE COMPOSITES	63
4. EXPERIMENTAL RESULTS AND DISCUSSION	70
<u>4.1 STRUCTURE OF 2-D C/C COMPOSITES</u>	70
4.1.1 FEATURES OF SOLID CONSTITUENTS AND INTERFACES IN THE COMPOSITES	70
4.1.2 VOIDS IN THE COMPOSITES AND THEIR CHARACTERISATION	72
4.1.3 PROPERTIES OF CARBONISED PREFORMS	75
4.1.3.1 Basic Properties of Carbonised Preforms	75
4.1.3.2 Voids in Carbonised Preforms	76
4.1.3.3 Discussion	78

<u>4.2 DENSIFICATION OF THE CARBONISED PREFORMS</u>	80
4.2.1 THE PAN FIBRE REINFORCED COMPOSITES	80
4.2.1.1 Densification by Multiple CVD	80
4.2.1.2 Densification by Multiple Resin Impregnation	85
4.2.1.3 Densification by Combined Processes	89
4.2.2 THE PITCH FIBRE REINFORCED COMPOSITES	92
4.2.2.1 Experimental Results	92
4.2.2.2 Remarks	94
4.2.3 THE RAYON FIBRE REINFORCED COMPOSITES	96
4.2.4 SUMMARY	98
<u>4.3 THE STRUCTURE IN RELATION TO MECHANICAL PROPERTIES OF THE COMPOSITES</u>	101
4.3.1 FRACTOGRAPHY	101
4.3.2 BONDING AT FIBRE/MATRIX INTERFACE	103
4.3.3 INFLUENCE OF VOIDAGE ON STRENGTHS OF THE COMPOSITES	106
4.3.1.1 Composites with Weak Bonding at Fibre/Matrix Interface	106
4.3.1.2 Composites with Strong Bonding at Fibre/Matrix Interface	108
<u>4.4 INFLUENCE OF PRE-DENSIFICATION PROCESSING ON VOID STRUCTURE IN THE COMPOSITES</u>	110
4.4.1 THE VOID FORMATION	110
4.4.2 MOULDING PROCESSING	111
4.4.3 CARBONISATION	113
5. CONCLUSIONS	117
6. RECOMMENDATIONS FOR FUTURE WORK	120
7. APPENDIX	121
8. REFERENCES	123
TABLES	
FIGURES	

SYMBOLS

For convenience in finding a particular symbol definition, the page numbers show the location of the first occurrence.

a	Inter-planar spacing, p13
a	Major semi-axis of an elliptical crack, p14
A_c	Cross-sectional area of a composite, p26
A_f	Cross-sectional area of fibres, p26
A_m	Cross-sectional area of matrix, p26
A_w	Areal weight of fibre cloth, p61
b	Minor semi-axis of an elliptical cracks, p14
C	1/2 crack length, p16
$[C_{ijkl}], [C_{ij}]$	Stiffness coefficient matrix, p9, p10
d	Fibre diameter, p30
D	Specimen diameter, p57
D_b	Bulk density, p59
D_t	True density, p60
$[e_{ij}]$	Strain matrix, p8
E	Young's modulus, p13
E_a	Young's modulus parallel to the basal planes of graphite, p12
E_c	Young's modulus parallel to the hexagonal axis of graphite, p12
E_c	Young's modulus of a composite, p25
E_f	Young's modulus of fibres, p25
E_{fl}	Flexural modulus, p56
E_m	Young's modulus of matrix, p25
$F(\sigma)$	Cumulative failure probability of a population of fibres, p36
F_d	Fibre density, p61
F_v	Fibre volume fraction, p61
G_i	Shear modulus of individual graphite layers, p12
G_o	Shear modulus parallel to the basal planes of graphite, p12
I_n	Crystallite orientation factor as defined in Eq.(2-30), p20
$I(\varphi)$	Distribution of layer normals, p19
L	Span, p56
l_{crit}	The minimum length of broken fibres, p29
m	Slope on load-deflection curve in elastic deformation range, p56
m_i	Mass, p60
n	Number of measuring frames, p68
N	Number of cloth layers, p61
N	Number of available frames, p68

P	Porosity, p39
P	Load at failure, p56
P_c	Load carried by a composite, p26
P_c	Closed porosity, p60
P_f	Load carried by fibres, p26
P_m	Load carried by matrix, p26
P_o	Open porosity, p59
P_t	Total porosity, p60
r	Fibre radius, p32
$[S_{ijkl}], [S_{ij}]$	Compliance matrix, p8, p10
S_n	Flexural strength, p56
S_{ILSS}	Interlaminar shear strength, p57
S_t	Longitudinal tensile strength, p58
S_{tc}	Transverse compression strength, p57
t	Thickness, p56
t_c	Composite thickness, p34
t_f	Fibre thickness, p34
t_m	Matrix thickness, p34
U	Work done by applied load, p15
U_E	Elastic strain energy, p15
U_s	Surface energy, p15
V_{crit}	Critical fibre volume fraction as defined in Eq.(2-54), p30
V_f	Fibre volume fraction, p26
V_m	Matrix volume fraction, p26
V_{min}	Minimum fibre volume fraction as defined in Eq.(2-52), p30
V_t	Transition volume fraction as defined in Eq.(2-56), p31
w	Width, p56
W	Weight, p59
$Z_{2/\alpha}$	Standardised normal variate, p68
$[\gamma_{ij}]$	Shear strain matrix, p10
γ	Surface energy, p13
γ_p	Energy expended in plastic deformation per unit area of crack, p7
δ_c	Composite elongation, p34
δ_f	Fibre elongation, p34
δ_m	Matrix elongation, p34
ϵ	Error limitation, p68
$[\epsilon_i]$	Strain matrix, p10
ϵ_c	Strain of a composite, p25
ϵ_f	Strain of fibres, p25
ϵ_m	Strain of matrix, p25

ϵ_f^*	Fibre failure strain, p28
ϵ_m^*	Matrix failure strain, p28
θ	Contact angle, p61
μ	Mean voidage, p68
ρ	Radius of curvature, p15
$[\sigma_{ij}], [\sigma_i]$	Stress component matrix, p8, p10
σ	Stress, p14
σ	Standard deviation
σ_c	Local stress, p14
σ_c	Stress of a composite, p25
σ_{cu}	Composite failure stress, p29
σ_f	Stress of fibres, p25
$(\sigma_f)_{em}^*$	Stress of the fibres at the matrix fracture strain, p32
σ_{fu}	Fibre failure stress, p29
σ_m	Stress of matrix, p25
$(\sigma_m)_{ef}^*$	Stress in the matrix at the fibre fracture strain, p29
σ_{mu}	Matrix failure stress, p29
σ_{th}	Theoretical maximum strength, p13
$[\tau_{ij}]$	Shear stress matrix, p10
τ	Shear stress at the fibre/matrix interface, p29
ϕ	Angle between c-axis of a crystallite and fibre axis, p20

1. INTRODUCTION

At the 1990 SAMPE conference, the world market of PAN-based carbon fibre was estimated to be 6000 tonnes per year and this accounted for the major share of the total market for carbon fibres. This market was predicted to grow at more than 10% annually during the 1990s^[1], the effect being a doubling of the market in the major trading areas of the world by 1995 (Figure 1.1). The advantages of carbon fibres which will stimulate this growth of demand are illustrated in Figures 1.2 and 1.3. These two figures show that carbon fibres have high specific strength and modulus in comparison with conventional materials. When they are embedded in matrices such as polymers or other carbon phases, the practical application of these properties are then realised. The properties of such composite materials, e.g., light weight, high corrosion resistance, extremely low thermal expansion coefficient and good fatigue resistance etc., soon received immediate attention for many applications. Their development initiated a "revolution in materials"^[4]. The perhaps premature description "miracle materials" even appeared^[5,6]. In the case of organic polymers as matrices, the composites are termed carbon fibre reinforced polymers, CFRP. If the matrix is another carbon phase, the materials are called carbon fibre reinforced carbon composites, CFRC or C/C composites. These are obtained by carbonising a CFRP and densifying the resultant carbonised preform.

Of the total carbon fibre production, more than 90% is used in CFRPs and only a minor part in C/C composites^[7]. However it is this latter application that will play the more important role in the future technology. High temperatures are unavoidable in many advanced applications. The surface temperature of a space shuttle, for instance, can rise to 1000 °C during the period of re-entry into the earth's atmosphere. In the now defunct British project, HOTEL, flying vehicles starting and landing in air fields like commercial airplanes, would fly from America to Asia in just 3 hours but it is calculated that the surface temperature of the vehicles would be over 1800 °C^[8]. In such cases, CFRP can not be used. The only suitable materials presently known are C/C composites. C/C composites consist of elemental carbon which possesses good thermal stability up to 2730 °C^[9]. This together with the light weight and high thermal shock resistance means that C/C composites can most impressively satisfy the needs of high technology. The principle applications of C/C composites includes their use as high temperature (>500 °C) materials, such as the cone-tip and edge of wings of the

INTRODUCTION

space shuttle^[10], nose and tip of missiles, heat shield materials, disk brakes for supersonic jets; intermediate temperature (250 - 500 °C) materials for car engines and gas turbines; refractory materials, e.g., moulds for hot moulding; corrosion resistance materials and biocompatible materials. The further development of C/C composites may also extend to the applications in transportation etc..

The major disadvantages of C/C composites are their sensitivity to high temperature oxidation and the lengthy and costly processing necessary to obtain an effective translation of fibre mechanical properties to the composite. The method currently used to protect C/C composites against oxidation is silicon carbide coating, but research into improved methods is continuing. The present study is concerned with the translation of the fibre properties to the composite.

Adequate adhesion between fibres and matrix is necessary for the composites to utilise the virtue of the fibres so as to obtain high mechanical properties. For CFRP, this problem can be solved by the surface treatment of carbon fibres. In the case of C/C composites, it is necessary to ensure poor adhesion between fibres and polymer matrix in the preforms, otherwise the fibres will be damaged by shrinkage of the matrix during carbonisation^[7,9]. This shrinkage results in fissures at the fibre/matrix interface. The only way to achieve the desired translation of fibre behaviour is then to densify this porous structure. Thus an understanding of the structure of the composites, its influence on mechanical properties and its development on densification is the first step in the approach to produce high quality C/C composites. The overall objective of this study was to gain such a understanding by investigating composites derived from different raw materials and produced in a variety of processes. The outcome of such work would be the ability to make recommendations for producing better quality C/C composites.

This thesis is divided into five sections. The relevant literature is reviewed in Section 2. Section 3 describes experimental procedure. Section 4 presents the experimental results which consist of the four phases of the experimental study. Characterisation of the composite structure was studied in the first phase. The second phase investigated the effect of void structure on densification route. An appreciation of relationship between the structure and the mechanical properties of the composites was obtained in the third phase. The final phase examined the effects of processing conditions on quality of the composites. The conclusions which follow lead to

INTRODUCTION

recommendations for further work.

2. LITERATURE REVIEW

As described in the Introduction, C/C composites exhibit outstanding performance in many important applications. A relatively detailed explanation of this performance and the fabrication of the composites will be reviewed in this section. The survey is based on the literature published to date and consists of two parts. Emphasis in the first part will be placed on the explanation of the high performance and the factors influencing the quality of the composites. The latter part is concerned with methods of fabrication.

2.1 STRENGTH OF C/C COMPOSITES

High thermal shock resistance and light weight are not only possessed by C/C composites. All materials which consist of almost pure elemental carbon have these properties. The superiority of C/C composites over the conventional carbon materials lies in their mechanical properties. The strength of current C/C composites exceeds those of conventional polygranular carbon and graphite materials by a factor of ten^[10]. The purpose of this section is to review the current understanding of high strength structures from carbon.

2.1.1 Fundamental Nature of Carbon

2.1.1.1 Bonding in Carbon Materials

The basis of the strength of carbon materials is the bonding between carbon atoms. Primary bonds are formed by a pronounced lowering of the energies of the electrons, i.e., chemical bonds. They are the basic units in forming the skeleton of carbon structure. Another kind of bonding between carbon atoms is that formed by van der Waals forces. This type of bond is much weaker than the chemical bonds but plays a very important role in the modification of carbon structure. At the atomic level, the strength of a carbon structure is characterised by the relative proportion of these different bonds and their arrangement.

The elemental number of carbon is six and the electronic configuration of a carbon atom in its ground state is $1s^2 2s^2 2p^2$. However this ground state is almost unknown

because of the energetic advantage of involving all four outer orbital electrons in bonding between carbon atoms themselves, or with other atoms^[11].

The commonly used method of treating the bonding in carbon materials and compounds was developed by Pauling^[12]. He suggested that the four atomic orbitals ($2s$, $2p_x$, $2p_y$, $2p_z$) in the L shell be replaced by three sets of equivalent hybrid orbitals, designated sp^3 , sp^2 and sp .

One $2s$ + three $2p$ ---- four sp^3

One $2s$ + two of the $2p$ ---- three sp^2

One $2s$ + one of the $2p$ ---- two sp

The bonding then is formed by overlap of the orbitals between the two atoms. When the electron distribution after overlapping is cylindrically symmetrical with respect to the internuclear axis, the bond is defined as a σ bond. If symmetry of the electron distribution refers to a plane in which the electron occupation is zero, the bond is called a π bond.

In the formation of carbon materials, sp - sp bonding tends to develop a linear chain structure. The angle of the neighbouring σ bonds is restricted by two π bonds formed by the p orbitals in an orthogonal arrangement. Such structures are difficult to use to build a high strength material. Just van der Waals force between the chains is not enough to hold them together in a preferred orientation. The only way for this type of bonding to participate in the skeleton of carbon materials is as a bridge form. However this hypothesis has not been confirmed in the literature.

The geometry of sp^2 and sp^3 hybridisation is predicted to be trigonal and tetrahedral respectively by the mathematical description. Under the geometrical restriction, sp^2 - sp^2 bonding can only develop in a 2-D plane. The bonding between C-C atoms with this development consists of one σ bond and one π bond. This bonding has potential to generate large 2-D networks which either remain as single layers or associate in stacks with or without layer ordering. Hexagonal networks are expected because their bond angle is the same as the hybridisation scheme, i.e., 120° . The development of sp^3 - sp^3 bonding leads to the formation of a rigid 3-D network as in

diamond. In this network, the neighbouring two atoms are bound by σ bonds. This type of bonding can also acts as a bridge in a carbon skeleton. Both sp^2 and sp^3 hybridisation participate in the formation of chemical bonds in carbon materials. In addition, sp^2 - sp^3 bonding often appears as a bridge in the carbon skeleton. Some materials such as coals also include a small number of bonds of carbon with other elemental atoms, e.g., oxygen, hydrogen and nitrogen etc.. The quatitative evaluation of the strength of bonds is given by bond lengths and energies. These data are shown in Tables 2.1 and 2.2 respectively.

2.1.1.2 Structure of Carbon

If carbon atoms are considered as bricks, the bonding forms between the atoms provide the mortar to bind the bricks into walls. The arrangement of these walls is of great importance in giving the building adequate strength and similarly the strength of a carbon material is determined by its structure at the microscopic level.

The allotropic forms of carbon in nature are diamond and graphite. Diamond is a perfect development of sp^3 hybridisation. The three dimensional network of σ bonds provides a very rigid, stable structure (Figure 2.1) making it one of the hardest materials known. From the thermodynamic calculation, synthesis of such a structure has to be under the conditions of a pressure > 60 GPa at room temperature. The difficulty of synthesis and the poor natural abundance restrict the use of diamond as an engineering material.

The crystal structure of graphite was first described correctly independently but nearly simultaneously by both Hassel^[14] and Bernal^[15]. It is a precise stacking of perfectly developed sp^2 - sp^2 hexagonal sheets. The distance between any two layers is 0.3354 nm. Figure 2.2 illustrates this structure with two different stacking forms. The hexagonal form, ABAB is the principal form in natural graphite, the rhombohedral form ABCABC etc. being less stable.

Carbon materials are essentially composed of solid carbons which have the basic structural unit of planar or approximately planar arrangements of carbon atoms in a hexagonal networks. Solid carbons can be considered as being the graphite

of defects. The order or regularity of a solid carbon is determined by the amount and types of these defects. A well-ordered material often has an almost perfect graphite lattice in a short range. But over a large range, the presence of defects, distortions and heteroatoms decreases the degree of order. In a less-ordered material, the disturbance of the defects is so serious that the material can not exhibit graphitic behaviour even in the short range.

A carbon structure may contain both the well-ordered and less-ordered materials. The variation in carbon structures depends on the proportion of ordered and less-ordered parts and the degree of alignment of the ordered structures. Solid carbons have two basic forms. According to the terminology suggested by International Committee for Characterisation And Terminology on Carbon (ICCTC), these two forms are termed graphitic carbons and non-graphitic carbons. Graphitic carbons are all varieties of substance consisting of the element carbon in the allotropic form of graphite irrespective of the presence of structure defects. The three-dimensionally ordered layer planes in graphitic carbon are measurable using X-ray diffraction analysis. Non-graphitic carbons consist mainly of the element carbon with two-dimensional long range order of the carbon atoms in planar hexagonal networks, but without any measurable crystallographic order in the c-direction apart from more or less parallel stacking[16,17].

Some carbons are thermally unstable. By heat treatment to above 2200 °C at atmospheric or lower pressure, thermally unstable carbon in non-graphitic form can be converted into graphitic carbon, while 3-D crystallographic order in thermally unstable graphitic carbon will develop further. This process is called graphitisation. Figure 2.3 illustrates the possibility of graphitisation for different carbon structures[18]. These models were proposed by Franklin as early as 1951. The term, "graphitizing", used in that time corresponds to the term, "graphitisable", used at present. The structure of non-graphitisable carbons is highly cross-linked. This structure derives from their precursors. During heat treatment, the precursors only lose small molecules and then develop the initial cross-linking, so that fusion can not take place. This non-fusing degradation forms a thermodynamically stable structure, hence further heat treatment up to the temperature of graphitisation can not generate 3-D crystallographic order.

Most graphitisable carbons are formed from or pass through a fluid stage on carbonisation. In this stage, mobile planar aromatic molecules have the opportunity to

align with each other to form a thermodynamically unstable precursor of the graphitic structure. Further heat treatment provides energy to the molecules so that the activated molecules rearrange to form thermostable graphitic carbon.

2.1.1.3 Stress Analysis of The Graphite Structure

Since solid carbon is based on the graphite modification, a detailed knowledge of the mechanical behaviour of graphite is essential before the synthesis of high performance materials can be considered. The discussion below is based on the hexagonal crystal form of graphite.

The structure of graphite illustrated in Figure 2.2 implies that graphite exhibits anisotropy in mechanical properties. The interatomic bonding within the basal plane is quite different from that between the neighbouring layers. Atoms within the aromatic sheets are covalently bonded. Breaking such bonds requires 699kJ/mol (Table 2.2)^[11]. However between the neighbouring sheets, there is no primary electron bonding so that the bond energy can only be similar in magnitude to van der Waal's force. This implies that the interatomic bonding within the basal planes (a-axis) is much stronger than that in the direction normal to the basal planes (c-axis). The distribution of stresses and elasticity in the graphite structure can be obtained by the use of following mathematical analysis.

For a three dimensional stress state in rectangular coordinates, such as that illustrated in Figure 2.4, the relations of the strain ϵ and stress σ for an anisotropic material can be expressed by the generalised Hooke's law.

$$\begin{pmatrix} \epsilon_{11} \\ \epsilon_{22} \\ \epsilon_{33} \\ \epsilon_{23} \\ \epsilon_{31} \\ \epsilon_{12} \\ \epsilon_{32} \\ \epsilon_{13} \\ \epsilon_{21} \end{pmatrix} = \begin{pmatrix} S_{1111} & S_{1122} & S_{1133} & S_{1123} & S_{1131} & S_{1112} & S_{1132} & S_{1113} & S_{1121} \\ S_{2211} & S_{2222} & S_{2233} & S_{2223} & S_{2231} & S_{2212} & S_{2232} & S_{2213} & S_{2221} \\ \text{---} & \text{---} & \text{---} & \text{---} & \text{---} & \text{---} & \text{---} & \text{---} & \text{---} \\ \text{---} & \text{---} & \text{---} & \text{---} & \text{---} & \text{---} & \text{---} & \text{---} & \text{---} \\ \text{---} & \text{---} & \text{---} & \text{---} & \text{---} & \text{---} & \text{---} & \text{---} & \text{---} \\ \text{---} & \text{---} & \text{---} & \text{---} & \text{---} & \text{---} & \text{---} & \text{---} & \text{---} \\ \text{---} & \text{---} & \text{---} & \text{---} & \text{---} & \text{---} & \text{---} & \text{---} & \text{---} \\ \text{---} & \text{---} & \text{---} & \text{---} & \text{---} & \text{---} & \text{---} & \text{---} & \text{---} \\ S_{2111} & S_{2122} & S_{2133} & S_{2123} & S_{2131} & S_{2112} & S_{2132} & S_{2113} & S_{2121} \end{pmatrix} \begin{pmatrix} \sigma_{11} \\ \sigma_{22} \\ \sigma_{33} \\ \sigma_{23} \\ \sigma_{31} \\ \sigma_{12} \\ \sigma_{32} \\ \sigma_{13} \\ \sigma_{21} \end{pmatrix} \quad (2-1)$$

Alternatively

$$\begin{pmatrix} \sigma_{11} \\ \sigma_{22} \\ \sigma_{33} \\ \sigma_{23} \\ \sigma_{31} \\ \sigma_{12} \\ \sigma_{32} \\ \sigma_{13} \\ \sigma_{21} \end{pmatrix} = \begin{pmatrix} C_{1111} & C_{1122} & C_{1133} & C_{1123} & C_{1131} & C_{1112} & C_{1132} & C_{1113} & C_{1121} \\ C_{2211} & C_{2222} & C_{2233} & C_{2223} & C_{2231} & C_{2212} & C_{2232} & C_{2213} & C_{2221} \\ \dots & \dots & \dots & \dots & \dots & \dots & \dots & \dots & \dots \\ \dots & \dots & \dots & \dots & \dots & \dots & \dots & \dots & \dots \\ \dots & \dots & \dots & \dots & \dots & \dots & \dots & \dots & \dots \\ \dots & \dots & \dots & \dots & \dots & \dots & \dots & \dots & \dots \\ \dots & \dots & \dots & \dots & \dots & \dots & \dots & \dots & \dots \\ C_{2111} & C_{2122} & C_{2133} & C_{2123} & C_{2131} & C_{2112} & C_{2132} & C_{2113} & C_{2121} \end{pmatrix} \begin{pmatrix} \epsilon_{11} \\ \epsilon_{22} \\ \epsilon_{33} \\ \epsilon_{23} \\ \epsilon_{31} \\ \epsilon_{12} \\ \epsilon_{32} \\ \epsilon_{13} \\ \epsilon_{21} \end{pmatrix} \quad (2-2)$$

In the stress and strain matrices, the first subscript i indicates that the surface on which the stress acts is perpendicular to the i-axis. The second subscript j indicates the component of the resultant force from which the stress is derived. The [S] matrix is the compliance matrix and [C] matrix is the stiffness coefficient matrix. Both matrices give the relations between the stress and strain or between the strain and stress and include 81 elastic constants in each. It can be proven that the stress, strain, compliance and stiffness coefficient matrices must be symmetrical^[19]. In other words,

$$\begin{aligned} \sigma_{12} &= \sigma_{21} & \epsilon_{12} &= \epsilon_{21} \\ \sigma_{23} &= \sigma_{32} & \epsilon_{23} &= \epsilon_{32} \\ \sigma_{13} &= \sigma_{31} & \epsilon_{13} &= \epsilon_{31} \end{aligned}$$

and (2-3)

$$\begin{aligned} S_{1122} &= S_{2211} & C_{1122} &= C_{2211} \\ S_{1121} &= S_{2111} & C_{1121} &= C_{2111} \\ \dots & \dots & \text{etc.} & \end{aligned}$$

With this symmetry, the size of equation (2-1) or (2-2) reduces to six independent stresses and strains and 36 components of the [S] or [C] matrix of which only 21 are independent. By introducing the following notation changes^[20]

$$\begin{aligned}
 \sigma_{11} &= \sigma_1 & e_{11} &= \epsilon_1 \\
 \sigma_{22} &= \sigma_2 & e_{22} &= \epsilon_2 \\
 \sigma_{33} &= \sigma_3 & e_{33} &= \epsilon_3 \\
 \sigma_{23} &= \sigma_4 = \tau_{23} & 2e_{23} &= \epsilon_4 = \gamma_{23} \\
 \sigma_{13} &= \sigma_5 = \tau_{13} & 2e_{13} &= \epsilon_5 = \gamma_{13} \\
 \sigma_{12} &= \sigma_6 = \tau_{12} & 2e_{12} &= \epsilon_6 = \gamma_{12}
 \end{aligned} \tag{2-4}$$

the end results are the constitutive relations as follows:

$$\begin{bmatrix} \epsilon_1 \\ \epsilon_2 \\ \epsilon_3 \\ \epsilon_4 \\ \epsilon_5 \\ \epsilon_6 \end{bmatrix} = \begin{bmatrix} \epsilon_1 \\ \epsilon_2 \\ \epsilon_3 \\ \gamma_{23} \\ \gamma_{13} \\ \gamma_{12} \end{bmatrix} = \begin{bmatrix} S_{11} & S_{12} & S_{13} & S_{14} & S_{15} & S_{16} \\ S_{12} & S_{22} & S_{23} & S_{24} & S_{25} & S_{26} \\ S_{13} & S_{23} & S_{33} & S_{34} & S_{35} & S_{36} \\ S_{14} & S_{24} & S_{34} & S_{44} & S_{45} & S_{46} \\ S_{15} & S_{25} & S_{35} & S_{45} & S_{55} & S_{56} \\ S_{16} & S_{26} & S_{36} & S_{46} & S_{56} & S_{66} \end{bmatrix} \begin{bmatrix} \sigma_1 \\ \sigma_2 \\ \sigma_3 \\ \tau_{23} \\ \tau_{13} \\ \tau_{12} \end{bmatrix} \tag{2-5}$$

and

$$\begin{bmatrix} \sigma_1 \\ \sigma_2 \\ \sigma_3 \\ \tau_{23} \\ \tau_{13} \\ \tau_{12} \end{bmatrix} = \begin{bmatrix} C_{11} & C_{12} & C_{13} & C_{14} & C_{15} & C_{16} \\ C_{12} & C_{22} & C_{23} & C_{24} & C_{25} & C_{26} \\ C_{13} & C_{23} & C_{33} & C_{34} & C_{35} & C_{36} \\ C_{14} & C_{24} & C_{34} & C_{44} & C_{45} & C_{46} \\ C_{15} & C_{25} & C_{35} & C_{45} & C_{55} & C_{56} \\ C_{16} & C_{26} & C_{36} & C_{46} & C_{56} & C_{66} \end{bmatrix} \begin{bmatrix} \epsilon_1 \\ \epsilon_2 \\ \epsilon_3 \\ \gamma_{23} \\ \gamma_{13} \\ \gamma_{12} \end{bmatrix} \tag{2-6}$$

For a hexagonal crystal, additional symmetrical relations can be applied, i.e.[21]

$$S_{11} = S_{22}$$

$$S_{13} = S_{23}$$

$$S_{44} = S_{55}$$

(2-7)

$$S_{14} = S_{15} = S_{16} = S_{24} = S_{25} = S_{26} = S_{34} = S_{35} = S_{36} = S_{45} = S_{46} = S_{56} = 0$$

Similarly

$$C_{11} = C_{22}$$

$$C_{13} = C_{23}$$

$$C_{44} = C_{55}$$

(2-8)

$$C_{14} = C_{15} = C_{16} = C_{24} = C_{25} = C_{26} = C_{34} = C_{35} = C_{36} = C_{45} = C_{46} = C_{56} = 0$$

Then the constitutive relationships between the stresses and strains for the hexagonal graphite structure are obtained.

$$\begin{bmatrix} \epsilon_1 \\ \epsilon_2 \\ \epsilon_3 \\ \gamma_{23} \\ \gamma_{13} \\ \gamma_{12} \end{bmatrix} = \begin{bmatrix} S_{11} & S_{12} & S_{13} & 0 & 0 & 0 \\ S_{12} & S_{11} & S_{13} & 0 & 0 & 0 \\ S_{13} & S_{13} & S_{33} & 0 & 0 & 0 \\ 0 & 0 & 0 & S_{44} & 0 & 0 \\ 0 & 0 & 0 & 0 & S_{44} & 0 \\ 0 & 0 & 0 & 0 & 0 & S_{66} \end{bmatrix} \begin{bmatrix} \sigma_1 \\ \sigma_2 \\ \sigma_3 \\ \tau_{23} \\ \tau_{13} \\ \tau_{12} \end{bmatrix} \quad (2-9)$$

and

$$\begin{bmatrix} \sigma_1 \\ \sigma_2 \\ \sigma_3 \\ \tau_{23} \\ \tau_{13} \\ \tau_{12} \end{bmatrix} = \begin{bmatrix} C_{11} & C_{12} & C_{13} & 0 & 0 & 0 \\ C_{12} & C_{11} & C_{13} & 0 & 0 & 0 \\ C_{13} & C_{13} & C_{33} & 0 & 0 & 0 \\ 0 & 0 & 0 & C_{44} & 0 & 0 \\ 0 & 0 & 0 & 0 & C_{44} & 0 \\ 0 & 0 & 0 & 0 & 0 & C_{66} \end{bmatrix} \begin{bmatrix} \varepsilon_1 \\ \varepsilon_2 \\ \varepsilon_3 \\ \gamma_{23} \\ \gamma_{13} \\ \gamma_{12} \end{bmatrix} \quad (2-10)$$

In eqs. (2-9) and (2-10), axes 1 and 2 are parallel to the basal planes of the graphite and axis 3 parallel to the hexagonal axis (c-axis). The values of elastic stiffness coefficients and elastic compliance are shown in Table 2.3^[22]. With these values, the Young's moduli and shear moduli can be calculated as follows^[22].

Young's modulus parallel to the hexagonal axis

$$E_c = S_{33}^{-1} = 36.4 \text{ GPa} \quad (2-11)$$

Young's modulus parallel to the basal planes

$$E_a = S_{11}^{-1} = 1020 \text{ GPa} \quad (2-12)$$

Shear modulus parallel to the basal planes

$$G_o = S_{44}^{-1} = C_{44} = 4.5 \text{ GPa} \quad (2-13)$$

Shear modulus of individual layers

$$G_i = C_{66} = 1/2 (C_{11} - C_{12}) = 440 \text{ GPa} \quad (2-14)$$

Eqs.(2-11) to (2-14) indicate that Young's modulus in the graphite structure is very high parallel to the basal planes and much lower in the direction of the hexagonal axis. Also the shear modulus parallel to the basal planes is quite small. From the data, it is evident that the tensile strength parallel to the basal planes would be the highest strength of the graphite. The compressive strength in this direction is reduced by buckling because of the low interlayer shear modulus. The lowest strength in the structure is the bending strength. During bending, the failure does not initiate fracture of the individual layers but cleavage between the layers. The mechanical behaviour of this structure is much like overlapped sheets of paper.

From the stress analysis of the graphite structure, it can be concluded that the

graphite structure has high performance mechanical properties within the graphite layers and low resistance against shear between the layers. For the synthesis of carbon materials with good mechanical properties, it is necessary to consider the utilisation of the merit in the direction of basal planes of the graphite structure and overcome the disadvantage in the direction of the hexagonal axis.

2.1.2 Strength of Carbon

Since it was realised that the basal plane of the graphite crystal possesses excellent mechanical properties, possible means of exploiting them have been investigated. The review in this section will provide an understanding of what forms of solid carbon are best suited to achieve high mechanical properties, their structure and classification.

2.1.2.1 Theoretical Maximum Values for Mechanical Properties of Carbon

Materials

To introduce a discussion of factors influencing mechanical properties of carbon materials, it is instructive to make an estimate of the theoretical modulus and strength of carbon materials and to compare these with the measured values. The theoretical maximum Young's modulus of a carbon material is the Young's modulus with value 1020 GPa in the direction parallel to the basal planes of the graphite crystal (see Eq.2-14). To date, 80% of the theoretical maximum modulus, i.e., 820 GPa, has been achieved by Union Carbide for Thornel P-120 carbon fibres^[23]. The high modulus was obtained by forming a high degree of preferred orientation.

The theoretical maximum strength of a material was estimated by Polanyi in 1921^[24]. From consideration of the action of strain on a perfectly brittle crystal, the elastic energy that resides between two atomic planes is equated to the energy of the two surfaces created when the crystal cleaves. The relationship obtained is

$$\sigma_{th} = (4 \gamma E / a)^{1/2} \quad (2-15)$$

Where σ_{th} is the theoretical maximum strength, γ the surface energy, E the Young's

modulus and a the interplanar spacing. For various materials, the theoretical strength is between $0.03E$ and $0.17E$ [25]. In the case of the graphite,

$$\sigma_{th} \approx 0.1 E \quad (2-16) [4, 23]$$

The best high strength solid carbons produced, i.e., graphite whiskers, had a Young's modulus of $E=680$ GPa and a tensile strength of $\sigma=20$ GPa[23] so that the elongation at failure, σ/E , is only 0.03.

Comparison of the achieved values with the theoretical maximum mechanical properties illustrate that improvement in strength is more difficult to achieve than improvement in Young's modulus. The explanation of this fact will involve consideration of the basic principles of fracture mechanics

2.1.2.2 Effects of Cracks on Strength

The basic principles of fracture mechanics to be introduced in this section are based on Griffith's energy-balance concept of fracture. Although this theory was derived from the behaviour of "model" materials, i.e., perfectly brittle materials, and is less satisfactory when applied to materials which exhibit less perfect behaviour, it does provide a common thread linking various aspects of empirically-based fracture theories at the fundamental level. The treatment which follows draws on the basic principles of this theory to illustrate the influence of cracks on strength while ignoring the localised anisotropy of carbon structure and the imperfectly brittle behaviour of solid carbons.

Fundamental principles of the fracture mechanics suggests that materials do not achieve the theoretical fracture stress because of the presence of flaws and defects. One of the basic forms of the flaws is a crack. When a material has been stressed, the cracks act to concentrate the stress at their tips. This was first noticed by Inglis[26]. He analysed an elliptical crack in a uniformly stressed plate and found that the ratio of the local to the applied stress, σ_c/σ was related to the major and minor semi-axes of the ellipse, a and b .

$$\sigma_c / \sigma = (1 + 2a/b) \quad (2-17)$$

For a narrow ellipse, where $a \gg b$, this equation can be rewritten in terms of the radius of curvature ρ at the crack tip as

$$\sigma_c / \sigma = 2(a/\rho)^{1/2} \quad (2-18)$$

From this equation, it can be seen that the irregularity of curvature of cracks induces stress concentration at localised positions. The finer the crack the greater the stress concentration. If the stress at the tip exceeds the theoretical fracture stress, it may be assumed that the crack will propagate through the material.

Ingli's work made progress in finding the conditions for crack propagation but did not include consideration of the size factor of the cracks. In most cases, large cracks propagate more readily than small ones. Thus there was considerable interest in finding the critical crack sizes which contribute to strength limitation. The progress in this consideration was made by Griffith^[27, 28]. He first introduced the energy-balance concept. This concept describes a thermodynamic equilibrium between an amount of work U done by the applied load, elastic strain energy, U_E stored in the material, and an increase in surface energy, U_s

$$U = U_E + U_s \quad (2-19)$$

Before the crack propagates, elastic strain energy is stored in the material. This is released when the material relaxes as the crack spreads. The crack propagates when the released energy is just sufficient to provide the surface energy necessary for the creation of the new surface.

By the application of this concept to a crack in a uniform stress. The decrease of stored strain energy due to that released is given by:

$$U_E = - \frac{\sigma^2 \pi C^2}{E} \quad (2-20)$$

The surface energy required to create new surface is

$$U_s = 4 \gamma C \quad (2-21)$$

By substituting Eqs.(2-20) and (2-21) into Eq.(2-19), the total energy can be expressed as

$$U = -\frac{\sigma^2 \pi C^2}{E} + 4 \gamma C \quad (2-22)$$

where σ and E are stress and Young's modulus. γ and $2C$ are surface energy per unit area and crack length respectively.

Figure 2.5 plots these energy terms as a function of crack length. The applied energy is maximum at length C_{critical} and consequently a crack of that length is unstable and reduces the total energy by growing. The maximum in U occurs when

$$\frac{dU}{dC} = \frac{dU_s}{dC} + \frac{dU_E}{dC} = 0 \quad (2-23)$$

Substituting U_s and U_E with Eqs.(2-20) and (2-21) results in

$$4 \gamma - \frac{2 \sigma^2 \pi C}{E} = 0 \quad (2-24)$$

Therefore

$$\sigma = \left(\frac{2 E \gamma}{\pi C} \right)^{\frac{1}{2}} \quad (2-25)$$

This is the Griffith equation for brittle materials. It shows that the stress necessary to cause a crack to propagate varies inversely as the square root of the crack length. This provides an explanation of why large cracks are favourable for crack propagation.

For materials exhibiting a small amount of plastic deformation, the Griffith equation can be modified as

$$\sigma = \left[\frac{E(2\gamma + \gamma_p)}{\pi C} \right]^{\frac{1}{2}} \quad (2-26)^{[29]}$$

where γ_p is the energy expended in plastic deformation per unit area of crack. This equation may be more suitable for carbons because they do not exhibit perfect brittle behaviour^[30].

The environment of voids in solid carbons and carbon materials is far more complicated than that of the crack assumed in deriving the Griffith equation. In this case, the term "Griffith flaws" was applied to account for breakage under an applied load. The Griffith flaws involve not only cracks and their environment but also grain boundary defects, grain size etc.. For example, it has been found that sometimes failure in carbon fibres does not initiate from large cracks but from small cracks^[31]. This does not mean that the trend indicated by the Griffith equation can not be applied but that the cracks are not simple cracks, in another words, the big and small cracks are present in different environments or they are different types of flaw. Reynolds and Sharp's research^[32] showed that the small cracks were present in misoriented region of graphite crystallites. Shear strain was introduced in this region so that the critical crack size was less than that for other regions. However for cracks in the same environment, failure still begins from the larger cracks.

All in all, Ingli's and Griffith's work illustrates that cracks in a material are the reason for material failure at a lower value than its theoretical strength. Hence reduction of the size and probability of the presence of flaws in carbons and carbon materials would be conducive to diminishing the difference between the practical and theoretical strengths.

2.1.2.3 Shear Resistance of Carbon Materials

To identify those crystallographic factors which have an important influence on

the shear resistance, it is convenient to regard solid carbons as aggregations of crystallites which may vary in a variety of degrees of imperfection. Under this assumption, the stiffness of any given carbon depends on the microstructural features of boundary restraint arrangement and imperfection of the crystallites. It is therefore possible to produce a desired set of mechanical and physical properties by controlling these features.

Imperfection in a graphitic structure can be characterised in two ways. One of these is to utilise traditional characterisation of the lattice defects of a crystal in crystallography. Types of lattice defects in an imperfect crystal structure may include point defects, line defects (dislocations) and surface defects in main groups. Point defects are localised disruptions of lattice involving one or possibly several sites. There are many types of point defects. When the disruption is an atom missing from a normal site, the defects are called vacancies. If an extra atom is inserted into the lattice structure at a site which is not a normal lattice point, an interstitial defect is formed. A substitutional defect is introduced when an atom is replaced by a different type of atom. The substitutional atom remains at the original normal lattice point. Once a vacancy-interstitial pair is formed, the defect is termed a Frenkel defect. Dislocations are line imperfection in an otherwise perfect lattice. Two types of dislocations are identified, the screw dislocation and the edge dislocation. A screw dislocation is produced by skewing a crystal so that one atomic plane produces a spiral ramp about the dislocation, while an edge dislocation is introduced by adding an extra half plane of atoms. The term surface defect refers to the boundaries, or planes, that separate a material into regions, each region having the same crystal structure but different orientations, such as material surface, stacking faults and grain boundaries etc.. All of these lattice defects are found in the graphitic structures. The studies based on such characterisation were systematically reviewed by Amelinckx et al^[33] and Kelly^[22].

Another solution to characterise the lattice defects in a graphitic structure is based on the laminar nature of the graphite structure^[4,34]. Three types of defects are described in this characterisation, namely defects within the layers, defects between the layers, mostly stacking faults which cause high lattice distance between the layers, and finally disclination of the layers. Such a description is quite easy to understand but further characterisation into sub-groups has to be supplemented with the traditional characterisation in crystallography.

Lattice defects produce a wide variety of topologies in carbon sheets by establishing strong boundaries beyond which sheet perfection can not extend. The shear stiffness, C_{44} , thus changes with the concomitance of the topology. Point defects and dislocations can give rise to an enormous change in the interlamellar shear stiffness of graphitic materials. With very small doses of neutron irradiation (about 10^{17} nvt, $E > 1$ mev) the shear stiffness of single graphite crystals increases by a factor of 16^[35-37]. In the first instance, low doses of irradiation produce immobile, isolated vacancies and very mobile interstitials. Dislocations are easy to form in this circumstance. The pinning of the dislocations then increases the cohesion between the sheets. Disclination and change in the separation of the layers often accompany this case. For example, out-of-plane distortion caused by unit c-axis dislocations brings about a disclination, modifies the distance between the layers and increases the interlamellar stiffness^[38]. However disclination and change in the distance between the layers without involving point defects may decrease interlamellar shear stiffness and act as a crack initiator^[39].

The arrangement of crystallites can be examined by introducing the limitation of uniform stress. With an anisotropic aggregation, cylindrical symmetry can usually be assumed. Such a symmetry can be treated as an anisotropic solid with five independent elastic constants as shown in Figure 2.6. If the degree of arrangement or preferred orientation of the crystallites is known, it should be possible to estimate aggregate elastic constants. This preferred orientation was defined in terms of the distribution of layer normals $I(\phi)$ determined by X-ray scattering techniques^[40]. On the condition that the voids in the anisotropic structure do not reduce the overall elastic moduli, it can be shown that the Young's modulus along the cylindrical axis, E_{33} , is given by^[41,42]

$$\begin{aligned} 1/E_{33} = & S_{33} + (2 S_{13} - 2 S_{33} + S_{44}) (I_3 / I_1) + \\ & (S_{11} - 2 S_{13} + S_{33} - S_{44}) (I_5 / I_1) \end{aligned} \quad (2 - 27)$$

while along a radial axis, E_{11} , is given by

$$\begin{aligned} 1/E_{11} = & S_{11} - (S_{11} - S_{13} - 1/2 S_{44}) (I_3 / I_1) + \\ & 3/8 (S_{11} - 2 S_{13} + S_{33} - S_{44}) (I_5 / I_1) \end{aligned} \quad (2 - 28)$$

Shear modulus along a radial axis, G_{44} , will be

$$1/G_{44} = S_{44} + (3 S_{11} + 2 S_{33} - S_{12} - 4 S_{13} - 5/2 S_{44}) (I_3 / I_1) - 2 (S_{11} + S_{33} - 2 S_{13} - S_{44}) (I_5 / I_1) \quad (2 - 29)$$

where

$$I_n = \int_0^{\pi/2} I(\varphi) \sin^n \varphi \, d\varphi \quad (n = 1, 3, 5) \quad (2 - 30)$$

$I(\varphi) \, d\varphi$ is the relative number of crystallites with c axes at an angle φ to the cylindrical axis while S_{ij} refers to elastic compliance for a single crystal.

Eqs (2 - 27) to (2 - 29) indicate that both Young's moduli and shear modulus are affected by the arrangement of the crystallites, i.e., I_3/I_1 and I_5/I_1 . The trend of the change of the moduli can be shown by the comparison between Type I carbon fibres and their ideal case where all crystallites are perfectly aligned, $I_3/I_1 = I_5/I_1 = 1$. The estimated elastic moduli of a single fibre for these two materials are given in Table 2.4^[41]. These data indicate that increase of preferred orientation will increase the Young's modulus with a concomitant decrease in shear modulus.

This analysis shows that the best way to improve the shear resistance of carbons is to modify the structure of the crystallites and boundary restraints between them. High preferred orientation can only be conducive to improve Young's modulus in the orientated direction.

2.1.2.4 Carbon Fibres for High Performance Materials

It is clear that carbon high strength and modulus can be achieved by reducing the size and proportion of voids in the body, introducing or preserving the highest degree of defects in the ultra-structure, and getting a high degree of preferred orientation. One of the ways of realising this is to make carbon in one-dimension form as fibres or whiskers. It has been known for many years that certain elements and compounds in whisker form exhibit outstanding strength and modulus, because they contain fewer flaws or defects than are present in the bulk form. This is obvious because the

geometry ensures that the cracks must be either very short, across a fibre, or parallel to the fibres and hence harmless. It is also easier to obtain preferred orientation in fibres than in the other forms by spinning and stretching during their production. Also, most carbon, either natural or produced, has a turbostratic rather than perfect graphite structure. Thus it is possible to control the shear resistance at a relatively satisfactory level. In fact, carbon fibres are one of the best solid forms achieving high mechanical properties, especially for engineering applications.

Carbon is neither fusible at atmospheric pressure nor soluble in any known solvent^[43,44]. The triple point of carbon is at temperature 3627 °C and pressure 10.1 GPa^[45]. These properties make it impossible to produce fibres directly from solid carbon using routine methods, i.e., melt spinning or extruding. Methods which have been used for either scientific exploration or commercial production are described as follows:

- A) in a carbon arc operating under a very high pressure of inert gas;
- B) deposition of pyrolytic carbon on fine dispersed catalysts by pyrolysis of CO or hydrocarbon gases; and
- C) carbonisation of infusible organic fibres.

Method A was exploited by Bacon^[46] to produce short graphitic whiskers. These whiskers are not dislocation-free single crystals but have the form of rolled-up scroll. Hence the axially strong bonds are orientated to a very high degree. The elastic moduli are more than 800 GPa while strengths are approximately 20 GPa estimated from the strain to failure.

For a long time, Bacon's technique was ignored since it was not found possible to develop this method into a industrially useful process. However last year Iijima discovered "buckytubes" by using a similar technique^[47], and considerable interest has been shown in this method for development of a variety of tube-fullerenes.

The formation of fibrous carbon by pyrolysis of gas was first observed nearly a century ago^[48]. Since then, several approaches by pyrolysis of a variety of hydrocarbons have been reported^[49-54]. Fibres obtained with this method are also short ones but have excellent graphitic structure after high temperature treatment. Although they are not suitable for reinforcement purpose, these fibres have already generated

interest for electrical applications, especially because of their suitability to form intercalation compounds.

High performance carbon fibres can only be formed by carbonisation of infusible organic fibres. This route was initiated by Edison who made carbon filaments for electric-light bulbs from natural cellulose fibres in 1879^[55]. However interest in carbon fibre for lamp application soon declined with the introduction of the tungsten filament. The true history of present-day carbon fibres begins in the 1950's with the requirement of the aerospace industry for strong but light materials. At this time, Abbott^[56] developed a process for converting rayon into a fibrous carbon material. When this material, produced by The Carbon Wool Corporation, was carbonised at temperature of up to 1000 °C; it possessed tensile strengths as high as 276 MPa. Since then carbon fibres have been produced from a multitude of precursor materials. Of these materials, viscose rayon, polyacrylonitrile (PAN) and pitch have been commercially utilised. Because of the low carbon yield of the rayon precursor, present high performance carbon fibres are mainly obtained from PAN and mesophase pitch.

A general process of the production of carbon fibres from organic precursors is illustrated in Figure 2.7. The precursor materials chosen for this purpose should have the ability to spin and a carbon yield as high as possible. PAN and pitch are thermoplastic materials so that melt spinning and extruding can be utilised to produce fibres. Cellulose materials undergo thermal decomposition without the presence of a melting stage. They have to be transformed into regenerated-cellulose solution and then spin into cuprammonium or saponified acetate solutions to form continuous filaments.

Before carbonisation, precursor fibres need to be converted into nonflammable, non-fusible fibres so as to maintain fibre form and to preserve the original preferred orientation during the further heat treatment. This step is called stabilisation. Since oxidation is widely used for this treatment, the terminology "pre-oxidation" is often used. For rayon fibres, heat treatment in an oxidising atmosphere will drive-off volatile to yield a permanently dehydrated material. The oxidation of PAN molecules cyclises the chain structure to form a ladder structure^[57]. Spun pitch exhibits a much more complicated structure. The oxidation of this type of materials is not well understood. Most explanations are based on the cross-linkages formed between the molecules. In addition to oxidation, some physical treatments such as vacuum devolatilisation^[58] and liquid extraction^[59] etc. can also be used to achieve the stabilisation for some

mesophase pitch fibres. Apparently the terminology "pre-oxidation" can not be used to describe these physical treatments. To meet this requirement, the terminology "infusibilisation", is also used to describe this process involving either oxidation or physical treatment.

The final treatment of the production is carbonisation or heat-treatment at graphitisation temperature depending on the products required. Both treatments give a nearly pure carbon material but carbonisation retains more imperfections and heteroatoms in the structure. The amorphous carbon and the heteroatoms perform a function similar to that of a matrix in a composite. They are supposed to link the "crystallites" and hence are beneficial to the tensile strength of the fibres^[60, 61].

Heat-treatment at a higher temperature, graphitisation temperature, allows the materials to absorb more energy. With this energy, the rearrangement of the carbon structure occurs. This process may involve graphitisation for graphitisable carbons and increase of the regularity of the structure of non-graphitisable carbons so that the modulus of the carbon fibres can be improved.

During the production, the preferred orientation has been achieved by the processing. It is introduced via different routes depending on the materials and processes applied. For mesophase pitch based carbon fibres, preferred orientation is formed by the spinning step. The pitch contains mesophase which is composed of the large planar poly-aromatic molecules having a tendency for parallel arrangement^[62, 63]. The spinning process makes the most of this and aligns the planar molecules in a preferred direction parallel with the fibre axis. The subsequent infusibilisation conserves the alignment and results in a permanent preferred orientation in the fibres. Rayon and PAN based carbon fibres are essentially non-graphitising^[64-66]. Considerable energy in some form must be given to achieve a parallel arrangement of layer planes. Two procedures, so called "stress graphitisation" and boron-doping, have been confirmed to realise this. "Stress graphitisation" refers to the process in which stretching is exerted on the fibres during heat-treatment at graphitisation temperature. High modulus rayon^[67-69] and PAN^[70] fibres have been produced using this technique. The boron-doping method was developed by Allen et al. for improving the modulus of PAN based carbon fibres^[71]. Another method to achieve the preferred orientation takes advantage of the PAN precursor consisting of chain molecules. Utilisation of stretching prior to cyclisation will draw the coiled chain molecules into a linear form parallel with

the fibre axis. The subsequent preoxidation then transforms the linear molecules into a ladder polymer and maintains the preferred orientation permanently^[72].

The mechanical properties of the various types of commercially produced carbon fibres are presented in Figure 2.8. Most of these data were collected from the recently published literature^[23, 34] while data for rayon fibres are based on the early products, Thornel 25 to 100, produced by Union Carbide^[73,74]. From the consideration of reinforcement purpose, these carbon fibres have been characterised into three groups, high strength (HT), high modulus (HM) and high strength with intermediate modulus (IM).

The term high strength refers to those fibres with a tensile strength above 3500 MPa. The Young's modulus of this type of fibre is around 250 GPa with a commensurate strain-to-failure of 1.7 to 2.4 %. This type of carbon fibres are produced from PAN precursor by heat treatment below 1400 °C. Their primary application is in carbon fibre reinforced plastics (CFRP).

In the case of high modulus fibres, the value of the modulus is over 350 GPa while their strain-to-failure is as low as 0.5%. These carbon fibres can be obtained by carbonisation or graphitisation of mesophase pitch, heat treatment of PAN at graphitisation temperature and "stress graphitisation" of rayon fibre precursors.

The IM type include fibres with the strength of HT type, but with improved modulus values. This type of carbon fibres are also produced from PAN precursor.

Instead of HM, HT and IM, in Britain, types I, II and III or A, are widely used. In American industry, graphitised fibres, i.e. those heat treated to graphitisation temperature, are termed graphite fibres. However it is known that high temperature treated PAN and rayon fibres do not exhibit a graphitic structure so that strictly the term graphite fibres can only be used to refer to carbon fibres produced from mesophase pitch.

So far, it is possible to achieve a Young's modulus as high as 800 GPa from a mesophase pitch precursor on a commercial scale. This value approaches the theoretical value of 1020 GPa. The achieved strength is still far from the theoretical fracture stress. However from the point of view of making C/C composites, great advances have been

made in producing high performance materials from carbon.

2.1.3 Carbon Fibre Reinforcement of Composites

The previous discussion has shown that carbon in fibre form has the highest strength and stiffness. However carbon fibres themselves are of little practical value unless they are converted into a form suitable for use in engineering applications. To do this, the fibres must be bonded together by matrix materials, giving a composite structure whose properties depend on the properties of the both the fibres and the matrix. The discussion in this section, based on an idealised model, presents some elementary theoretical considerations of fibre reinforcement of composites, the implications for C/C composites being drawn.

2.1.3.1 General rules of fibre reinforcement

The Rule of Mixtures

Analysis of the mechanism of fibre reinforcement can be simplified if a unidirectional composite is considered with a perfect bonding between the fibres and the matrix. This unidirectional composite may be modelled by further assuming fibres to be uniform in properties and diameter, and continuous, and parallel throughout the composite. Under these conditions, the strains experienced by the fibre ϵ_f , matrix ϵ_m and composite ϵ_c should be same if the composite is subjected to a tensile stress in the longitudinal or fibre axial direction.

$$\epsilon_f = \epsilon_m = \epsilon_c \quad (2 - 31)$$

If the fibres and matrix behave elastically, the stress are as

$$\sigma_f = E_f \epsilon_f \quad (2 - 32)$$

$$\sigma_m = E_m \epsilon_m \quad (2 - 33)$$

Stresses σ_f and σ_m act over the cross-sectional areas of the fibres A_f and the matrix A_m respectively. Thus the loads P_f and P_m carried by the fibres and the matrix are

$$P_f = \sigma_f A_f = E_f \epsilon_f A_f \quad (2 - 34)$$

$$P_m = \sigma_m A_m = E_m \epsilon_m A_m \quad (2 - 35)$$

The resultant load P_c carried by the composite is the sum of the loads carried by the fibres and the matrix

$$P_c = P_f + P_m \quad (2 - 36)$$

This resultant load P_c causes an average stress σ_c in the composite acting over the entire cross-sectional area $A_c = A_f + A_m$. Thus

$$P_c = \sigma_c A_c = \sigma_f A_f + \sigma_m A_m \quad (2 - 37)$$

$$\sigma_c = \sigma_f (A_f / A_c) + \sigma_m (A_m / A_c) \quad (2 - 38)$$

For a composite with parallel fibres, the volume fraction can be written in terms of the areas as

$$V_f = A_f / A_c, \quad V_m = A_m / A_c \quad (2 - 39)$$

Thus

$$\sigma_c = \sigma_f V_f + \sigma_m V_m \quad (2 - 40)$$

Where V_f and V_m are respectively the volume fraction of the fibres and matrix in the composite. The differentiation of Eq (2-40) with respect to strain yields

$$\frac{d\sigma_c}{d\varepsilon} = \frac{\partial\sigma_f}{\partial\varepsilon_f} v_f + \frac{\partial\sigma_m}{\partial\varepsilon_m} v_m \quad (2-41)$$

In the range of elastic deformation

$$d\sigma_c/d\varepsilon = E_c, \quad \partial\sigma_f/\partial\varepsilon_f = E_f, \quad \partial\sigma_m/\partial\varepsilon_m = E_m \quad (2-42)$$

therefore

$$E_c = E_f V_f + E_m V_m \quad (2-43)$$

Eqs. (2-40) and (2-43) indicate that the strength as well as the stiffness varies linearly with the amount of fibres or matrix the composite contains. Such a relationship is called the rule of mixtures.

It is of interest to know the extent to which the load is shared between the fibres and matrix and the stresses to which they may be subjected. For this purpose, the following ratios of stresses and loads can be obtained from Eqs. (2-31) to (2-43)

$$\frac{\sigma_f}{\sigma_m} = \frac{E_f}{E_m}, \quad \frac{\sigma_f}{\sigma_c} = \frac{E_f}{E_c} \quad (2-44)$$

$$\frac{P_f}{P_m} = \frac{\sigma_f V_f}{\sigma_m V_m} = \frac{E_f}{E_m} \frac{V_f}{V_m} \quad (2-45)$$

$$\frac{P_f}{P_c} = \frac{E_f \varepsilon_f V_f}{E_f \varepsilon_f V_f + E_m \varepsilon_m V_m} = \frac{\frac{E_f}{E_m}}{\frac{E_f}{E_m} + \frac{V_m}{V_f}} \quad (2-46)$$

These equation indicate that the ratio of the stresses is the same as the ratio of

corresponding elastic moduli. The ratio of load depends on the ratio of elastic moduli of the fibres and the matrix and also on the ratio of their volume fractions. Thus a higher extent of stresses and load in the composite are undertaken by the fibres because of their higher performance. This achieves the aim of utilising the advanced properties of the fibres in bulk form. For effective reinforcement, high values of the modulus ratio of fibres and matrix, and fibre volume fraction are required.

Failure Behaviour of Composites

The ultimate tensile strength (maximum load/original cross-sectional area) of a composite depends on the stress-strain behaviour of the matrix and fibres, and the relative volume fraction. For C/C composites, the stress-strain behaviour of the constituents, fibres and matrix varies widely depending on their precursors so that the different combinations of fibres and matrix in a composite could give rise to three cases:

a) fibre failure strain, $\epsilon_f^* \approx$ matrix failure strain, ϵ_m^* ,

b) fibre failure strain, $\epsilon_f^* <$ matrix failure strain, ϵ_m^* ,

c) fibre failure strain, $\epsilon_f^* >$ matrix failure strain, ϵ_m^* ,

Which case predominates has not been confirmed because of the lack of reported data of the strain-to-failure of the matrix. Some researchers suggested that CASE C might be the most frequent^[75]. However from the point of view of structural features, it is difficult to imagine the failure strain of a high modulus carbon fibre produced from mesophase pitch to be greater than that of the matrix carbon produced from polyacrylonitrile. Thus the failure mechanism described in the following and based on the idealised model established previously, will cover all the possible situations.

CASE a: $\epsilon_f^* = \epsilon_m^*$

In this case, the fibres and the matrix will fail at the same time. The failure stress of the composite can be expressed as

$$\sigma_{cu} = \sigma_{fu} V_f + \sigma_{mu} V_m \quad (2-47)$$

where σ_{cu} , σ_{fu} and σ_{mu} are the ultimate strengths of the composite, the fibres and the matrix respectively. This equation provides an upper limit to the tensile strength of the composite. The properties of the fibres and the matrix can be fully utilised in this instance.

CASE b: $\epsilon_f^* < \epsilon_m^*$

If the fibres break at a much lower elongation than the matrix (Figure 2.9a), the ultimate tensile strength of the composite can be expressed by the rule of mixtures at the moment of fibre failure when the fraction of the fibres exceeds a value, V_{min}

$$\sigma_{cu} = \sigma_{fu} V_f + (\sigma_m)_{\epsilon_f^*} (1 - V_f) \quad (2-48)$$

where $(\sigma_m)_{\epsilon_f^*}$ is the stress in the matrix at the fibre fracture strain ϵ_f^* . In this range, the failure of one fibre leads to fracture of the others at the cross-section where the first one fails. This is called single fracture. The single fracture occurs because $(\sigma_m)_{\epsilon_f^*}$ is very small with respect to fibre failure stress, σ_{fu} . After fibre failure, the matrix can not sustain the load thrown upon it, hence the ultimate strength of the composite must exceed that borne by the matrix

$$\sigma_{cu} = \sigma_{fu} V_f + (\sigma_m)_{\epsilon_f^*} (1 - V_f) \geq \sigma_{mu} (1 - V_f) \quad (2-49)$$

Out of this range, there is more matrix in the composite, As shown in Figure 2.9 a, even if all the fibres fail, the load thrown upon the matrix is still less than the limit which the matrix can bear, $\sigma_{mu} V_m$. In this case, the fibres fracture into many pieces in different cross-section of the composite. This is called multiple fracture of the fibres.

The minimum length of the broken fibres, l_{crit} can be calculated by using shear stress, τ at the fibre-matrix interface introduced by straining of the matrix

$$l_{\text{crit}} = \frac{\sigma_{fu} d}{2 \tau} \quad (2-50)^{[76]}$$

where d is the fibre diameter. The ultimate strength of the composite is determined by the limit of matrix fracture

$$\sigma_{cu} = \sigma_{mu} (1 - V_f) \quad (2-51)$$

When Eqs.(2-49) and (2-51) are plotted in Figure 2.9 b, it is clear that the value, V_{\min} is the minimum fraction of the fibres to result in single fracture of the composite. This value is given by the combination of the two equations:

$$V_{\min} = \frac{\sigma_{mu} - (\sigma_m) \epsilon_f^*}{\sigma_{fu} + \sigma_{mu} - (\sigma_m) \epsilon_f^*} \quad (2-52)$$

On Figure 2.9 b, it can also be seen that the composite ultimate strength σ_{cu} is less than matrix strength σ_{mu} when the fibre volume fraction is below a value V_{crit} . Apparently the composite with this composition can not meet the requirement for reinforcement. For reinforcement, the ultimate strength of the composite must exceed that of the matrix, i.e.,

$$\sigma_{cu} = \sigma_{fu} V_f + (\sigma_m) \epsilon_f^* (1 - V_f) \geq \sigma_{mu} \quad (2-53)$$

so that the minimum volume fraction of the fibres for reinforcement, V_{crit} should be

$$V_{\text{crit}} = \frac{\sigma_{mu} - (\sigma_m) \epsilon_f^*}{\sigma_{fu} - (\sigma_m) \epsilon_f^*} \quad (2-54)$$

An examination of Eqs.(2-52) and (2-54) shows that V_{\min} and V_{crit} possibly arise due to work-hardening and plastic flow of the matrix and the matrix strength being higher than the matrix stress at the fibre fracture strain. For C/C composites, although the

carbon matrix does not exhibit perfect brittle behaviour, the breaking strain of all carbons is very limited with respect to a ductile material. Thus the effect of work-hardening and plastic flow can be ignored. The main factor attributing to V_{\min} and V_{crit} should be the difference of the stresses of the matrix at matrix fracture and at fibre fracture. Table 2.5 gives estimated V_{\min} and V_{crit} for two model composites. These two supposed composites are made using phenolic resin coke combined with two types of high modulus mesophase pitch based carbon fibres Thornel P-120 and P-100 respectively. The strength and modulus of the phenolic resin coke are taken from Fitzer's results^[77], the resin being carbonised at 1200 °C. The ratio of failure stress and modulus is 0.42% so that the failure strain for the resin coke must exceed this value. This ensures that the supposed composites could satisfy the requirement of the discussion, $\epsilon_f^* < \epsilon_m^*$. The estimated results indicate that V_{\min} and V_{crit} are very small for C/C composites. The range of multiple fracture of the fibres can be ignored. Therefore single fracture should be expected when the combination $\epsilon_f^* < \epsilon_m^*$ occurs.

CASE c: $\epsilon_f^* > \epsilon_m^*$

This is another case which may occur for C/C composites. In this case, the matrix fails first. Whether the fibres can sustain the load thrown upon them after breaking of the matrix again depends on the volume fraction of the fibres. This volume fraction is termed transition volume fraction, V_t . Single fracture of the composite will occur when the fibres can not bear the load after matrix failure

$$\sigma_{cu} = (\sigma_f)\epsilon_m^* V_f + \sigma_{mu} (1 - V_f) \geq \sigma_{fu} V_f \quad (2 - 55)$$

therefore

$$V_f \leq \frac{\sigma_{mu}}{\sigma_{fu} + \sigma_{mu} - (\sigma_f)\epsilon_m^*} \quad (2 - 56)$$

or

$$V_t \leq \frac{\sigma_{mu}}{\sigma_{fu} + \sigma_{mu} - (\sigma_f)\epsilon_m^*} \quad (2-56a)$$

$$\sigma_{cu} = (\sigma_f)_{\epsilon_m^*} V_f + \sigma_{mu} (1 - V_f) \quad (2-57)$$

where $(\sigma_f)_{\epsilon_m^*}$ is the stress of the fibres at the failure strain of matrix failure. Eq.(2-56) indicates that failure of the matrix results in failure of the composite at smaller volume fractions than given by eq.(2-57). For large volume fractions the matrix is split into a series of thin discs by a set of parallel cracks running normal to the fibres. This is called multiple fracture of the matrix. The spacing of the cracks varies between X' and $2X'$ and can be given by:

$$X' = \left(\frac{V_m}{V_f} \right) \frac{\sigma_{mu} r}{2 \tau} \quad (2-58)$$

where r is the fibre radius. After cracking is complete the stress-strain behaviour of the composite is totally determined by the fibres until failure of the composite occurs at a stress

$$\sigma_{cu} = \sigma_{fu} V_f \quad (2-59)$$

The failure strain of the composite is within the range

$$\left(\epsilon_{fu} - \frac{\alpha \epsilon_{mu}}{2} \right) < \epsilon_{cu} < \left(\epsilon_{fu} - \frac{\alpha \epsilon_{mu}}{4} \right) \quad (2-60)^{[78]}$$

where

$$\alpha = \frac{E_m V_m}{E_f V_f} \quad (2-61)$$

Figure 2.10 shows the deformation behaviour and the relationship between the ultimate tensile strength and the fibre volume fraction. Over V_b , the stress of the composite at starting failure of the matrix is on the dotted line under the shadow. This is the limit of the composite without losing its re-use value. For convenience, it is named as failure strength of the composites. Although further increase of load will not result in

complete failure of the composite until the ultimate strength is reached, the original solid form has been destroyed. Therefore the strength of the composite for a designer should be regarded as the failure strength. The difference between the ultimate strength and the failure strength is the toughness of the composites consisting of relative brittle fibres and matrix.

Thus from the results derived from the rule of the mixtures, it is evident that the advantage of carbon fibres can be utilised in their composite form. The efficiency of transition of the fibre properties into the composites depends on the relative failure strain of the fibres and matrix, and the volume fraction of the fibres. Although the failure strain is not available for most carbon matrices, it may be expected that CASES a and b occur when high modulus fibres are used. In these cases, the fibre properties can be utilised to the full. A high volume fraction and a high strength of high modulus fibres will give rise to a good quality C/C composite. When carbon fibres with high strain-to failure, such as IM and HT PAN-based fibres are used, CASE c may occur. The efficiency of the transition in such a case is controlled by a fibre volume fraction, V_f . The composites with smaller fibre volume fractions than V_f can fully utilise the strength of the fibres. If the volume fraction of the fibres exceeds V_f , part of the fibre strength will not contribute to the composite failure strength but to the toughness of the composites. This is not an economic solution to increase the toughness of the composites. As will be seen later for C/C composite, the perfect bonding between fibres and matrix is neither attainable nor entirely desirable. The imperfect bonding will result in tough composites. Therefore high modulus carbon fibres are favoured for the fabrication of C/C composites with high strength and modulus.

2.1.3.2 Multidirectional Reinforcement

Unidirectional composites have highly anisotropic properties. The previous discussion considered only the tensile loading in the longitudinal direction. In the case of tensile loading in the transverse direction, the stress borne on the fibres is the same as the stress borne on the matrix and the composite, i.e.,

$$\sigma_c = \sigma_f = \sigma_m \quad (2 - 62)$$

The elongation of the composite in the direction of the load, δ_c is the sum of the fibre elongation, δ_f , and the matrix elongation, δ_m

$$\delta_c = \delta_f + \delta_m \quad (2 - 63)$$

The elongation of the material can be written as the product of the strain and its cumulative thickness, t , so that

$$\delta_c = \epsilon_c t_c, \quad \delta_f = \epsilon_f t_f, \quad \delta_m = \epsilon_m t_m \quad (2 - 64)$$

where footnotes c, f and m represent composite, fibres and matrix respectively. Substituting Eq.(2-64) in Eq.(2-63) gives

$$\epsilon_c t_c = \epsilon_f t_f + \epsilon_m t_m \quad (2 - 65)$$

Dividing both sides of Eq.(2-65) by t_c and recognising that the thickness is proportional to the volume fraction yields

$$\epsilon_c = \epsilon_f \frac{t_f}{t_c} + \epsilon_m \frac{t_m}{t_c} \quad (2 - 66)$$

or
$$\epsilon_c = \epsilon_f V_f + \epsilon_m V_m \quad (2 - 67)$$

If the fibres and the matrix deform elastically, the strain can be written in terms of the corresponding stress and the elastic modulus as follows:

$$\frac{\sigma_c}{E_c} = \frac{\sigma_f}{E_f} V_f + \frac{\sigma_m}{E_m} V_m \quad (2 - 68)$$

From Eq.(2-62), it is known that Eq.(2-68) can be written in following form

$$\frac{1}{E_c} = \frac{V_f}{E_f} + \frac{V_m}{E_m} \quad (2 - 69)$$

Figure 2.11^[79] shows the relationship between E_c and the fibre volume fraction predicted by Eqs.(2-69) and (2-43) respectively. These relationship together with Eq.(2-62) indicate that the fibres are much less effective in raising the composite modulus in the transverse direction than in the longitudinal direction unless the percentage of fibres is very high. The strength of the composite in the transverse direction has not been enhanced by the fibres. This causes the strength in a unidirectional composite to decrease sharply when the load changes away from the fibre direction. In recognition of the drawbacks of the unidirectional composites, multidirectional reinforced structure have been developed to meet the directional property requirements of complex designs.

The common forms of woven structure for multidirectional reinforcement are fabrics, orthogonal derived construction and their combination. The basic unit in these structure is yarn, a yarn being a continuous length of plied fibres held together by fibre twisting or by an added coating, or both. A fabric is generated by interweaving the yarns. This technique provides the possibility to produce a variety of two-directional (2-D) complex pattern and three-directional (3-D) structures with limited thickness^[80]. More than three directional reinforced structures are realised by the modification of 3-D orthogonal construction. In this way, woven preforms with 4, 5, 7 and 11 directions of reinforcement have been obtained^[80,81]. The third form of widely used reinforced structure is the combination of interweaving and orthogonalisation to produce 3-D reinforced materials ^[82,83]. To do this, woven fabric layers are pierced over an array of metal rods which are normal to the layer planes. The metal rods are then replaced by carbon fibre yarns or pre-cured (rigidized) yarn-resin rods as the final step of the process. In addition to these configurations, reinforcement of fibres in cylindrical construction has also been developed^[84]. In the future, more and more geometrical and directional structure are expected to be generated to meet a variety of special requirements.

Mechanical properties achieved by multidirectional reinforcement are shown in Figure 2.12^[7,75]. As the number of reinforcing directions increases, the composites become more isotropic. Also for structures with 3 or more reinforcing directions, the

possibilities of debonding and delamination presented in 1-D and 2-D structures have been reduced. However some disadvantages also arise from increasing the number of reinforcing directions, eg, the fibre volume fraction has to be reduced due to the limitation of the geometrical arrangement. Thus tensile or flexural strengths of a multidirectional composite can not achieve the high value shown by a unidirectional composite in the fibre axial direction. What structure should be produced in practice totally depends on the demands of application design.

2.1.3.3 Additional Factors Influencing Strength And Stiffness

Many assumption were used in the derivation of the rule of mixtures. It is rare that all the assumption can be completely met in a practical situation. Also the strength and stiffness of a composite are influenced by other factors. These factors include misorientation of fibres; fibres of nonuniform strength; residual stresses; interfacial conditions and porosity.

The influence of fibre orientation with respect to the loading axis has been discussed in 2.1.3.2. The contribution of the fibres to the composite properties is a maximum only when they are parallel to the loading direction. Composite strength and stiffness will be reduced when the fibre orientation differs from the loading direction.

The analysis of failure mechanism has indicated that the strength of fibres affects the strength of the composites in a very direct manner. A high strength composite will be obtained when all the fibres are uniform in their strength values. Nonuniform strength of the fibres causes the fracture of the individual fibres in a composite starting at loads much smaller than the composite failure load. This early failure of the fibres throws a heavier load on the unbroken constituents. As a result, the composite fails at a lower stress than the composite consisting of uniform fibres whose strength is the same as the average strength of the nonuniform fibres.

The failure of fibres is usually assumed to follow the Weibull statistic distribution^[85]. This assumption is also suitable for carbon fibres^[4]. According to the Weibull formulation, the cumulative failure probability of a population of fibres, $F(\sigma)$, is relative to the stress applied, σ

$$F(\sigma) = 1 - \text{EXP} \left[-V \left(\frac{\sigma - \sigma_u}{\sigma'} \right)^m \right], \quad \sigma > \sigma_u \quad (2-70)$$

where V is the volume of the fibre, σ' and m are constant, and σ_u is the value of the stress below which $F(\sigma)=0$.

From Eq.(2-70), the mean strength, σ_{mean} of a fibre along the length, L can be derived

$$\sigma_{\text{mean}} = \frac{\sigma'}{L^{1/m}} \Gamma \left(1 + \frac{1}{m} \right) \quad (2-71)$$

This equation indicates that strength of a fibre reduces with increasing fibre length. This trend is in accord with the measurements of strength of carbon fibres in different gauge length made by Moreton^[86].

The diversity of fibre strength is affected by not only the length of fibres but also the variation in fibre diameter. As indicated in 2.1.2.4, thinner fibres give rise to a higher strength. In commercial carbon fibres, the diversity of fibre diameter can be controlled in a relative satisfactory level for PAN and rayon based carbon fibres. Carbon fibres produced from pitch usually have a wide distribution in fibre diameter^[87,88].

During the fabrication of composites, residual stresses are inevitably introduced into the constituents and at various interfaces. They are primarily caused by two effects: (1) the difference in the coefficients of thermal expansion for the constituents and (2) the difference in fabrication temperature and the temperature at which they are used. C/C composites are produced from the carbonisation of organic matrix precursors. High shrinkage occurring in the process generates more residual stresses than in other composite materials. Moreover thermal expansion of a unidirectional composite varies with the fibre orientation so that residual stresses are easily formed in an inter-woven structure such as 2-D laminates. Since the residual stresses affect the in situ properties

of the matrix and the actual state of stress resulting from the service loads, strengths of the composites are affected by the residual stresses. Detailed discussion on this subject have been presented by Chamis^[89] and Tsai et al.^[90].

The mechanical properties of composites are markedly dependent upon the interfacial bonding between the fibres and the matrix. The interface is responsible for transmitting the load from the matrix to the fibres, which contribute the greater portion of composite strengths. Generally, composites with weak interfaces have relatively low strength and stiffness but high toughness whereas materials with strong interfaces have high strength and stiffness but are very brittle. Thus maximum utilisation of fibre properties requires optimum bonding across the interface.

Another important factor influencing the mechanical properties of the composites is porosity. The behaviour of a crack under uniform stress in a brittle material has been discussed in 2.1.2.2. The propagation of crack in a composite is more complicated than in an isotropic brittle material. Cracking strain in an isotropic material is governed by the presence of Griffith cracks. This case can be only suitable for the composite whose surface to surface separation of the fibres, S is less than the Griffith crack length, $2C$. If the plane of the crack is normal to the fibre orientation and $S < 2C$, the strain for crack propagation is also dependent on the elastic modulus of fibres and matrix, relative volume fraction and interfacial conditions etc.. Therefore the criteria for cracking in a composite relies not only on crack shape and size but also on the relative position and orientation of crack to fibres and loading direction, and the bonding between the constituents.

The influence of crack size on the fracture of the composite is similar to the case of isotropic material when a crack is large. For a small crack, the tensile stress at the crack tip calculated from the elastic analysis may become considerably greater than the composite tensile strength before fracture occurs^[91,92]. This infringement is caused by the formation of a stable damage zone at the end of the crack. Such a damage zone may contain cracks parallel to the fibres in individual layers, delaminated layers, and some times broken fibres. By reducing the stress concentration, these damage zones effectively blunt the crack, and give the composite toughness.

If a crack is near the interface between fibres and matrix, or between fibre bundles or layers, the direction of crack propagation is determined by the ratio of fracture

energy at the interface and at the matrix^[93]. A small value of the ratio, i.e., weak bonding at the interface can result in a change of propagation direction from normal to parallel to the interface, whilst strong bonding at the interface leads to propagation of the crack following the original direction normal to the interface.

The capacity of crack propagation is also affected by the relative orientation of the crack tip and fibres. Figure 2.13 shows a given length of crack orientated in three different directions to the fibre axis. The crack propagates in opening mode, i.e., the applied stress normal to the propagating direction. The strain-energy release rate in three cases follows the sequence of $c > b > a$. This implies that the resistance of cracking is the least in a plane parallel to the fibres (Figure 2.13 a), a small value parallel to the fibres (Figure 2.13 b) and the largest normal to the fibres (Figure 2.13 c).

The influence of porosity on tensile and flexural strength for carbon felt/carbon matrix composites was quantitatively described by Pierson et al.^[94]. The form of the equation is similar to that used for polycrystalline materials^[95] and can be expressed as

$$\sigma = \sigma_0 (1 - b P)^{1/2} \quad (2-72)$$

where σ and σ_0 are the strengths of porous and non-porous composites respectively, b is an empirical constant and P is the volume porosity. This relationship indicates that the decrease of composite strengths from their non-porous form is due to the presence of porosity for carbon felt/carbon matrix composites.

The theoretical consideration described in this section has shown that the use of carbon fibres in C/C composites is a practical method of achieving high strength and stiffness. The efficiency of achievement depends upon the choice of fibre types, the fibre volume fraction, the matrix properties, the residual stresses, the interface between fibres and matrix, and the porosity. Once the fibres have been chosen, the other factors have to be improved by processing. Therefore to achieve the best possible mechanical properties, advanced fabrication techniques are also required.

2.2 FABRICATION OF C/C COMPOSITES

The advent of the technology of C/C composites goes back to the early 1960's, as carbon fibres began to appear commercially, and steps were taken to use carbon fibres to produce or replace other carbon products. Under the sponsorship of the U.S. Air Force, by 1960 the world's first carbon fibre reinforced carbon composites were demonstrated by two American industrial laboratories^[96].

In the middle 1960's, several commercial processes were invented to produce materials which were not cited as strong materials but as useful in electrical and nuclear applications such as brushes, furnace electrodes^[97] and containment of nuclear fission products^[98].

By the late 1960's, C/C composites were beginning to emerge as a new class of engineering materials^[99,100] developed to produce strong, ablative and light weight materials for aerospace application^[101,102]. Starting from 1970, C/C composites have been under extensive development, first in U.S.A., followed by Europe, Japan, and other Asian countries^[103-105].

This part of the review will consider some past and present methods of fabrication. It should be remembered that these methods are being continuously improved and that new techniques are under development. Moreover many techniques in this field are proprietary so that, in this respect, this review may not be comprehensive.

2.2.1 General Process

The fabrication of C/C composites is similar to the classical methods as used in synthetic graphite. The analogy between the two processes is illustrated in Figure 2.14. During processing of C/C composites, carbon fibres act as the filler or primary carbon which combines with a temporary binder to form the precursor or "green" composite. The subsequent carbonisation results in an all-carbon material with two different phases. The temporary binder in this treatment forms a secondary carbon termed binder or matrix carbon. Since the temporary binder is normally thermoplastic or thermosetting

polymeric material, mass loss and shrinkage occurs during the carbonisation to form the carbonised preform with a highly porous structure. These high porosity materials seldom meet the quality requirements for most applications so that a subsequent treatment, namely densification, is required to fill the pores and/or cracks in the material. This step is achieved by impregnation with carbon precursor compounds, liquid or gaseous, and subsequent re-carbonisation. The procedure may be repeated several times. Thus a third type of carbon, the impregnation carbon is present in a multi-phase all-carbon composite.

In some cases, processing does not stop after the densification. Heat treatment at graphitisation temperature may be also included to provide further structural stability and better thermal shock resistance.

The above description gives a general outline of the procedures used to produce C/C composites. Some special processes, such as production of carbon felt / pyrolytic carbon composites, may not necessarily involve a temporary binder. The carbon fibre felt directly goes through densification^[106,107]. Materials produced in this way contain only two carbon phases. They are often used where a high degree of thermal shock resistance is required^[108].

2.2.2 Green Fabrication

Green fabrication refers to processing before the first carbonisation. In this process, fibres and carbon matrix precursor are appropriately mixed and constructed to give a desired shape. For unidirectional and bidirectional (2-D) reinforcement, there is no obvious difference in processing at this stage between CFRC and CFRP. Indeed much of the technology used in C/C production has been adopted from the plastic industry. The most widely used method in this processing is compressive moulding.

The simplest compressive moulding is to take individual fibre tows or cloth layers, soak them in carbon matrix precursor, and lay them up in a mould in order to form a desired geometrical shape. Pressure is applied to the top plunger of the mould, together with heat to semi-cure the resin or to maintain a molten state in the case of pitch binder. The subsequent treatment fully cures the resin or converts the pitch to semi-coke. This operation may be carried out either before or after cooling down and

opening the mould.

The disadvantages of such a process are the difficulties associated with controlling the content of the matrix precursor, alignment of the fibres, and removal of the air entrapped in the moulded preform. To overcome these disadvantages, pre-impregnation of fibre tows with thermosetting resin has been used before moulding.

The pre-impregnation technique involves coating tows with resin, aligning them on a suitable non-stick siliconised paper or plastic sheet and then rolling between the two sheets to flatten the coated tows. This process can produce both well-aligned fibre tows for making woven fabrics and unidirectional fibre sheets by controlling the distance between the coated fibre tows in the sheet. Preforms produced by moulding these rolled tows or cloths have highly reproducible resin content, less entrapped air in the moulded preforms and well-aligned fibre orientation.

Other techniques often used in the plastic industry include various kinds of injection moulding, pultrusion etc.^[109]. Injection moulding has been developed to produce precisely shaped materials. This method may be operated in a highly automated machine but unavoidably results in failure and poor orientation of the fibres. The pultrusion method consists of drawing fibres through a resin bath, followed by passage through a bush of the required shape to remove the excess resin and any entrapped air. The drawn material is then passed continuously through an oven to harden the resin. This method is suitable for producing large beams, tubes and channel sections.

For production of multi-directional C/C composites, wide distribution of fibre orientation and reinforcing configurations restrict the use of traditional moulding technology. The methods to fix the reinforcing configurations of the fibres are related to the techniques used to construct the configurations. The fixing phase, i.e., carbon matrix precursor or carbon matrix (eg. pyrolytic carbon) may be induced into the fibre skeleton in different processing stages. For example, a process developed by McCoy^[110] to produce conical C/C composites consists of pre-impregnation of the fibres in a resin bath, winding the fibres in a conical mandrel and curing the resin completely to form a rigid green composite. In this process, resin is mixed with fibres before the formation of the reinforcing configuration. In a similar process^[111], a binder was introduced between the fibres after winding the fibres into a desired shape. Binders

may also be introduced between the fibres during winding. Many techniques can be utilised to introduce the fixing phase into the reinforcing configurations. Coating a carbonisable binder by liquid impregnation is a relatively easy method. Other methods involve vapour deposition and building solid blocks. Process developed by Rohl, et al.^[101] and DeMunda^[112] deposit pyrolytic materials directly onto the fibres to form bonded constructions. Jacob, et al.^[113] designed a solid carbon frame to support a 3-D orthogonal reinforced fibre skeleton. The frame had many holes whose configuration is the same as the fibre skeleton. The reinforced green composite was formed by inserting fibre tows into these holes.

From the above discussion, it may be observed that different aspects are emphasised in the stage of green fabrication between multi-directional composites and uni- or bi-directional composites. Processing of uni- and bi-directional composites puts emphasis on producing dense material because their geometrical shape and reinforcing configuration are readily achieved. In the case of multi-directional reinforcement, the emphasis is placed on the preservation of the complicated fibre reinforcing configuration and geometrical shape. Dense material are expected to be achieved by a subsequent densification process.

2.2.3 Densification Processing

The aim of densification is to insert carbon into the void spaces in the carbonised preforms. In this process, solid carbon is required not only to fill the voids but also to form good bonding with the original carbon so as to provide a better translation of applied stresses. It is difficult to use solid carbon directly in this purpose. To do this, pyrolysis of organic materials is again utilised. The available precursors for pyrolysis include hydrocarbons, thermosetting and thermoplastic resins and pitches, etc.. In some cases, certain inorganic precursors have also been used^[114,115], but these materials, of course, are not intended to form solid carbon, but an anti-oxidation phase. Nevertheless they are often considered in the study of the densification and fabrication of C/C composites^[116]. In the production of all-carbon composites, densification is realised by two techniques, chemical vapour deposition for impregnating hydrocarbon vapours, and liquid infiltration for impregnating liquid matrix precursors.

2.2.3.1 Chemical Vapour Deposition

Chemical vapour deposition is a process which combines gaseous and mass transfer. In this process, both gaseous and liquid hydrocarbons can be used as the precursors and it involves vaporisation of the hydrocarbon if a liquid, pyrolysis of the hydrocarbon gas, and deposition of carbon on a substrate.

Chemical vapour deposition was the first densification technique used for producing C/C composites^[98,102]. The technique was originally developed for producing pyrolytic graphite structures and coatings and was later further developed for the fabrication of C/C composites. The process can be performed using three different methods. These include isothermal^[117-121], thermal gradient^[118,119,121,122-124], and differential pressure^[100,119] techniques. They are shown schematically in Figure 2.15^[125].

The isothermal CVD process is the most widely used of the three densification processes for improving the physical properties and reducing the gas permeability of C/C composites. As shown in Figure 2.15a, a constant temperature zone surrounding the C/C substrate is established by the radiative heating from the induction furnace susceptor. Hydrocarbon and carrier gases are introduced and allowed to pass over the surfaces of the part to be infiltrated. The gaseous hydrocarbon diffuses into the voids and deposits pyrolytic carbon. This infiltration continues as a function of time until the voids are narrowed to a point where surface overcoating occurs. In order to make the further infiltration possible, the processing is usually accomplished in multiple cycles, with intermediate grinding to clean away the surface coating which blocks the porosity. Optimum time per cycle is usually 60 to 120 hours^[121].

The isothermal CVD process is operated at temperature below 1400 °C, low pressure or near atmospheric, and low concentration of hydrocarbon with high dilution of an inert gas. The conditions chosen in this way tend to produce a uniform deposit through the substrate. However the problems is that long operational time is required to achieve a high density composite. To overcome this disadvantage, thermal gradient and differential pressure methods were used to improve the mass transfer through the carbonised preforms.

Figure 2.15b is a schematic drawing of the thermal gradient process. The arrangement inside the furnace, in practice, may vary with the geometrical shape of the

substrates. In this example of the process, a substrate is placed between the inductor coil and the susceptor so that a thermal gradient is generated across the thickness of the substrate. The temperature on the surface in contact with the susceptor is higher than that on the outside surface near to the water-cooled induction coil. The gradient obtained depends on the thermal conductivity, the structure of the substrate and the rate of the gas flowing over the substrate. In general, high porosity, poor coupling and non-graphitic structure can create a large thermal gradient.

During the processing, the temperature on the relatively cool surface is kept below the threshold pyrolysis temperature of the carbon-bearing gas or at a temperature where the deposition rate at the surface is below the deposition rate of carbon within the voids. Thus the deposition of a surface coating is minimised. This minimisation reduces the rate of void closing so that the process uses a shorter time cycle to reach a desired density as compared with the isothermal technique.

The differential pressure technique can be considered as a variation of the isothermal technique. As shown in Figure 2.15c, a mandrel is attached to a gas feed tube so that the inner portion of the substrate is isolated from the furnace chamber by sealing part of the substrate to the feed tube. Gases are fed into the inner substrate at a positive pressure with respect to the furnace chamber. This creates a pressure gradient across the thickness of the substrate, forcing the gases to flow through the voids.

In addition to the three kinds of techniques, there were other CVD techniques, such as vapour-consolidation^[126] and combined thermal gradient and differential pressure^[121] etc., which have been used for the densification of C/C composites. From recent reports, they have not gained wide acceptance. The techniques presently used in industry are based on isothermal and thermal gradient methods.

2.2.3.2 Liquid Impregnation

Liquid impregnation is a two-stage process with repeated infiltration of the carbonised preform with an organic precursor and carbonisation to convert the precursor into carbon. The efficiency of the processing is influenced by the properties of the precursor and processing techniques. The available precursors used for this purpose are almost limitless. However when all of the process and property

requirements are considered, the selection is reduced to relatively few materials. The basic requirements of the precursors for liquid impregnation are low viscosity and high carbon yield. A further consideration is the ability to adhere to the original carbon in the preforms and the microstructure of the coke formed. Low viscosity provides sufficient fluidity during infiltration while high carbon yield tends to reduce the processing cycles. To achieve this, thermosetting resins and pitches are commonly used.

Thermosetting resins used in composite fabrication are composed of materials which polymerise at low temperature to form a highly cross-linked, thermosetting, non-melting, amorphous solid. Research on their application in C/C composites started in the early 1970's. In the early stage, the resins which were used in C/C composites were tested^[77,127-132]. They include epoxy, phenolic, furfuryl alcohol, divinyl benzene, furane, polyimide, polyacrylonitrile and dimethyl formamide resins. The advantage of using these materials is their low viscosity at low temperature, considerable strength of their coke and relatively high carbon yields (50-70%). However high shrinkage occurs with these materials, especially epoxy resin, during carbonisation. The high shrinkage tends to cause severe damage in the C/C composites. Hence later work in this field concentrated on the modification of relatively low shrinkage resins such as phenolic and furfuryl alcohol resins. In 1986, a new type of thermosetting resin, namely COPNA, was synthesised using 1,4-benzene dimethanol and pyrene and phenathrene at Gunma University, Japan^[132]. The resin consists of condensed aromatic nuclei cross-linked with methylene bridges. Its carbon fibre bonded preforms could undergo carbonisation without any "trouble". The weight loss of the resin is in the middle grade of the other thermosetting resins used for C/C composites. Since the resin is produced from cheap precursors, it may gain a wider application and further modification in the future.

The use of pitches as matrix precursors in C/C composites began at almost the same time as the thermosetting resins^[129]. A variety of coal tar, petroleum and synthesised pitches could serve for this purpose. Pitch materials are thermoplastic. The plastic state may cover a wide temperature range from the melting point to about 500 °C where solidification occurs. In this range, pitches undergo various changes including volatilisation of low molecular weight compounds, polymerisation, cleavage and rearrangement of the molecular structure, formation of mesophase and coalescence of the mesophase. Since viscosity and the coke structure are dependent on every step in these changes, control of densification with pitches is more complicated than with

thermosetting resins. The advantage of using pitches as matrix precursors is that a high carbon yield, up to 90%, can be achieved by pressure carbonisation^[134].

In addition to solitary thermosetting resins and pitches, their mixtures have also been used. Inagaki et al.^[135] mixed pitch with either polyethylene terephthalate (PET) or phenolic resin as carbon matrix precursors and obtained 68-86% carbon yield by carbonisation of the precursors at 30 MPa and 650 °C.

The choice of technique for liquid impregnation is dependent on the carbon yield of the impregnant on carbonisation and the microstructure of the carbon formed. Both properties change with pressure. This results in two impregnation techniques whose difference lies in the pressure range applied during densification. At atmospheric pressure, the carbon yields of the pitch materials (about 50 wt%) are a little lower than those of the resins (50-70 wt%). Increase of pressure during processing can largely raise the carbon yields of the pitches^[134,136] but slightly decreases the carbon yields of the thermosetting resins^[137]. From this point of view, high pressure processing should be applied for pitch impregnation while low pressure processing can be used for both resin and pitch impregnation.

Low pressure impregnation is the most widely used approach to achieve the required densification. In this process, the carbonised preforms are usually evacuated first to reduce impregnating resistance. Then the evacuated preforms are plunged into molten resin or pitch. In some cases, pressure is applied as part of the impregnation cycle to ensure penetration of all available porosity in the composite structure. Before carbonisation, resin impregnated preforms have to be cured while pitch impregnated preforms will be subjected directly to carbonisation in an inert atmosphere. Carbonisation is normally carried out at a programmed heating rate to temperatures in the range of 650 to 1100 °C. If a high thermal stability of the products is required, the carbonised structure will be further subjected to heat treatment at graphitisation temperature. This procedure is usually repeated several times until the porosity in the composites is reduced to an acceptable level.

All aspects of a densification cycle using high pressure impregnation are the same as for a low pressure cycle except for the use of isostatic pressure during the melting and coking stages of the carbonisation^[138-141]. A schematic illustration of high pressure impregnation is shown in Figure 2.16. Before impregnation, the carbonised

preforms are held in thin-metal canisters. The process starts with conventional impregnation in which molten pitch in a heated reservoir is transferred to the metal canisters containing the preforms under vacuum, via pipes connecting both tanks. This is accomplished by backfilling the reservoir tank with an inert gas. Once the preforms are fully subjected to the hot liquid pitch, the canister is backfilled with the inert gas to equalise the pressure in both tanks and stop the transfer of pitch. The canisters are then sealed off under vacuum with metal lids. After that step, the canisters are placed in a gas-pressure vessel where carbonisation occurs under a high pressure. During the carbonisation, isostatic pressure in the gas phase is applied to the thin metal of the sealed container and hence transmitted to the molten pitch via the metal wall. This step is a combined process involving both pressure impregnation and coking. After the carbonisation, the carbonised composites are taken out of the container and cleaned up being ready for either graphitisation or recarbonisation. This operation is carried out several times until a desired density of the composites is achieved.

A comparison of the pore-filling and pore-blocking mechanisms using pyrolytic carbon on the one hand and resin and pitch on the other enables comment to be made on the above mentioned densification techniques. These mechanisms have been proposed by Ford^[142] and are shown schematically in Figure 2.17. In resin and pitch impregnation, even though the pores are initially filled, the subsequent heat treatment can still give rise to residual porosity due to the devolatilisation and shrinkage. Fortunately these residual pores are still open so that whatever pores are initially filled before the heat treatment, multiple densification should always be applied in order to reduce the residual porosity further. Infiltration with pyrolytic carbon does not have the drawbacks of volatiles and shrinkage but still can not avoid the formation of residual porosity by blocking bottle-neck-like pores. Porosity blocked in this way can not be further reduced.

In conclusion, the different densification techniques have their own specific advantages. Resin impregnation is an easy technique to apply, but high shrinkage during carbonisation results in a lot of problems as regard improving the strength of the composites. Pitch is a cheap carbon matrix precursor. A high carbon yield can be achieved by employing high pressure impregnation technique. The difficulties in this field are poor reproducibility and highly operational cost. CVD techniques have demonstrated the ability to obtain significant improvement in the physical properties of the composites but it is not easy to fill the porosity completely. Therefore the

application of these techniques has to consider comprehensively the influence of structure and properties of the carbonised preforms, and processing conditions on the quality of the composites.

2.3 OUTLINE OF RESEARCH

The whole procedure of the approaches to achieve high strength from carbon has been described in the literature review. From this, it can be seen that the mechanical properties of C/C composites are dependent on the types of fibres used, the efficiency of translation of fibre properties to the composites and the porosity present. The overall aim of the present research project was to gain an appreciation of the relationship between raw materials and processing and the structure and quality of composites so that materials with superior strength can be produced, ideally at the lowest cost.

The project developed into two concurrent studies. The objective of the first was to seek an understanding of the structure, especially the porous structure, of 2-D C/C composites and to probe the mechanism by which this was altered during the densification process. The second aimed to identify raw material and processing factors necessary to achieve high strength composites.

In the first, materials obtained from various stages of a commercial process, were used at the start of this project, and preforms subjected to multiple CVD and furfuryl alcohol impregnation were examined. Polarised light microscopy was used to identify the various forms of carbon present and image analysis to quantify pore structural parameters.

Knowledge of the availability of raw materials and the capability of the processing equipment meant that, inevitably, the initial stages of the second study involved the examination of materials commercially produced to meet a specification. From the preliminary results obtained, it was possible to recommend combinations of raw materials and processing conditions likely to produce high strength composites. These were adopted and the composites were produced for examination. The structure of selected composites was studied in an attempt to explain the variation in their mechanical properties.

3. EXPERIMENTAL METHODS

3.1 MATERIALS STUDIED

3.1.1 Raw Materials And Processing Conditions

The materials used in this study were 2-D C/C composites produced by New Metals And Chemicals, U.K., and Sintec Keramik GmbH, Germany. The general fabrication process used is schematically illustrated in Figure 3.1. The raw materials for the preregs included two types of phenolic resin and three types of fibre cloth produced from three types of carbon fibres, i.e., PAN, pitch and rayon based carbon fibres. For the convenience of future discussion, the two types of phenolic resin are termed PHA and PHB. The three types of fibre cloth is designated PAN-5H, Pitch-5H and Rayon-8H according to their contained fibre type and weaving structure, the symbols behind the hyphen standing for the weaving pattern, i.e., 5H for five harness satin weave and 8H for eight harness satin weave. The properties of the carbon fibres and the fibre cloths are given in Tables 3.1 and 3.2 respectively. As shown in Table 3.1, the rayon fibres had been heat-treated to graphitisation temperatures ($>2500^{\circ}\text{C}$), while the other two types of fibres were only heat-treated to carbonisation temperatures (about 1400°C). According to the classification shown on Figure 2.8, the PAN fibres have high strength and median modulus. The values of the strength and the modulus for both the pitch and the rayon fibres lie within the low range. The fibres chosen in this way may not fully satisfy the basic principles for fabrication of very high quality C/C composites. However choice of fibres was made by the composite manufacturers after comprehensive consideration of the costs and the requirements for the quality of the products.

During fabrication, the prepregged fibre cloths were laid-up with alternate layers rotated through 90° and moulded together to give disk or bar shaped moulded-preforms. The composites studied were produced from three moulding conditions which involved two techniques, i.e., constant thickness and constant pressure moulding. Figure 3.2 schematically illustrates the difference between the two techniques. In the case of constant thickness moulding, the pressure is increased with

the core plate and the cavity plate touching, the thickness of the composite then being equal to the difference in depth of the core and the cavity. The depth difference is varied depending on the number of layers being used. In this study, laminated materials with 18 layers and 4.7 mm thickness were produced using this technique. In constant pressure moulding, the depths of the core and cavity are similar and the thickness of the moulded preforms depends on both layer content and moulding pressure. The moulding pressure selected for this study was 4 to 140 Pa for low pressure moulding and 2.1 to 3.6 KPa for high pressure moulding.

After moulding, the materials are subjected to carbonisation and densification to form C/C composites. The carbonisation was carried out under two conditions depending on the group of the materials. Condition A applied a relatively high heating rate, 60 °C/h, to heat the materials to a maximum temperature of 870 °C. A slower heating rate was employed in condition B, running 48 hours to a maximum temperature of 1050 °C.

In densification of the carbonised preforms, many processing routes based on CVD and resin impregnation methods were investigated. In chemical vapour deposition, xylene was used as precursor, the conditions studied being:

- A -- Furnace pressure 7252 mPa, Temperature 870 °C,
- B -- Furnace pressure 580 mPa, Temperature 870 °C,
- C -- Furnace pressure 29-73 mPa, Temperature 825 °C,
- D -- Furnace pressure 29-73 mPa, Temperature 870 °C,
- E -- Furnace pressure 29-73 mPa, Temperature 1050 °C.

Resin impregnation was carried out under vacuum using furfuryl alcohol as precursor, 2% oxalic acid being added as polymerisation catalyst. The impregnated materials were then carbonised at 180 °C/h to 870 °C.

3.1.2 Materials Examined

Materials for structural and processing studies were obtained from various stages of the fabrication of composites varying in precursors and densification routes. The processing conditions are given in Table 3.3. In this phase of the work, three groups of

precursors were investigated. They are PAN-5H cloths prepregged with phenolic resin PHA, Pitch-5H cloths prepregged with phenolic resin PHB and Rayon-8H cloth prepregged with phenolic resin PHB. The identification of the groups corresponds to the names of the fibres with a suffix "-SR". The materials in groups PAN-SR and Pitch-SR were processed using same conditions. The materials in group PAN-SR contained 12 cloth layers and the materials in group Pitch-SR contained 8 layers. Different conditions were applied to produce materials in group Rayon-SR. These conditions were used in the manufacturer's original production process to obtain composites for a particular application. The materials in this group were made using 12 cloth layers.

Table 3.4 shows materials for the studies of the effects of processing conditions on the quality of the composites. These materials were produced from the same prepreps as used in group PAN-SR and contained 18 layers. They are termed group PAN-RC. Two cycles of CVD were used in densification of the materials in this group. The conditions used in processing varied in moulding techniques, carbonisation conditions and CVD pressure and temperature.

3.2 MEASUREMENTS OF THE MECHANICAL PROPERTIES

Many methods have been devised quantitatively to characterise the mechanical properties of composites. In most cases, it is not necessary to use all of these tests to get adequate information on a material. The tests to be utilised totally depend on the requirements of proposed use. A material for a complex application may require more tests to supply sufficient information for designers, whereas for some specific scientific research, a few limited tests will be sufficient to satisfy the research objectives. There are also different views in the selection of mechanical measurements for engineering application and scientific research. The mechanical tests for engineering application lay emphasis on the satisfaction of the application environment, while the mechanical tests for scientific research are aimed at understanding the inherent properties of a material. For example, a flexural bending test can lead to failure of a composite in either tensile or shear mode. No matter what failure mode occurs, the engineering application only considers whether the failure load exceeds the limitation on bending resistance. The scientific research, however, has to consider the reason for the material failing so as to decide what properties should be improved.

In some ways, the structure of 2-D C/C composites is analogous to the structure of graphite. This analogy is reflected by the mechanical properties of 2-D C/C composites and the graphite shown in Tables 3.5^[143] and 2.3 respectively. Both structures are strong within an individual layer (aromatic layer in the graphite and fibre cloth layer in the composites) and have poor strengths in the direction normal to the layers. Facing such a structure at least two strength parameters are required to assess the quality of the composites, one of them to evaluate the reinforcement of the fibres, the other to judge the bonding between the layers.

The direct way to assess the quality of the fibre reinforcement is to determine a tensile failure using a tensile strength test in the fibre orientated direction. The strength measured in such a way is known as longitudinal tensile strength. This test is not easy to perform on 2-D C/C composites because of their extremely high ratio of tensile strength in the longitudinal direction to interlaminar shear strength. Two problems can arise during the measurement. Firstly, load is normally transferred from the test machine to the specimen by shear and if large loads are required to produce failure at

the test section then large shear stresses will concentrate at the specimen ends. Secondly, the residual shear stress introduced by twisting during fixing of the specimen may increase to the critical value for shear fracture before the limit of tensile failure is achieved. In addition to these problems, the tensile strength test is relative expensive. It usually requires large pieces of specimens with special machined ends such as dog-bone geometries, pin-type connection and serrated-jaw-type joints. This undoubtedly increases the difficulty for large scale research on expensive materials like C/C composites. In this work, only a few specimens have been subjected to tensile strength test for qualitative fracture examination.

A cheaper method to create failure in the tension mode is by the flexural bending test. An ideal flexural bending test results in half the thickness of the specimen being in tension and the other half being in compression. Calculation of a tensile failure stress is complicated and requires certain assumptions. Nevertheless, the test is frequently carried out because not only is it cheap but also composites in application are often subjected to bend loads. In this project, the test was chosen to assess the quality of the reinforcement in the fibre direction.

The bonding between the layers can be assessed by either the interlaminar shear strength test or a transverse (normal to cloth layers) tensile strength measurement. For bar-shaped, thin laminates, it is relatively difficult to measure a transverse tensile strength. The easiest way to assess inter-layer bonding is to use a three-point-bend test to measure the interlaminar shear strength. For disc-shaped test pieces, a tensile strength can be obtained by using diametral compressive test. This test was initially developed to measure tensile strength in the direction normal to applied load but perpendicular to the disc planes for concrete^[144-148], ceramics^[149] and carbon materials^[150-152]. For 2-D C/C composites, high ratio of tensile strength in the longitudinal direction to interlaminar strength would be expected to result in delamination.

In this work, the strength measurements on bar-shaped composites were based on the three-point-bend test measuring flexural strength and modulus and interlaminar shear strength. Limited direct tensile strength tests were tried. Also disc-shaped specimens were used for diametral and transverse compression tests. An Instron universal test machine was utilised to measure flexural strength and modulus, interlaminar shear strength and diametral compressive load. Transverse compression

testing was carried out on a Dartec machine. Attempts were made to measure longitudinal tensile strength using both ESH and Instron machines. The mode of failure in the various tests was studied using a scanning electron microscope (SEM). The detail procedure for these tests will be described below.

3.2.1 Flexural Strength And Modulus Measurement

Flexural strength and modulus measurements were made using composite bars 100mm long, 20mm wide and 3 to 5mm thick. The specimens were strained in three-point bending over a span of 80mm between a 20mm diameter loading roller and 10 mm diameter supporting rollers. The machine cross-head speed used was 1 mm/min. A deflection gauge was placed beneath the specimen, opposite to the loading roller to measure the deflection for the modulus calculation. The flexural strength, S_{fl} , and modulus, E_{fl} , are given by the following formulae:

$$S_{fl} = 14.715 \frac{PL}{wt^2}, \quad (\text{MPa}) \quad (3-1)$$

$$E_{fl} = \frac{S^3 m}{4 w t^3}, \quad (\text{MPa}) \quad (3-2)$$

where P is the load at failure, kg; L , w and t are the span (mm), specimen width (mm) and thickness (mm); and m is the slope on load-deflection curve in the elastic deformation range, N/m.

The results quoted are the mean values calculated from eight specimens for each material.

3.2.2 Interlaminar Shear Strength Measurement

The interlaminar shear strength (ILSS) was measured using bars 30mm long, 10mm wide and 3-5mm thick. The specimens were strained in a three-point bending rig having a supporting span of five times of the specimen thickness. The supporting rollers were 6 mm and loading roller was 10 mm. The rate of loading was 0.5 mm/min. The interlaminar shear strength, S_{ILSS} , can be obtained from:

$$S_{ILSS} = 7.3575 \frac{P}{wt} , \quad (\text{MPa}) \quad (3-3)$$

where P is the failure load, kg, and w and t are the width and thickness of the test piece, mm. Mostly, twelve specimens for each material were tested to give a mean ILSS.

3.2.3 Diametral Compression Test

This test was carried out using disc shaped specimens 31 mm diameter and with various thicknesses. The specimens were loaded across the diameter parallel to fibre orientation at a speed of 0.5 mm/min. A jig was used to hold the specimens vertical and to prevent buckling. Since failure occurred by delamination usually in several planes, it is impossible to calculate a valid tensile strength. Hence the ultimate failure load is quoted as a measurement of strength.

3.2.4 Transverse Compression Strength Measurement

In this test, an increasing uniform stress was applied on the planar surface of 31mm diameter discs until fracture occurred. The machine cross-head speed was 0.1 mm/min. The transverse compressive strength, S_{tc} is obtained by dividing the failure load by the disc surface area.

$$S_{tc} = 12.5 \frac{P}{D^2} , \quad (\text{MPa}) \quad (3-4)$$

where P is the load at failure, kg, and D is the specimen diameter, mm.

3.2.5 Longitudinal Tensile Strength Measurement

A few materials were measured using specimens either with or without end tabs.

Specimens with end tabs had a size of 200mm long, 37mm wide and 3-4mm thick. Aluminium end tabs 50 mm by 37 mm were attached to each side of the ends,

using aradite adhesive, leaving a free length of 100 mm, These specimens were tested on the Dartec machine with a load speed 1 mm/min.

Specimens without end tabs were 100 mm long, 15 mm wide and 2.5-3.4 mm thick. These specimens were directly fixed in a jig on the Instron machine, leaving a free length of 40 mm. The machine cross-head speed used in this tests was 0.5 mm/min.

For both methods, fracture occurred in either the gauge length or at the joining position of the end tabs or the jig. The main aim of these tests was to create tensile fracture surfaces for scanning electron microscopy study. However for specimens broken within the guage length, longitudinal tensile strength, S_t values were calculated from the failure load, P (kg) divided by the area of the cross-section of the specimens.

$$S_t = 9.81 \frac{P}{w t} \quad , \quad (\text{MPa}) \quad (3-5)$$

where w (mm) and t (mm) are width and thickness of the specimens respectively.

3.3 DETERMINATION OF DENSITY, VOLUME POROSITY AND FIBRE VOLUME FRACTION

3.3.1 Bulk Density And Open Porosity

Bulk density of a composite is defined as the weight of the composite per unit volume which includes solid and all pores. Open porosity refers to the volume fraction of the pores which can be penetrated with a measuring medium. The measurements of bulk density and open porosity were based on ASTM C-20 using water as measuring medium. This involves obtaining the weight of a dried specimen in air, W_a (g), when suspended in water after filling the pores with water by boiling, W_{su} (g), and in air with the pores water filled, W_{sa} (g). Bulk density and open porosity were then obtained by using following equations.

$$D_b = \frac{W_a}{W_{sa} - W_{su}} \times 1000, \quad (\text{kg/m}^3) \quad (3-6)$$

$$P_o = \frac{W_{sa} - W_a}{W_{sa} - W_{su}} \times 100, \quad (\%) \quad (3-7)$$

3.3.2 True Relative Density And Total And Closed Porosity

True density of a material is the density of its solid part, i.e., the weight per unit volume which only includes solid material. This value is usually assumed to be equal to the X-ray density of the material. For C/C composites, interest is normally focused on macropores (diameter greater than 50 nm) so that the density of a powdered composite, measured by liquid displacement in a gravity bottle, can be reasonably used to represent the solid density of the composite. The density measured in this way is termed true relative density. The measurement of true relative density in this project is based on the method described in BSI 1902.

For the test, the sample was prepared by crushing to pass a 240 mesh (63 microns) sieve, and drying for 1 hour at 105 °C. Then 3 g of sample were transferred

to a density bottle of 10 cm³ capacity. Any powder adhering to the neck of the bottle was washed down with distilled water, and the bottle half-filled with distilled water. The air in the water was removed by evacuation of the density bottle in a vacuum desiccator. The operation of adding water and evacuation was repeated several times until the bottle was completely filled with air-free water.

The measurements in this procedure include the mass of the density bottle fully filled with air-free water, m_1 (g), the mass of the sample in the density bottle, m_2 (g), and the mass of the density bottle fully filled with sample and air-free water, m_3 (g). From these data, the true relative density, D_t can be obtained by:

$$D_t = \frac{m_2 D_w}{m_1 + m_2 - m_3} , \quad (\text{kg/m}^3) \quad (3-8)$$

where D_w is the water density at the temperature of the measuring environment.

After the measurement of bulk density and true density, the total porosity, P_t and the closed porosity P_c can be calculated by the following equations.

$$P_t = \left(1 - \frac{D_b}{D_t} \right) \times 100\% , \quad (\%) \quad (3-9)$$

and

$$P_c = P_t - P_o , \quad (\%) \quad (3-10)$$

3.3.3 Fibre Volume Fraction

The fibre volume fraction was determined by the method recommended by Booth and Yeager^[153]. The method makes use of the areal weight (A_w , kg/m²) of the fibre cloth, and fibre density (F_d , kg/m³). Using composite thickness (t , m) and number of cloth layers (N), the fibre volume fraction, F_v is given by:

$$F_v = \frac{A_w N}{F_d t} \times 100 \quad , \quad (\%) \quad (3-11)$$

3.3.4 Open Volume Porosity Distribution

The size distribution of open pores was measured using a computerised porosimeter, Micromeritics Pore Sizer 9310. The mechanism of the measurement was based on the equation proposed by Washburn^[154]

$$r = - \frac{2 \sigma \cos \theta}{\Delta p} \quad (3-12)$$

where r is the pore radius, σ is the surface tension of mercury, θ is the contact angle and $\Delta p = p^l - p^g$ is the difference between the pressure applied to the liquid mercury and that of the gas in the pore. When mercury is forced into a pore in a solid material, the pressure, Δp required to fill the pore completely is in inverse proportion to the size of the pore. Therefore the open pore size distribution can be obtained by measuring the volume of mercury penetrating into the composite at different pressures.

In this test, the porosimeter operated from 4.83 KPa to 52.27 MPa, equivalent to a pore radius range of 268 μm to 23.9 nm. In processing the data, the contact angle was assumed to be 130° , the surface tension of mercury being 485mN/m.

3.4 CHARACTERISATION OF THE COMPOSITE STRUCTURE

3.4.1 Preparation of Samples for Microscopy

The examination of the composites under optical microscopy and image analysis was based on 31mm diameter disc-shaped specimens. For carbonised materials, surfaces for examination were obtained by embedding pieces of composite in epoxy resin, cutting back and smoothing the surfaces using various grades of silicon carbide paper, and finally polishing to a scratch- and relief-free finish using alumina powder on a cloth pad. The preparation of samples of moulded and impregnated but uncarbonised preforms employed the same procedures as used for carbonised materials but without embedding the preforms in epoxy resin. The surfaces examined comprised sections of the composites, sized (the radius of the disc by the disc thickness), cut perpendicular to the fibre-cloth layers and at $0^\circ/90^\circ$ and $45^\circ/45^\circ$ to the fibre direction.

Surfaces for scanning electron microscopy were prepared by cleaning the pieces of composite ultrasonically in a water bath, drying and then coating with gold to eliminate charging when exposed to the electron beam.

3.4.2 Polarised Light Microscopy (PLM)

Qualitative examination of the polished surface was performed using a Leitz Ortholux II Pol-BK microscope with crossed polars. It is well known that the appearance of carbon surface under polarised light is dependent on the nature of the carbon^[155]. Hence the fibres and different matrix components could be identified from their optical appearance and geometrical shape. In most cases, a λ -retarder plate was used to create a multi-chromatic image. With this λ -retarder plate, isotropic carbon and upper planes aligned normal to the incident light appear purple. Carbon layer planes aligned parallel to the incident light appear respectively purple, blue, purple and yellow when the planes are at 0° , 45° , 90° , and 135° to the planes of vibration of the incident polarised light. Another advantage of using λ -retarder plate is that voids are readily distinguished by their black appearance. Sometimes, observation without a λ -retarder plate was also applied to confirm orientation direction of the crystallines and to identify

some pyrolytic carbon which appears quite dull when observed using a λ -retarder plate.

In addition to qualitative investigation, the microscope was also used to measure the thickness of pyrolytic carbon. A video camera was used to transfer the microscope image to a TV screen, the thickness of pyrolytic carbon then being measured with a calibrated ruler.

The micrographs in this thesis were taken using a Reichert MeF3 polarising microscope with crossed polars and a λ -plate.

3.4.3 Scanning Electron Microscopy (SEM)

In this research, a Cambridge Steroscan S604 scanning electron microscope was used to gain a knowledge of three-dimensional structure of the composites and to determine their failure mode by the examination of fracture surfaces. The acceleration voltage was set to 25 kv for most samples. However for fracture surfaces and the Si-SiC skeleton remaining after burning-off the carbon from the Si-impregnated composites, a lower acceleration voltage of 7.5kv was chosen to prevent surface damage by the electron beam.

3.4.4 Development of Image Analysis Technique to Characterise Pore Structure in The Composites

The Literature Review showed that the strength of composites is influenced by void size, geometrical shape and volume fraction. Water penetration and mercury porosimetry can give information on the volume and entrance diameters of open pores. The porosity of the closed pores can be indirectly obtained using the density bottle method, but these techniques do not provide information on the geometrical shape of pores. However when polished surfaces of the composites are examined under an incident light microscope, the geometrical shape of open and closed pores on the two dimensional surfaces, their relative position to the solid constituents and distribution in the composites can be established. On such surfaces, discrete dark areas are the voids whereas the solid constitutes the continuous bright phase. If the microscope is

connected to an image analysis system as shown in Figure 3.3, it is possible to characterise quantitatively void structure in the C/C composites.

The application of image analysis techniques to characterise void structures of C/C composites has already received attention^[156]. However, one problem arising from the application is that the fundamental stereological relationship^[157,158] can not be easily applied. This fundamental stereological relationship considers that the area fraction of voids in any randomly distributed 2-D cross-section of a material corresponds to the volume fraction of the voids in the material. Voids in a C/C composite are highly anisotropic. Thus the apparent porosity depends on the angle between the polished surface and the fibre direction. Also voids in 2-D C/C composites vary widely in size and shape. Therefore, a characterisation of void structures in the composites has to be made. Without this, it would be impossible to obtain useful data by means of image analysis.

A method developed in this work characterises the voids in a cross-section of the composites into four types. They are planar cracks, bundle cracks, inter-fibre pores and inter-fibre cracks. Figures 3.4 a and b show the appearance of these four types of voids on the cross-section cut $0^\circ/90^\circ$ to the fibre direction. The planar cracks (also sometimes termed inter-layer cracks or coplanar cracks) are long cracks more or less oriented in the horizontal direction in the micrograph, Figure 3.4 a. The wide cracks predominantly orientated in the vertical direction and having a length of about one bundle thickness in the carbonised preforms are called bundle cracks. The bundle cracks may be shorter in a densified composite due to their blockage by new matrix carbon introduced by the densification process. However they can be readily identified under the microscope. Inter-fibre pores and cracks refer to the voids within fibre bundles. They are differentiated according to their areas on the cross-section normal to the fibre axis; inter-fibre pores were defined as pore areas below $150 \mu\text{m}^2$ with inter-fibre cracks being in the range of $150\text{--}500 \mu\text{m}^2$. A detail discussion on qualitative characterisation of the voids will be given in the next chapter. Following such a characterisation, the useful data, relevant to studies of the densification of the composites and of the influence of the voids in them on their mechanical behaviour, could be obtained.

Corresponding to the above characterisation, a suitable operational procedure for the image analysis was also developed. This involves calibration of light source,

arrangement of measuring fields, and development of programmes for measurements. The characterised voids were measured using a Joyce-Loebel Mini-Magiscan computerised image analysis system.

The essential principles of this system are shown in Figure 3.3. In this system, a TV image of a microscope field of view is captured as a 512 X 512 pixel array, the brightness of each pixel being allocated to one of either 64 or 256 grey levels (energy levels) depending on the capture methods. This process converts the microscope image into digitised signals. Such digitised signals are called the grey image. Directly measuring the energy level of the grey image will give the average brightness of the microscope image. In this work, this operation was used to calibrate the light source of the microscope. It was achieved by using a 7.4% reflectance standard and adjusting the light intensity to give a particular mean grey level.

For void measurement, segmentation is required to convert the digitised grey image into a binary signal. This can be done by setting a value of grey level. Then all pixels with grey level over the value result in a output of 1 (black), and pixels with lower levels giving a zero output, i.e., white output which may be displayed in a selected colour on the screen. By this conversion, dark voids corresponding to white output are detected on the binary image. For the materials studied, a grey level of 30 using threshold segmentation was found to be suitable for accurately separating voids and constituents under the calibrated microscope-illumination condition.

In some cases, only parts of the voids are of interest so that the binary image after segmentation needs further processing to delete unwanted voids. The Joyce-Loebel system provides image processing facilities such as isolation, deletion, dilation, erosion etc. to meet this requirement. In this work, a binary image of either planar or bundle cracks were achieved by isolation and programming and manual deletion. A binary image of inter-fibre pores and cracks was achieved by programming deletion.

The final step of the image analysis is the measurement of the desired voids and data processing. In Joyce-Loebel Magiscan system, the terminology of measured parameters relevant to this work includes:

Total detected area, FD:	area based on the number of white pixels within the measuring frame;
--------------------------	--

Field area, FA:	area of the measuring frame;
Detected area, OD:	based on the number of white pixels enclosed by and on the boundary, this area takes account of any holes;
Length, OL:	the maximum Feret diameter;
Breadth, OB:	the Feret diameter normal to the length;
Field objects, FO:	the number of objects (voids) detected in the field.

By data processing, void structural parameters used in this work were derived from the above measurements:

PARAMETER	SYMBOL	EXPRESSION
Voidage, %	(V)	$= \frac{FD}{FA} \times 100\%$
Mean area / voids, μm^2	(A)	$= \frac{\sum_{i=1}^{FO} OD}{FO}$
Mean length, μm	(L)	$= \frac{\sum_{i=1}^{FO} OL}{FO}$
Mean breadth, μm	(B)	$= \frac{\sum_{i=1}^{FO} OB}{FO}$
Number of voids per frame area, μm^{-2}	(NV)	$= \frac{FO}{FA}$

During the measurements, a X4 objective lens was used to measure the planar and bundle cracks, whereas the measurement of inter-fibre pores and cracks required a X10 objective lens. The size of a pixel was 3.3 by 2.9 μm when using the X4 lens and 1.1 by 1.0 μm when the X10 lens was used. From a later discussion it will be seen that the measurements of all types of voids could be performed on a 0°/90° cross-section, i.e., in which the fibres lay perpendicular and parallel to the surface of section. However polishing 0°/90° sections usually resulted in some fibres parallel to the surface being

torn away. If the torn away fibres are near the planar cracks, it is impossible to distinguish a planar crack from a fibre cavity. To overcome this problem, a $45^\circ/45^\circ$ cross-section was chosen for measuring planar cracks. Figure 3.4 c shows a polished $45^\circ/45^\circ$ cross-section of the same materials as used in Figure 3.4 a. Obviously a better view of planar voids was given on the $45^\circ/45^\circ$ section. The measurements of the other types of voids were carried out on a $0^\circ/90^\circ$ cross-section.

The measuring frame used is relevant to the size of the unit cell, the smallest volume representative of all the structural features in the materials under examination. The unit cell for 2-D C/C composite has a length equal to the distance between the two neighbouring crimps and a height equal to the thickness of three cloth layers. Table 3.6 gives mean dimensions of the unit cells for the materials studied. These data indicate that the length of the unit cell does not change during processing while the height of the unit cell varies with moulding conditions and the thickness of the composites. Therefore the height of the frame needs frequent adjustment according to the thickness of specimens.

When measuring planar and bundle cracks, the height of the unit cells could be accommodated on the viewing screen leaving a suitable size frame area but the lengths of the unit cells could not. Thus the measuring frames used had heights equal to those of the unit cells and for the composites produced from PAN-5H, Pitch-5H and Rayon-8H, lengths of the frames equal to $1/5$, $1/6$, and $1/2$ of the lengths of the corresponding unit cells. Since when using a low magnification lens, few fields are available for each specimen, all the available fields were measured. The diagrams in Figure 3.5 illustrate, for twelve and eight carbon-cloth layer composites respectively, the position, from the surfaces to the centre, across the composites thickness, i.e., in the Z-direction, of the measuring frames from which measurements were taken. Each frame contained three inter-layer interfaces. For composites consisting of 12 and 18 layers, the measuring frames exactly cover all the area of the section, but for composites consisting of 8 layers, the frames overlapped on the third layer counted from the surfaces. The central area was measured twice, the average value of the two measurements being quoted as the value for the central area. In the Y-direction, measurements were taken within the available area along the length of the unit cell before moving to the neighbouring unit cell.

When measuring inter-fibre pores and cracks, the fields of view were restricted to

areas containing only views of the fibres orientated perpendicular to the surface. The system was programmed to ignore any voids with areas greater than $500\mu\text{m}^2$ and less than $10\mu\text{m}^2$. The measuring frame used had a height of 80% of the fibre bundle height and an arbitrarily chosen width of $500\mu\text{m}$. With such a size of frame, there were very many possible frames available on each section. To measure all of these frames would take a very long time. Therefore a method was developed to determine a reasonable number of fields to be measured within the limitation of acceptable error. The method consisted of choosing a typical specimen for each type of material, measuring voidage V_i for all available fields within unit cells of the whole specimen, calculating the mean voidage μ and standard deviation σ of mean voidage μ for all available fields and finally using the following equation to decide the number of measuring frame, n under an error limitation ϵ :

$$n \geq \frac{\sigma^2 Z_{\alpha/2}^2 N}{\mu^2 \epsilon^2 (N - 1) + \sigma^2 Z_{\alpha/2}^2} \quad (3 - 13)$$

where N is the available number of fields in the specimen, and $Z_{\alpha/2}$ is a standardised normal variate. The relative error ϵ is defined as the difference between the measured value X_m and true value μ , divided by μ :

$$\epsilon = \frac{X_m - \mu}{\mu} \quad (3 - 14)$$

A detailed derivation of Eq. (3-13) is given in Appendix.

Under the restriction of 5% relative error, the n values of three typical composites corresponding to PAN-5H, Pitch-5H and Rayon-8H fibre cloths were obtained using this method. The results are shown in Table 3.7. The numbers of measuring fields per unit cell, 9, 16 and 6 respectively for composites made using PAN-5H, Pitch-5H and Rayon-8H fibre cloths, were chosen to measure the inter-fibre pores and cracks.

The voidage and number of voids per frame area were measured on a different basis of frame area when using different lenses. Actually it is not so important what frames are used because the voidage does not truly represent the volume porosity in voids of the types considered. However comparison of V and NV between bundle cracks and inter-fibre voids on a $0^\circ/90^\circ$ cross-section is possible since both of these voids appear on the area where the fibre direction is normal to the cross-section. From this consideration, V and NV were corrected to the same basis, i.e., the area per unit cell. For the inter-fibre pores and cracks, since the measuring frame did not include an area containing 0° fibres, V and NV were corrected by dividing the two parameters by a factor of two.

4. EXPERIMENTAL RESULTS AND DISCUSSION

4.1 STRUCTURE OF 2-D C/C COMPOSITES

An understanding of the structure of 2-D C/C composites is an essential preliminary step before an unequivocal explanation of their densification and mechanical properties can be developed. In the present context, structure is used to imply the three dimensional arrangement of solid constituents, interfaces and voids, rather than the organisation of the carbon in the fibres and matrix. With such an understanding, information obtained from the two-dimensional cross-sections of the composites could be applied to explain the mechanism of densification and the factors influencing the mechanical properties of the composites.

4.1.1 Features of Solid Constituents And Interfaces in The Composites

There is a certain regularity in the arrangement of fibres in a 2-D C/C composite so that it is possible to choose a small volume of the composite to represent structural features of the whole composite. The smallest such unit is called a unit cell. The concept of a unit cell was originally established in crystallography^[159] and later was introduced into the study of composites by Jortner to describe the structure of 3-D C/C composites^[160,161]. For 2-D C/C composites, the unit cell structure proposed in this study is schematically illustrated in Figure 4.1. The illustration is based on the study of the arrangement of the fibres in 2-D composites as revealed by SEM examination. For simplicity, the diagram in Figure 4.1 shows a 3-harness satin-weave composite. The weft and warp fibre bundles are orientated in the X- or Y-directions in Figure 4.1 while four fibre cloth layers are shown laid-up in the Z-direction.

The length and width, i.e., dimensions in X- and Y-directions of a unit cell are equal to the distance between two neighbouring crimps. At a crimp position, fibre bundles pass over and under each other forming a wavy pattern. The fibres at this position are not orientated in the reinforcing direction so that, when responding to various applied loads, they have a significantly different behaviour from those fibres lying in the plane of the laminate. With the defined length and width of a unit cell, each

layer in a unit cell on a cross-section such as Y-Z or X-Z faces includes one crimp. Hence the investigation of any changes in the planar direction could be made by comparison of the variation between each length or width of the unit cells. It has been recognised by some authors^[162] that there are a certain differences in crimp angle between weft and warp sides and between the length and width of a unit cell for some fibre cloths. For the materials studied in this work, these differences were found to be very small. Therefore the treatment in this study ignored the difference between warp and weft bundles. Mean values obtained from a large number of measurements are quoted as length or width of a unit cell for each type of material.

In the Z-direction, the skeleton of the composite is formed by stacking of fibre cloths. Regardless of crimp positions, two types of interface at layer boundaries may result from processing; one interface, termed, inter-layer parallel (ILP), at which fibres on the two sides are orientated in the same direction, and another, inter-layer normal (ILN), at which fibres on the two sides are orientated normal to each other. On a two-dimensional cross-section such as the Y-Z face in Figure 4.1, the two types of interfaces may appear in one of the three forms, X-X, X-Y and Y-Y depending on the fibre directions at the two sides of the interface. These are indicated by some dashed, horizontal lines. X-X, Y-Y inter-layer interfaces constitute ILP interfaces while a X-Y inter-layer interface is an ILN interface. Since the three types of interface may be present in a composite, representation of the composite structure in the stacking direction (Z) requires at least four layers to cover three inter-layer interfaces. However during measurement by image analysis, a frame size slightly thicker than three layers is adequate to include three inter-layer interfaces by following the method described in 3.4.4. Although the diagram in Figure 4.1 shows all three types of inter-layer interfaces on the Y-X face, it should be recognised that this is only one of the stacking combinations in a unit cell of 2-D composites. Three inter-layer interfaces in a unit cell on a randomly chosen field could consist of three X-Y interfaces or two X-Y interfaces and one X-X interface etc..

In addition to inter-layer interfaces, Figure 4.1 also illustrates two types of inter-bundle interfaces and one type of intra-bundle inter-face on the Y-Z face. These interfaces are present within the cloth layers. An X-Y inter-bundle interface is the planar boundaries between crossed weaving bundles. Viewing the top X-Y face in Figure 4.1, it could be imagined that X-Y inter-bundle interface would continuously spread along the line a. It would appear as many diagonal bands which are isolated by bands formed

by crimps as indicated along the line *b*. On a Y-Z cross section, X-Y inter-bundle interfaces are orientated in the horizontal direction.

A X-X inter-bundle interface is formed between two parallel bundles. This is also a type of planar interface having a shape similar to an ellipse viewed in three dimension. The major axis of such an "ellipse" is equal to (number of harness - 1) times the bundle width with the minor axis being the height of the bundle. On a Y-Z face, X-X inter-bundle interfaces are orientated in the vertical direction.

The appearance and the height of a X-X intra-bundle interface on a Y-Z face is similar to a X-X inter-bundle interface. However X-X intra-bundle interfaces are present within fibre bundles.

Other interfaces which occur in the composites include those between fibres and matrix and between different matrices or between the same type of matrix formed at different processing stages.

The matrix in the composites is relatively uniform within the fibre bundles in respect to inter-layer and inter-bundle interfaces. These two types of interfaces are matrix-rich areas especially at an inter-layer interface where cavities formed by crossed crimping-bundles may accommodate a relatively large volume of matrix carbon.

4.1.2 Voids in The Composites And Their Characterisation

Voids may occur at interfaces of all types. In addition to the interfaces described in the above, a very small proportion of the total porosity is present within the matrix. Like the porosity in the fibres, this porosity is considered as the in situ properties of the matrix so that it will not be considered further.

Large voids identified under polarised light microscopy and SEM are illustrated in Figure 4.2. Corresponding to the interfaces shown in Figure 4.1, the voids in Figure 4.1 include X-X, X-Y and Y-Y inter-layer cracks, X-X and X-Y inter-bundle cracks and X-X intra-bundle cracks. Another type of large void also shown on the diagram is a crimp void.

Small voids within the fibre bundles are too small to be drawn in Figure 4.2. Their position relative to the surrounding fibres is shown by the micrograph in Figure 3.4 b. These small voids are classified according to size. The voids being surrounded by less than five fibres are termed inter-fibre pores, the bigger voids being known as inter-fibre cracks.

In order to help to understand the three-dimensional structure of the voids, rough outlines of the voids were obtained by impregnating the target voids with silicon and burning-off the carbon constituents. These outlines of the voids are the remaining silicon skeletons covered by a thin layer of SiC which was formed by silicon and carbon at the boundaries between voids and carbon constituents. Although such Si-SiC skeletons may be slightly thicker and inter-connected more than real voids, most of voids features still remain. Therefore the skeletons were investigated using SEM. Their morphology under SEM is shown in Figure 4.3.

The skeleton in Figure 4.3a resulted from a composite in which silicon only infiltrated the large voids illustrated in Figure 4.2. On the picture, planar sheets orientated in horizontal direction are the rough outlines of either various inter-layer cracks or X-Y inter-bundle cracks, whereas the planar sheets orientated in the vertical direction represent either X-X inter-bundle cracks or X-X intra-bundle cracks. The real morphology of these cracks may not be the perfectly planar sheets but either discontinuous or continuous planar sheets with many solid islands on them. X-X, X-Y and Y-Y inter-layer cracks and X-X and X-Y inter-bundle cracks were formed within the range of their corresponding interfaces as indicated in 4.1.1. The depth of X-X intra-bundle cracks in the X-direction is shown in Figure 4.4. The surface visible in the micrograph was obtained by cleaning a composite at an inter-layer interface. Many of the cracks appear to run from one crimp to another (e.g. at A). Others may stop at intermediate position within the distance but when this happens, an adjacent crack is initiated (see B).

The final type of void illustrated in Figure 4.2 is a crimp void which is present at the corner between wavy and horizontal fibre bundles. The rough outline of this type of void is shown at position C in Figure 4.3a. Geometrical considerations suggest that the maximum penetration of the cracks from the Y-Z plane can not exceed the width of one fibre bundle. Crimp voids occur in a position of resin coke concentration and result from cracking either within the resin coke itself, or at the interface between the resin

coke and the fibres orientated in X- or Y-directions. Their appearance in Y-Z section, as Figure 4.5 shows, is somewhat variable. The number of crimp voids in a composite depends on the types of weave used in the fibre cloth. A plain-weave composite contains more positions for crimp voids than the satin-weave composites.

Both the morphology shown on Figure 4.3a and the good penetration of silicon into the large cracks suggest that the large cracks shown in Figure 4.2 are highly inter-connected. X-X inter- and intra-bundle cracks act as bridges between inter-layer cracks and X-X inter-bundle cracks forming a large crack network. The degree of the inter-connection may not be quite as high as the Si-SiC skeleton shows due to the reaction between silicon and carbon and varies with the types of the composites and stage of processing.

The Si-SiC skeletons of inter-fibre pores and cracks are shown in Figures 4.3b and 4.3c respectively. The inter-fibre pores in three-dimension appear as many, more or less parallel, bars. The pores at the interfaces between the fibres and the matrix appear as split hollow sheaths while the pores surrounded by matrix look like rhombic bars. The inter-connection between the pores, as illustrated in Figure 4.6, results from local mergence of the pores in the fibre direction. The inter-fibre cracks viewed in three-dimension appear as long and narrow bands.

For quantitative study, the classification of the voids described above was simplified. The inter-layer cracks and X-Y inter-bundle cracks are both suitably orientated to influence the strength of delamination of the composites and they were therefore allocated to one class termed planar cracks since they lay in planes parallel to those of the fibre layers. X-X inter-bundle and intra-bundle cracks orientated perpendicular to the cloth layers were classified as bundle cracks. Such cracks are considered to be important in relation to flexural strength^[163]. The studies in this work were mostly based on satin-weave composites for which the contribution of crimp voids to the total porosity is small. Hence in this work they are regarded as either planar or bundle cracks according to their orientation. The classification of small voids within the fibre bundles still use the names of their identification. However for purposes of quantitative measurement, the differentiation between inter-fibre pores and cracks were based on their cross-sectional area rather than the number of fibres surrounding them. It was found that inter-fibre pores had areas below $150\mu\text{m}^2$, the areas of inter-fibre cracks being in the range of $150\text{-}500\mu\text{m}^2$. Both types of voids are considered to be related to

load transfer among fibres^[164,165] but inter-fibre pores are more important in relation to physical bonding conditions between the fibres and the matrix, whereas inter-fibre cracks are associated with the looseness of the solid constituents in the fibre bundles.

4.1.3 Properties of Carbonised preforms

Before the densification study is described, the current understanding of features present in carbonised preforms is presented. Studies in this phase were based on three types of material, i.e., carbonised preforms PAN-SR, Pitch-SR and Rayon-SR. They were produced from three different types of carbon fibre which cover all types of fibre precursor used widely in commercial production today. As seen in section 3.1.2, the subsequent densification studies were also based on these materials.

4.1.3.1 Basic Properties of Carbonised Preforms

The properties of the fibres and the prepregged cloths as used in the three types of carbonised preforms have already been described in sections 3.1.1 and 3.1.2. Some basic properties of the preforms obtained from the density measurements and observations of polarised-light microscopy are given in Table 4.1. As shown in the table, the PAN and rayon fibre based preforms contained twelve cloth layers and had similar thickness and fibre content. In contrast to these two types of preforms, the pitch fibre based preform only contained eight cloth layers and had a little higher thickness and lower fibre content. The bulk density of these materials follows a sequence of Pitch-SR > PAN-SR > Rayon-SR. This sequence appears to correspond with the density of the fibres contained as given in Table 3.1.

Under a polarised-light microscope, the types of the carbonised preforms could be easily distinguished from the morphology of the constituent fibres and weaving structure. The micrographs shown in Figures 3.4 b, 4.7 a and b were respectively taken from the PAN, pitch and rayon fibre based carbonised preforms using a X100 lens. These pictures display the microstructure within fibre bundles of the materials. The individual fibres differed significantly in appearance. In cross-section, the PAN fibres in PAN-SR were optically isotropic and circular, the pitch fibres in Pitch-SR anisotropic and circular while the rayon fibres in Rayon-SR were isotropic and crenellated.

Differences could also be found in the distributions of fibre diameters. The PAN fibres all had diameters close to $7.5\text{ }\mu\text{m}$, while the diameter of the pitch fibres was widely distributed, ranging from 9 to $14\text{ }\mu\text{m}$. Most of the rayon fibres had a maximum Feret diameter between 9 to $11\text{ }\mu\text{m}$ with a small proportion being around $5\text{ }\mu\text{m}$. The fibre bundles in the pitch fibre based materials appeared looser than those in PAN-SR and Rayon-SR.

The resin coke in the carbonised preforms basically exhibits optical isotropy in the bulk and weak anisotropy near the fibres. The fibres/resin interface is usually cracked. The physical bonding between the fibres and the resin coke appears better in PAN based materials than in Pitch-SR and Rayon-SR. In the latter materials, it is easy to find fibres which are totally debonded from the resin coke as shown in position I on Figures 4.7a and 4.7b, whereas this situation rarely occurs in the cross section of a PAN based preform. The mass fraction of the resin coke listed in Table 4.1 indicates that the pitch fibre based preforms contain more resin coke than the PAN and rayon fibre reinforced preforms.

$0^\circ/90^\circ$ cross-sections of the preforms viewed using a X5 lens are shown in Figure 4.8. The shape of the cross-section of the fibre bundles in Rayon-SR is not as flat as that observed in the PAN and pitch fibre based preforms. The measured mean crimp angle was 6° for PAN-SR, $8^\circ 51'$ for Pitch-SR and $15^\circ 51'$ for Rayon-SR.

4.1.3.2 Voids in Carbonised Preforms

Volume porosity of voids in the carbonised preforms is shown in Figure 4.9. A similar value of total porosity, around 23 vol %, was observed for all three types of material. Of the total porosity, more than 95% of the voids in the pitch and rayon based preforms were open while in PAN reinforced preforms, 36% were closed.

The distribution of the voids in the preforms was measured by image analysis. Figures 4.10 to 4.14 show the voidage, mean area per voids, average length, breadth and number of voids per frame area of various types of voids of the preforms. When measuring planar cracks, some cracks were too long to be included within a measuring frame so that the true mean area per void and the true average length could be larger

than quoted while the number of voids per frame area would be lower than the figures indicated. However since the measurements on all materials examined were obtained by the same method, it is considered that the values quoted provide useful means of comparing materials containing different cloth and at various stages of densification.

As Figure 4.10 shows, marked differences were observed for the planar, bundle and inter-fibre cracks in the three types of carbonised preform. The PAN based preforms contained a considerably higher voidage as planar and bundle cracks than the pitch and rayon fibre preforms while the pitch fibre reinforced materials contained a higher voidage as inter-fibre cracks than the others. In this respect, the differences between the pitch and rayon fibre based preforms in planar and bundle cracks and between the three types of materials in inter-fibre pores are small.

Comparing the voidage data with that in Figures 4.11 to 4.14 indicates that the high voidage of planar and bundle cracks in the PAN based materials results from cracks with a large mean area. This large area is due primarily to a large crack length. The average breadth of the cracks in the PAN fibre based preforms are also wider than in the pitch and the rayon fibre based preforms. In contrast, the high voidage of inter-fibre cracks in the pitch fibre based materials is due to a high number of cracks.

The micrographs shown in Figures 3.4b, 4.7 and 4.8 explain the other differences in voidage shown in Figure 4.10. From Figure 4.8, it can be seen that the higher voidage and number of planar cracks in the rayon fibre based preforms compared to the pitch fibre based materials are caused by a high number of crimp voids some of which were quoted as planar cracks during the measurement. In contrast, the higher voidage of bundle cracks in the pitch fibre based preforms is due to a high number of bundle cracks with a fairly regular spacing as indicated in Figure 4.8 b. Such cracks were observed in the PAN and pitch fibre based preforms but could not be found in the rayon based materials. The voidage of bundle cracks in the rayon fibre preforms, Figure 4.10, is made up of crimp voids orientated in vertical direction. Another confusion with the bundle cracks is the average breadth. Figure 4.12 shows that the PAN fibre preforms have a higher average breadth than the pitch fibre based preforms. This seems impossible because the bundle thickness in the PAN fibre preforms is lower. The answer from the micrographs is that the bundle cracks in the pitch fibre preforms appear to be blocked by one or a few fibres since they are thin in these places. Therefore one bundle crack could be measured as two or more cracks

when taking measurements from the pitch fibre based preforms.

Microscopic observation of inter-fibre pores indicates that the small difference in voidage between the three types of preform can not be ignored. The lower voidage of inter-fibre pores in the PAN fibre preforms corresponds to the better physical bonding between the fibres and the resin coke as described previously.

4.1.3.3 Discussion

Although the variety of 2-D C/C composites is potentially very large because of the wide selection of suitable fibres, reinforcement geometries, matrix precursors and processing conditions, the three types of carbonised preform studied may include the structural features of voids for all types of 2-D C/C composite. In the PAN fibre based preforms, planar and bundle cracks are prominent, the pitch fibre preforms contain many inter-fibre cracks, and inter-fibre pores are present in all three types of material. These materials therefore form a group of model materials ideally suited to the study of the densification of 2-D C/C composites.

The results obtained suggest:-

- (1) In spite of dependence on the density of the constituents and the content of carbon fibres, matrix and voids, the bulk density of the studied carbonised preforms was governed primarily by the density of the fibres they contained.
- (2) The voids structures of the three types of preform are a consequence of both processing and the types of fibre and resin used. The similar total and closed porosity in the pitch and rayon fibre based preforms indicates that almost all types of voids are open and highly inter-connected in these two types of material. The PAN fibre based preforms contained 8.2 vol% closed porosity. This, together with the good penetration of silicon into planar and bundle cracks in a composite in the PAN-SR group (Figure 4.3a), appears to show that the closed voids are inter-fibre pores and cracks. Hence the inter-fibre pores and cracks in the PAN fibre based preforms are in a different environment from those in the other two types of preform. The environments depend on the bonding between the fibres and the matrix, in another words they are related with the surface properties of the fibres and the resins used.

The inter-fibre cracks are associated with the relative content of the fibres and the matrix in the carbonised preforms. Compared to the other two types of material, the higher number of inter-fibres cracks in the pitch fibre based preforms is due to their lower fibre volume fraction and high resin content. This is understandable because the richer resin within the fibre bundles is surrounded with more fibres. Figure 4.15 schematically illustrates well bonded resin in a moulded preform with the fibres which are in close contact with each other in the fibre bundles and a moulded preform with a low fibre content. In the former situation (Figure 4.15a), resin is isolated by the fibres so that only inter-fibre pores could occur during further processing. In the case of low fibre content (Figure 4.15b), resin is a continuous phase which contacts with all the fibres within a bundle. Whether the voids are formed at fibre/resin interface or within the resin phase, there is a greater probability of forming inter-fibre cracks during the subsequent processing.

Bundle cracks with fairly regular spacing have been found in PAN-based carbon fibre reinforced 2-D C/C composites by many researchers^[161-163,166]. For the materials studied, this type of void was observed in both the PAN and pitch fibre preforms but not in the rayon fibre based materials. It appears that the cracks are associated with the weaving structure of the fibre cloths. The cracks are likely to occur when the length of the unit cell is long.

A considerable difference in length and breadth of planar cracks was observed between the PAN based preforms and the other two types of materials. No explanation can be given at this stage.

4.2 DENSIFICATION OF THE CARBONISED PREFORMS

The densification of the model carbonised preforms will be discussed in this chapter. The densification processes studied involved two techniques, i.e., resin impregnation and chemical vapour deposition. Many densification routes were investigated, aimed at gaining an appreciation of the relationship between the void structure and densification processing.

4.2.1 PAN Fibre Reinforced Composites

4.2.1.1 Densification by Multiple CVD

Experimental Observation

To study multiple CVD densification of the PAN based composites, the carbonised preforms were given up to five CVD treatments, each treatment being 72 hours in duration. The materials processed to each stage were investigated. Figure 4.16 shows the weight gained by the composites during processing, expressed as a percentage of the weight of the carbonised preform, while the bulk densities of the composites are shown in Figure 4.17. In these figures, C1 refers to the carbonised preform and D1 to D5 the composites after one to five CVD treatment. Significant weight gains occurred on the first two CVD treatments but only small gains were recorded thereafter. The bulk density generally follows the weight gains except for the composite D4 which was slightly thicker than the other specimens.

The open porosity of the composites, determined by the water penetration method, is shown in Figure 4.18 to fall to a constant value of about 6% after two CVD treatments.

The behaviour of the individual type of voids was investigated qualitatively by polarised-light microscopy and quantitatively by image analysis. In the whole densification process, pyrolytic carbon, as Figure 4.19 shows, was observed in both planar and bundle cracks. Deposits were not generally observed in inter-fibre cracks. Figures 4.20 and 4.21 give the changes in voidage of the planar and bundle cracks

respectively. Apparent decreases in voidage of the two types of voids occurred in the early cycles of CVD treatment. The planar cracks were densified to a great extent than the bundle cracks, especially in the first CVD treatment.

The micrographs in Figures 4.22 to 4.24 illustrate the position of pyrolytic carbon deposited in the composites. In the first CVD treatment, pyrolytic carbon can be observed in planar and bundle cracks in the outer layers (Figure 4.22a) and at the centre (Figure 4.22b) of the composites. The deposit near the surface is clearly thicker than that at the centre. In the outer layer, the thin deposit did not greatly influence the entrance of the bundle cracks but considerably narrowed the planar cracks, especially at the tip of the cracks as indicated in position A on Figure 4.22 a. After the second cycle, as Figure 4.23 shows, pyrolytic carbon at both the edge and the centre is noticeably thicker, the deposit near the surface being much thicker than in the centre position. In the outer layer, all planar cracks appear blocked at their necked positions on the observed cross-section, and so do some bundle cracks (Figure 4.23a) but other bundle cracks were still open to the atmosphere (Figure 4.23b). In the subsequent three cycles of treatments, the thickness of pyrolytic carbon in the outer layer and external surface further increased, and the bundle cracks open to the external surface appeared to be progressively blocked. At the same time, bundle cracks without any pyrolytic carbon were observed at both the centre and the outer layer. Figure 4.24 a shows such a crack (F) and a crack with a similar width but deposited with pyrolytic carbon (G) at the centre of a composite. It is considered that they were newly formed during the densification. Reopened cracks were also observed in the outer layer (at E in Figure 4.24b). The changes of carbon deposit in the centre area are difficult to determine by qualitative observation.

The quantitative information on the variation of the thickness of pyrolytic carbon during densification was obtained by transferring the microscopic image on to a TV screen via a video camera, and then measuring the thickness of pyrolytic carbon using a calibrated ruler. In every layer, seven fields were measured. Each field corresponded to 2 mm in length. Since some planar cracks were completely filled, the measurements were mainly based on bundle cracks. Figure 4.25 shows the distribution of the thickness in the direction normal to the layers. Layers 1 and 6 correspond to the surface layer and middle of the central layer of the composites respectively. The first CVD treatment created a small difference of the thickness between the first layer and the interior. The carbon deposited in the first layer was approximately twice that in each of

the other layers. On further treatment, the thickness in the first layer increased much more rapidly than in the inner layers so that after five CVD treatment the pyrolytic carbon in the outer layer was five times thicker than that in the interior. In the inner layers from the second to the sixth treatment, the average thickness of pyrolytic carbon increased progressively even after the second CVD treatment (Figure 4.26).

In the layer direction, the variation of the average thickness from the rim to the centre of the circular composites is shown in Figure 4.27. The average thickness of pyrolytic carbon does not include the thickness in the first layer because the data for the first layer were influenced too much by the infiltration in the direction normal to the layers. The thickness of pyrolytic carbon showed a gradual diminution from the rim to the centre after the first and the second CVD treatments. After that, the difference in the thickness in the layer direction tended to decrease. Only the carbon deposited near the rim became increasingly thicker.

On the external surface, variation of the average thickness of pyrolytic carbon is shown in Figure 4.28. The thickness on the external surface increased with the number of CVD treatments.

Mechanism of CVD Densification

From the experimental results obtained, the mechanism of the CVD densification can be explained. The inter-fibre pores and cracks, because either the pore diameter at the boundaries of the fibre bundles was too small or they were closed to the gaseous atmosphere, were inaccessible to the pyrolytic carbon precursor. By using a coordinate system shown in Figure 4.2, the behaviour of the densification for planar and bundle cracks can be schematically illustrated as in Figure 4.29. For a Y-Z section, the crack network formed by planar and bundle cracks is simplified to a glass bulb inter-connected by thin tubes. The planar cracks act as the thin tube or the necks of the bulbs while the bundle cracks behave as the bulbs. On the external surface, the bulbs rather than the necks are exposed to the outside atmosphere.

At the beginning of the first CVD treatment, both planar and bundle cracks were accessible to the vapour of the carbon precursor so that the concentration of the reactive gas can be assumed to be uniform within the composite. Thus the overall reaction rate is controlled by the chemical reaction. As the deposition continued, carbon deposited on

the crack walls was not thick enough to influence the vapour flowing through bundle cracks but did have a considerable influence on the resistance of the planar cracks to vapour flow. Progressively, carbon deposits narrowed the planar cracks and reduced the rate of mass transport from the surface to the centre. Thus the concentration of the reactive gas, C_g , in the bundle cracks within a half layer distance to the external surface was similar to that in the external gas phase so that the necks of the network, i.e., the X-Y inter-bundle cracks within the first layer, were narrowed, or in some cases blocked, at a faster rate than the planar cracks in the inner area, thus restricting but not completely stopping ingress of reactant to the inner layer. This gives rise to a situation shown in the bottom curve on Figure 4.25, i.e., a marked difference between the first and the inner layers in the thickness of pyrolytic carbon present (or more exactly at the X-Y inter-bundle interfaces within the layers). The cracks in the inner layers were uniformly deposited with pyrolytic carbon because the thickness of the deposits in them was not sufficient to affect the resistance to mass transport. At the end of the CVD treatment, the overall reaction rate was dominated by diffusion control. As shown on the right hand side in Figure 4.29a, a barrier to the mass transport of reactive species was built up at half layer thickness from the external surface.

In the layer direction, a similar mechanism to that discussed above can be applied. Carbon deposited on the rim in the first densification was over $2.2\ \mu\text{m}$ thick. By comparing this datum with those shown for densification stage D1 in Figure 4.27, it appears that the hindrance of the rate of mass transportation occurred at the rim surface. In the inside of the composite, pyrolytic carbon deposited in the planar cracks increased the resistance of the mass transport from the rim to the centre due to narrowing and blocking. Since the mass transport in this direction was through the planar cracks, a progressive reduction of the gas concentration was then created. This resulted in the progressive decrease of the thickness of pyrolytic carbon at the end of the deposition.

The arrangement and geometric shape of the planar and bundle cracks suggest that a planar crack has more open channels than a bundle crack. A planar crack is not only connected with a large number of bundle cracks but also with other planar cracks in the same interface so that blocking of even several connections would not necessarily stop the mass transport to any point taking place via other cracks. However most bundle cracks are connected to the planar cracks at their ends, hence blocking a few opening sections of the planar cracks would result in closing some bundle cracks. From this

point of view, the planar cracks would be filled to a great extent than the bundle cracks. The experimental results shown in Figures 4.20 and 4.21 support this view.

The carbon deposited in the planar and the bundle cracks and blocking of some planar cracks certainly contributed to the decrease of the open porosity during the first CVD treatment. However whether this was fully responsible for the sharp decrease of the open porosity shown in Figure 4.18 can not confirmed at this stage because it is not clear to what extent there is any open porosity in inter-fibres pores and cracks in the carbonised preforms. The question can be expected to be answered by the study of the densification by resin impregnation.

Because of the structure created by the first CVD treatment, the whole stage of the second deposition was controlled by diffusion. At an early stage of this second treatment, the rate of carbon deposited in the inner layers depended on the diffusion rate of the vapour passing through the barriers at the rim surface and at half layer distance from the external surface. As the deposition continued, a considerable number of positions of the planar cracks at the barriers were blocked. The carbon deposited in the bundle cracks near the external surface also starts to influence the mass transport through them. The average concentration of the reactive gas in these bundle cracks was no longer the same as that in the gas phase outside of the composite. This is therefore an early stage in the formation of a second barrier at the external surface. At the end of the second CVD, although some bundle cracks in the half layer thickness from the external surface appear blocked, the thickness of pyrolytic carbon in these cracks does not vary markedly with position (Figure 4.23). Hence the reaction in this area was still predominantly controlled by the chemical reaction. Perhaps more like the "transition zone A" as described by Hedden et al.^[167] and Vohler et al.^[168]. The distribution of the reactant in the latter stage of the second CVD is schematically shown in Figure 4.29b.

After the second CVD, the penetration from the rim to the centre through the planar cracks almost stopped so that the multiple densification curves in Figure 4.27 tend to be horizontal. This is probably caused by the carbon deposited in the inner layers of the composite arising from reactant which penetrated from the direction normal to the cloth layers. In that direction, the changes of the penetration in the later cycles are shown in Figures 4.29 c to e. The barrier to mass transport generally moved from the X-Y inter-bundle interface in the first layer to the external surface. This gave

rise to the continuous increase in the thickness of pyrolytic carbon in the first layer and external surface. The interesting point is that, after the second CVD, the open porosity and weight gain remained almost unchanged while the thickness of pyrolytic carbon both on the external surface and in the interior of the composites increased. These results lead to only one explanation, i.e., some weight loss and newly formed cracks are also involved in the densification process. This view was confirmed by the microscopic observation and a re-carbonisation study of the composites from different processing stages. The micrographs shown in Figure 4.24 indicate the new cracks formed at both outer and inner layers of the composite. Weight losses and the increase in open porosity of the carbonised preforms and the composite after two CVD treatments, by re-carbonisation in nitrogen are given in Table 4.2. This change tended to decrease as the number of processing cycles increased. This implies that at the end of the first carbonisation, the devolatilisation of the carbonised preforms was not complete. Siebold's study on Resinox SC-1008 phenolic resin showed that weight losses continued until about 1300 °C^[169]. The complete devolatilisation of the PAN fibre based composites studied required heat treatment at a higher temperature than that presently used. Therefore the densification of the composites involved both reduction of the open porosity and weight gain due to the deposition of pyrolytic carbon and increase of the open porosity and weight loss due to the further devolatilisation and new crack formation. At an early stage of the densification, the former factor predominated. As the cracks narrowed and blocked, deposition was more and more difficult. As a result, a balance was formed between the void opening and closing and the weight loss and gain leading to the results observed.

4.2.1.2 Densification by Multiple Resin Impregnation

Experimental Observation

Multiple resin impregnation of the PAN based carbonised preforms was performed using four impregnation/carbonisation cycles. The weight gain by the composites in this process, expressed as a percentage of the weight of the carbonised preform, is shown in Figure 4.30, whilst the bulk density of the composites is shown in Figure 4.31. In these figures, C1 refers to the carbonised preform and C2 to C5 the composites after one to four treatments by resin impregnation. The weight gain and bulk density increased progressively with number of the treatments. The open porosity

of the composites (Figure 4.32) was generally in agreement with these findings, the value for C5 being considered to be slightly anomalous.

The changes of the voidage during the densification, measured by image analysis, are shown in Figures 4.33 to 4.35. Figure 4.33 shows that the densification occurred in not only the planar and the bundle cracks but also the inter-fibre voids (pores and cracks). The voidage for the planar cracks decreased sharply in the first cycle and progressively afterwards. The densification of the bundle cracks mainly occurred in the treatments after the first cycle. The detailed changes of the voidage for the inter-fibre pores and cracks are illustrated in Figures 4.34 and 4.35 respectively. The voidage of the inter-fibre pores smoothly decreased with processing whereas the voidage of the inter-fibre cracks changed little after the first resin impregnation.

Figures 4.36 and 4.37 give the distribution of the voidage in the composites. It appears that resin impregnation affects the voids in all positions within the composites to approximately the same extent during the densification.

For each densification cycle, the materials both before and after carbonisation were examined by polarised-light microscopy. In carbonised materials, furfuryl alcohol coke in the bundle cracks could be easily identified because there was no resin coke on the crack wall in the carbonised preform. However the carbon formed by furfuryl alcohol resin in the planar and the inter-fibre pores and cracks was difficult to differentiate from the phenolic resin coke originally present in the composites. To overcome this difficulty, impregnated composites without carbonisation were studied. The impregnating resin in such composites had a dark pink appearance which was easily distinguished from the phenolic resin coke due to a marked difference in reflectance. One problem arising from this approach was that the impregnating resin appeared identical to the epoxy resin normally used for block preparation. Hence the surfaces of uncarbonised composites were prepared without embedding the materials in the epoxy resin.

Figure 4.38 shows the composite after the first resin impregnation without carbonisation. The dark pink areas on the micrographs are the furfuryl alcohol resin. At this stage, furfuryl alcohol resin impregnated almost all the planar cracks (position A), the narrow bundle cracks (position B), and the inter-fibre pores (position C) and cracks (position D). For the wide bundle cracks, new resin phase was only observed at their

narrowed necks but not inside the cracks. After carbonisation, the new carbon phase was difficult to distinguish from the original resin coke in the planar cracks and the inter-fibre pores and cracks. In the narrow bundle cracks, the carbon formed from the impregnating resin was incompletely attached to the crack walls (Figure 4.39). From the second cycle, impregnating resin was observed readily in all types of voids. Multiple-layer resin coke appeared in the narrowed cracks (Figure 4.40), whilst in the wide bundle cracks, impregnated resin coke was observed in the middle of the cracks in the early densification cycles (Figure 4.41) and latter became multiple layers loosely attached or unattached to the crack walls (Figure 4.42). The interfaces between the resin coke formed from different impregnation cycles were recognisable.

Mechanism of The Densification

The capillary effect appears to play an important role during impregnation with furfuryl alcohol resin. During the impregnation, when a composite is immersed in the liquid resin, the voids in a void network in the composite are analogous to a soap bubble with different curvatures at its surface. As the resin impregnates the void network, the "bubble" is compressed and the gas pressure inside the "bubble" increases. When the gas pressure reaches a certain value, a balance will be formed between the power driving the resin into the void network and the resistance formed by the internal gas pressure so that mass transportation stops. At this state, the voids with smaller radii share a higher pressure than the voids with bigger radii according to the Young and Laplace equation^[170]. As a result, the voids with small radii are compressed to a greater extent, or in another words, are filled to a greater extent compared to voids with bigger radii. This could result in a structure in which the "bubble" is divided into several smaller bubbles by the resin. The "smaller bubbles" tended to be present in the wide bundle cracks while the planar cracks act as thin capillaries. The data in Figure 4.13 indicate that the average breadth was 25.6 μm for the planar cracks and 35.1 μm for the bundle cracks in the carbonised preform. Thus the planar cracks would be preferentially filled during the impregnation. In the first cycle, a great decrease in voidage of the thin voids (the planar cracks and the inter-fibre voids) and poor filling of the wide bundle cracks may be attributed to this explanation.

Following this approach, the imbibition of the resin into the wide bundle cracks on subsequent densification can be explained. The pressure created in the first cycle in the wide bundle cracks would be released on solidification and carbonisation by

opening cracks due to resin shrinkage. To achieve the same pressure build up in the wide bundle cracks in the second cycle, the resin would have to invade some of the crack space because the volume of the void network has been reduced. In this way, in the later cycles, the wide bundle cracks would become densified.

Drainage may also play a role in the densification. After impregnation, some resin drawn into the composites might flow out. Although the change of the environmental pressure of the composites from a vacuum to atmospheric in the operation would hinder drainage, it might not be completely prohibited. During the first resin impregnation, when the void structure is relatively open, resin might drain from the wide bundle cracks to the neighbouring thin planar cracks or inter-fibre pores and cracks. This provides an alternative explanation for the lack of impregnating resin coke in the bundle cracks after one impregnation cycle. Following the first densification, considerably narrowed planar cracks (Figure 4.33) increased the "dependent behaviour"^[171] of the void network. This increased resistance to drainage and may enable the resin to stay in some wide bundle cracks. Therefore the wide bundle cracks could be densified by the second and subsequent cycles.

The capacity for imbibition and drainage of porous materials, with three-dimensional inter-connectivity like the void structure in the composites studied, depends on many factors. The experiments in this study were not designed to provide detail information on this subject. Thus it is not possible to decide unequivocally which of the two is more realistic. However imbibition is considered the more likely explanation.

It is not surprising to observe the multiple layers of the impregnated carbon in both thin and wide cracks from the mechanisms suggested above. As a result, from the second cycle, the bulk density and the weight progressively increased and voidage in all types of the voids, except the inter-fibre cracks, progressively decreased. The small change of the voidage in the inter-fibre cracks can be explained by two simultaneous processes; the filling of the inter-fibre cracks and the generation of further cracks in that size range from filling of the bundle cracks.

Since the mechanism of the densification is considered to be predominantly by the capillary effect, narrowing of the open channels would not significantly influence the mass transport from the external surface or the rim to the centre of the composites.

Therefore the voids in all positions were filled to almost the same extent.

The remaining question from the multiple CVD densification can also be answered from the resin impregnation results. The penetration of resin into the inter-fibre pores and cracks indicates that a certain proportion of the inter-fibre pores and cracks in the carbonised preforms were open voids.

4.2.1.3 Densification by Combined Processes

In addition to multiple CVD and multiple resin impregnation, densification involving both CVD and resin impregnation was also studied. The materials used in this study were produced in two batches. This resulted in a small difference in thickness between the materials. The composites whose first densification was achieved using the CVD technique had thickness of 2.80 mm to 2.85 mm, while the composites whose first densification involved resin impregnation were 3.00 mm to 3.05 mm thick. Comparison between the materials of different thickness, and hence voidage is difficult. However a comprehensive understanding of the two densification techniques in various pore structures present could still be achieved by investigation of selected densification processes involving both CVD and resin impregnation.

Figure 4.43 a to c compares the variation of voidage in all types of the voids during the densification using a DCD sequence together with the data on multiple CVD treatments. In this, D refers to CVD treatment and C to resin impregnation plus carbonisation so that DCD implies that the densification process started with CVD, then with resin impregnation and finally again with CVD. Compared to the multiple CVD, when the second treatment was a resin impregnation, i.e., DC, the voidage in all types of voids decreased to a greater extent. This was expected because the cracks being narrowed after the first CVD were conducive to resin impregnation, especially to densify the wide bundle cracks (Figure 4.43b) according to the mechanism on the multiple resin impregnation. The decrease of voidage in the inter-fibre pores and cracks by resin impregnation implies that these voids were not completely closed in the CVD treatment used in the first cycle. As a result, a higher density and lower open porosity were obtained when resin impregnation was applied in the second densification (Figures 4.44 and 4.45). The further densification using CVD after DC does not appear to effect the voidage in all types.

The changes of voidage for all types of voids in combined processes initiated by a resin impregnation are shown in Figures 4.46 a to c. Compared to the multiple resin impregnation, the second densification using CVD decreased more voidage in the planar cracks (Figure 4.46a) but was less efficient in filling the bundle cracks (Figure 4.46 b). To find the reason, the thickness of the pyrolytic carbon deposited in CD was measured. Figure 4.47 gives variation of the thickness of pyrolytic carbon in CD together with the data in the early two cycles of the multiple CVD densification. The two lines from CD and D1 almost overlap. This indicates that the first densification using resin impregnation not only did not affect the mass transport in the subsequent CVD treatment but would also provide more deposition area for the following CVD due to shrinking of the impregnated resin away from the crack walls during the re-carbonisation stage. This resulted in a more efficient densification for the planar cracks in the CD process. As Figure 4.48 shows, three or four layers of pyrolytic carbon (see A region) could be observed in the planar cracks in the composite processed by CD. For the bundle cracks, a large amount of resin coke could be introduced into a wide bundle cracks when the second densification treatment was a resin impregnation. In contrast, the thin layer of pyrolytic carbon deposited in such a crack in the CD process was small compared to the impregnated resin coke. Thus the voidage in the bundle cracks was reduced to a less extent. As expected, the voidage in the inter-fibre pores and cracks could not be reduced by the second densification using CVD (Figure 4.46 c). Corresponding to these changes, a similar density to CC and lower open porosity resulted from the densification by CD (Figures 4.44 and 4.45).

After CD processing, further densification using either CVD or resin impregnation failed to reduce the voidage in the planar cracks but decreased further the voidage in the bundle cracks. At this stage, resin impregnation appears to be more effective. In addition to the bundle cracks, a little decrease in the voidage of the inter-fibre pores and cracks can also be observed in the third cycle densified by resin impregnation (Figure 4.46c).

From the results obtained from the densification of the PAN based composites, a general view regarding the application of the densification techniques can be made. The inter-fibre pores and cracks in the PAN based composites were so narrow at their necked positions that the resistance to the mass transportation in the CVD treatment was too high to permit access of reactant. Thus to densify these voids, the CVD technique

could not be utilised. Only resin impregnation is applicable. If the processes must involve CVD treatment, resin impregnation should be the early densification stage, thus preventing some inter-fibre pores and cracks being sealed off by the CVD treatment.

To densify the planar cracks, if the densification includes two cycles, both DC and CD are superior to the corresponded DD and CC. As indicated earlier, the cracks narrowed by the first densification by CVD increased the resistance to the mass transportation for the subsequent CVD but was favourable to the subsequent resin impregnation, whereas the first densification using resin impregnation did not affect the resistance to mass transport for the subsequent CVD and also created more area for deposition. Based on this analysis, the ease of the above processes for further densification is likely to follow such a sequence: $CD < DC < DD < CC$. In this sequence, the materials after CD treatment is the most difficult to be subjected to further densification. During the processing, the infiltrated resin cracking away from the crack walls left thin cracks which, on the subsequent CVD treatment, were amenable to blockage. Thus after CD, neither CVD nor resin impregnation could further reduce the voidage in the planar cracks (Figure 4.46 c). Being easier than CD, DC may be suitable for further resin impregnation. After DC processing, the planar cracks were densified to a state which corresponded to the three cycles of densification by multiple CVD (Figure 4.43 a). According to the mechanism of multiple CVD densification, the planar cracks in the composites after DC processing are difficult to densify further using the CVD technique. However it is possible to utilise further resin impregnation because the second densification by resin impregnation tended to densify the cracks mostly by way of narrowing rather than blocking. The lowest voidage in the planar cracks is expected to be achieved by the multiple resin impregnation. This would involve many treatment cycles. From economic considerations, DC and CD are recommended.

For the bundle cracks, the best route seems to be the first densification using CVD, followed by resin impregnation. From the the previous discussion, it has been established that many bundle cracks are wide in the PAN fibre based composites. If the first densification uses resin impregnation, the wide bundle cracks would not be densified according to the mechanism of multiple resin impregnation. Therefore the efficiency of the whole densification process initiated by this route would not be high, especially for a low number of cycles of densification because one cycle is wasted. In contrast, the first densification using CVD has high efficiency to densify the wide

bundle cracks. The more important factor is that the cracks narrowed by the first CVD are favourable for subsequent resin impregnation. From the results obtained, two cycles of the densification by DC could reduce the voidage to a level which required at least three cycles of densification by other processes. A very low voidage of the bundle cracks is expected to be achieved by either DC followed by multiple resin impregnation or continuous multiple impregnation.

It should be recognised that the rules discussed above were based on the consideration of how to fill the various types of voids effectively. In fact, improvement of the quality of the composites rely on not only how much carbon is introduced into the voids but also the properties of the infiltrated matrix and its ability to bond to the void walls. Therefore in application of the rules, these factors together with the influence of the types of voids on the mechanical properties have to be considered.

4.2.2 Pitch Fibre Reinforced Composites

Densification of the pitch fibre reinforced composites was carried out using the same conditions as applied when densifying the PAN based composites. Studies on these materials concentrated on two cycle processes. However selected routes for further densification were also investigated.

4.2.2.1 Experimental Results

The voidage of the composites processed by two cycles of densification were measured by image analysis. An outline of changes in voidage is shown in Figure 4.49 while the changes in detail are illustrated in Figures 4.50 to 4.53. In the figures, C1 again refers to the carbonised preforms and D and C to a CVD and a resin impregnation/carbonisation stage respectively. In contrast to the voidage in the PAN fibre reinforced carbonised preform, it is clear from Figure 4.49 that for the carbonised preform based on the pitch fibres, changes of voidage primarily occurred in the inter-fibre voids, and it is this voidage which is influenced mostly by the densification processes. For these two types of voids, the lowest voidage was obtained by CC processing. The other three processes filled the inter-fibre pores to the same extent (Figure 4.50). However, for inter-fibre cracks, densification by DD was less efficient. DD and DC again gave rise to a similar volume of voidage (Figure 4.51).

Voidage distributions of the inter-fibre pores and cracks were also measured. Figure 4.54 shows the variation of the voidage in the direction normal to the cloth layers. The difference in the voidage between the area near the external surface and that at the centre generally increased in the order of CC, CD, DC and DD, the central area containing a higher voidage.

The bundle and planar cracks were not markedly influenced by the densification. In Figure 4.52, DD and DC appear to be more effective than CC and CD in the densification of the bundle cracks. The pitch fibre reinforced carbonised preform contained a low voidage in the planar cracks. Thus changes in this type of voidage during densification are difficult to observe. Nevertheless, some filling of the cracks did occur on densification (Figure 4.53).

Additional information on the processes was obtained by investigation using polarised-light microscopy. For the composite densified by the DD process, pyrolytic carbon was observed in all types of voids and was apparently thicker in the area near the external surface. Here a thicker layer of carbon was deposited in the wide cracks than in small pores but the carbon in the wide cracks was concentrated at the crack entrance. The carbon deposited in the central area was quite thin, its thickness appearing similar to that in the small pores. Viewed under low magnification, only the entrances of the bundle cracks were apparently narrowed by the CVD densification. Otherwise the size of the bundle cracks was not much affected. It seems that the reduced voidage of the bundle cracks shown in Figure 4.52 was a result primarily of narrowing of the crack entrances.

In the composite densified by the CC process, furfuryl alcohol resin coke was observed in the planar and inter-fibre pores and cracks but not in the bundle cracks. The resin coke appeared to be well bonded to void walls in the inter-fibre pores and exhibited stronger anisotropy than the original resin coke formed by the phenolic resin PHB, whereas in the inter-fibre cracks, bonding between the penetrated resin coke and the crack walls was poor. The resin appeared either suspended in the crack centre or incompletely attached to the crack walls.

Examination of the composites processed by CD and DC showed that the new matrix phase introduced by the second densification was rarely observed in the

inter-fibre pores. It was readily identified in the inter-fibre cracks near the external surface but became less and less obvious towards the centre of the composites. For the bundle cracks, a few pieces of impregnated resin coke could be seen near the external surface in the composite processed by DC. However such a phase was not present in the composite densified by CD.

Further densification following the above two cycles of treatment was investigated by application of a few selected routes. Variation of voidage in these processes is given in Table 4.3. The data suggest that further CVD treatment after either CD or DC does not densify all types of void. In each stage, densification by CDCD appears to be effective in filling the planar cracks and the inter-fibre pores and cracks.

4.2.2.2 Remarks

A quite different behaviour from the PAN fibre based composites was observed in the densification of the pitch fibre reinforced composites. For the pitch fibre based composites, the densification mainly occurred by filling the inter-fibre pores and cracks rather than the planar and bundle cracks. This is the consequence of the pitch fibre reinforced carbonised preform containing a large number of open inter-fibre pores and cracks and a small proportion of planar cracks. Such a structure is analogous to the globe domain as illustrated in Figure 4.55. The difference between this structure and the domain shown in Figure 4.29 is that the thin capillaries connecting the globes are no longer only planar cracks but mostly inter-fibre pores and cracks. The bundle cracks as well as some planar cracks act as the globes. For such a structure, densification would be controlled by the properties of the thin capillaries, i.e., the inter-fibre pores and cracks. Capability of densification in every stage depends on the structure of the thin capillaries resulting from the previous treatment.

In such a situation, the globes would be difficult to fill by both CVD and resin impregnation. When using the CVD technique, even supposing a concentration gradient of the reactant is not established in the mass transport routes, the thickness of pyrolytic carbon deposited in the void walls could not exceed the radius of the thin capillaries. As a result, the infiltrated carbon may take up a high proportion of the volume of the thin capillaries but only a minor volume fraction of the globes.

Resin impregnation appears a useful approach to fill the globes. However, long processing involving many cycles would be required. In the first cycle, according to the analysis in 4.2.1.2, it is difficult for the resin to penetrate into the globes. For the pitch fibre composites, even the second cycle is also difficult because the equivalent length of the thin capillaries in Figure 4.55 is much longer than that in the PAN fibre composites.

From these analyses, the combined process CD should not be effective in densification of the globes since the first densification by resin impregnation is ineffective and the subsequent CVD, even if the thin capillaries were not narrowed or blocked, can only fill the globes to a small extent.

In the process DC, although the void network narrowed by CVD would be favourable for the densification of the globes in the subsequent resin impregnation, some blockage of thin capillaries by CVD tends to isolated globes and to form one dimensional ink-bottle structures as shown in Figure 4.56. Thus the isolated globes can not be further densified. A one dimensional ink-bottle structure is likely to hinder the ingress of the resin over a long distance. The consequence of these effects is that only a few bundle cracks near the external surface can be densified.

In general, resin impregnation has a stronger capability of densifying small voids than CVD according to the discussion in 4.2.1. However this ability is influenced by void size and structure. If the neck diameter of the voids is very small, only resin impregnation can be utilised. The inter-fibre pores and cracks in the PAN fibre composites belong to this type. As the neck diameter increases, the resistance to mass transportation in CVD treatment decreases. At a certain diameter, the voids become accessible to CVD densification in the first cycle. However the second densification is still hindered because most of the voids are blocked. The inter-fibre pores in the pitch fibre composites are this type of void. Compared to the PAN fibre reinforced carbonised preform, poorer physical bonding at the fibre/matrix interface and the high proportion of open voids in the pitch fibre carbonised preform suggest that the neck diameter of the inter-fibre pores in the pitch fibre carbonised preform was larger than the inter-fibre pores and cracks in the PAN fibre based carbonised preform. For this structure, the second densification in processes DD, DC and CD was hindered. In the first two processes, hindrance was caused by blocking with pyrolytic carbon while in CD, the voids were narrowed by the resin impregnation in a manner similar to the inter-fibre pores and cracks in the PAN fibre composites so that the second

densification using CVD is ineffective. However the voids narrowed in the first densification using resin impregnation would not hinder the subsequent resin impregnation. As a result, the lowest voidage in the four processes was obtained by two cycles of resin impregnation (Figure 4.50). From this discussion, further densification after DD and DC would be difficult. Multiple resin impregnation seems the best process for densification of the inter-fibre pores. However it was of interest that voidage of the inter-fibre pores could be further decreased by CDCD processing (Table 4.3). Perhaps further devolatilisation of the furfuryl alcohol resin coke introduced in the first cycles and the newly impregnated resin, reopened some of the closed voids. Thus the third densification using resin impregnation behaved more as void re-opening rather than void filling. The little change in the voidage by the third densification and marked decrease in the final densification using CVD appear to support this point of view.

When the neck diameter of the voids increased to the range corresponding to the inter-fibre cracks in the pitch fibre reinforced carbonised preform, the first densification by CVD did not block all the voids but generated a certain number of narrowed open voids. For such a structure, the subsequent densification using resin impregnation manifested its advantage so that DC processing exhibited a higher efficiency in densification of the inter-fibre cracks than DD (Figure 4.51). A higher efficiency than DD was also obtained by CD because less blocking occurred during the first densification using resin impregnation. After the two cycles of densification, the cracks were blocked or narrowed to a similar environment to the inter-fibre pores, hence rules for further densification as discussed for the inter-fibre pores could be utilised.

Capillary effect of resin impregnation is confirmed from the order shown in Figure 4.54. Densification using resin impregnation tended to fill the voids in all positions while a degradation, in terms of degree of densification, resulted from CVD treatment. On this basis and in conjunction with the above discussion, multiple resin impregnation appears to be the optimum route to fabricate dense pitch fibre reinforced composites.

4.2.3 Rayon Fibre Reinforced Composites

Structural features of the carbonised preforms presented in 4.1.3 suggest that the

rayon fibre reinforced composites should be analogous to the pitch fibre based composites in terms of densification behaviour. The simplified void model shown in Figure 4.55 can be also applied to the rayon fibre composites. The main difference is that the globes in the rayon fibre composites were mostly crimp voids rather than X-X inter- and intra-bundle cracks. Nevertheless behaviour on densification of this type of composite would be expected to obey to some extent the rules derived for the densification of the pitch fibre composites. Thus in formulating the research programme, extensive study on the densification of the rayon fibre composites was not included. Only a DCDCD fabrication process was investigated to confirm the prediction.

The change of voidage during the process, as measured by image analysis, is shown in Figure 4.57. As stated earlier, a large proportion of the planar and bundle cracks were crimp voids in the rayon fibre composites so that the sum of the voidage of the planar and bundle cracks could approximately represent the voidage of the crimp voids or globes. The trend of the changes is similar to those for densification of the pitch fibre composites. Marked decrease in voidage occurred in the inter-fibre pores and cracks in the first two cycles of densification, DC. Further densification after DC was ineffective in filling these two types of void. The globes were almost unaffected by the densification treatment. Detailed information on the variation of voidage of the planar and bundle cracks, shown in Figure 4.58, indicates that small decrease of voidage in the planar cracks and bundle cracks in Figure 4.57 is due primarily to the decrease of voidage in of inter-layer cracks and X-X inter-bundle cracks in the first two cycles of the densification. Some of these cracks also acted as thin capillaries in the simplified void model. This was confirmed by the investigation of the composites using optical microscopy. Figures 4.59 a and b show the individual change of voidage of the inter-fibre pores and inter-fibre cracks respectively. In contrast to effects observed during densification of the pitch fibre reinforced composites, following the first densification using CVD, the second densification using resin impregnation was still effective in filling of the inter-fibre pores. This implies that the neck diameter of inter-fibre pores in the rayon fibre reinforced carbonised preform is larger than that in the pitch fibre based preform. In fact, of the three types of carbonised preforms, the poorest bonding at fibre/matrix interface was observed in the rayon fibre reinforced materials.

Volume porosity of the composites at selected stages of the densification process

was measured by the water penetration method. These results are illustrated in Figure 4.60. During the early stage of densification, processing filled some voids and closed others. However in the later stages, possibly starting after DC treatment according to Figure 4.60 as well as Figure 4.57, processing tended to close some of the remaining open voids without filling them. Apparently surface coating occurred. This result illustrates a very important fact that closed porosity could be present in the composites processed at any stage. Hence mechanical properties of a composite are not necessarily dependent on open porosity, although good correlation of mechanical properties and open porosity can be achieved in some cases^[172]. This again emphasises the importance of using image analysis to develop an understanding of the influence of voids on mechanical properties of composite materials.

4.2.4 Summary

The void structures of the materials studied could be described by two models according to their densification behaviour. Both models were three dimensional ink-bottle domains connected by thin capillaries. For the PAN fibre based composites, the planar cracks acted as thin capillaries and the bundle cracks as globes, whereas for the pitch and rayon fibre reinforced composites, the thin capillaries were mostly the inter-fibre pores and cracks. During the densification, the thin capillaries behaved as roads for mass transport so that their properties, and the changes therein on processing, controlled the overall densification rate and efficiency.

Densification mainly occurred in planar and bundle cracks for the PAN fibre based composites and in inter-fibre pores and cracks for the pitch and rayon fibre reinforced composites. The capillary effect played an important role during resin impregnation while in CVD densification, for the conditions applied, the overall reaction rate was controlled by diffusion.

The efficiency of the densification depends on the void structure and densification technique applied. In general, thin voids are filled readily by resin impregnation due to the capillary effect and on carbonisation, shrinkage of the resin away from the void walls creates further narrow voids which are susceptible to further resin impregnation. These voids tend to be blocked easily by CVD treatment. As void thickness increases, the capillary effect in resin impregnation tends to weaken, while resistance to mass

transport would decrease. In the medium range, alternate utilisation of the two densification techniques can give a higher efficiency than other combinations using two densification cycles. The reason is that first densification using CVD increases the capillarity of the voids by narrowing the voids without substantial blockage so that the narrowed voids are more suitable for subsequent resin impregnation, whereas the first densification using resin impregnation can create more deposition area for the subsequent CVD treatment due to the resin shrinkage from the void walls. For wide cracks, the capillary effect no longer plays an important role during the resin impregnation. Hence they are difficult to fill in the first cycle treatment using resin impregnation. Consequently they are more readily filled by the CVD treatment. These cracks are globes in the ink-bottle domain system. Therefore their position and surrounding thin capillary structure are also important in determining the densification efficiency.

The breadth of the voids and their densification behaviour in two cycles of densification treatments are summarised in Figure 4.61. The four types of void in the three types of carbonised preform are divided into six groups, A to F, each being shaded differently in the figure depending on its behaviour in the two stage densification processes. The thin capillaries are in groups A to D. The minimum thickness (neck diameter) of the voids also increases in this order. It can be seen that the change of the average breadth of the voids does not relate well to the increase of the minimum thickness of the voids when the voids are small. This is because the breadth measured here is the minimum Ferets' diameter which does not truly represent the real breadth for ring- and crescent- shaped voids. The small (thin) voids mentioned above have average breadth less than 20 μm and are in the groups A to C. These three groups differ in the sequence of densification efficiency with the exception of the CC process. The advantage of resin impregnation over CVD can be hindered in these processes if the minimum thickness of the voids is too small and is generally shown up as the minimum thickness of the voids increases. Behaviour of group D is in accord with that of the voids in the medium size range. This range is likely to have average breadth between 20 to 28 μm . Above this size range, the voids are wide cracks. Groups E and F are in this category and are globes in the ink-bottle domain networks. Densification of these cracks is not only influenced by the crack thickness but also by the thin capillary structure. Densification of these cracks in the rayon and pitch fibre reinforced composites is more effective using CVD treatment than that in the PAN fibre composites.

Disregarding processing time, the maximum degree of densification of all types of voids is possibly obtained by multiple resin impregnation with infinite cycles of densification. However it is doubtful whether mechanical properties would be a corresponding maximum due to the poor bonding between the impregnated resin coke and void walls, and to thermal damage by long periods of repeated heating and cooling. To solve these problems, the influence of the voidage in different types of voids has to be studied. This will be addressed in the next chapter.

4.3 THE STRUCTURE IN RELATION TO MECHANICAL PROPERTIES OF THE COMPOSITES

The previous chapter discussed approaches to maximise the filling of all types of voids in the composites. In fact, mechanical properties of C/C composites are determined not only by voids but also by properties of fibres and matrix, bonding at fibre/matrix interface, fibre orientation and weave pattern etc.. Hence the influence of some types of voids on mechanical properties can be obscured by either of these factors. When this occurs, comprehensive consideration of densification of the voids should concentrate on those void types having a noticeable effect.

Contribution of the mechanical properties of the fibres and the matrix to the strength of composites has been discussed in the literature review. Results in this chapter are intended to give an appreciation of the relationship between the structure and mechanical properties of the composites so as to find how to improve weak properties.

4.3.1 Fractography

Failure behaviour of fully processed composites subjected to longitudinal tensile, flexural and delamination tests was studied by scanning electron microscopy (SEM). It was found that, no matter what densification processes had been utilised, composites produced from the same type of fibre cloth prepreg exhibited a similar fracture morphology. These morphologies are shown in Figures 4.62 to 4.64.

Fractographs in Figure 4.62 are for the three types of composites subjected to the longitudinal tensile strength test. The graph on the left illustrates a corresponding typical stress/strain diagram. For the PAN fibre reinforced composites, the fibres fractured in groups. Each group had a relative flat and common fracture (Figure 4.62c). Such a fracture corresponds to catastrophic failure of the composites as shown line c of the graph. Before the catastrophic failure, the composites experienced a stage where the stress/strain curve indicated a departure from purely elastic behaviour.

Fractographs of both the pitch and rayon fibre reinforced composites show large amounts of fibres protruding out of the major fracture plane. The stress/strain curve of

these composites also has a similar appearance. Tough behaviour is exhibited after the elastic range. The stress firstly increased to an ultimate stress and then decreased until complete failure.

Fracture surfaces of the composites which failed by flexural bending are similar to those broken by longitudinal tension (Figure 4.63). Stress/strain relations in flexural bending test appear to decrease step-wise after the ultimate point and the composites exhibited tougher behaviour due to non-uniform stresses than that obtained in the longitudinal tensile strength test. Among the materials studied, a much steeper curve was observed for the PAN fibre based composites.

Delamination of the composites was studied by both short beam three-point-bending test and manual cleavage. The manual cleavage was designed to obtain a delaminated fracture normal to the layer direction. Figure 4.64 depicts micrographs of delaminated fracture surfaces created by cleavage together with the stress/strain curves recorded from the short beam bending test. A flat, compact and brittle fracture was observed for the PAN fibre reinforced composites (Figure 4.64c). Failure in this type of material appears as matrix fracture and fibre debonding from the matrix at inter-layer interfaces. Neither debonded fibres within the bundles nor broken fibres can be seen on the fracture surface. In contrast, cleavage surfaces of the pitch and rayon fibre composites were observed to have broken and debonded fibres (Figures 4.64 a and b). The broken fibres were mostly present at crimp positions. The rayon fibre reinforced composites appears to have more broken fibres on the fracture surface. Debonding of fibres was observed both at interlayer interfaces and within the fibre bundles.

On the typical stress/strain diagram shown, the rate of stress decrease after the ultimate point is much slower than that in longitudinal tensile and flexural bending tests. The pitch and rayon fibre composites have a relative smooth curve while for the PAN fibre reinforced composites, a crenellated shaped line is seen when the strain exceeds the ultimate point.

Fracture by all the above mentioned tests tended to show that stress transfer within the bundles was sufficient in the PAN fibre reinforced composites. Mechanical properties of the composites are weakened by insufficient stress transfer at interfaces between cloth layers or fibre bundles. Hence they would be controlled by bonding and

voids at these interfaces. Improvement of strength of this type of material should be attained by to improving these factors. Toughness of the composites, when subjected to a uniform tensile stress (longitudinal tensile stress test), would not be much affected by the strengthening due to original brittle behaviour within the bundles. However, when non-uniform tensile and compressive stresses (flexural strength test) and shear stresses are applied, the toughness might be reduced by the strengthening.

Failure behaviour of the rayon and pitch fibre reinforced composites is similar and exhibited tough fracture in all the tests utilised. Damage initiation and propagation could be influenced by properties at interfaces of all types. Even in delamination tests, fracture could occur within the fibre bundles. Figure 4.65 shows fracture of a fully processed rayon fibre composite tested to failure in the interlaminar shear strength test. Failure involved both interlaminar and intra-laminar fracture. Thus improvement of strength of the rayon and pitch fibre composites should be directed towards strengthening all types of interfaces. In all the densification processes studied, toughness of the composites did not decrease markedly so that there is still further potential to strengthen the interfaces without markedly reducing toughness. It is interesting to find that fibre strength also contributes to interlaminar shear strength for these two types of materials. From geometrical consideration, composites with a large crimp angle would involve more fibres participating in this effect. As a result, rayon fibre reinforced composites contained more broken fibres on the fracture surface than the pitch fibre reinforced composites.

4.3.2 Bonding at Fibre/Matrix Interface

From the above results, it appears that fracture behaviour of the composites is related to bonding at the fibre/matrix interface. Also in the densification study, it was found that properties at the fibre/matrix interface were important in determining densification behaviour of the composites. The diversity of bonding at the fibre/matrix interface is likely caused by surface properties of the raw materials as used in the composites. To understand this, X-ray photoelectron spectroscopy (XPS) was used to study surface properties of the carbon fibres and the cured resin.

XPS measurements were carried out on a VG ESCALAB MK1 using Al K α X-rays of energy 1486.6 eV at a power of 200W and in a residual vacuum 10^{-6} Pa.

Measurements were made with the analyser in a fixed transmission mode and normal to the plane of the sample surface. All peaks were referenced to the major C-C/C-H 1s peak at 284.6 eV. Surface composition was calculated using the areas of the respective photoelectron peaks after background correction.

Surface composition of the raw materials measured by XPS is shown in Table 4.4. The PAN fibres supplied were resin prepregs so they were not measured. However since it is known that the PAN fibres are medium modulus type, their surface composition should lie between high and low modulus PAN based carbon fibres. Surface properties of these two types of fibres were supplied by the Institute of Surface Science And Technology, Loughborough University of Technology. These data are listed at the bottom of the table.

In the fibres listed, high and low modulus PAN based carbon fibres contained a high content of oxygen on their surfaces. It can be reasonably assumed that oxygen on the PAN fibres studied should not be less than that on the high modulus PAN based carbon fibres. Hence the PAN fibres must contain a higher content of surface oxygen than the rayon and pitch fibres. The surface oxygen content of the rayon and pitch fibres is small. The pitch fibres, being treated by carbonisation, contained 1.8 mol% oxygen on the surfaces while the rayon fibres, being treated at graphitisation temperature, only had 0.9 mol% oxygen on the surfaces. The two types of phenolic resin, as expected, contained much higher oxygen levels than the carbon fibres.

Many researchers have found that chemical bonding of carbon fibres with the matrix is achieved via surface oxide groups^[173-175]. During pyrolysis, the chemical bonding between the surfaces of carbon fibres and the free functional groups in the resin undergo rearrangements. Some of the chemical bonds may change to C-C or C=C linkages between the carbon fibres and the resin coke, whilst others may lead to enhanced physical adhesion between the two. Hence strong bonding at fibre/matrix interface in C/C composites could be associated with a high oxygen content on surfaces of the carbon fibres. The PAN fibre composites, with a high content of oxide groups on the fibre surfaces, exhibited strong bonding at the fibre/matrix interfaces and gave rise to brittle fracture in the mechanical tests, whereas for the rayon and pitch fibre composites, the small amounts of oxide groups on the fibre surfaces were not sufficient to form strong bonding at their fibre/matrix interfaces and thus led to pull-out of the fibres in tensile and flexural strength tests and debonding of the fibres and intra-laminar

fracture in delamination tests.

Structure of voids located between the fibres is also strongly influenced by the fibre surface properties. On the micrographs illustrated in Figure 3.4b and Figure 4.7, voids between the fibres consist of discrete, short and crescent-shaped cracks, intra-matrix pores and cusp-shaped pores in the PAN fibre based carbonised preform, long crescent-shaped cracks in the pitch fibre based carbonised preform and interlinking cracks which almost encircle each of the fibres in the rayon fibre based carbonised preform. Strong bonding of fibres with the matrix is associated with the structure of the inter-fibre voids in the PAN fibre composites. The voids in this type of material appear to be poor interlinked in the two dimensional polished section. The unvoided fibre/matrix interface is tightly contacted. The discrete, short and crescent-shaped cracks are probably formed by shrinkage of resin due to variable strength of initial bonding with surrounding fibres. Resin is then forced to shrink away from the relatively poorly contacted fibres and firmly to bond with the others during pyrolysis. If resin is equally bonded with its surrounding fibres, pyrolysis of the resin tends to form intra-matrix pores. Formation of the cusp-shaped pores is considered to be due primarily to a tight packing arrangement of the fibres.

Structures of inter-fibre voids in the rayon and pitch fibre composites correspond to poor bonding at the fibre/matrix interface. The difference in oxygen content on fibre surfaces between the two types of fibre brings about a diversity in the morphology of the voids between the fibres. The pitch fibres, having a relatively high content of oxide groups on their surfaces, appear to have a larger contact area at the fibre/matrix interface than the rayon fibres (Figure 4.7). The inter-fibre pores in the pitch fibre reinforced carbonised preform are basically long crescent-shaped cracks, while in the rayon fibre reinforced carbonised preform, the fibres are almost debonded from the matrix.

With such an understanding, the reason for differences in behaviour on densification of the materials studied can be sought. The structure of the globe/thin capillary domains is determined by bonding conditions at the fibre/matrix interface. In the case of fibre surfaces containing a high content of oxide groups such as the PAN fibres studied, pyrolysis of resin tends to form plenty of closed porosity within the fibre bundles and large planar and bundle cracks. This results in poor interlinking between the inter-fibre voids and the bundle cracks, while planar cracks act as thin capillaries. The formation of closed porosity by obtaining a tight bonding at the

fibre/matrix interface was also observed by Manocha et al.^[176]. In their work, open porosity of unidirectional carbonised preforms decreased as improvement of bonding at fibre/matrix interfaces occurred.

Poor bonding at the fibre/matrix interface in the rayon and pitch fibre composites ensures a good interlinking of the voids within the bundles so that, in Figure 4.9, almost all voids were open in the carbonised preforms of these two types of material. In such a case, a majority of the thin capillaries are inter-fibre pores and cracks. The difference in content of surface oxide groups between the two types of composite results in different morphology of inter-fibre pores, which lead to different behaviour in densification. The inter-fibre pores in the composites with the poorest bonding at the fibre/matrix interface (rayon fibre based composites) are more amenable to multiple cycles of densification treatments than those in the pitch fibre reinforced composites. From this discussion, it is clear that the different behaviour in densification between groups A, B and C shown in Figure 4.61 is controlled by the bonding conditions at the fibre/matrix interface.

4.3.3 Influence of Voidage on Strengths of The Composites

Much of the work in fabrication of C/C composites is spent on reducing the porosity of the highly porous carbonised preforms. Thus it is important to understand the influence of porosity on mechanical properties of the composites. However it has been recognised that many factors are related to mechanical properties of the composites. Changing any of them may cause striking fluctuations in the strengths of the composites. Hence the influence of porosity on the strengths has to be studied under conditions in which other factors are relatively constant. With such a restriction, it is not surprising that mechanical property data useful for this purpose is very limited despite a large number of materials having been examined in this project. In the following discussion, a quantitative correlation of porosity or voidage and mechanical properties will be attempted, with reference to a particular densification process for composites with weak bonding at the fibre/matrix interface and a process involving two CVD densification steps with composites with strong bonding at the fibre/matrix interface.

4.3.3.1 Composites with Weak Bonding at The Fibre/Matrix Interface

Quantitative study of the relationship between composite strength and porosity for the composites with weak bonding at the fibre/matrix interface was based on the rayon fibre reinforced composites at various stages of the densification process, DCDCD. These materials were 31mm diameter disks so that only ultimate diametral compression-failure-load (UDCFL) and transverse compressive strength were measured.

The densification process, DCDCD has been studied in 4.2.3. It was expected that the mechanical properties of the composites would not respond markedly to the change of open porosity in this process because a large amount of closed porosity formed as processing progressed. Especially in the last resin impregnation/CVD cycle, the remaining porosity was not densified but some of the open voids were blocked forming closed porosity. The expectation was confirmed by the relationship of the UDCFL and open porosity as shown in Figure 4.66. The increase of UDCFL was not invariably accompanied by a corresponding reduction of the open porosity .

Correlations of UDCFL and voidage of planar cracks and inter-fibre pores and cracks are illustrated in Figures 4.67 and 4.68 respectively. Good linear relationships appear on the two graphs. There is also an excellent linear relationship between UDCFL and transverse compressive strength for these materials (Figure 4.68). Thus both UDCFL and transverse compressive strength would have similar relationships with open porosity, voidage of planar cracks and voidage of inter-fibre pores and cracks.

In the diametral compression test, failure occurred by delamination. The effect is similar to transverse tension. Thus both UDCFL and transverse compressive strength represent delamination resistance. This appear to be the reason for a linear relationship present between UDCFL and transverse compressive strength. Based on this analysis, the above correlations demonstrate relations between voids fraction and delamination resistance. Fractographic study discussed in 4.3.1 has shown that the fraction in delamination of the composites with weak bonding at fibre/matrix interface involves both interlaminar and intra-laminar fracture (Figure 4.65). Hence interface quality at inter-layers, X-X inter-bundles and fibre/matrix need to be enhanced in order to improve the ability to resist delamination. This was achieved by filling voids at the interfaces with matrix carbon so that, in Figures 4.67 and 4.68, UDCFL increases

with decrease of voidage of planar cracks and inter-fibre pores and cracks. Experiments in the present study were not organised to obtain a relationship between relevant voids fraction and strength in fibre direction. However it can be predicted from the results of fractographic study that reduction of all types of voids tends to increase strength in the fibre direction for the rayon and pitch fibre composites.

4.3.3.2 Composites with Strong Bonding at The Fibre/Matrix Interface

Study of the influence of voidage on mechanical properties of the composites with strong bonding at fibre/matrix interface was based on the PAN fibre composites in the group PAN-RC. These materials contained 18 cloth layers and were densified by two cycles of CVD treatments. The variation of voidage in the different types of voids was created by changing processing conditions. These conditions are listed in Table 4.5.

Table 4.5 also shows the mechanical properties of the materials. Although these mechanical properties include flexural strength and modulus and interlaminar shear strength (ILSS), many data are invalid because an inappropriate failure mode occurred during the tests. It appears that only flexural strength and modulus of the composites processed by constant thickness moulding can be utilised for the purpose of this study.

In the four types of void characterised, previous results have shown that inter-fibre pores and cracks can not be densified for the PAN fibre composites in CVD treatments. This was also observed for the listed materials subjected to two cycles of CVD densification under various conditions. Therefore Table 4.5 only gives information on the planar and bundle cracks.

Relationships of voidage with flexural strength as well as modulus for the composites processed by constant thickness moulding are plotted in Figures 4.70 to 4.73. It is surprising to find that flexural strength and modulus are related to the voidage of the planar cracks rather than the bundle cracks. A divergent distribution was obtained between voidage of bundle cracks and flexural strength as well as flexural modulus (Figures 4.70 and 4.71), whilst flexural strength and modulus data are linearly related to the voidage of the planar cracks (Figures 4.72 and 4.73). The flexural strength and modulus increase as voidage of the planar cracks falls. This result appears to be contradictory to common knowledge and the result obtained by Kohno et al.^[163].

However microscopic observation revealed that the voids in the composites used for correlation were somewhat unusual. Some planar cracks in these materials have a high breadth which was similar to the length of the bundle cracks (Figure 4.74 position A). Actually they are much bigger than a normal bundle crack and act as both planar and bundle cracks. Hence this type of void would be more effective in influencing flexural properties. As a result, tensile failure occurred in both short and long beam bending tests, yet flexural strength and modulus were not dependent on voidage of the bundle cracks but voidage of the planar cracks.

This result adds a complexity to consideration of the contribution of the voidage of planar and bundle cracks to the mechanical properties of the composites. Their influence is not as simple as initially expected. Not only bundle cracks but also planar cracks can participate in determining flexural strength and modulus depending on the breadth of the planar cracks. In case of all planar cracks being thin, though local high stresses could be created in a fibre bundle adjacent to planar cracks, much higher stresses, either tension or shear, could be present in the inter-layer matrix surrounded by interlayer cracks. Hence the matrix between cloth layers and at X-X inter-bundle interfaces would be the weakest sites in the bending tests. Failure, in this situation, is likely to initiate and propagate from planar cracks. Composites tend to fail in shear mode. The composites processed by constant pressure moulding, their properties and microstructure are given in Table 4.5 and Figure 4.74b, show this type of behaviour. ILSS of these materials would be associated with voidage of planar cracks. If the above composites have a good bonding at inter-layer, and X-X inter-bundle interfaces, or contain many weak sites in the fibre bundles, tensile fracture could occur in the long beam bending test. In this case, flexural strength and modulus would be governed by voidage of bundle cracks. The final situation is that the composites contain very thick planar cracks as observed in the particular group of materials studied. Tensile failure could occur in both long and short beam bending tests. Flexural strength and modulus of the composites should be predominantly controlled by voidage of the planar cracks.

Thus to improve tensile and shear resistances of the composites with strong bonding at fibre/matrix interface, densification should be aimed at filling the voidage of planar and bundle cracks. For these materials, if bonding at the fibre/matrix interface is too good, undesirable brittle fracture in the fibre bundles will result. Thus densification should avoid filling those voids any further.

4.4 INFLUENCE OF PRE-DENSIFICATION PROCESSING ON VOID STRUCTURE OF THE COMPOSITES

It has been acknowledged that voids are the major factor to influence quality of C/C composites. To achieve desired mechanical properties, an expensive operation, the densification, has to be applied to fill the voids in the composites. Almost all voids in C/C composites are formed in processing before the densification. Thus if the void formation could be controlled effectively in these stages, the production cost would be reduced by shortening the densification process. In addition to the consideration of the production cost, it is clear from the results obtained that some types of void such as the "globes" in the ink-bottle domain models, have a significant effect on the mechanical properties of the composites but these are difficult to fill effectively using the densification techniques investigated. Hence efforts should be made towards effective control of the void formation in processing before the densification. The results presented here permit comment on these subjects.

4.4.1 The Void Formation

The void formation in the composites has been mentioned in 4.1 and 4.3.2. The results given here aim to identify what type of void was created in which processing stage rather than mechanism of the void formation. The mechanism of the formation of voids in different stages will be discussed in the following relevant section.

The void formation was studied by examining both the moulded and carbonised preforms using polarised-light microscopy. The micrographs of the three types of carbonised preform have already been given in Figures 3.4, 4.7 and 4.8. Figures 4.75 and 4.76 respectively show micrographs of the three types of moulded preform viewed at high and low magnification. The resin in the moulded preforms has a relatively low reflectance and appears similar to the epoxy resin used to embed the samples for the carbonised preforms. The black areas in the micrographs of the moulded preforms are voids.

By comparison of Figure 4.75 to Figures 3.4b and 4.7, it is clear that the inter-fibre pores and cracks in the carbonised preforms were essentially formed during the

carbonisation stage. Almost all the space between the fibres in the moulded preforms was fully filled with the cured resins. The perfect physical bonding at fibre/resin interface was observed in the PAN fibre reinforced moulded preform (Figure 4.75a), whereas, in the moulded preforms produced from the pitch and rayon fibres, incomplete bonding of the fibres occurred in a few areas (Position D in Figure 4.75 b and c).

Some bundle cracks in the PAN and pitch fibre reinforced composites were initiated in moulding processing (Figures 4.76 a and b) and were further widened and lengthened in the carbonisation stage. Since the number of the bundle cracks in the moulded preforms was less than in the carbonised preforms, it is considered that the other bundle cracks in the carbonised preforms were created during the carbonisation stage. Jortner's results obtained from the observation of the crack formation using a microscope with a hot stage^[162] support this view. In his experiments, when a moulded preform was heated to 500 °C, it was observed that new bundle cracks were formed during the heating.

The planar cracks in the PAN fibre composites were formed in a similar way to the bundle cracks in the PAN and pitch composites. However major planar cracks in the rayon and pitch fibre composites were created in the carbonisation stage. A crimp position in the rayon and pitch fibre reinforced moulded preforms were well filled with resin (Figures 4.76 b and c) so that the crimp voids in these materials were formed in the carbonisation stage (Figures 4.7 b and c). In the PAN fibre reinforced moulded preform (Figure 4.76a), cracks in crimp positions can be observed. Similar to the planar and bundle cracks, both moulding and carbonisation participated in initiation and propagation of the crimp voids in the PAN fibre composites.

4.4.2 Moulding Processing

The above results indicated that crack formation in the moulding process mostly occurred in processing of the PAN fibre reinforced materials. Based on this type of material, influence of different moulding techniques applied on the crack formation was investigated.

It is clear from the results shown in Table 4.5 and Figure 4.7 that the composites

processed by constant pressure moulding contained less planar and bundle cracks and exhibited a higher bending strength. In contrast, constant thickness moulding processed composites had a higher content of planar and bundle cracks and a lower bending strength. The average thickness of the composites was respectively 4.1 mm and 4.7 mm for the materials processed from constant pressure and constant thickness moulding methods, yet they both contained 18 layers of carbon fibre cloth. The two techniques utilised the same heating programme during the operation. Thus the major difference between the two moulding methods lies in the moulding pressure applied. It is apparent from the thickness data that the constant pressure moulding applied a higher pressure than the constant thickness method.

During the curing process, the pressure applied acts to consolidate the fibre cloth layers and plies and to squeeze out excess resin and entrapped air so that the void content in the composites can be minimised. Thus it is not surprising that the content of the planar cracks is reduced by increasing the moulding pressure. However picturing how the formation of the bundle cracks is affected by the moulding pressure is not straightforward.

The formation of the bundle cracks appears to be associated with surface properties at the fibre/resin interfaces. Purslow has found that the surface tension at the fibre/resin interface tends to draw the fibres together under zero pressure applied at the commencement of curing^[177]. By this effect, resin rich positions between which the fibres are gathered into several groups may be formed within a fibre bundle so that the X-X intra-bundle cracks could be created at the resin rich positions on shrinkage during solidification. The X-X inter-bundle cracks are also readily formed in this case because bulk shrinkage of the composites can not accommodate the larger bundle shrinkage. This situation is likely to occur in the materials with strong bonding at the fibre/matrix interface because strong bonding at the fibre/matrix interface corresponds with a high surface tension. This explains why the materials with a high content of surface oxygen (the PAN fibre composites) more readily form bundle cracks than the materials with a low surface oxygen content, e.g. the rayon fibre composites.

The decrease of voidage of the bundle cracks on increasing the moulding pressure is considered to result from the increasing spatial constraint of the fibres. It was observed from the experiments that the fibre volume fraction increased with the moulding pressure. In the constant pressure moulding processed composites, the

materials contained 70 vol% carbon fibres, whilst the fibre volume fraction in the constant thickness moulding processed composites was only 61vol%. The mobility of the fibres within a bundle is reduced by the increased compaction at the commencement of curing. Thus the possibility to form resin rich areas within the fibre bundles is decreased. Further the formation of the X-X intra-bundle cracks is also decreased. In addition to the X-X intra-bundle cracks, the formation of the X-X inter-bundle cracks also tends to decrease when a high moulding pressure is applied. The reason is that the decreased resin content reduces the bundle shrinkage and thus improves the compatibility between the bulk and bundle shrinkage.

Although the planar and bundle cracks in the PAN fibre composites can be reduced by applying a high moulding pressure, the moulding pressure should not be too high, otherwise breakage and distortion of the fibres could occur. This, of course, does not improve the quality of the composites.

4.4.3 Carbonisation

Influence of carbonisation conditions on quality of the composites was studied using the PAN fibre based carbonised preforms and fully processed composites, containing 18 cloth layers. The carbonisation was carried out under two conditions. Condition A applied a relatively slow heating rate, 20 °C/h, to heat the materials to a maximum temperature of 1050 °C. A relatively fast heating rate, 60 °C/h, was utilised in condition B to heat the materials to a maximum temperature of 870 °C. The fully processed composites were fabricated by using two further cycles of CVD treatment under a pressure of 29-73 mPa and a temperature of 875 °C.

Some properties of the carbonised preforms and fully processed composites are given in Table 4.6. In both the moulding processes applied, the fully processed composites produced from the condition A exhibited better mechanical properties than those from the condition B. It appears that improvement of the mechanical properties in the former materials is due primarily to a high weight gain obtained during the densification so that porosity in these materials is filled more effectively. However, the weight gain data are not easy to reconcile with the open porosity of the carbonised preform. The open porosity of the carbonised preforms was independent of the moulding conditions applied. Values of approximately 15% and 21% respectively were

found for the preforms carbonised under conditions A and B. Usually the more open porosity a carbonised preform contains, the more weight should be gained in the composites during the densification. In contrast, for these materials, the results obtained indicate that the preforms with lower open porosity gained more pyrolytic carbon. One possible explanation is that carbonisation condition A favoured large voids and B small voids. To test this view, the open porosity distribution was studied using mercury porosimetry. This result is shown in Figure 4.77.

In Figure 4.77, the content of the open voids is expressed as cumulative intrusion volume of the voids per unit weight material, P_m , in the ordinate axis, while the values in the abscissa axis are natural logarithm of the void diameter in the macropore range (void diameter > 50 nm). The two curves almost overlap in the overall macropore size range except the void diameter exceeding 15 μm , i.e., 2.7 ($\ln 15$) in the abscissa axis on the graph. The close values of P_m at the void diameter 50 nm ($\ln 0.05 = -3$) for the two materials indicate that the "extra" open porosity in the preform carbonised under the condition B is indeed small voids whose size is below the macropore range. The voids with diameter over 15 μm are considered as large voids relevant perhaps to the planar and bundle cracks because this value is close to the upper limit of diameter of the inter-fibre cracks, $(500/\pi)^{1/2} = 12.6 \mu\text{m}$ calculated by assuming the cracks to have circular cross-section. This result appears to support the above view.

The difference in open porosity of the carbonised preforms is likely to be caused by the heating rate rather than the maximum temperature applied during the carbonisation. Otherwise the preforms carbonised at the higher temperature should generate more open porosity. The influence of the heating rate on void formation of the composites could be through affecting either pyrolysis or pressure and temperature gradients. The pressure and temperature gradients formed across the thickness of the composites were studied by Nam and Seferis^[178]. Pressure build-up in the composites is caused by decomposed gases being trapped within the matrix network, while the temperature gradients result from heat transfer via the solid constituents and energy loss by gas evolution. Both the pressure and temperature gradients may introduce internal stresses and undesirable deformation leading to development of the void structure in the composites. In a certain range, the heating rate could markedly influence the pressure and temperature gradients. Nam and Seferi's results showed that the pressure and temperature gradients tended to increase with the heating rate. Thus more porosity

could be generated by applying a higher heating rate.

In order to confirm whether the above mechanism can be applied to explain the current results obtained, plates of phenolic resin PHA varying in thickness were carbonised using the same conditions as used for the composites. Open porosity of the resin chars is given in Table 4.7. The data in the table do not appear to support the above explanation. Firstly, for the resin plates with a same thickness, the resin chars carbonised using a higher heating rate contained a much higher open porosity than those carbonised using a lower heating rate. This implies that the "extra" open porosity in the carbonised preforms processed from the condition B are small pores present within the matrix. The voids caused by high pressure and temperature gradients are usually large cracks rather than the small voids within the matrix. Secondly, for the same carbonisation condition, the thicker plates of resin chars contained a lower open porosity than the thin plates. If the "extra" open porosity in the preforms carbonised by the condition B is caused by high pressure and temperature gradients, the thicker plates should contain more open porosity because a higher pressure and temperature gradients could be built-up in the thicker plates. This contravention may have resulted from different heating ranges applied in the studies. In this study, the maximum heating rate was 60 °C/h, whilst the heating rates used in Nam's experiments exceeded 120 °C/h. Due to a lower heating rate being applied in the current study, the pressure and temperature gradients may no longer play an important role in exerting a marked influence on the void formation in the composites.

The influence of the heating rate on the void formation is then considered to be via its effect on the pyrolysis of the resin under the conditions used. It is common knowledge that increasing the heating rate can shift the apparent temperature of the resin decomposition and gas evolution to a higher range. This is caused by the lack of sufficient time to complete the decomposition reaction at a higher heating rate. As a result, more decomposition gases generate and flow out of the material in a narrower range, resulting in turbulent gas flow and forming more open porosity in the resin char. In the case of carbonisation of a thicker resin plate, permeability of gas evolution is lower in comparison with a thin plate. The poorer permeability tends to resist the decomposed gases flowing out of the materials leading to the generation of lower open porosity.

It is clear from this result that the heating rate during the carbonisation is

important in development of void structure in the PAN fibre based carbonised preforms. The influence of heating rate on void formation is through its effect on pressure and temperature gradients in the case of higher heating rates, $>120\text{ }^{\circ}\text{C/h}$ and on the pyrolysis of the resin at lower heating rates of less than $60\text{ }^{\circ}\text{C/h}$. In the higher range, a fast heating rate can cause formation of large cracks in the preforms, while in the lower range, a quick heating rate is associated with the generate of small open voids within the matrix. No matter in what range, a slow heating rate is favourable for the production of the desired structure of the carbonised preforms for subsequent densification and fabrication of high quality of the composites.

5. CONCLUSIONS

(1) Careful study of the structure of carbonised preforms has revealed the presence and positions of many types of voids in two directional woven carbon fibre reinforced carbon composites. Large voids were classified according to orientation into planar and bundle cracks. The planar cracks, most of which occur between fibre cloth layers, are considered to be essentially important in consideration of interlaminar shear strength, while the bundle cracks are appropriately aligned perpendicular to the cloth layers and are considered essentially important in influencing the flexural strength of the composites. Small voids within the fibre bundles were classified according to their cross-sectional size into inter-fibre pores and cracks which are associated with physical bonding at the fibre/matrix interface.

(2) Based on this classification, a quantitative method to characterise the void structure in the composites was developed by means of image analysis. This method is able to give quantitative information of the highly anisotropic void structure by analysis of voidage and geometrical properties of the characterised voids on $0^\circ/90^\circ$ and $45^\circ/45^\circ$ cross-sections of the composites. The data obtained have proved useful in understanding the structure of the composites, the mechanisms of densification and the relationship between the structure and mechanical properties of the composites.

(3) Three types of carbonised preforms studied included all the structural features of voids present in a wide variety of 2-D woven carbon/carbon composites. The planar and bundle cracks are prominent in the PAN fibre reinforced carbonised preforms, inter-fibre cracks in the pitch fibre preforms and inter-fibre pores in the rayon fibre preforms. These materials form a group of model materials ideally suited to the study of the densification of 2-D C/C composites.

(4) The void structure in the carbonised preforms is associated with surface oxygen of the carbon fibres. A higher content of surface oxygen in the PAN fibres tends to form tight bonding at the fibre/matrix interface via chemical reaction. As a result, the PAN fibre reinforced carbonised preforms contained large amounts of planar and bundle cracks and many closed inter-fibre pores and cracks. The rayon and pitch fibres had a low oxygen content on the surfaces so that, in their carbonised preforms, more than 95% of total porosity was open. A relatively higher voidage in the inter-fibre cracks in

CONCLUSIONS

the pitch fibre reinforced carbonised preforms is due primarily to a lower fibre content within the fibre bundles.

(5) The planar and bundle cracks in the PAN fibre composites are initiated at both the moulding and carbonisation stages of processing. Within the range of conditions applied, these cracks in the moulded preforms can be reduced by applying a higher moulding pressure.

(6) The inter-fibre pores and cracks in all types of composite studied and crimp voids in the rayon fibre composites were essentially formed during the carbonisation step of the processing. Formation of these voids can not be avoided and changing carbonisation conditions has little effect.

(7) For the two conditions applied to carbonise the PAN fibre materials, the preforms carbonised at a higher heating rate contained 7% more open porosity than those carbonised at a low heating rate. This "extra" open porosity occurred as small pores present within the matrix and could not be filled by CVD densification.

(8) The void structure of the materials studied could be described by two models according to their densification behaviour. Both models were three-dimensional ink-bottle domains connected by thin capillaries. For the PAN fibre based composites, the planar cracks acted as thin capillaries and the bundle cracks as globes, whereas for the rayon and pitch fibre reinforced composites, the thin capillaries were mostly the inter-fibre pores and cracks.

(9) The densification mostly occurred in the planar and bundle cracks for the PAN fibre based composites and in inter-fibre pores and cracks for the rayon and pitch fibre reinforced composites. The capillary effect played an important role during resin impregnation while in CVD treatment under the conditions used, the overall reaction rate was diffusion controlled.

(10) The efficiency of the densification depends on the void structure and the densification technique applied. In general, thin voids are filled readily by resin impregnation due to the capillary effect and are easily blocked by CVD treatment. In contrast, wide cracks are more readily filled by CVD than resin impregnation. In this case, the capillary effect no longer plays an important role during the resin

CONCLUSIONS

impregnation. In the medium size range, alternative utilisation of the two techniques can give a higher efficiency than other combination processes if the densification involves two cycles. For the materials studied, the thin voids had average breadth less than 20 μm , the medium range 20 to 28 μm and the wide cracks over 28 μm . The wide cracks are usually globes in the ink-bottle domain void system so that their position in the composites and surrounding thin capillary structure are also important in determining the densification efficiency.

(11) In delamination tests of the rayon and pitch fibre composites, both interlaminar and intra-laminar failure occurred. Hence the delamination strengths were influenced by not only the planar cracks but also the inter-fibre pores and cracks. Linear relationships between diametral compression load and both voidage of the planar cracks and voidage of inter-fibre pores and cracks were obtained for the rayon fibre composites. The diametral compression load of the composites did not respond markedly to the change of the open porosity since a large proportion of closed voids formed during the densification. In addition to the voids, the fibre tensile strength also participates in contributing to the ILSS of the rayon and pitch fibre composites. It was observed that some fibres fractured at crimp positions in the rayon and pitch fibre composites during delamination tests. The number of fractured fibres was related to crimp angle of the fibre cloths. A larger crimp angle resulted in more fractured fibres on the fracture surface.

(12) For the PAN fibre reinforced composites, flexural properties of the composites could also be controlled by the planar cracks when the planar cracks had a breadth similar to the length of the bundle cracks. A good linear relationship between voidage of the planar cracks and the flexural properties (strength and modulus) was obtained in this case.

(13) For all the densification processes applied, the PAN fibre reinforced composites exhibited brittle fracture in tensile, flexural and interlaminar shear strength tests, whereas tough fracture occurred in the rayon and pitch fibre composites. To improve strengths of the composites, densification should aim towards filling the planar and bundle voids in the PAN fibre composites and all types of voids in the rayon and pitch fibre composites.

6. RECOMMENDATIONS FOR FUTURE WORK

6.1 CAPILLARITY OF MODELLED VOID STRUCTURES IN RESIN IMPREGNATION

It has been recognised from this project that the wide bundle cracks in the ink-bottle domains were difficult to fill during the resin impregnation. It has not been confirmed whether imbibition or drainage played the more important role during the densification. Therefore a detail study of capillarity of modelled structure in various environments of liquid impregnation is necessary to develop effective technology to fill the wide cracks.

6.2 MODELLING OF FAILURE INITIATION AND DEVELOPMENT IN 2-D C/C COMPOSITES

Significant progress on the quantitative characterisation of void structure and correlation of void structure with mechanical properties of the composites has been achieved in this project. However, the limited number of samples and the strength tests used were insufficient to give a thorough understanding of failure initiation and development in the composites and to allow modelling of the influence of void structure on mechanical properties. Future work on this field is recommended to achieve prediction of strength and reproduction of high quality of 2-D C/C composites.

7. APPENDIX DEVELOPMENT OF STATISTICAL METHOD FOR DETERMINING NUMBER OF MEASURING FIELDS

Translated into statistical language, the question of how many fields are needed to provide a good representation of all the available fields may be expressed as what minimum sampling size should be taken from a population under a given error restriction. With this translation, the average voidage obtained from all available fields, N will be the true value or population mean voidage, μ ; and the standard deviation of μ will be the population standard deviation, σ :

$$\mu = \frac{\sum_{i=1}^N V_i}{N} \quad (A-1)$$

$$\sigma = \sqrt{\frac{\sum_{i=1}^N (V_i - \mu)^2}{N-1}} \quad (A-2)$$

where V_i is voidage on an individual field.

According to the central limit theorem, no matter what a population distribution is like, sampling distribution is exactly normal for any sampling size, n , i.e.

$$\frac{X_m - \mu}{\sigma_{X_m}} = Z_{\alpha/2} \quad (A-3)$$

where

$$X_m = \sum_{i=1}^n \frac{V_i}{n}$$

is the mean voidage for a sampling size, n . The sampling standard deviation, $\sigma_{X_m}^2$ equals:

$$\sigma_{X_m}^2 = \frac{N-n}{N-1} \frac{\sigma^2}{n} \quad (A-4)$$

By changing Eq.(A-3) to the following form

$$\frac{X_m - \mu}{\mu} = \frac{Z_{\alpha/2} \sigma_{X_m}}{\mu} \quad (A-5)$$

it is found that the left side of the equation is the relative error, ϵ which is relevant to the sampling size, n . When setting a certain restriction of relative error ϵ , a minimum sampling size can be obtained by the replacement of σ_{X_m} in Eq. (A-5) with (A-4)

$$\frac{Z_{\alpha/2}}{\mu} \sqrt{\frac{N-n}{N-1} \frac{\sigma^2}{n}} \leq \epsilon \quad (A-6)$$

Finally

$$n \geq \frac{\sigma^2 Z_{\alpha/2}^2 N}{\mu^2 \epsilon^2 (N-1) + \sigma^2 Z_{\alpha/2}^2} \quad (A-7)$$

8. REFERENCES

- [1] **Advanced Composites Engineering** 1990, **5**, p. 7.
- [2] Fitzer, E and Heine, M., Paper presented at **World Conference on Resource Material Conversion**, Den Haag, June 25-29, 1984.
- [3] Gill, R. M., **Carbon Fibres in Composite Materials**, The Butterworth Group, London, 1972, p. 9.
- [4] Fitzer, E., **Carbon Fibres And Their Composites**, Ed. Fitzer, E., Springer-verlag, New York, 1983, pp. 4-45.
- [5] **Financial Guardian**, Tuesday, April 19, 1983, p. 23.
- [6] **Newsweek**, February, 1982, p. 36.
- [7] Fitzer, E., **Journal de Chimie Physique** 1984, **81**, 718.
- [8] Fitzer, E., **Pure And Applied Chemistry** 1988, **60**, 288.
- [9] Fitzer, E., **Carbon** 1987, **25**, 163.
- [10] Curry, D. M.; Scott, H. C. & Webster, N. C., **SAMPE** 1979, 1524-1539.
- [11] Edwards, I.A.S., **Introduction to Carbon Science**, Ed. Marsh, H., Butterworths, London, 1989, p. 3.
- [12] Pauling, L., **Journal of American Chemical Society** 1931, **53**, 1367.
- [13] Dewar, M. J. S. and Thiel, W., **Journal of American Chemical Society** 1977, **99**, 4907.
- [14] Hassel, D. and Mark, H., **Zeitschrift fur Physik** 1924, **25**, 317.
- [15] Bernal, J. D., **Proceedings of The Royal Society of London** 1924, **A106**, 749.
- [16] **ICCTC, Proceedings of The Fifth London International Carbon And Graphite Conference**, Vol. 3, Society of Chemical Industry, London, 1978, pp. 113-115.
- [17] **ICCTC, Carbon** 1982, **20**, 445.
- [18] Franklin, R. E., **Proceedings of The Royal Society of London** 1951, **A209**, 196.
- [19] Lekhnitskii, S. G., **Theory of Elasticity of An Anisotropic Elastic Body**, Holden-Day, Inc., NewYork, 1963.
- [20] Ashton, J. E.; Halpin, J. C. and Petit, P. H., **Primer on Composite Materials: Analysis**, Technomic, Inc., Stamford, 1969.
- [21] Love, A. E. H., **A Treatise on The Mathematical Theory of Elasticity**, Cambridge University Press, London, 1927.

REFERENCES

- [22] Kelly, B. T., **Physics of Graphite**, Applied Science Publishers Ltd., London, 1981.
- [23] Johnson, D. J., **Introduction to Carbon Science**, Ed. Marsh, H., Butterworths, London, 1989, p. 203.
- [24] Polanyi, M., *Zeitschrift fur Physik* 1921, 7, 323.
- [25] Brenner, S. S., **Fibre Composite Materials**, American Society for Metals, Metals Park, 1965, p. 12.
- [26] Inglis, C. E., *Trans. Inst. Naval Arch.* 1913, 55, 219.
- [27] Griffith, A. A., *Phil. Trans. R. Soc. London* 1920, A221, 163.
- [28] Griffith, A. A., **Proceedings of The First International Congress on Applied Mechanics**, Ed. Biezeno, C. B. and Burgers, J. M., Waltham, Delft, 1924, p. 55.
- [29] Anderson, J. C., Leaver, K. D. and Rawlings, R. D. et al., **Materials Science, Fourth Edition**, Chapman And Hall, London, 1990, p.220.
- [30] Losty, H. H. W., **Modern Aspects of Graphite Technology**, Ed. Blackman, L. C. F., Academic Press, London, 1970, pp.202-221.
- [31] Sharp, J. V. and Burnary, S. G., **Plastics And Polymers-Conference Supplement No.6**, 1971, p68.
- [32] Reynolds, W.N. and Sharp, J. V., *Carbon* 1974, 12, 103.
- [33] Amelinckx, S., Delavignette, P. and Heerschap, M., **Chemistry And Physics of Carbon, Vol. 1**, Ed. Walker, P. L., Jr., Edward Arnold Ltd., London, 1965, PP. 1-71.
- [34] Fitzer, E. and Heine, M., **Composite Materials Series, 2: Fibre Reinforcements for Composite Materials**, Ed. Bunsell, A. R., Elsevier, Amsterdam, 1988, pp. 73-148.
- [35] Blakslee, O. L., Proctor, D. G., Seldin, E. J. et al., *Journal of Applied Physics* 1970, 41, 3373.
- [36] Jenkins, G. M. and Jouquet, G., *Nature* 1966, 212, 1507.
- [37] Jenkins, G. M. and Jouquet, G., *Carbon* 1968, 6, 85.
- [38] Jenkins, G. M., *Carbon* 1969, 7, 9.
- [39] Johnson, D. J., *Chemistry And Industry* 1982, 18, 692.
- [40] Bacon, G. E., *Journal of Applied Chemistry And Biotechnology* 1956, 6, 477.
- [41] Reynolds, W. N., **Chemistry And Physics of Carbon, Vol. 11**, Eds. Walker, P. L., Jr., Thrower, P. A., Marcel Dekker, New York, 1973, pp. 1-67.

REFERENCES

- [42] Jenkins, G. M., **Chemistry And Physics of Carbon**, Vol. 11, Eds. Walker, P. L., Jr., Thrower, P. A., Marcel Dekker, New York, 1973, pp. 190-242.
- [43] Clauser, H. R., **Encyclopedia / Handbook of materials, Parts and Finishes**, Technomic, Westport, 1976, p. 55.
- [44] Brady, G. S. and Clauser, H. R., **Materials Handbook**, Twelfth Edition, McGraw-Hill, New York, 1986, p. 137.
- [45] CRC, **Handbook of Chemistry And Physics**, 72nd Edition, Ed. Lide, D. R., CRC press, Boca Raton, 1991, pp. 4-7.
- [46] Bacon, R., **Journal of Applied Physics** 1966, **31**, 283.
- [47] Iijima, S., **Nature** 1991, **354**, 56.
- [48] Schutzenberger, P. and Schutzenberger, L., **C. R. Acad. Sci.** 1890, **111**, 774.
- [49] Gibson, J., Riley, H. L. and Taylor, T., **Nature** 1944, **154**, 554.
- [50] Hillert, M and Langer, N., **Z. Krist.** 1958, **111**, 24.
- [51] Onuma, Y. and Koyama, T., **Oyo Butsuri** 1963, **32**, 875.
- [52] Tibbetts, G. G., **Applied Physics Letters** 1983, **42**, 666.
- [53] Koyama, T., Endo, M. and Onuma, Y., **Japanese Journal of Applied Physics** 1972, **11**, 445.
- [54] Weisbeck, R., **Carbon** 1971, **9**, 525.
- [55] Edison, T. A., **U.S. Patent 223989**, 1879.
- [56] Abbott, W. F., **U.S. Patent 3053775**, 1962.
- [57] Cohota, K., Shinoya, I and Metzler, A., **Extended Abstracts of International Symposium on Carbon**, Toyohashi, Carbon Society of Japan, Tokyo, 1982, p. 30.
- [58] Schulz, D. A., **U.S Patent 3919376**, 1975.
- [59] Singer, L. S., **U.S. Patent 3919387**, 1975.
- [60] Johnson, D. L. and Tyson, C. N., **Journal of Physics, D, Applied Physics** 1970, **3**, 526.
- [61] Franklin, R. E., **Proceedings of The Royal Society of London** 1950, **A209**, 196.
- [62] Brooks, J. D. and T aylor, H., **Carbon** 1965, **3**, 185.
- [63] Sanada, Y., **Fuel** 1973, **52**, 143.
- [64] Bacon, R., **Chemistry And Physics of Carbon**, Vol. 9, Ed. Walker, Jr., P. L. and Thrower, P. A., Marcel Dekker, New York, 1973, pp. 2-102.
- [65] Fourdeux, A., Perret, R. and Ruland, W., **Proceedings of The First**

REFERENCES

- International Conference on Carbon Fibres**, Plastics Institute, London, pp. 57-62.
- [66] Johnson, D. J., **Chemistry And Physics of Carbon**, Vol. 20, Ed. Thrower, P. A., Marcel Dekker, New York, 1973, pp. 2-102.
 - [67] Bacon, R. and Schalamon, W. A., **The Eighteenth Biennial Conference on Carbon**, American Carbon Committee, Buffalo, N. Y., June 1967, Paper MI-58.
 - [68] Spry, W. J., **British Patent 1093084**, 1967; **U.S. Patent 3454362**, 1969.
 - [69] Gibson, D. W. and Langlois, G. B., **ACS Polymer Preprints** 1968, 9, 1376.
 - [70] Johnson, D. J. and Tyson, C. N., **Journal of Physics, D, Applied Physics** 1969, 2, 787-795.
 - [71] Allen, S., Cooper, G. A., Johnson, D. J., et al. **Proceeding of The Third London International Conference on Carbon and Graphite**, Society of Chemistry and Industry, London, 1970, pp. 456-461.
 - [72] Great Lakes Carbon Corp., **U.S. Patent 3533743**, 1970.
 - [73] Dauksys, R. J. and Ray, J. D., **Journal of Composite Materials** 1969, 3, 684.
 - [74] Jenkins, G. M. and Kawamura, K., **Polymeric Carbon: Carbon Fibre Glass And Char**, Cambridge Univ. Press., New York, 1976, P. 44.
 - [75] Fitzer, E. and Huttner, W., **Proceedings of The International Meeting on Strength And Structure in Carbon And Graphite**, The Institute of Physics, Bath, 1979, p.32.
 - [76] Kelly, A. and Tyson, W. R., **High Strength Materials**, Ed. Zackay, V. F., Wiley, New York, 1965, p.578.
 - [77] Fitzer, E. and Burger, A., **Proceedings of The First International Conference on Carbon Fibres**, Plastic Institute, London, 1971, p.134.
 - [78] Aveston, J., Cooper, G. A. and Kelly, A., **The Properties of Fibre Composites**, National Physical Laboratory, IPC Science And Technology Press Ltd., Surrey, Guildford, 1971 pp. 15-26.
 - [79] Agarwal, B. D. and Broutman, L. J., **Analysis And Performance of Fibre Composites**, John Wiley & Sons, NewYork, 1980, p. 36.
 - [80] Lackman, W. L., Crawford, J. A. and McAllister, L. E., **Proceedings of International Conference on Composite Materials**, Eds. Noton, B. et al., Metallurgical Society of AIME, NewYork, 1978.

REFERENCES

- [81] Crawford, J. A., U. S. Patent 3949126, 1976.
- [82] McAllister, L. E. and Taverna, A. R., **Proceedings of The Seventeenth National SAMPE Symposium**, SAMPE, Azusa, 1972, p. III-A-3.
- [83] McAllister, L. E. and Taverna, A. R., **Proceedings of International Conference on Composite Materials**, Vol. 1, Eds. Scala, E., et al., Metallurgical Society of AIME, New York, p. 307.
- [84] Mullen, C. K. and Roy, P. J., **Proceedings of The Seventeenth National SAMPE Symposium**, SAMPE, Azusa, 1972, p. III-A-2.
- [85] Weibull, W., **Journal of Applied Mechanics** 1951, 18, 243.
- [86] Moreton, R., **Fibre Science And Technology** 1968, 1, 273.
- [87] Barker, R. L., **Journal of Engineering for Industry** 1978, 100, 1.
- [88] Hsiung, P. L. and Rowe, G. R., **The Fourteenth Biennial Conference on Carbon**, American Carbon Committee, PennState University, 1979, p.226.
- [89] Chamis, C. C., **Fracture And Fatigue**, Ed., Broutman, L. J., Academic, New York, 1974.
- [90] Tsai, S. W. and Azzi, V. D., **AIAA Journal** 1966, 4, 296-301.
- [91] Whitney, J. M. and Muismer, R. J., **Journal of Composite Materials** 1974, 8, 253.
- [92] Potter, R. T., **Proceedings of The Royal Society of London** 1978, A361, 325.
- [93] Kendall, K., **Proceedings of The Royal Society of London** 1975, A344, 287.
- [94] Pierson, H. O., Granoff, B., Schuster, D. M., et al., **Proceedings of The First International Conference on Carbon Fibres**, Plastic Institute, London, 1971, p.161.
- [95] Hasselman, D. P. H., **Journal of The American Ceramic Society** 1963, 46, 564.
- [96] Schmidt, D. L., **SAMPE J.** 1972, 8, 9.
- [97] Gibson, D. W., McGhee, K. B. and Stroup, R. C., U.S. Patent 3174859, 1965.
- [98] Bickerdike, R. L. and Hughes, G., U.S. Patent 3233014, 1966.
- [99] Stoller, H. M. and Frye, E. R., **Proceedings of AIAA / AIME of The Tenth Structures, Structural Dynamics And Materials Conference**, New Orleans, 1969, p.193.
- [100] Kotlensky, W. V. and Pappas, J., **The Ninth Biennial Conference on Carbon**, American Carbon Committee, Boston, 1969, Paper MP-26.

REFERENCES

- [101] Rohl, C. W. and Robinson, J. H., U.S. Patent 3462289, 1969.
- [102] Hough, R. L., U.S. Patent 3462340, 1969.
- [103] Zhao, J., Liu, J., Zhou, D. and Zhu, K., The Nineteenth Biennial Conference on Carbon, American Carbon Committee, PennState, 1989, p. 328.
- [104] Sohn, K. Y., Oh, S. and Lee, J., Carbon 1988, 26, 157.
- [105] Manocha, L. M., Bahl, O. P. and Singh, Y. K., Carbon 1989, 27, 381.
- [106] Lieberman, M. L. and Pierson, H. O., Carbon 1974, 12, 233-241.
- [107] Pierson, H. O. and Northrop, D. A., Journal of Composite Materials 1975, 9, 118-137.
- [108] Stoller, H. M., Irwin, J. L. and Granoff, B. et al., The Tenth Biennial Conference on Carbon, American Carbon Committee, Lehigh University, 1971, Paper FC-57.
- [109] Newman, S., Composite Materials Technology: Processing And Properties, Eds., Mallick, P. K. and Newmans, S., Hanser Publishers, New York, 1990, pp.1-26.
- [110] McCoy, J. C. and Steele, J. W., U.S. Patent 3700535, 1972.
- [111] Martin, G. R., U.S. Patent 3712428, 1973.
- [112] DeMund, G. P., U.S. Patent 4178413, 1979.
- [113] Jacobs, K. M., Laskaris, A. T. and Herrick, J. W., AIAA 4th Propulsion Joint Specialist Conference, Cleveland, 1968, Paper NO. 68-598.
- [114] Delmonte, J., Technology of Carbon And Graphite Fibre Composites, Van Nostrand Reinhold Company, NewYork, p. 398.
- [115] Leeds, D. H., U.S. Patent 3713865, 1973.
- [116] Sittig, M., Carbon And Graphite Fibres, Manufacture And Applications, Noyes Data Corporation, Park Ridge, New Jersey, 1980, p. 231.
- [117] Williams, R. M., Advances in Structural Composites, Vol. 12, SAMPE, Azusa, 1967.
- [118] Pierson, H. O., Proceedings of 14th National SAMPE symposium, Cocoa Beach, 1968, II4B-2.
- [119] Stoller, H. M. and Frye, E. R., Paper presented at 73rd Annual meeting American Ceramic Society, Chicago, 1971.
- [120] Warren, J. W. and Williams, R. M., Paper presented at 4th National SAMPE Technical Conference, Palo, Alte, 1972.
- [121] Kotlensky, W. V., Chemistry And Physics of Carbon, Vol. 9, Eds.

REFERENCES

- Walker, P. L., Jr and Thrower, P. A., Marcel Dekker, New York, 1973, pp. 173-257.
- [122] Pierson, H. O. and Smatana, J. F., **Chemical Vapour Deposition, Second International Conference**, Eds. Blocher, J. M. Jr. and Withers, J. C., the Electrochemical Society, New York, 1970, p.487.
- [123] Frye, E. R., **Carbon Composite Technology Symposium**, University of New Mexico, 1970, pp. 173-191.
- [124] Gebhardt, J. J., **The Tenth Biennial Conference on Carbon**, American Carbon Committee, Lehigh University, 1971, P.53.
- [125] Leeds, D. H., Kotlensky, W. V. and Smith, W. H., **Proceedings of The 17th Refractory Composites Working Group**, 1971, p.559.
- [126] Pfeifer, W. H., Wilson, W. J. and Griesenauer, N. M. et al., **Chemical Vapour Deposition, Second International Conference**, Eds. Blocher, J. M. Jr. and Withers, J. C., the Electrochemical Society, New York, 1970, p.463.
- [127] Newling, D. o. and walker, E. J., **Proceedings of The First International Conference on Carbon Fibres**, Plastic Institute, London, 1971, p.142.
- [128] Walker, P. L., Jr., **Carbon** 1972, 10, 369.
- [129] Fitzer, E. and Terwiesch, B., **Carbon** 1972, 10, 383.
- [130] Yamada, S. and Tamada, K., **Journal of Composite Materials** 1973, 7, 119.
- [131] Hishiyama, Y., Tamada, K. and Inagaki, H., **High Temperature And High Pressure** 1973, 5, 353.
- [132] Hishiyama, Y., Inagaki, H. and Kimura, S., **Carbon** 1974, 12, 249.
- [133] Raskovic, V. and Otani, S., **Proceedings of 4th International Carbon Conference**, DKG, 1986, p.749.
- [134] Fitzer, E. and Berwiesck, T., **Carbon** 1973, 11, 570.
- [135] Inagaki, M., Washiyama, M. and Kobayaski, K., et al., **Tanso** 1990, No.141, 17.
- [136] Huttinger, K. H. and Rosenblatt, V., **Carbon** 1977, 15, 69.
- [137] McAllister, L. E. and Lachman, W. L., **Handbook of Composites, Vol. 4, Fabrication of Composites**, Eds. Kelly, A. and Milliko, S. T., Elsevier Science Publishers, B. V., New York, 1983, pp. 111-175.
- [138] Burns, R. L. and Cook, J. L., **Petroleum Derived Carbons**, ACS Symposium series Vol. 21, Eds. O'Grady, T. M. and Deviney, M. L.,

REFERENCES

- American Chemical Society, Washington D. C., 1974, p. 139.
- [139] Chard, W., Conaway, M. and Neisz, D., **Petroleum Derived Carbons, ACS Symposium series Vol. 21**, Eds. O'Grady, T. M. and Deviney, M. L., American Chemical Society, Washington D. C., 1974, p. 155.
 - [140] Burns, R. L. and McAllister, L. E., Paper presented at **AIAA/SAE 12th Propulsion Conference**, Palo Alto, 1976.
 - [141] Dietrick, H and McAllister, L. E., Paper presented at **American Ceramic Society 80th Annual Meeting**, Detroit, 1978.
 - [142] Ford, A. R., **Engineer** 1967, 224, 444.
 - [143] Kowbel, W. and Shan, C. H., **Carbon** 1990, 28, 287.
 - [144] Carneire, F. L. L. B. and Barcellos, A., **Union of Testing And Research Laboratories for Materials And Structures, No.13**, 1953.
 - [145] Akazawa, T., **Union of Testing And Research Laboratories for Materials And Structures, No.16**, 1953.
 - [146] Peltier, R., **Union of Testing And Research Laboratories for Materials And Structures, No.19**, 1954.
 - [147] Wright, P. J. F., **Magazine of Concrete Research**, July, 1955, 87.
 - [148] Mitchell, N. B., Jr., **Materials Research And Standard** 1961, 1, 780.
 - [149] Rudnick, A., Hunter, A. R. and Holden, F. C., **Materials Research And Standard** 1963, 3, 283.
 - [150] Patrick, J. W., Stacey, A. E., **Fuel** 1972, 51, 81.
 - [151] Patrick, J. W., Stacey, A. E. and Wilkinson, H. C., **Fuel** 1972, 51, 174.
 - [152] Patrick, J. W. and Walker, A. W., **Journal of Materials Science** 1987, 22, 3589.
 - [153] Booth, R. E. and Yeager, R. E., **International Conference on Carbon'88**, Eds. McEnaney, B., and Mays, T. J., U.K., 1088, p417.
 - [154] Washburn, E. W., **Phys. Rev.** 1921, 17, 273.
 - [155] Moreland, A., **The Structure And Strength of Metallurgical Coke**, PhD Thesis, Loughborough University of Technology, 1990.
 - [156] Mays, T. J. and McEnaney, B., **Proceedings of The Eighteenth Biennial Conference on Carbon**, American Carbon Committee, Worcester, 1987, p438.
 - [157] Delesse, M.A., **C. R. Acad. Sci. Paris** 1847, 15, 544.
 - [158] Underwood, E.E., **Quantitative Stereology**, Addison-Wesley, Massachusetts, 1970.
 - [159] Anderson, J. C., Leaver, K. D., Rawlings, R. D. and Alenander, J. M.,

REFERENCES

- Materials Science, Fourth Edition**, Chapman And Hall, London, p91.
- [160] Jortner, J., **Proceedings of Army Symposium on Solid Mechanics**, AMMRS MS 76-2, U.S. Army Materials And Mechanics Research Centre, 1976, pp.81-97.
 - [161] Jortner, J., **Carbon** 1986, **24**, 603.
 - [162] Jortner, J., **Carbon** 1992, **30**, 153.
 - [163] Kohno, T., Kurosaki, K. and Herai, T., **The Twentieth Biennial Conference on Carbon**, American Carbon Committee, Santa Barbara, 1991, p394.
 - [164] Peebles, L.H., Meyer, R.A. and Jortner, J., **Interfaces in Polymer, Ceramic And Metal Matrix Composites**, Ed. Ishid, H., Elsevier, NewYork, 1988, pp.1-16.
 - [165] Meyer, R.A., **The Nineteenth Biennial Conference on Carbon**, American Carbon Committee, PennState, 1988, p.334.
 - [166] Ford, B.A., Cooke, R.G. and Harris, B., **The Seventeenth Biennial Conference on Carbon**, American Carbon Committee, Kentucky, 1985, p.233.
 - [167] Hedden, K. and Wicke, E., **Proceedings of The Third Conference on Carbon**, Pergamon Press, Oxford, 1957, p.249.
 - [168] Vohler, O., Reiser, P.L. and Sperk, E., **Carbon** 1968, **6**, 397.
 - [169] Seibold, R.W., **SAMPE National Symposium**, Vol. 20, San Diego, California, 1975, p.327.
 - [170] Adamson, A.W., **Physical Chemistry of Surfaces**, Fifth Edition, John Wiley & Sons, Inc., New York, 1990, p.8.
 - [171] Walsh, T.J., **Capillary Properties of Model pores**, PhD Thesis, Loughborough University of Technology, 1989, p.65.
 - [172] Yasuda, E. and Tanane, Y., **Proceedings of The 34th Japan Congress on Materials Research**, Japanese society of materials science , Kyoto, 1991, p.35.
 - [173] Horie, K., Murai, H. and Mita, I., **Fibre Science And Technology**, 253, 1976.
 - [174] Donnet, J. P., Papirer, E. and Dauksch, H., **International Conference on Carbon Fibres**, London, 1974, Paper 9.
 - [175] Fitzer, E., Geigl, K. H. and Manocha, L. M., **Proceedings of 5th Conference on Carbon And Graphite**, Vol. 1, London, 1978, p.405.
 - [176] Manocha, L. M., Bahl, O. P. and Singh, Y. K., **Carbon** 1989, **27**, 381.

REFERENCES

- [177] Purslow, D. and Childs, R., **Composites** 1986, **17**, 127.
- [178] Nam, J. and Seferis, J. C., **Carbon** 1992, **30**, 751.

TABLES

Table 2.1 Bond Lengths (Å) [13]

<u>Hybridisation</u>	<u>Types of bonds</u>	<u>Bond lengths, (nm)</u>
sp^3	C -- H	0.109
sp^2	C -- H	0.1086
sp	C -- H	0.106
sp^3-sp^3	C -- C	0.154
sp^3-sp^2	C -- C	0.150
sp^3-sp	C -- C	0.147
sp^2-sp^2	C -- C	0.146
sp^2-sp^2	C = C	0.134
$sp-sp$	C \equiv C	0.120
	C -- O	0.142
	C = O	0.122

Table 2.2 Bond energies (kJ mol⁻¹) [11]

C -- C	348	C = C	699	C \equiv C	962
C -- H	435	C -- O	351	C = O	581
C -- S	259	C -- N	292	C -- F	441
C - Cl	328	C - Br	276	C -- I	240

Table 2.3 Elastic Constants of Perfect Graphite Crystals^[20]

<u>Elastic stiffness coefficient</u> (GPa)	<u>Elastic compliance</u> (X 10 ⁻¹³ m ² /N)
C ₁₁ = 1060	S ₁₁ = 9.8
C ₁₂ = 180	S ₁₂ = -1.6
C ₁₃ = 15	S ₁₃ = -3.3
C ₃₃ = 36.5	S ₃₃ = 275
C ₄₄ = 4.5	S ₄₄ = 2200

Table 2.4 Estimated Elastic Moduli of A Single Fibre

<u>Fibre type</u>	<u>Modulus, GPa</u>		I ₃ /I ₁	I ₅ /I ₁
	E ₃₃	G ₄₄		
Type I	392	25	0.9882	0.9769
Ideal	1020	15	1	1

Table 2.5 Estimated V_{\min} And V_{crit} for Model C/C Composites

<u>Constituents</u>	<u>Thornel</u>		<u>Phenolic resin</u>
	<u>P-120</u>	<u>P-100</u>	
<u>Tensile strength</u> (MPa)	2200	2200	118
<u>Young's modulus</u> (GPa)	820	690	28
<u>Failure strain</u> (%)	0.2	0.3	(σ/E) =0.42
<hr/>			
<u>Composites</u>	<u>P-120/Phenolic resin</u>		<u>P-100/Phenolic resin</u>
<u>Estimated</u> σ_{Ef}^* , MPa	56		84
V_{\min} , %	2.74		1.52
V_{crit} , %	2.89		1.61

TABLES

Table 3.1 Properties of The Carbon Fibres Used for Producing Woven Cloths

<u>IDENTIFICATION</u>	<u>PAN</u>	<u>Pitch</u>	<u>Rayon</u>
<u>PRECURSORS</u>	PAN	Mesophase pitch	Rayon
<u>TEMPERATURE OF HEAT TREATMENT</u>	Carbonisation	Carbonisation	Graphitisation
<u>BULK DENSITY</u> (kg/m ³)	1760	1880	1500
<u>TENSILE STRENGTH</u>	High	Low	Low
<u>TENSILE MODULUS</u>	Medium	Low	Low

Table 3.2 Properties of The Carbon Fibre Cloths

<u>IDENTIFICATION</u>	<u>PAN-5H</u>	<u>Pitch-5H</u>	<u>Rayon-8H</u>
<u>FIBRES</u>	PAN	Pitch	Rayon
<u>WOVEN</u>	5 H*	5 H	8H**
<u>STRUCTURE</u>			
<u>WEIGHT PER CLOTH AREA</u> (g/m ²)	280	510	250

Note

* 5H: five harness satin weave

**8H: eight harness satin weave

Table 3.3 Densification Route And Processing Conditions of The Materials for Structural And Processing Studies

<u>MATERIALS</u>	<u>Group PAN-SR</u>	<u>Group Pitch-SR</u>	<u>Group Rayon-SR</u>
<u>PREPREGS</u>	PAN-5H + resin PHA	Pitch-5H + resin PHB	Rayon-8H + resin PHB
<u>NUMBER OF LAYERS</u>	12	8	12
<u>DENSIFICATION PROCESSES</u>	Mutiple D multiple C DC, CD DCD, CDD CDC, CCD	CC, DD DC, CD DCD, CDD CDC, CCD CDCD	DCDCD
<u>MOULDING PRESSURE</u> (kPa)	2.1-3.6	2.1-3.6	2.1-3.6
<u>CARBONISATION TEMPERATURE</u> (°C)	1050	1050	870
<u>CVD PRESSURE</u> (mPa)	29-73	29-73	7252
<u>CVD TEMPERATURE</u> (°C)	1050	1050	870

Processing code:

C -- Resin impregnation + carbonisation
D -- Chemical vapour deposition

TABLES

Table 3.4 Materials Varying in Raw Materials, Thickness And Processing Conditions

<u>MATERIALS</u>	<u>Group PAN-RC</u>
<u>PREPREGS</u>	PAN-5H + resin PHA
<u>NUMBER OF LAYERS</u>	18
<u>DENSIFICATION PROCESS</u>	DD
<u>MOULDING PRESSURE</u> (kPa)	2.1-3.6 (CP*), 4-140 (CT**)
<u>CARBONISATION TEMPERATURE</u> (°C)	870, 1050
<u>CVD PRESSURE</u> (mPa)	29-73, 580
<u>CVD TEMPERATURE</u> (°C)	870, 1050

Processing code:

D -- Chemical vapour deposition
 CP -- Moulded by constant pressure method
 CT -- Moulded by constant thickness method

Table 3.5 Typical Mechanical Properties of 2-D C/C Composites^[143]

<u>MATERIALS</u>	<u>I</u>	<u>II</u>	<u>III</u>
<u>TENSILE STRENGTH</u> (MPa)	60	75	61
<u>TENSILE MODULUS</u> (GPa)	65	65	65
<u>FLEXURAL STRENGTH</u> (MPa)	80	120	83
<u>FLEXURAL MODULUS</u> (GPa)	25	28	23
<u>ILSS. (MPa)</u>	3.5	5.0	3.5

TABLES

Table 3.6 Dimensions of A Unit Cell for Studied Materials

<u>CLOTH TYPE</u>	<u>BUNDLE DIMENSIONS</u>		<u>LENGTH OF A UNIT CELL, mm</u>
	<u>WIDTH, μm</u>	<u>HEIGHT, μm</u>	
<u>PAN-5H</u>	1300	140	7.50
<u>Pitch-5H</u>	2000	305	10.50
<u>Rayon-8H</u>	300	215	2.70

<u>MATERIALS</u>	<u>CLOTH TYPE</u>	<u>THICKNESS PER LAYER, mm</u>	<u>DIMENSIONS OF A UNIT CELL</u>	
			<u>LENGTH, mm</u>	<u>HEIGHT, mm</u>
<u>Group PAN-SR</u>	PAN-5H	0.250	7.50	0.75
<u>Group Pitch-SR</u>	Pitch-5H	0.430	10.50	1.29
<u>Group Rayon-SR</u>	Rayon-8H	0.250	2.70	0.75
<u>Group PAN-RC</u>	PAN-5H	0.225, 0.260	7.50	0.68, 0.78

Table 3.7 Minimum Number of Measuring Frames And Relevant Statistical Results

<u>TYPICAL MATERIALS</u>	<u>SPECIMENS WITH CLOTH PAN-5H</u>	<u>SPECIMENS WITH CLOTH Pitch-5H</u>	<u>SPECIMENS WITH CLOTH Rayon-8H</u>
<u>NUMBER OF LAYERS</u>	12	8	12
<u>NUMBER OF UNIT CELLS</u>	8	4	20
<u>μ, %</u>	10.91	9.32	1.63
<u>σ, %</u>	3.53	2.87	0.89
<u>N</u>	196	96	180
<u>$\frac{n}{N}$ CALCULATED</u>	69	58	115
<u>NORMALISED</u>	72	64	120
<u>n PER UNIT CELL</u>	9	16	6

Table 4.1 Basic Properties of Carbonised Preforms

<u>MATERIALS</u>	<u>PAN-SR</u>	<u>Pitch-SR</u>	<u>Rayon-SR</u>
<u>BULK DENSITY</u> (kg/m ³)	1359	1435	1199
<u>THICKNESS</u> (mm)	3.02	3.38	3.04
<u>NUMBER OF LAYERS</u>	12	8	12
<u>VOLUME FRACTION OF FIBRES, %</u>	63.2	57.1	65.7
<u>MASS FRACTION OF FIBRES, %</u>	81.85	74.82	80.19
<u>MASS FRACTION OF MATRIX, %</u>	18.15	25.18	17.81
<u>MEAN CRIMP ANGLE</u>	6°	8°51'	15°51'

Table 4.2 Changes of Weight Loss And Open Porosity of The Composites by Re-carbonisation

<u>MATERIALS</u>	<u>OPEN POROSITY, %</u>		<u>WEIGHT LOSS, %</u>
	<u>Before re-carbonisation</u>	<u>After re-carbonisation</u>	
C1	15.81	23.98	1.84
D2	5.84	6.56	0.80

**Table 4.3 Variation of Voidage during The Densification of The Pitch
Fibre Reinforced Composites**

<u>PROCESSES</u>	<u>PLANAR CRACKS</u>	<u>VOIDAGE, %</u>		<u>INTER-FIBRE CRACKS</u>
		<u>BUNDLE CRACKS</u>	<u>INTER-FIBRE PORES</u>	
<u>C1</u>	0.42	0.91	3.38	1.53
<u>CD</u>	0.25	1.00	2.40	0.69
<u>CDC</u>	0.24	0.72	2.17	0.58
<u>CDCD</u>	0.14	0.87	1.84	0.46
<u>C1</u>	0.42	0.91	3.38	1.53
<u>CD</u>	0.25	1.00	2.40	0.69
<u>CDD</u>	0.39	1.11	2.66	0.84
<u>C1</u>	0.42	0.91	3.38	1.53
<u>DC</u>	0.33	0.68	2.46	0.72
<u>DCD</u>	0.31	0.69	2.88	1.00

Table 4.4 Surface Composition Measured by X-Ray Photoelectron Spectroscopy (XPS)

<u>MATERIALS</u>	<u>ELEMENTAL COMPOSITION ON SURFACE, mol%</u>		
	<u>C</u>	<u>O</u>	<u>N</u>
<u>CURED RESIN</u>			
<u>PHA</u>	88.5	9.0	2.4
<u>PHB</u>	84.2	14.5	1.4
<u>CARBON FIBRES</u>			
<u>Rayon</u>	99.1	0.9	0
<u>Pitch</u>	98.2	1.8	0
<hr/>			
<u>High Modulus PAN</u>			
<u>Carbon Fibres*</u>	96.5	3.2	0.3
<u>Low Modulus PAN</u>			
<u>Carbon Fibres*</u>	92.0	4.7	3.3

* Data supplied by Dr. R. H. Bradley, Institute of Surface Science And Technology, Loughborough University

**Table 4.5 Mechanical Properties And Voidage of The Composites with
Strong Bonding at Fibre/Matrix Interface Processed by Two Cycles of
Densification**

<u>MATERIALS</u>	<u>MOULDING METHODS</u>	<u>CARBONISATION TEMP., °C</u>	<u>CVD PRESSURE, mPa</u>	<u>TEMP., °C</u>
PAN-RC298	CT*	1050	580	875
PAN-RC280	CT	1050	29-73	875
PAN-RC334	CT	1050	29-73	825
PAN-RC343	CT	1050	29-73	1050
PAN-RC289	CT	870	29-73	875
PAN-RC307	CP**	1050	29-73	875
PAN-RC316	CP	870	29-73	875

<u>MATERIALS</u>	<u>FLEXURAL BENDING TEST</u>			<u>ILSS TEST</u>	
	<u>STRENGTH MPa</u>	<u>MODULUS GPa</u>	<u>FAILURE MODE</u>	<u>ILSS MPa</u>	<u>FAILURE MODE</u>
PAN-RC298	45.8	44.2	F***	5.49	F
PAN-RC280	58.4	47.6	F	5.86	F
PAN-RC334	43.5	38.3	F	4.16	F
PAN-RC343	79.3	51.6	F	9.31	F
PAN-RC289	45.2	43.4	F	4.45	F
PAN-RC307	176.6	63.7	S*****	6.56	S
PAN-RC316	124.9	57.1	S	5.21	S

<u>MATERIALS</u>	<u>PLANAR CRACKS</u>		<u>BUNDLE CRACKS</u>	
	<u>VOIDAGE, %</u>	<u>BREADTH, µm</u>	<u>VOIDAGE, %</u>	<u>BREADTH, µm</u>
PAN-RC298	3.30	34.1	2.17	28.3
PAN-RC280	2.78	35.2	1.80	28.7
PAN-RC334	3.37	33.0	2.38	31.4
PAN-RC343	2.12	33.0	1.95	31.8
PAN-RC289	3.15	31.0	1.84	28.1
PAN-RC307	0.70	23.4	0.43	18.7
PAN-RC316	1.93	17.0	0.37	19.3

Note

- * CT: constant thickness moulding
- ** CP: constant pressure moulding
- *** F: tensile fracture
- **** S: shear fracture

**Table 4.6 Properties of The Carbonised Preforms And Composites
Processed from Different Carbonisation Conditions**

	<u>MATERIALS</u>			
	<u>PAN-RC</u> <u>276-284</u>	<u>PAN-RC</u> <u>285-293</u>	<u>PAN-RC</u> <u>303-311</u>	<u>PAN-RC</u> <u>312-320</u>
CARBONISED PREFORMS				
<u>CARBONISATION</u> <u>TEMPERATURE, °C</u>	1050	870	1050	870
<u>HEATING RATE</u> <u>°C/h</u>	20	60	20	60
<u>MOULDING</u> <u>METHODS</u>	CT*	CT	CP**	CP
<u>OPEN POROSITY</u> <u>%</u>	15.9	21.5	15.2	21.6
FULLY PROCESSED COMPOSITES				
<u>WEIGHT GAIN BY</u> <u>CVD TREATMENT, %</u>	6.06	5.51	6.74	4.99
<u>OPEN POROSITY, %</u>	9.78	8.99	5.43	5.41
<u>BULK DENSITY</u> <u>kg/m³</u>	1449	1431	1509	1504
<u>FLEXURAL</u> <u>STRENGTH, MPa</u>	58.4 (F ^{\$})	45.2 (F)	176.6 (S ^{\$\$})	124.9 (S)
<u>ILSS, MPa</u>	5.86 (F)	4.45 (F)	6.56 (S)	5.21 (S)
<u>DIAMETRAL</u> <u>COMPRESSION</u> <u>LOAD, kg</u>	137.6	99.2	205.0	97.8

NOTE:

*CT -- constant thickness moulding

**CP -- constant pressure moulding

^{\$}F -- tensile failure^{\$\$}S -- shear failure

Table 4.7 Open Porosity of Chars of The Phenolic Resin PHA
Carbonised at Different Conditions

<u>MATERIALS</u>	<u>THICKNESS</u>	<u>CARBONISATION</u>		<u>OPEN</u>
	<u>mm</u>	<u>TEMPERATURE</u>	<u>HEATING</u>	<u>POROSITY</u>
		<u>°C</u>	<u>RATE, °C/h</u>	<u>%</u>
PHA1	1.8	1050	20	4.14
PHA2	1.8	870	60	13.16
PHA3	2.6	1050	20	2.62
PHA4	2.6	870	60	9.07

FIGURES

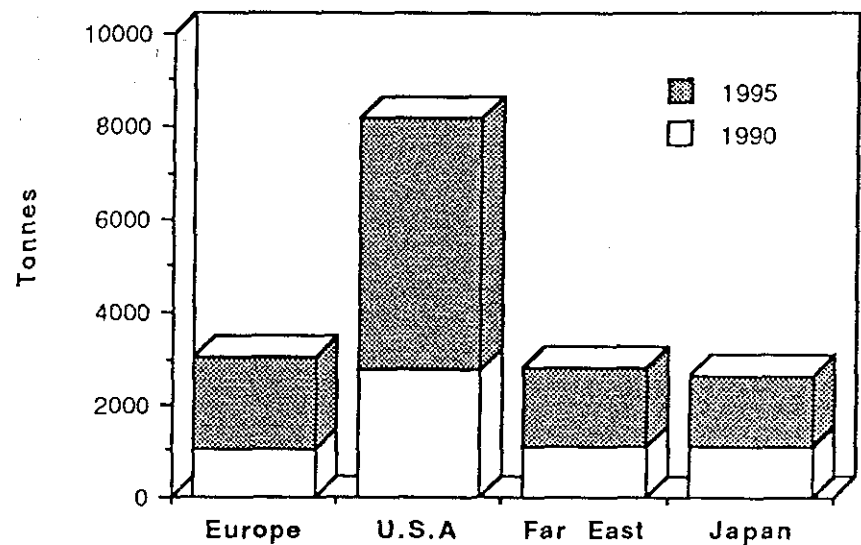


Figure 1.1 Forecast of world market for carbon fibres^[1]

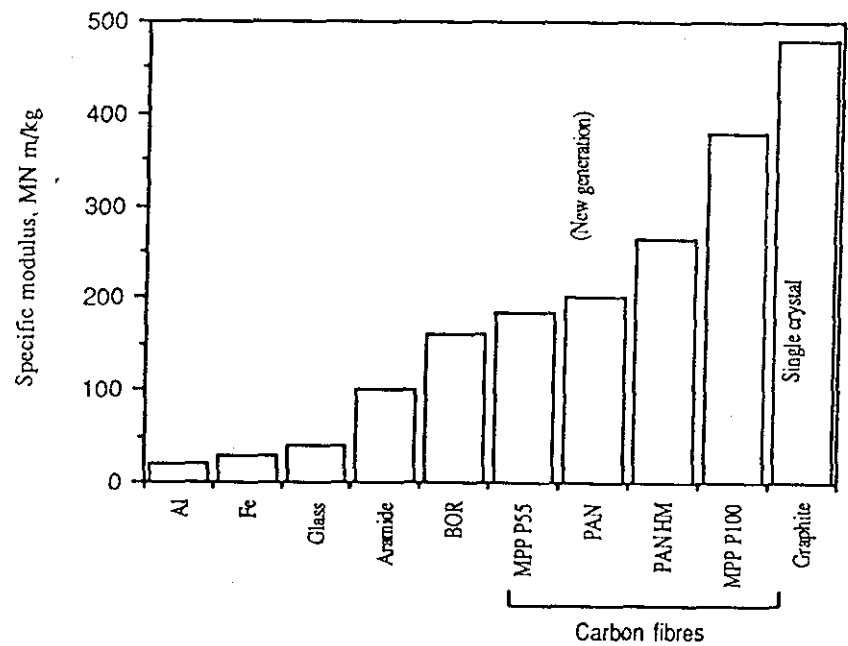


Figure 1.2 Specific Young's modulus of carbon fibres and conventional materials^[2]

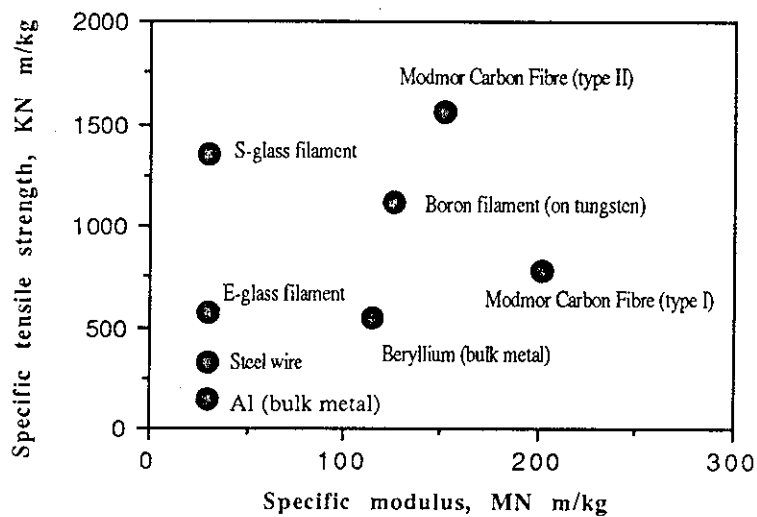


Figure 1.3 Specific tensile strength and modulus of carbon fibres and some conventional reinforcing materials^[3]

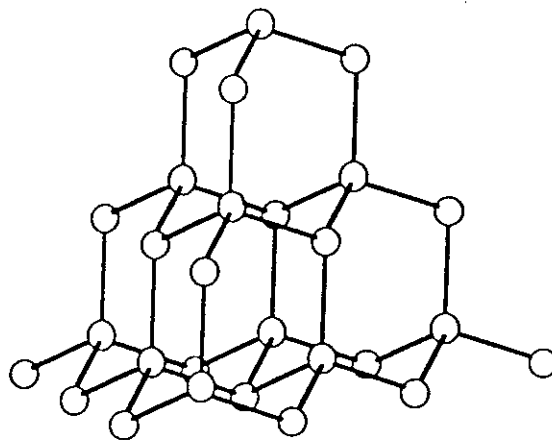


Figure 2.1 Structure of diamond

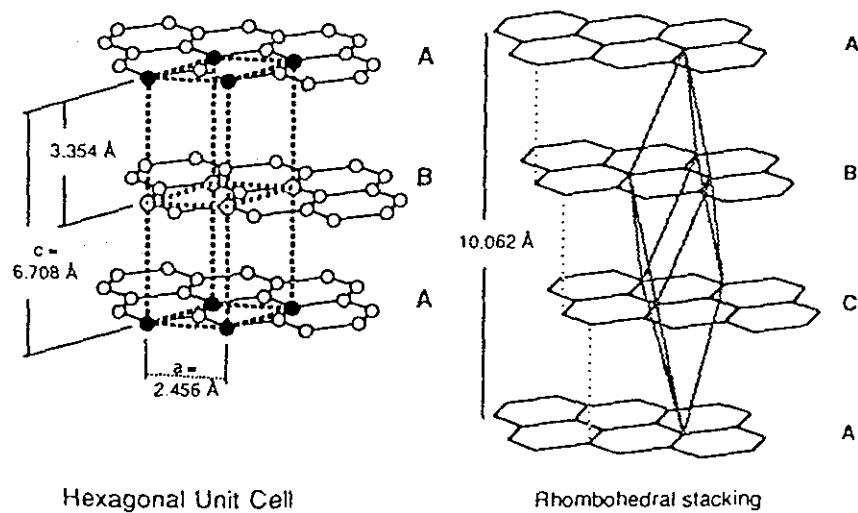


Figure 2.2 Structure of graphite^[11, 14, 15]

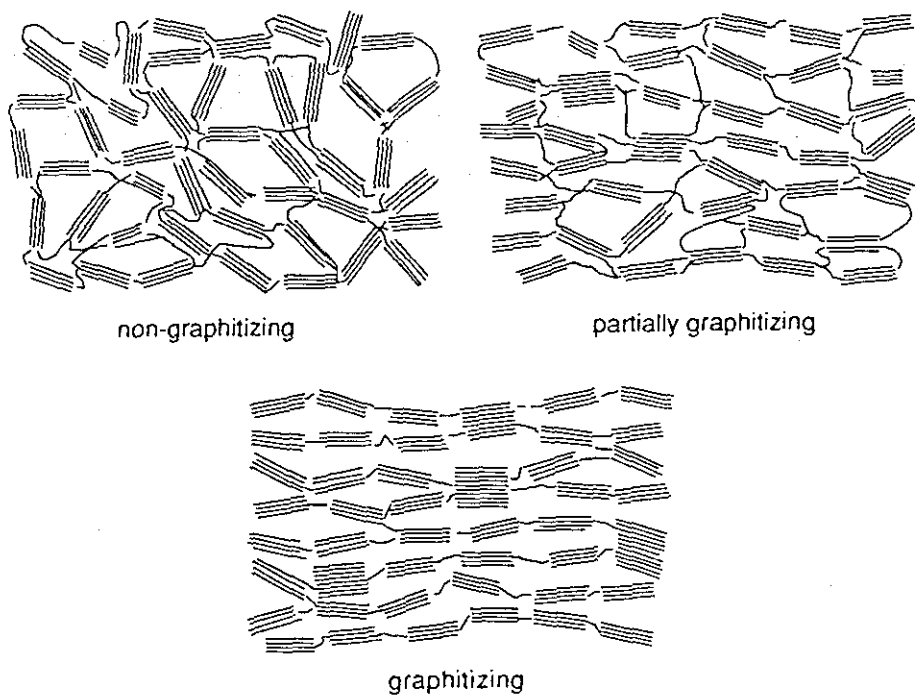


Figure 2.3 Models of carbon structure^[16]

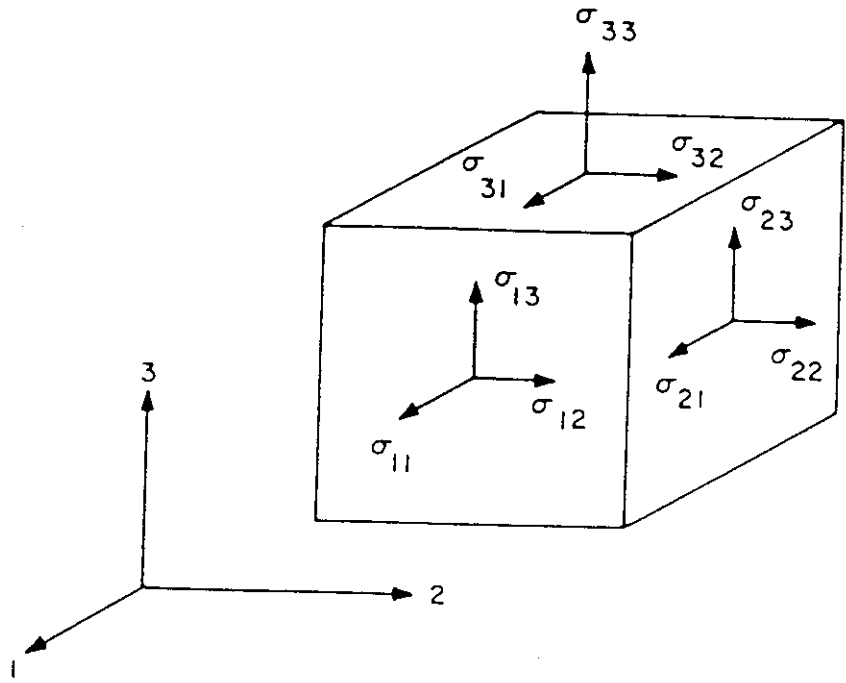


Figure 2.4 Three dimensional state of stresses

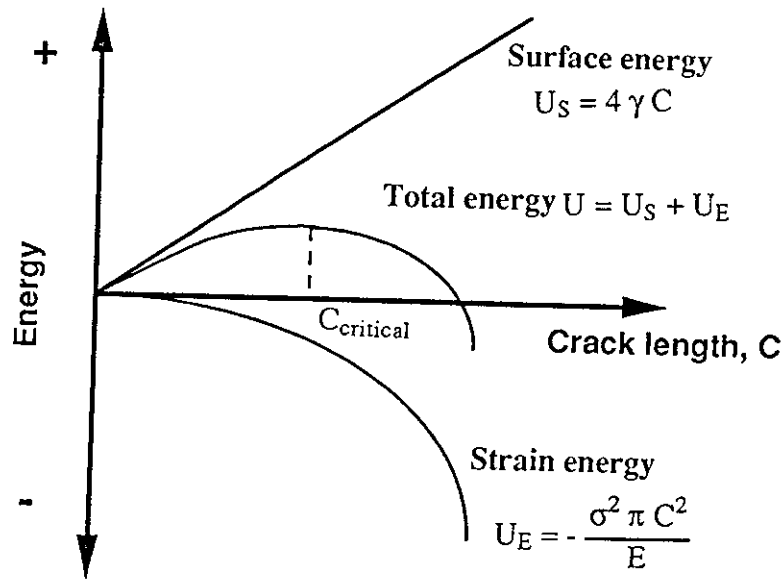


Figure 2.5 Variation of the surface energy, strain energy and total energy with crack length

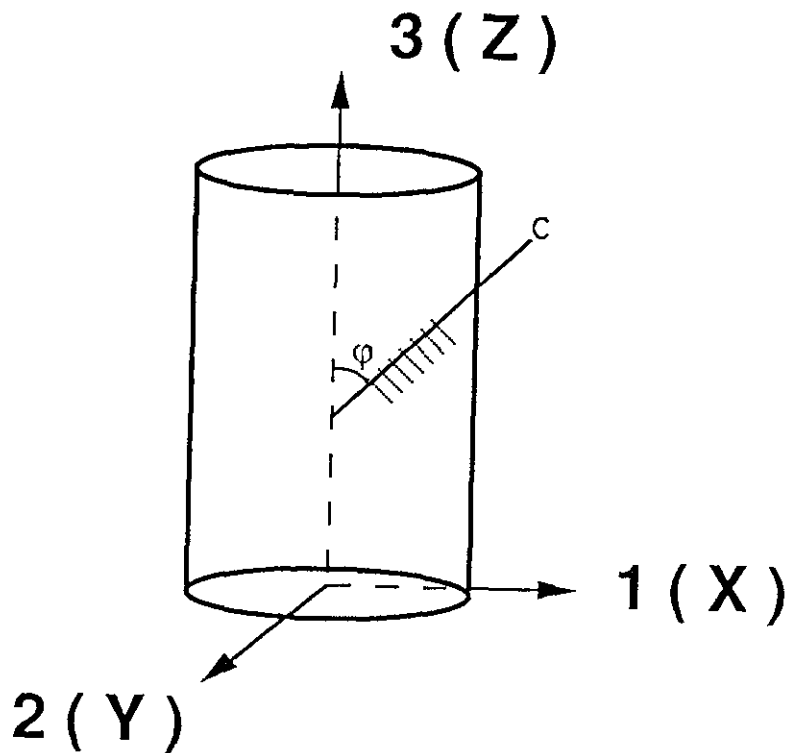


Figure 2.6 Uniform stress in an anisotropic structure with cylindrical symmetry

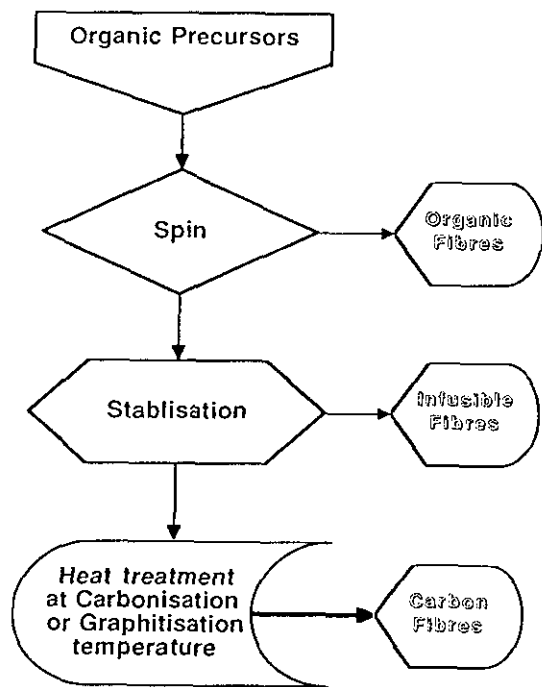


Figure 2.7 General process of the production of carbon fibres

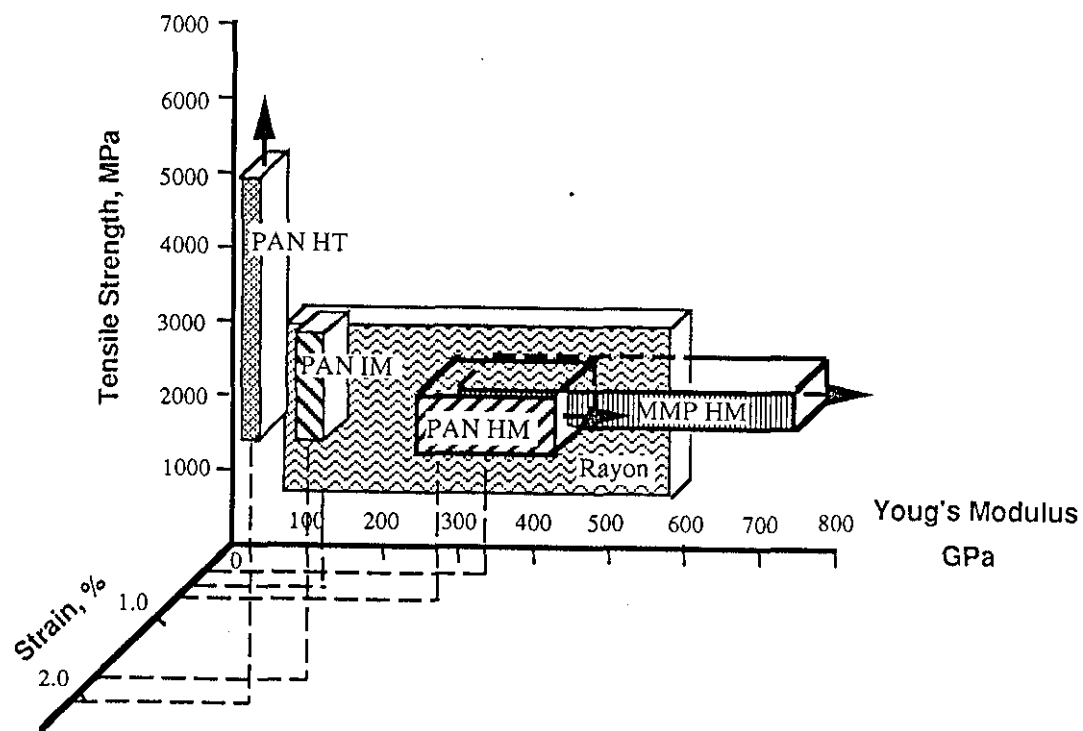
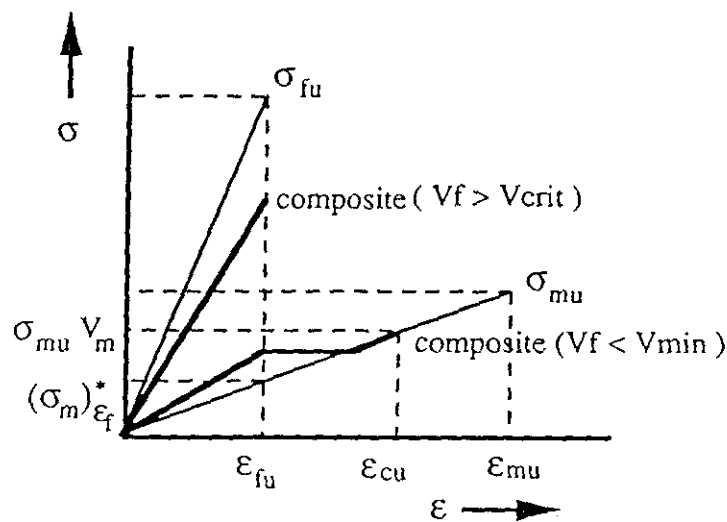
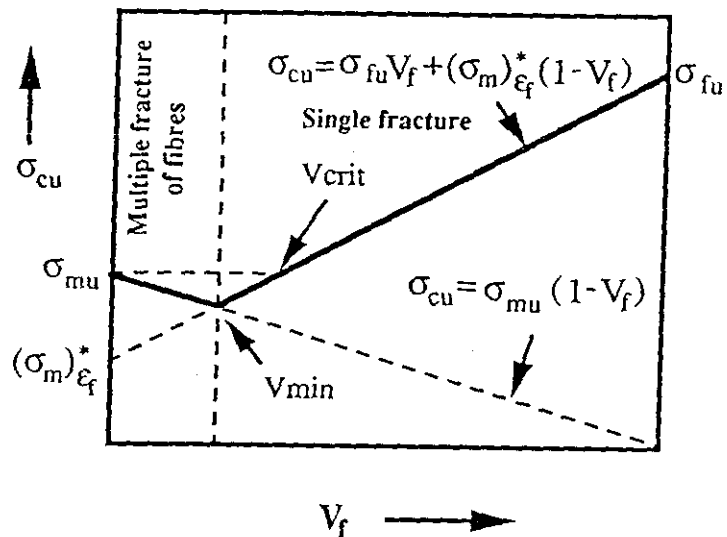


Figure 2.8 Mechanical properties achieved in various types of carbon fibres



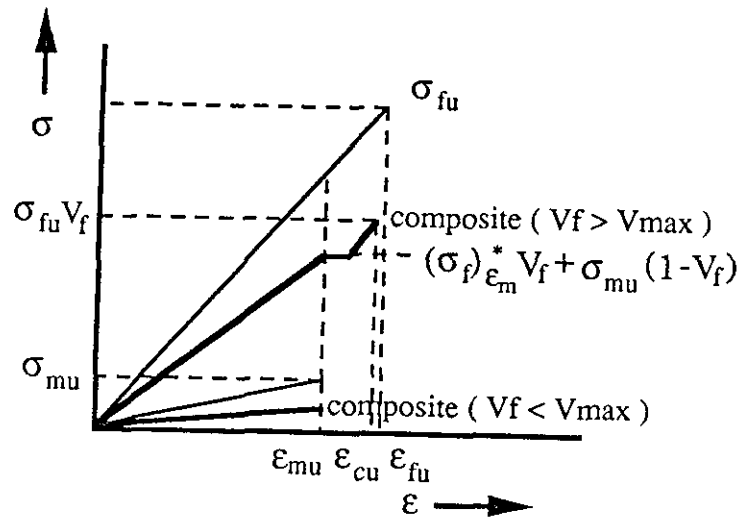
(a) Stress-strain curve



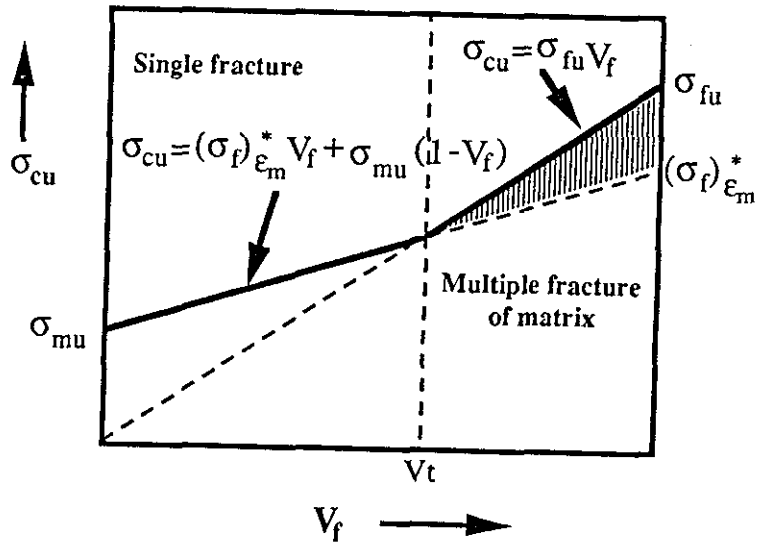
(b) Ultimate strength of the composite as function of fibre volume fraction

Figure 2.9 Behaviour of deformation and relationship between the ultimate tensile strength and the fibre volume

fraction in the case of $\epsilon_m^* > \epsilon_f^*$



(a) Stress-strain curve



(b) Ultimate strength of the composite as function of fibre volume fraction

Figure 2.10 Behaviour of deformation and relationship between the ultimate tensile strength and the fibre volume fraction in the case of $\epsilon_m^* < \epsilon_f^*$

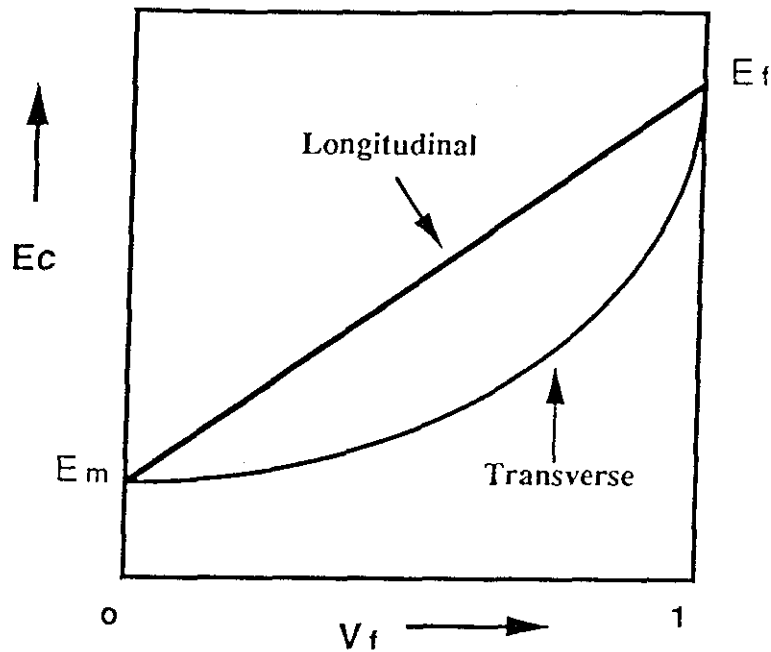


Figure 2.11 Relationship between composite modulus and fibre volume fraction

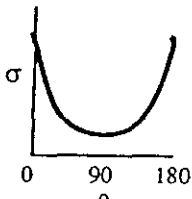
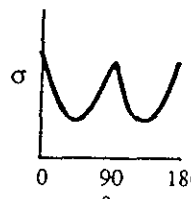
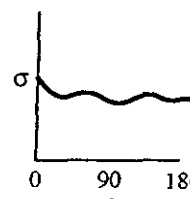
Structure of the composites	1-D	2-D	3-D
Variation of flexural strength with the composite orientation			
ILSS, MPa	20-40	20-40	50-80
Theoretical maximum of fibre volume fraction	90.6 %	78.5 %	67.9 %
Experimental maximum of fibre volume fraction	> 60 %	< 60 %	~ 50 %

Figure 2.12 Mechanical properties and possibilities for fibre arrangement in different direction reinforced structure

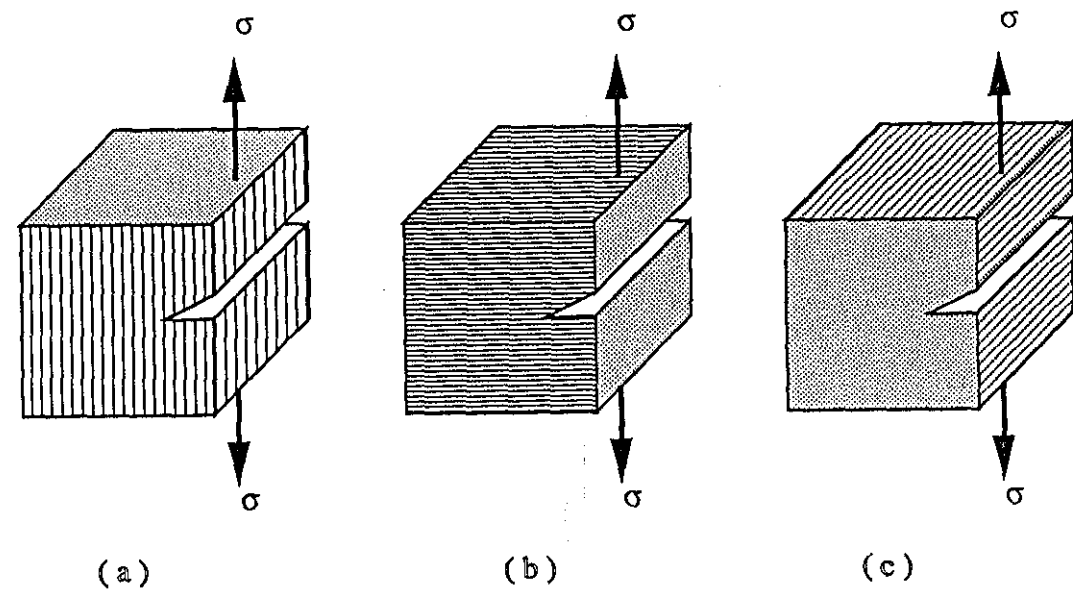


Figure 2.13 A given length of crack for opening mode in three directions to fibre axis

SYNTHETIC GRAPHITE

C/C COMPOSITES

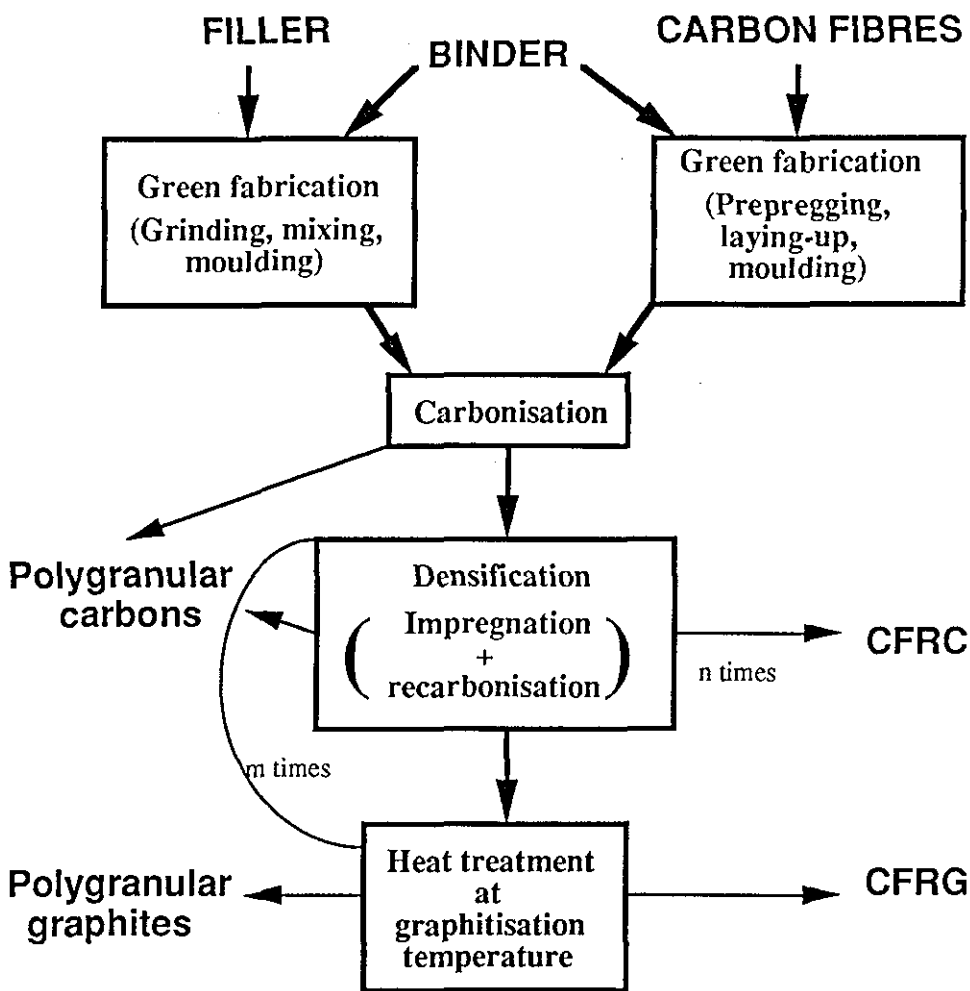


Figure 2.14 General processes of the production of C/C composites and synthetic polygranular graphite^[9]

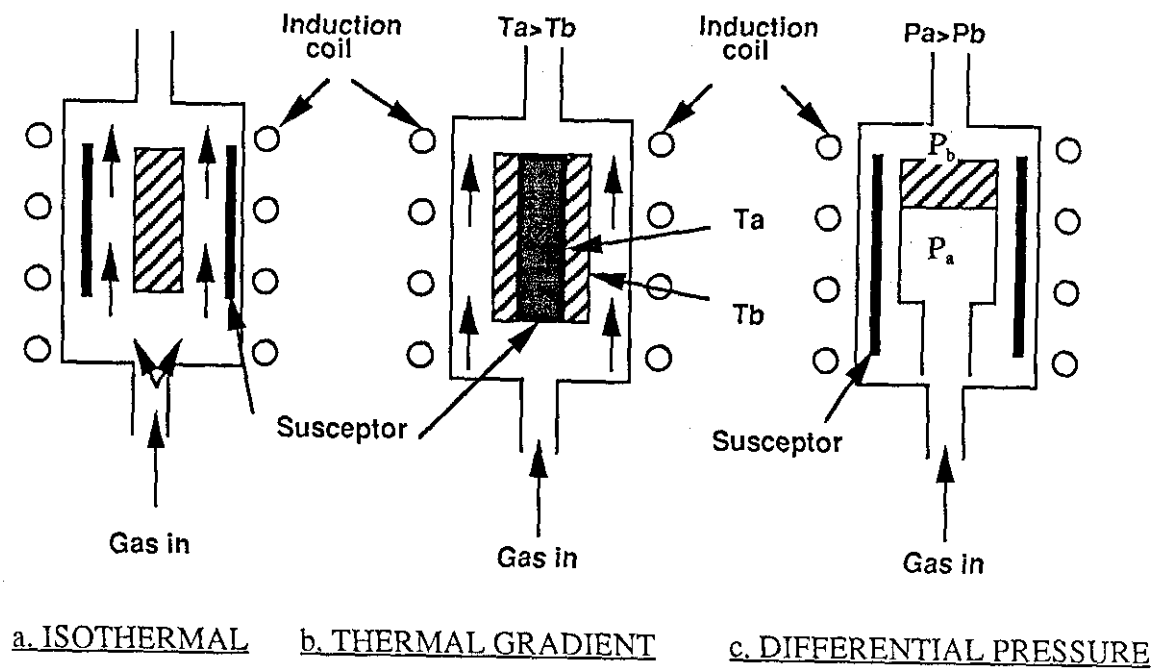


Figure 2.15 Chemical vapour deposition techniques

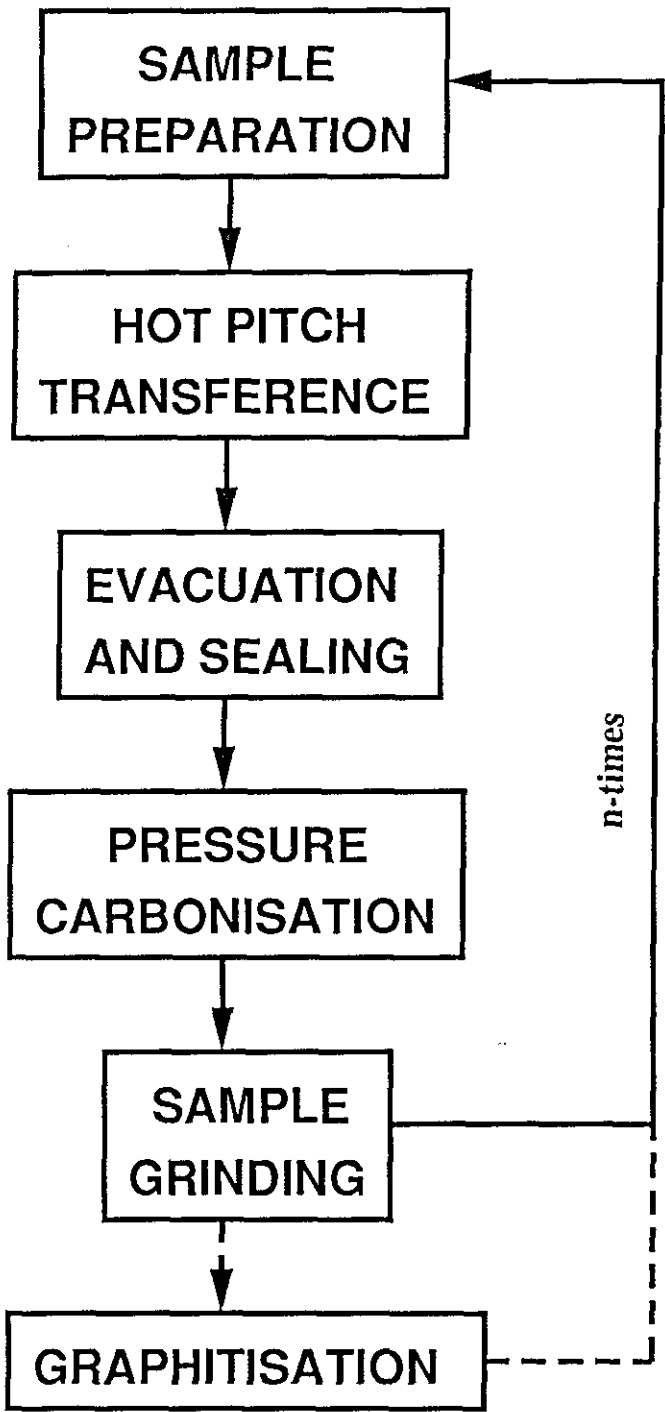


Figure 2.16 Schematic of high pressure impregnation process

FIGURES

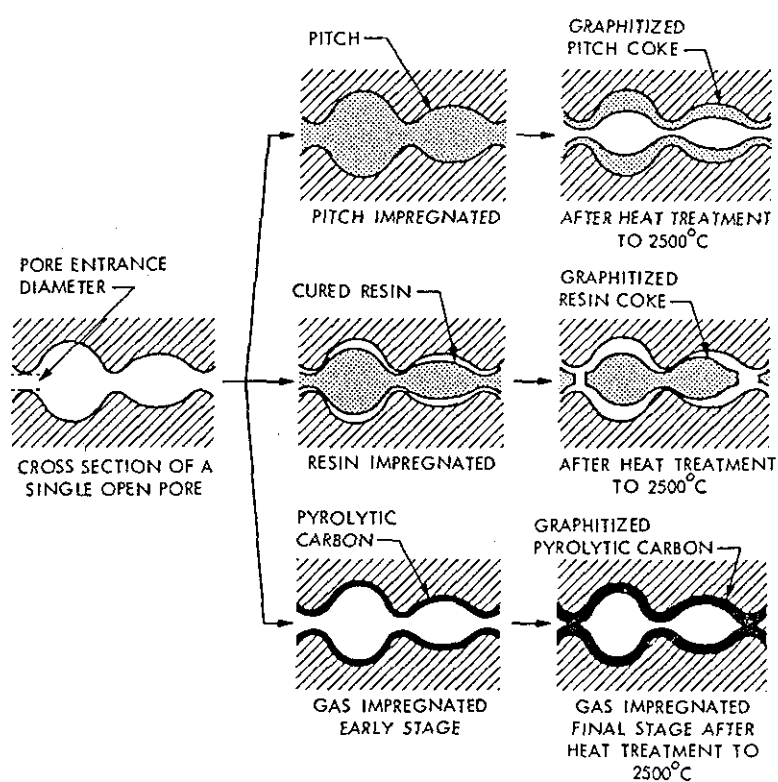


Figure 2.17 Schematic illustration of pore-filling and pore-blocking mechanisms during CVD and liquid impregnation^[142]

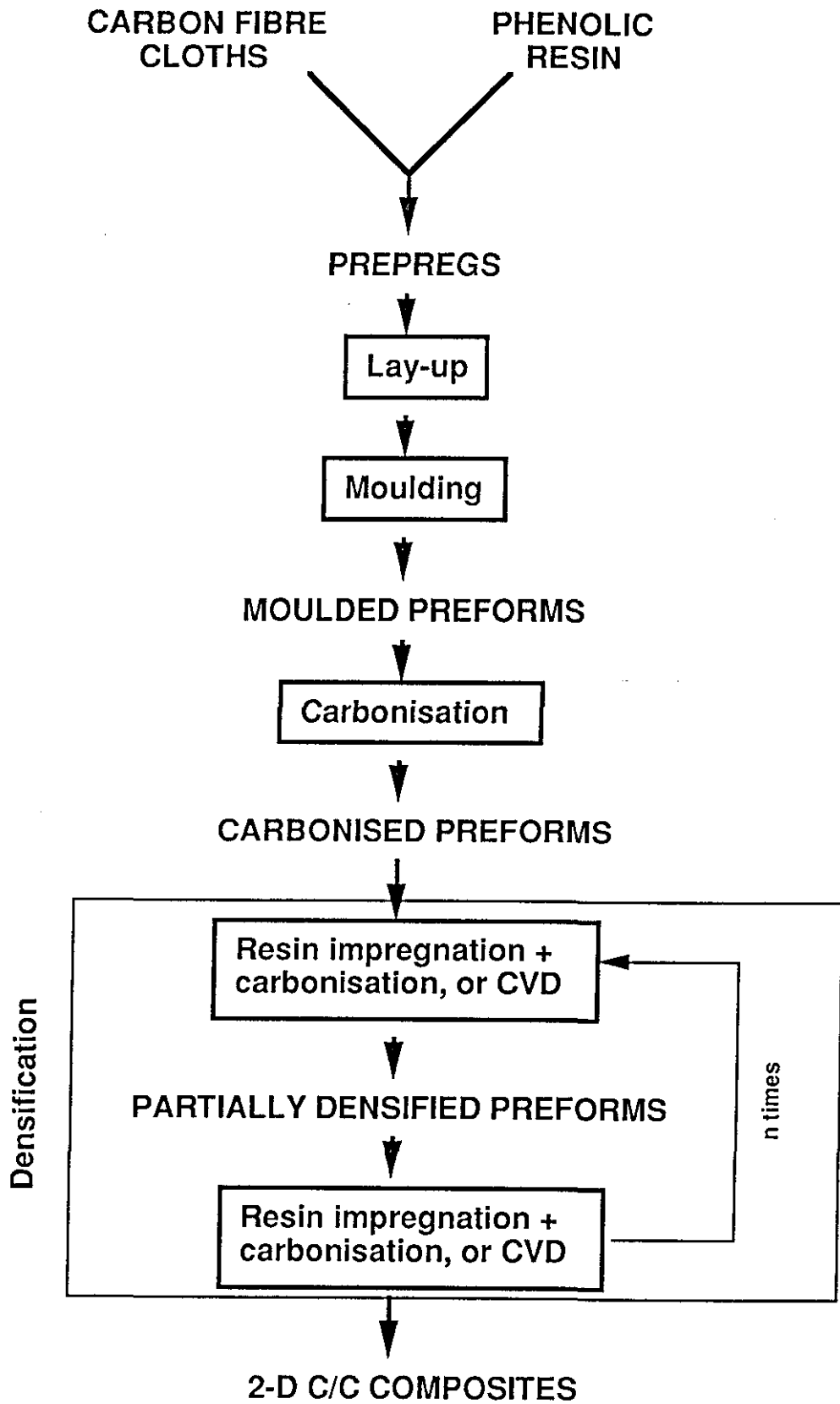
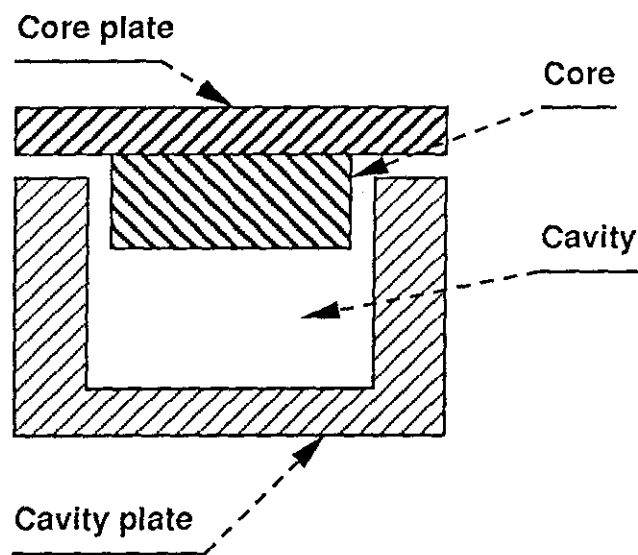
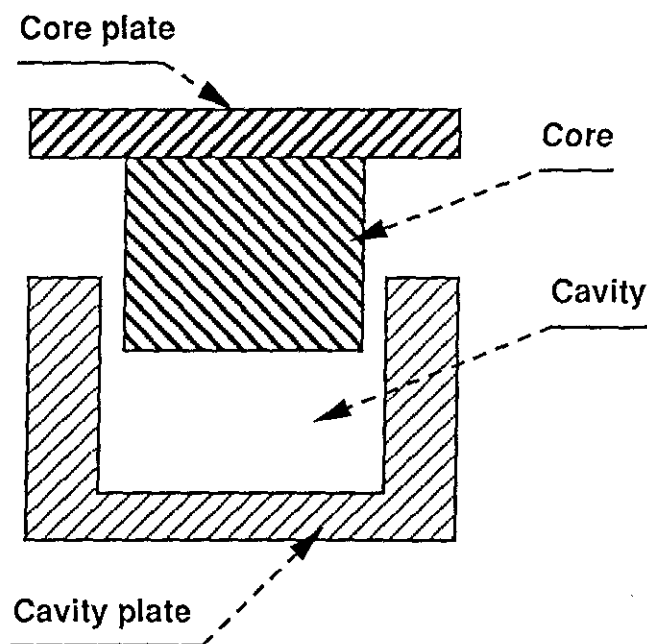


Figure 3.1 Fabrication process of New Metals And Chemicals and Sintec Keramik



(a) Constant thickness moulding



(b) Constant pressure moulding

Figure 3.2 Schematic illustration of constant thickness and constant pressure moulding techniques

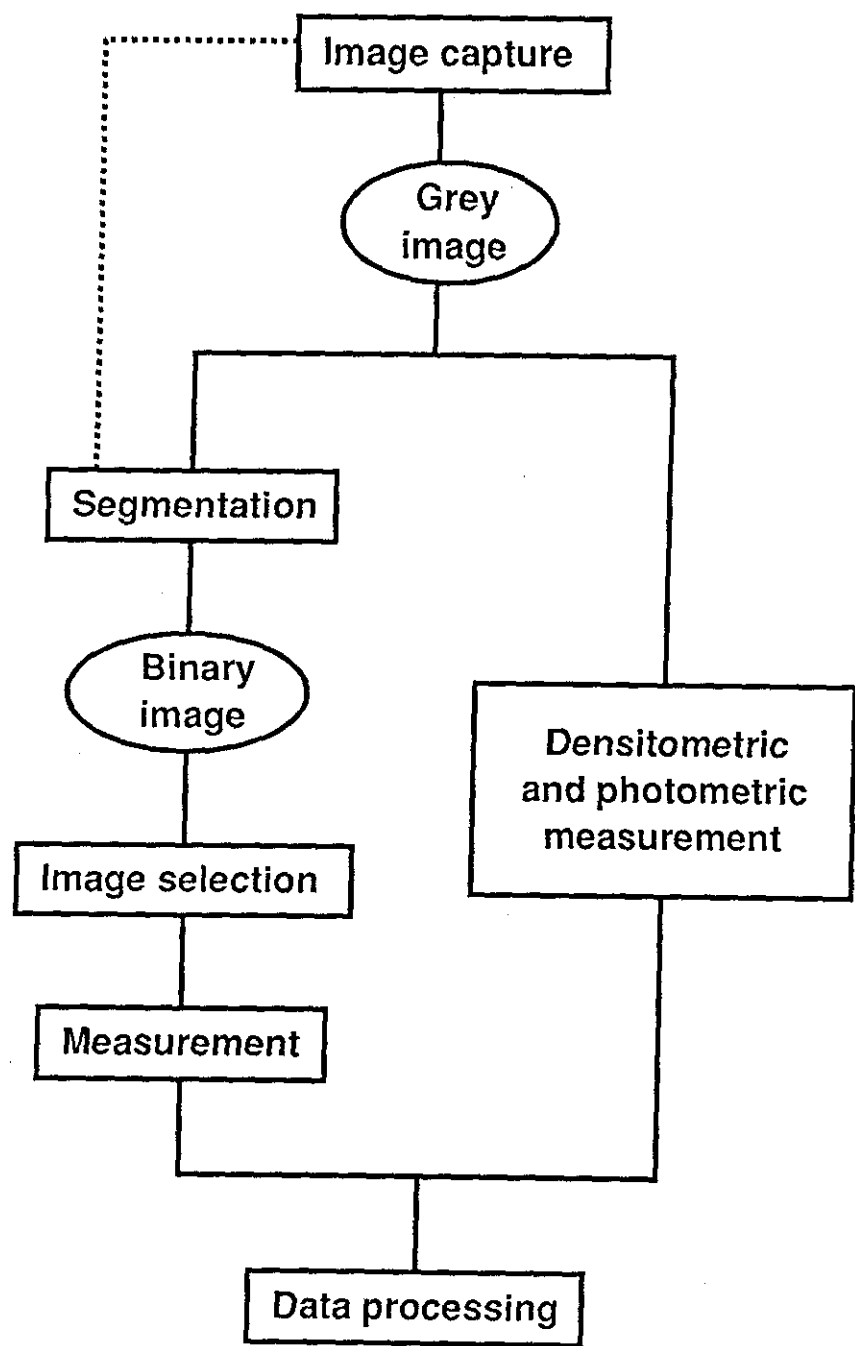
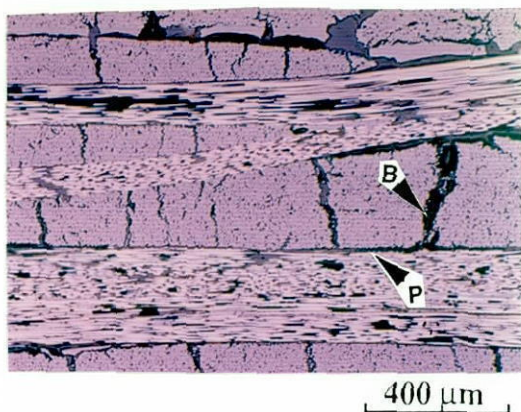


Figure 3.3 The essential principles of image analysis

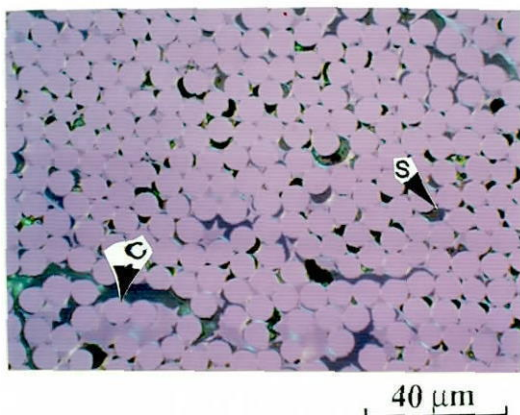
FIGURES



a. Planar and bundle cracks
on a $0^\circ/90^\circ$ cross-section.

P -- planar crack

B -- bundle crack

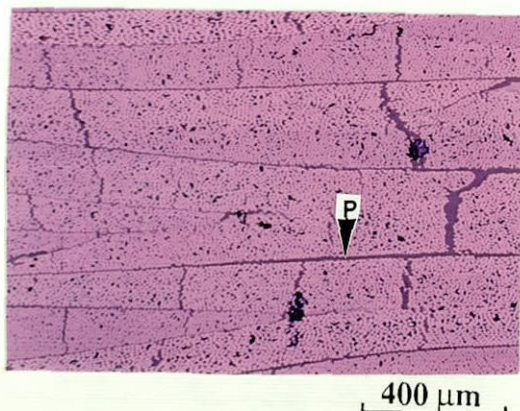


b. Inter-fibre pores and cracks
on a $0^\circ/90^\circ$ cross-section.

S -- inter-fibre pore

C -- inter-fibre crack

M -- matrix



c. Planar cracks on a $45^\circ/45^\circ$
cross-section.

P -- planar crack

Figure 3.4 Appearance of different types of voids on cross-sections of a carbonised preform in Group PAN-SR

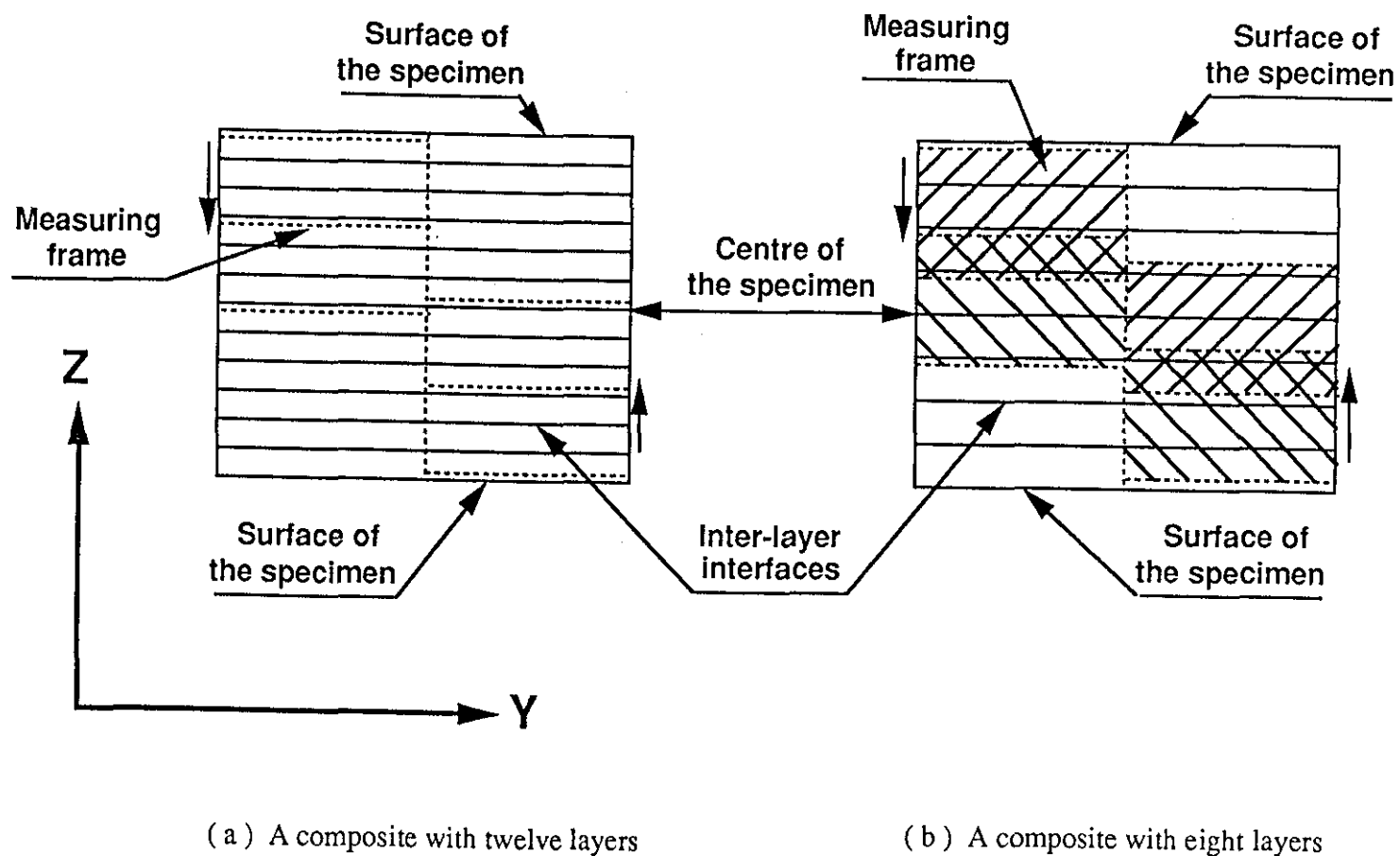


Figure 3.5 Diagrams of measuring frames across the thickness of the polished surfaces of the composites

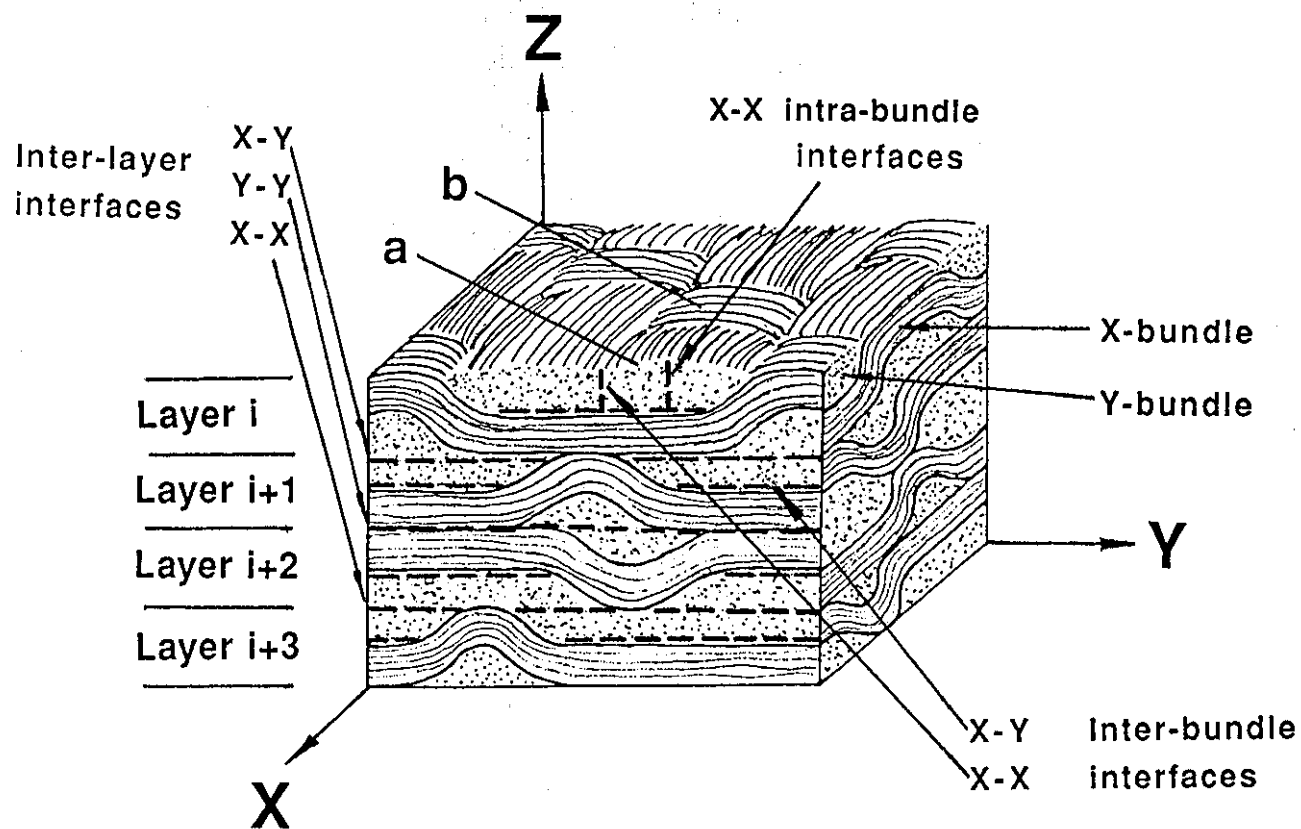


Figure 4.1 Three-dimensional view of the arrangement of the fibres in a unit cell of a 2-D C/C composite

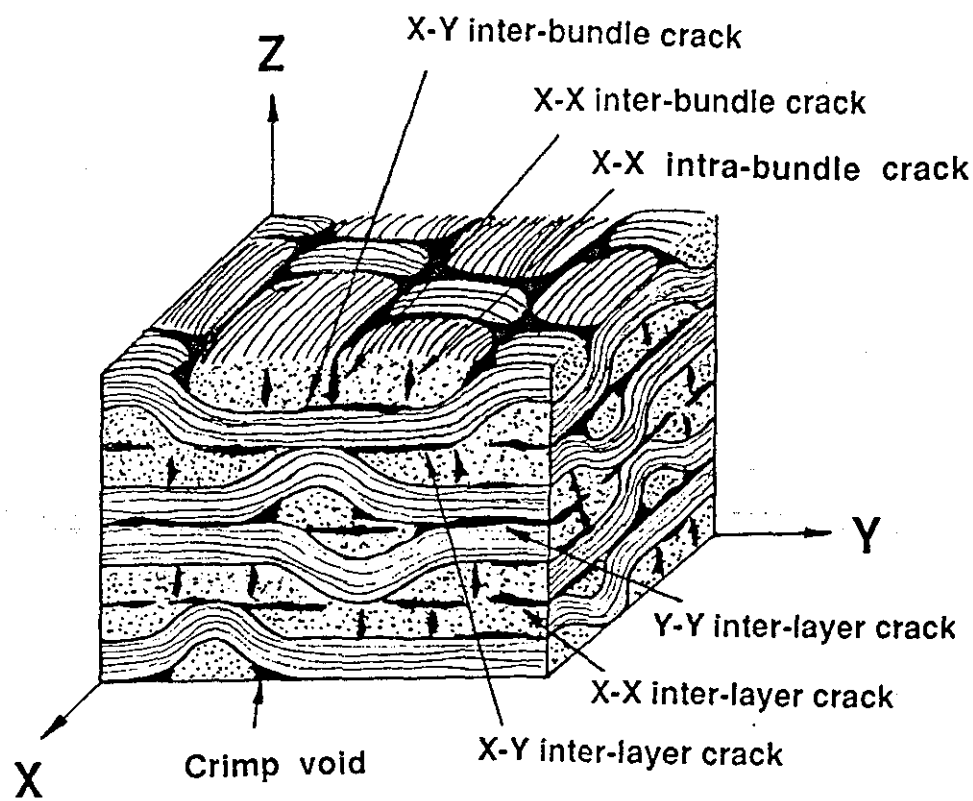
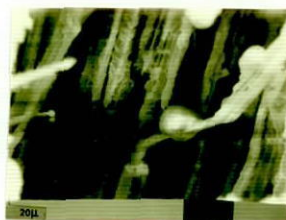
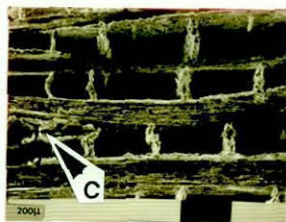


Figure 4.2 Large voids in a 2-D C/C composite



- a. Si-SiC impregnated into inter-layer, inter-bundle and intra-bundle cracks and crimp voids, PAN-SR.
C -- crimp void

- b. Si-SiC impregnated into inter-pores, Rayon-SR.

- c. Si-SiC impregnated into inter-fibre cracks, Rayon-SR.



Figure 4.3 Micrographs of Si-SiC skeleton remaining after burning-off the carbon, SEM

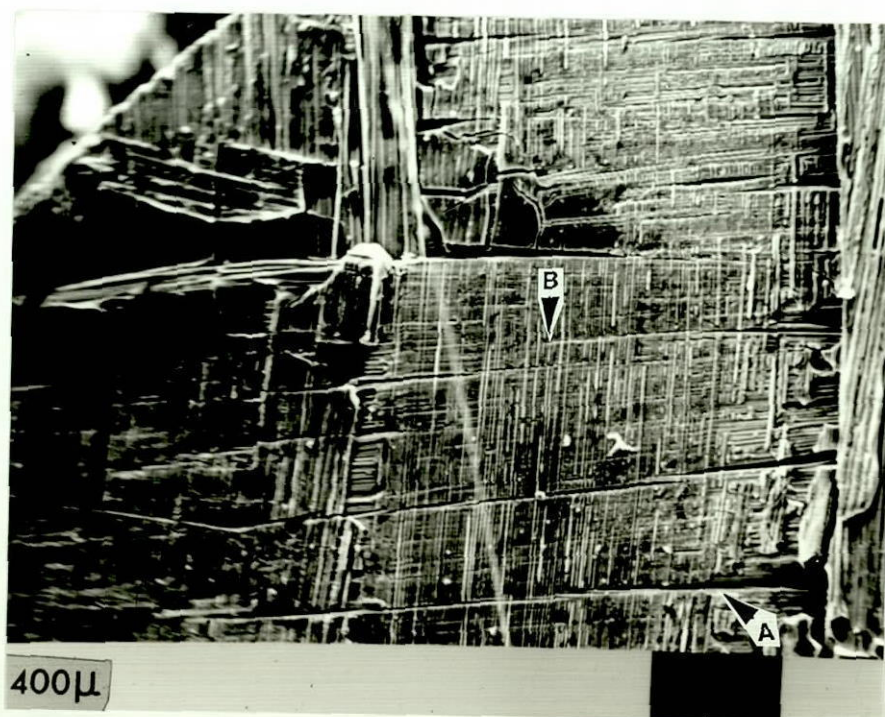


Figure 4.4 X-X intra-bundle cracks on X-Y face, SEM, PAN-SR

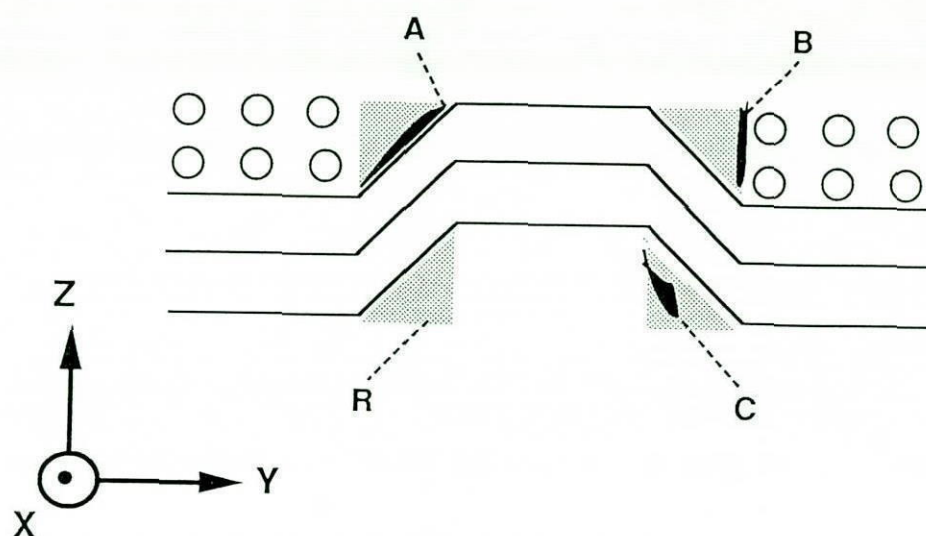


Figure 4.5 Various types of crimp voids, (A) and (B) at fibre/resin coke interfaces and (C) with the resin coke. Uncracked resin coke is at R.

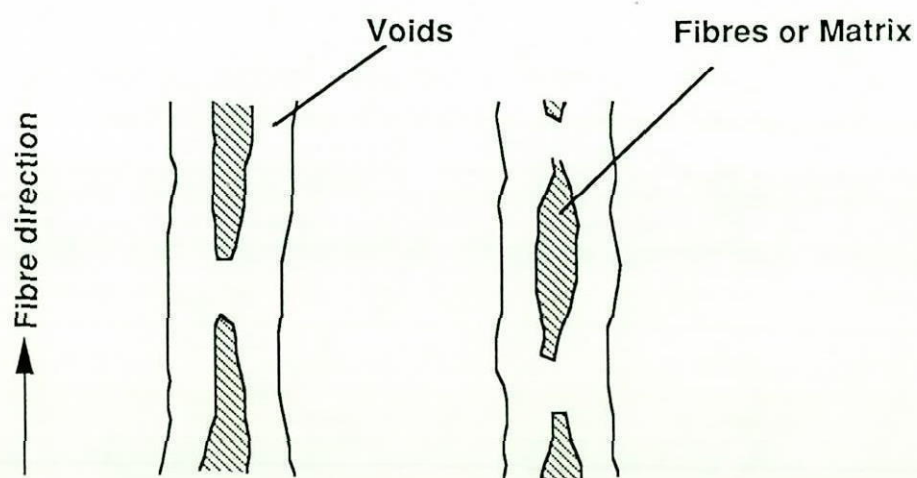
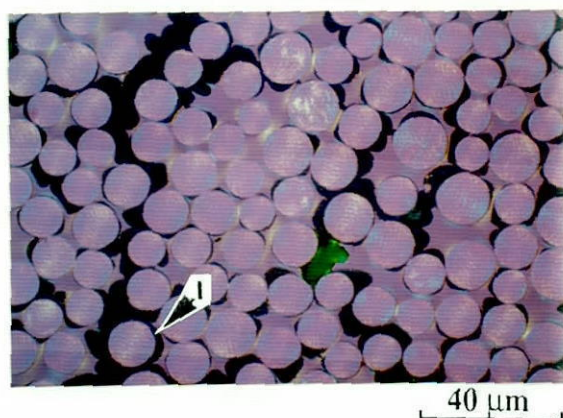
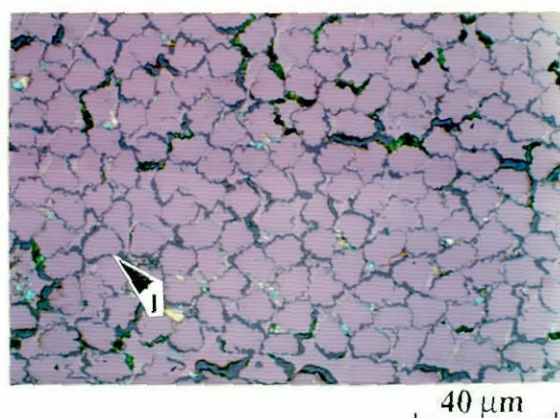


Figure 4.6 Inter-connection between the inter-fibre pores

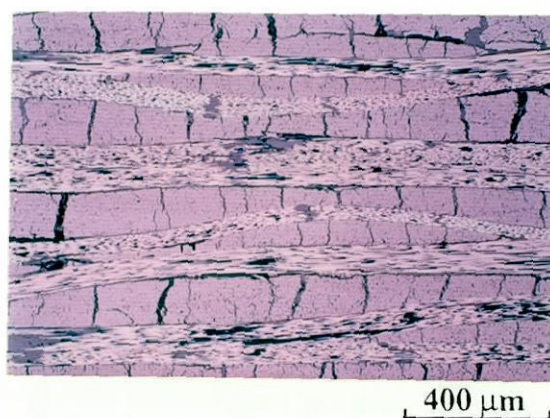


a. Pitch-SR

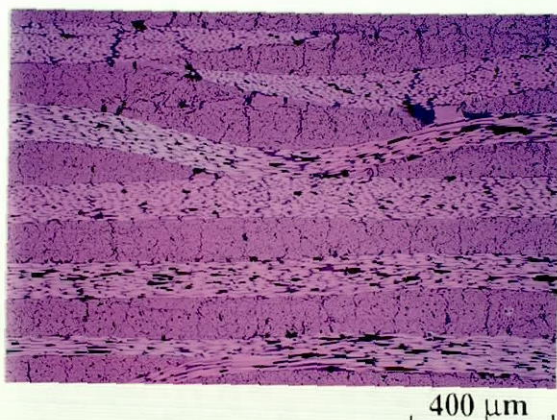


b. Rayon-SR

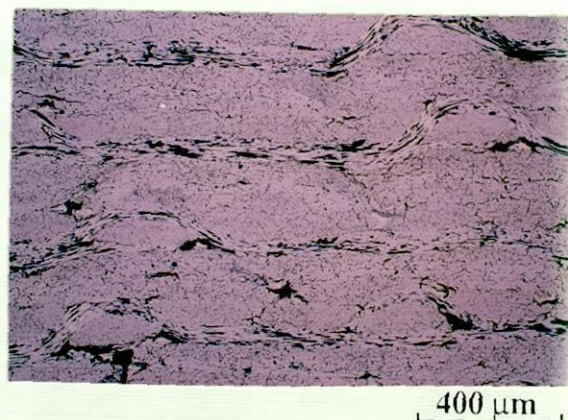
Figure 4.7 Micrographs of the carbonised preforms on cross-sections normal to the fibre direction, polarised-light



a. PAN-SR



b. Pitch-SR



c. Rayon-SR

Figure 4.8 The carbonised preforms on 0°/90° cross-sections viewed at a low magnification, polarised-light

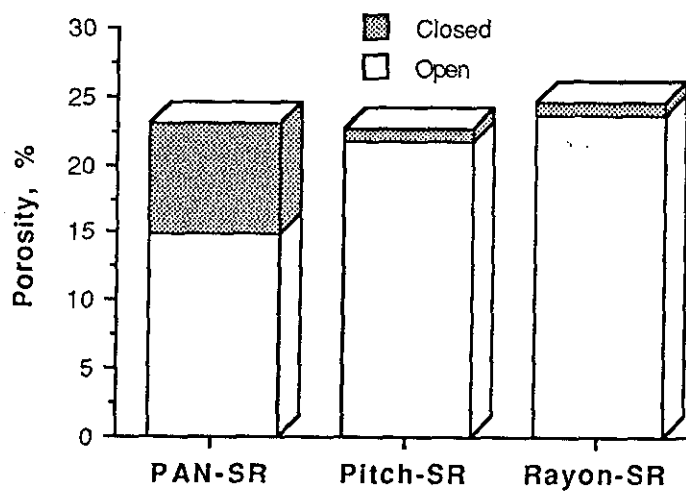


Figure 4.9 Open and closed porosity in the carbonised preforms

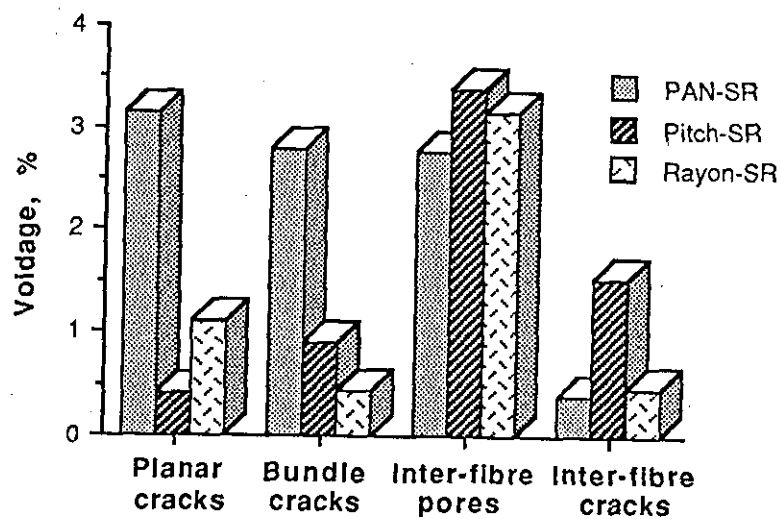


Figure 4.10 Voidage of the characterised voids in the carbonised preforms

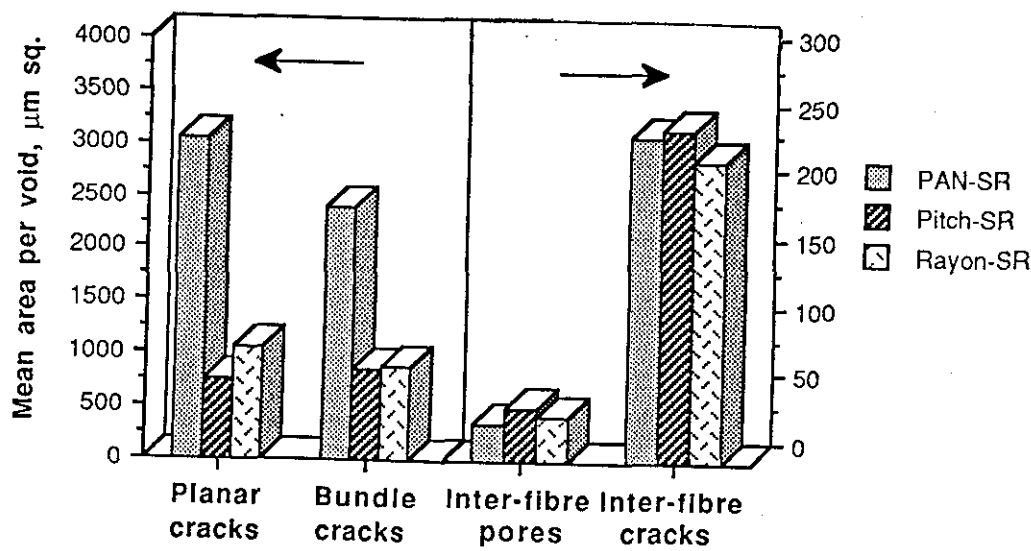


Figure 4.11 Mean area per void of the characterised voids in the carbonised preforms

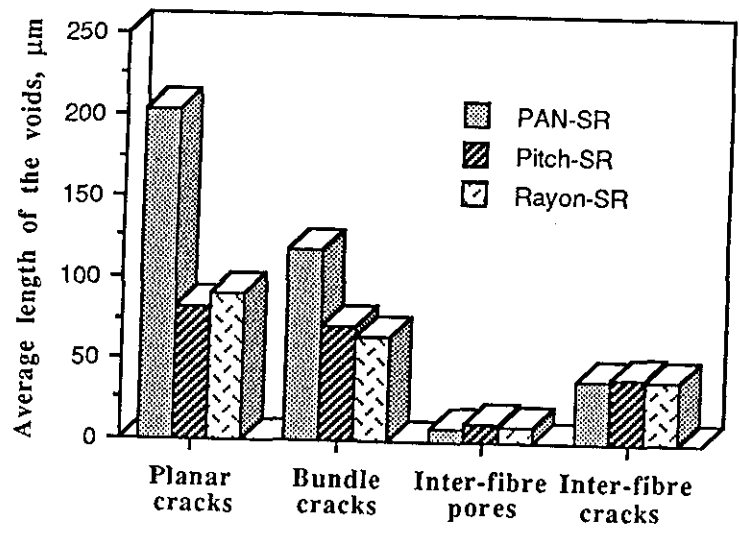


Figure 4.12 Average length of the characterised voids in the carbonised preforms

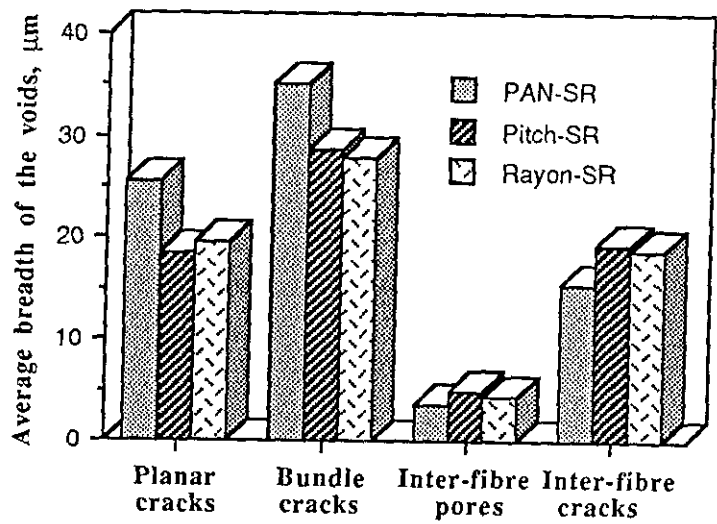


Figure 4.13 Average breadth of the characterised voids in the carbonised preforms

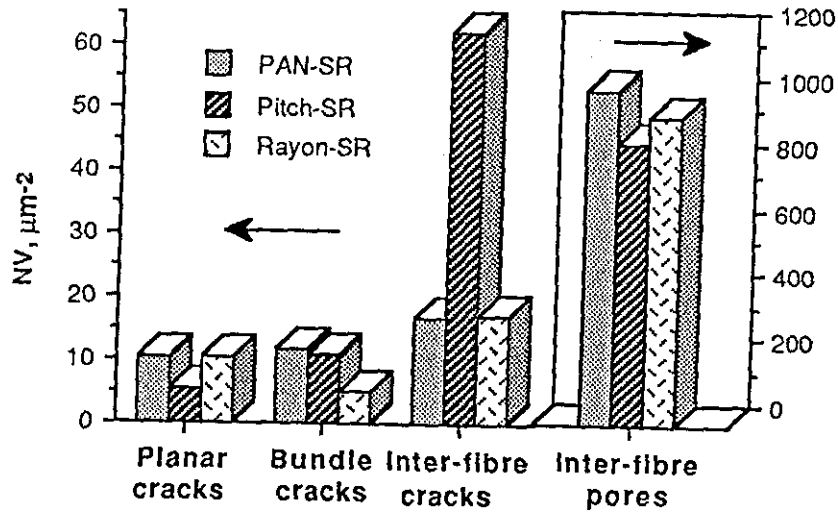


Figure 4.14 Number of voids per frame area of the characterised voids in the carbonised preforms

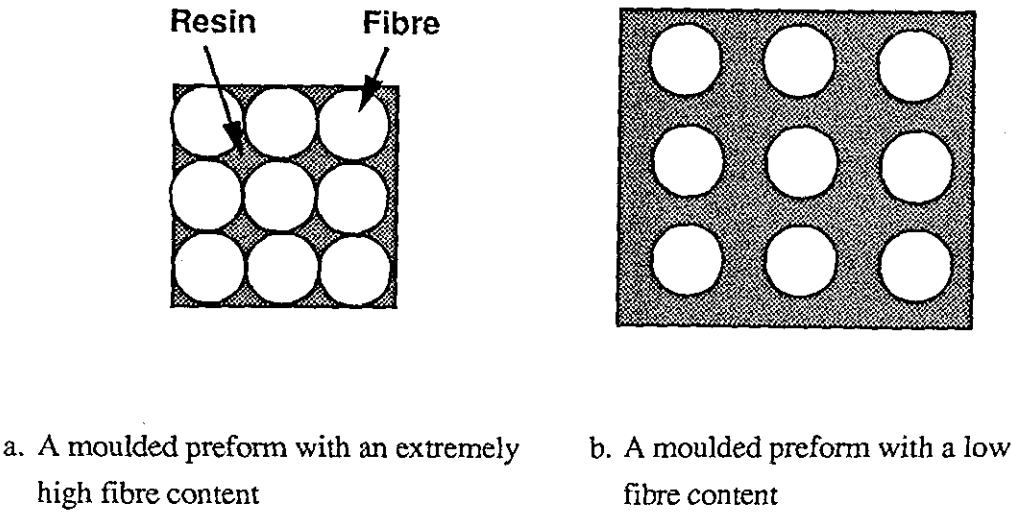


Figure 4.15 Schematic illustration of well-bonded resin within a fibre bundle on a cross-section of moulded preforms with different volume fractions

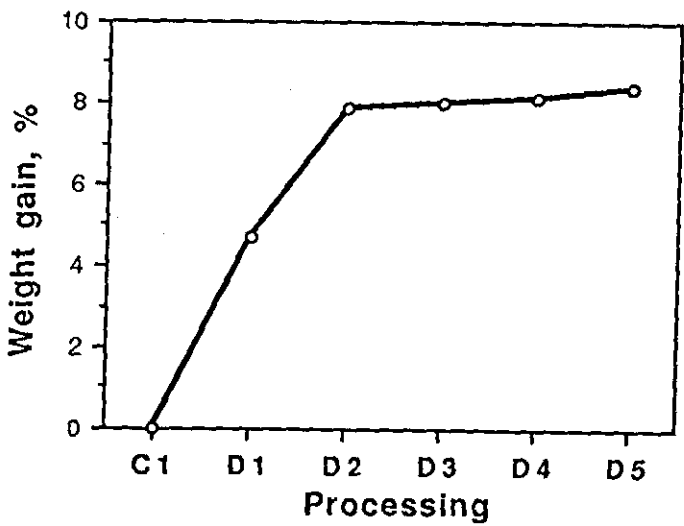


Figure 4.16 Weight increases on multiple CVD treatment

FIGURES

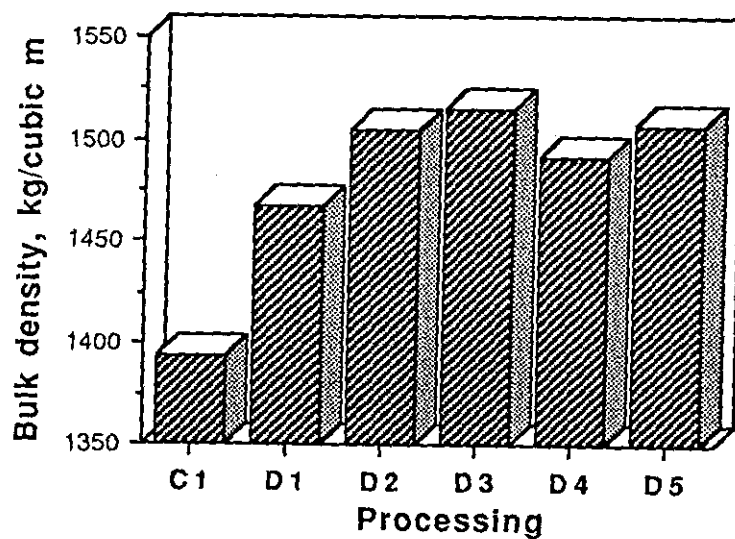


Figure 4.17 Variation of bulk density on multiple CVD treatment

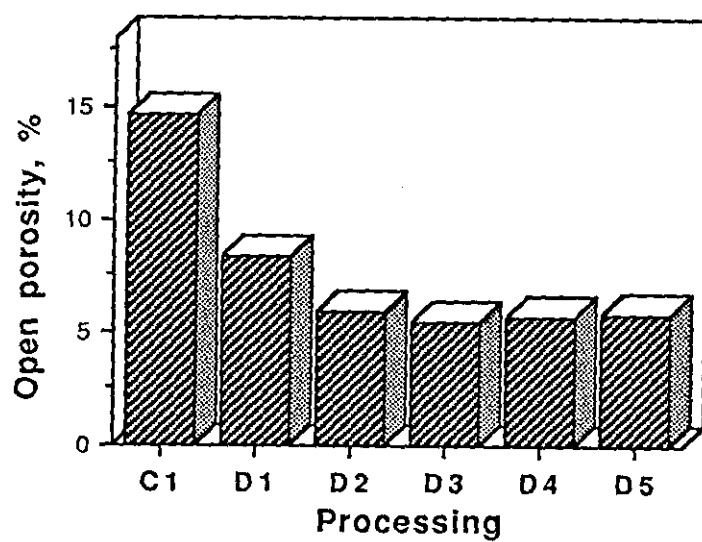


Figure 4.18 Open porosity changes on multiple CVD treatment

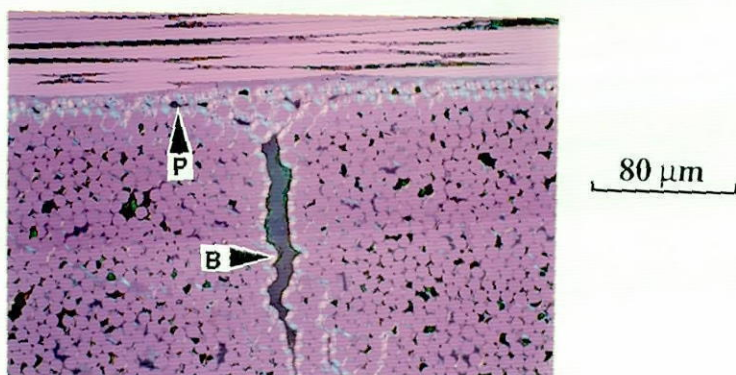


Figure 4.19 Pyrolytic carbon deposited in the planar (at P) and the bundle (at B) cracks rather than the voids within the fibre bundles, D3

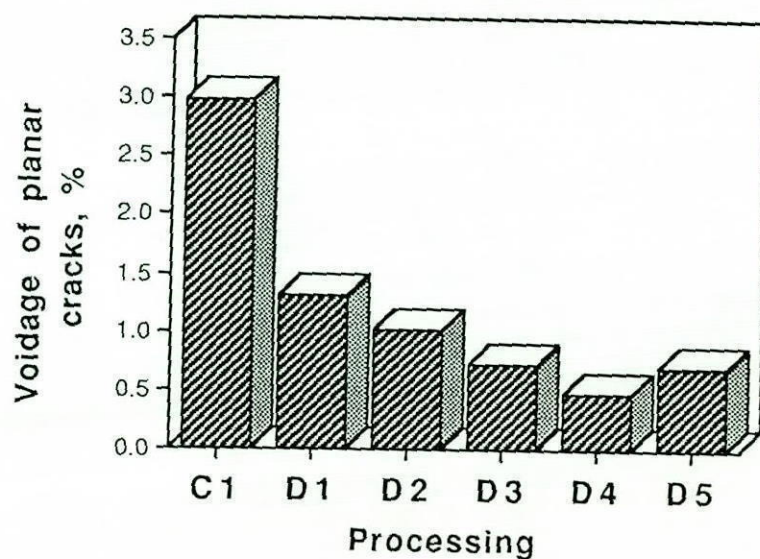


Figure 4.20 Variation of voidage in planar cracks on multiple CVD treatment

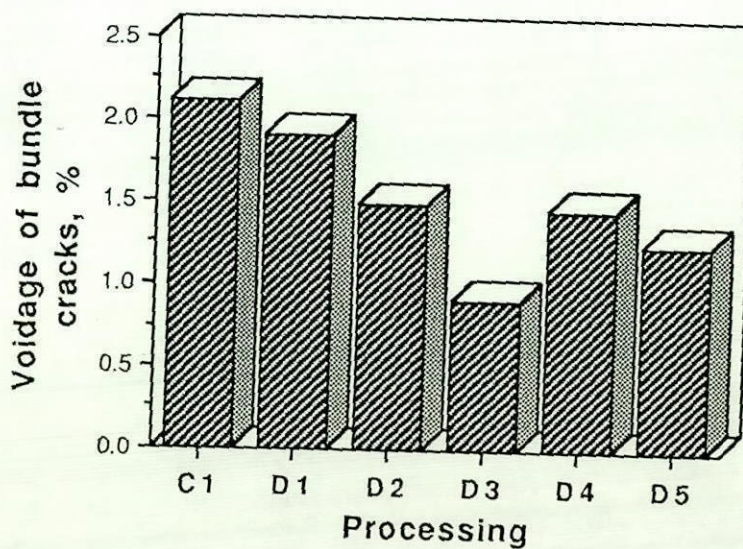
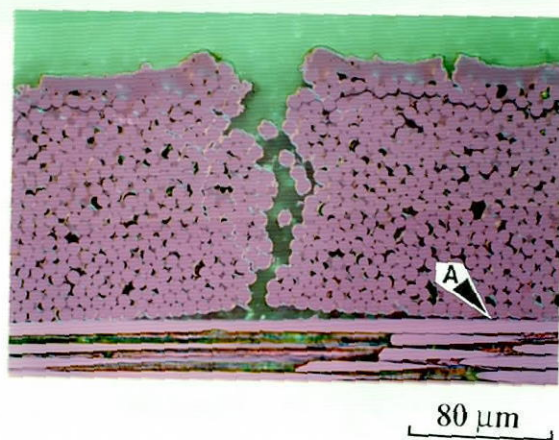
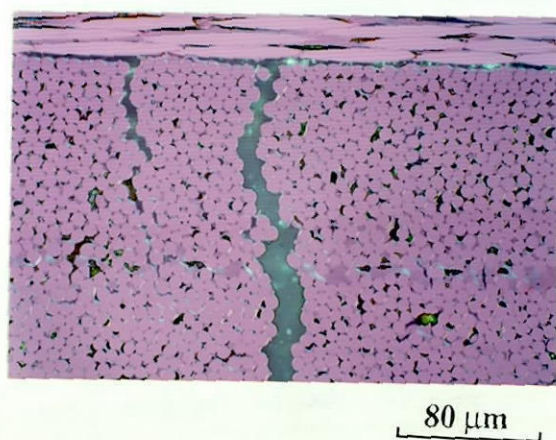


Figure 4.21 Variation of voidage in bundle cracks on multiple CVD treatment

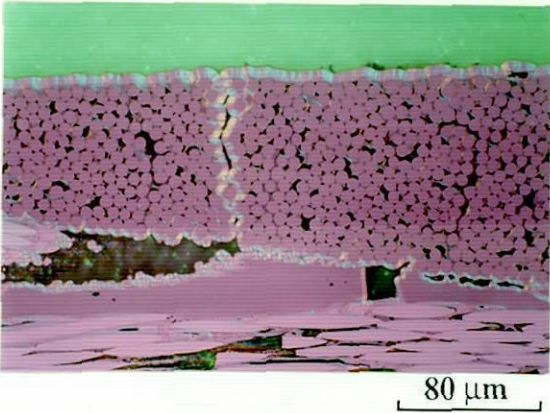


a. Outer layer

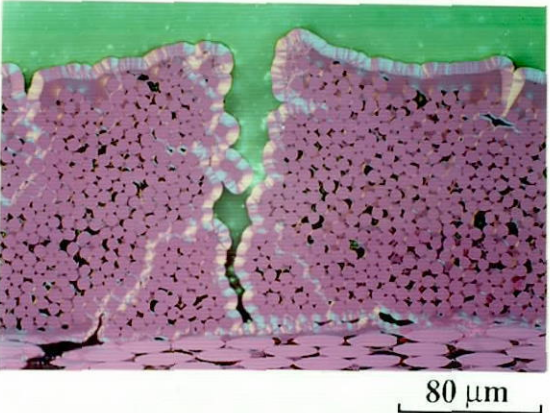


b. The centre of the composite

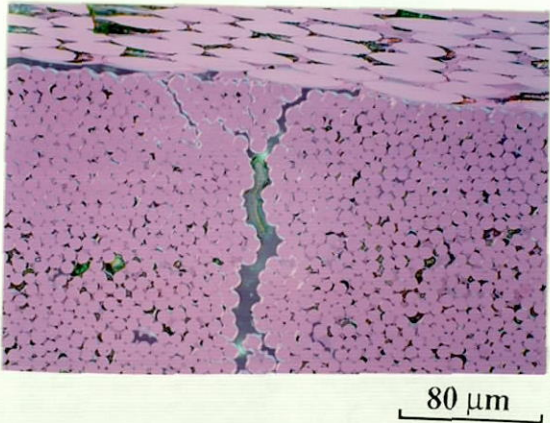
Figure 4.22 Polarised-light micrographs of the composite after the first CVD treatment



a. Blocked planar and bundle cracks in the outer layer



b. Narrowed bundle crack and blocked planar crack in the outer layer



c. The centre of the composite

Figure 4.23 The composite after the second CVD treatment

FIGURES

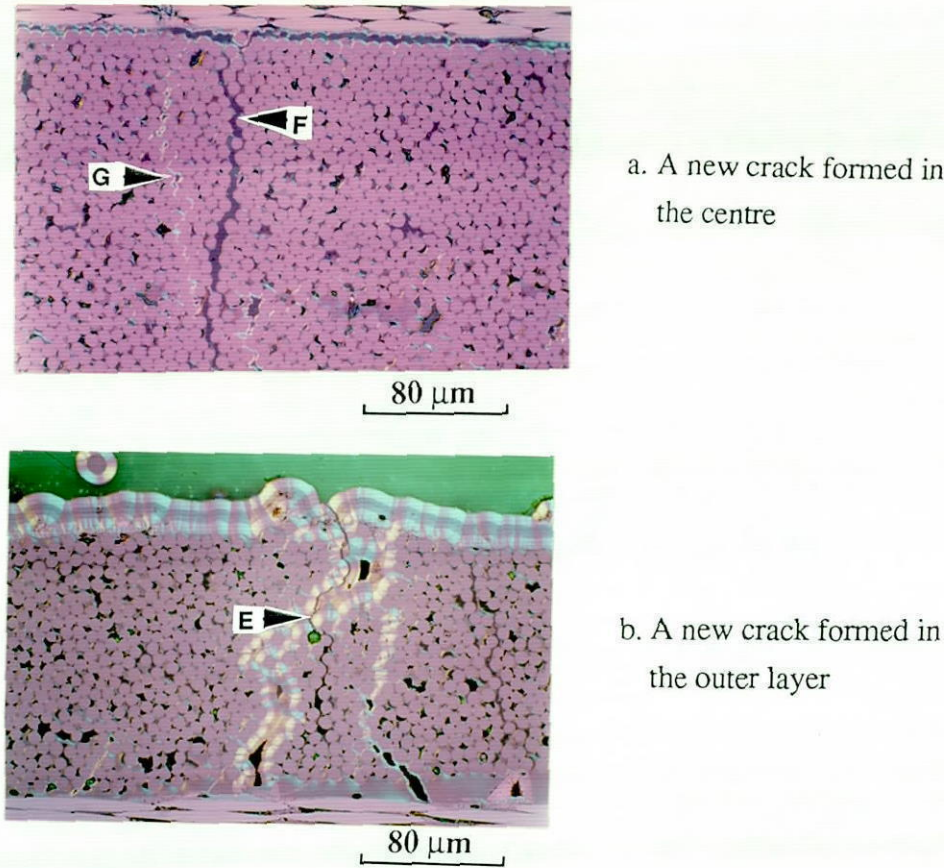


Figure 4.24 Newly formed cracks during multiple CVD treatment, D5

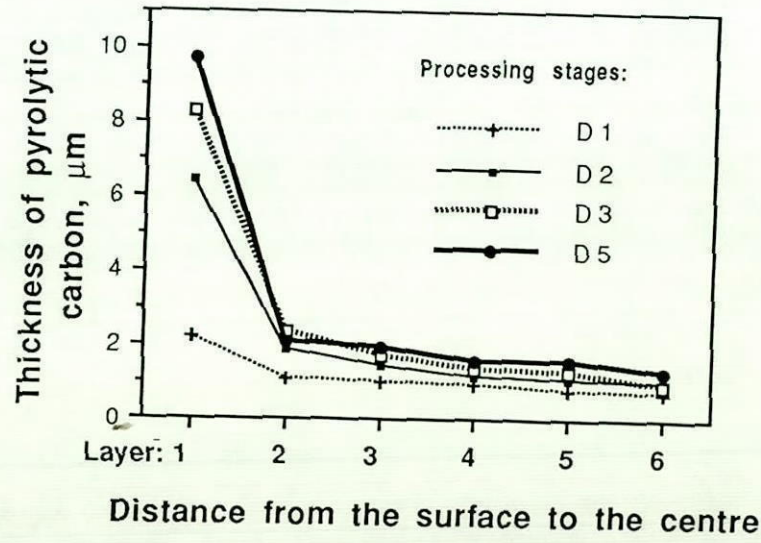


Figure 4.25 Variation of thickness of pyrolytic carbon from the surface to the centre on multiple CVD treatment

FIGURES

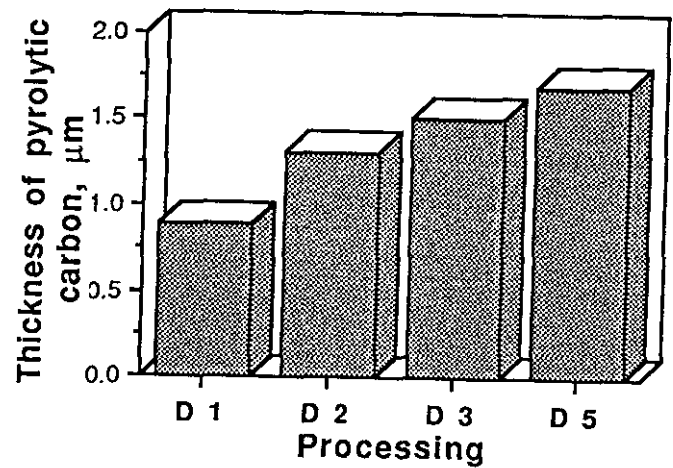


Figure 4.26 Thickness of pyrolytic carbon deposited in layer 2 to 6 on multiple CVD treatment

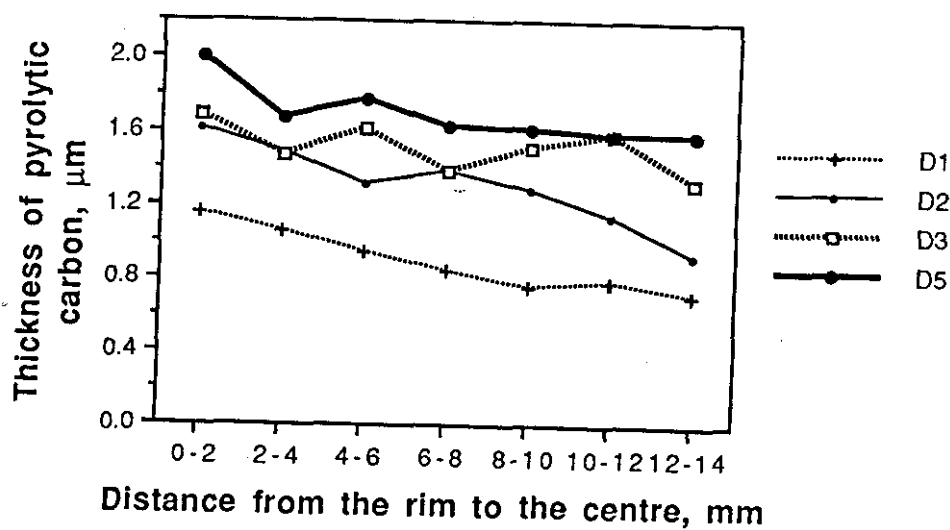


Figure 4.27 Variation of thickness of pyrolytic carbon in layer 2 to 6 from the rim to the centre on multiple CVD treatment

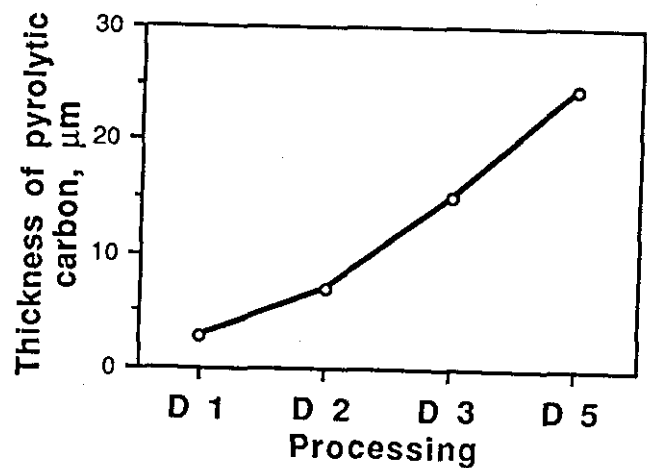
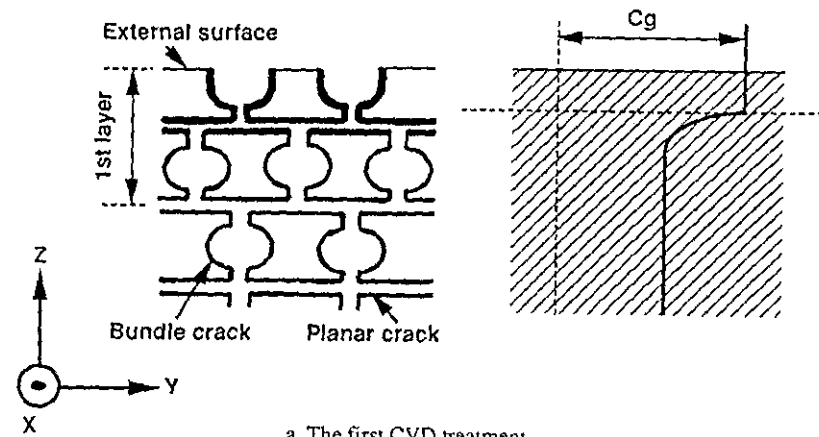
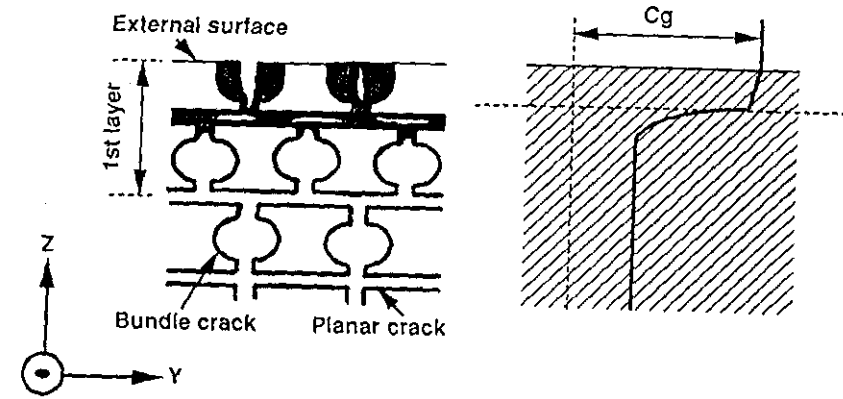


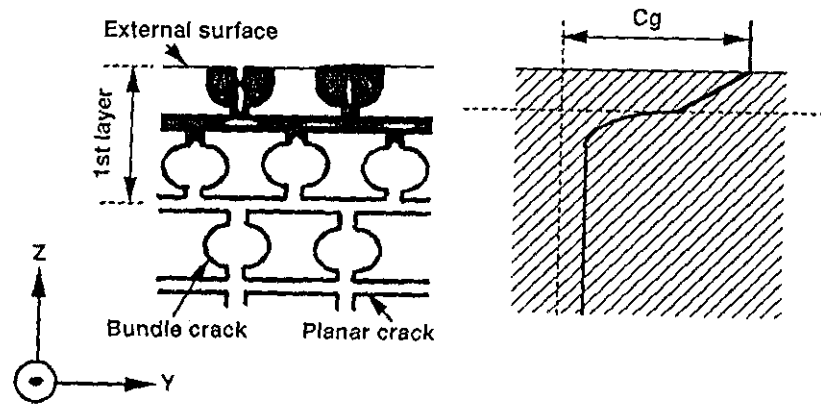
Figure 4.28 Increasing average thickness of pyrolytic carbon deposited on the external surface on multiple CVD treatment



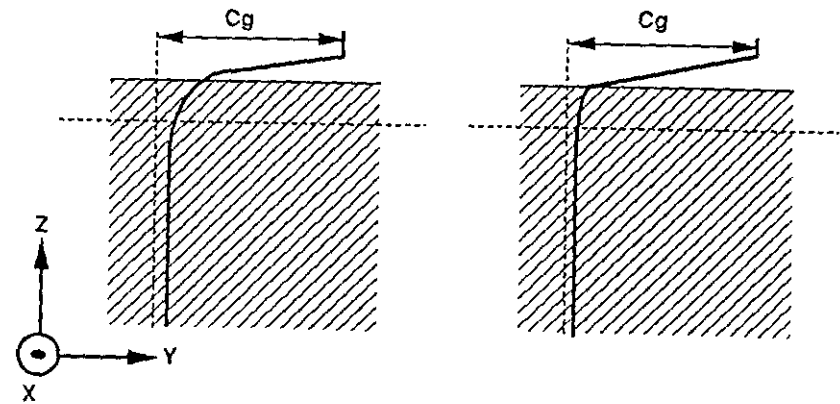
a. The first CVD treatment



b. The second CVD treatment



c. The third CVD treatment



d. The fourth CND treatment

e. The fifth CVD treatment

Figure 4.29 Schematic illustration of infiltration in the direction normal to the cloth layers

FIGURES

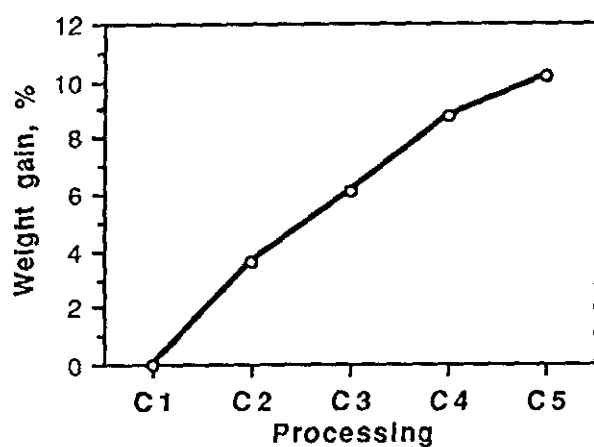


Figure 4.30 Weight increases on multiple resin impregnation

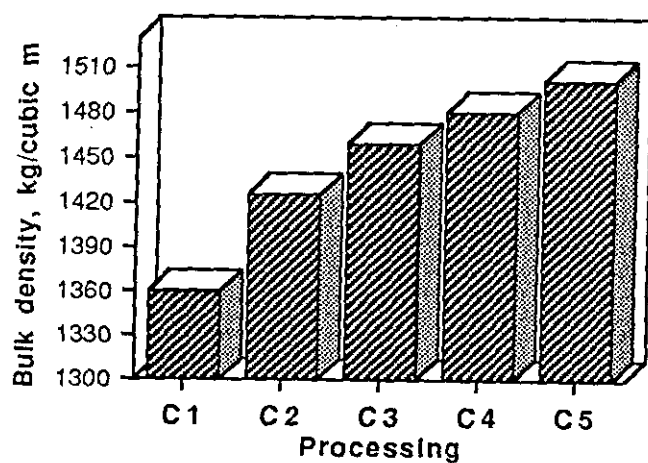


Figure 4.31 Variation of bulk density on multiple resin impregnation

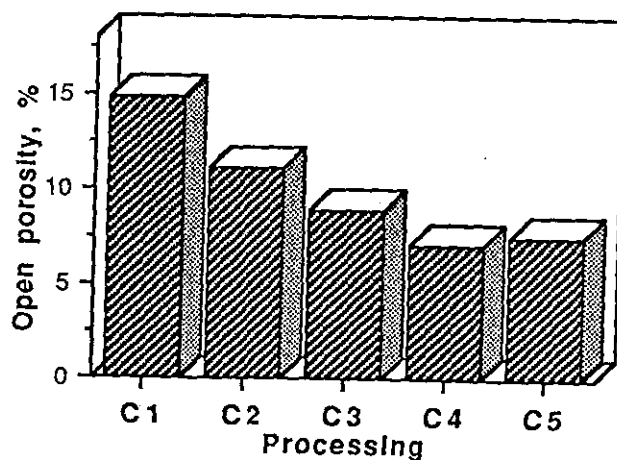


Figure 4.32 Open porosity changes on multiple resin impregnation

FIGURES

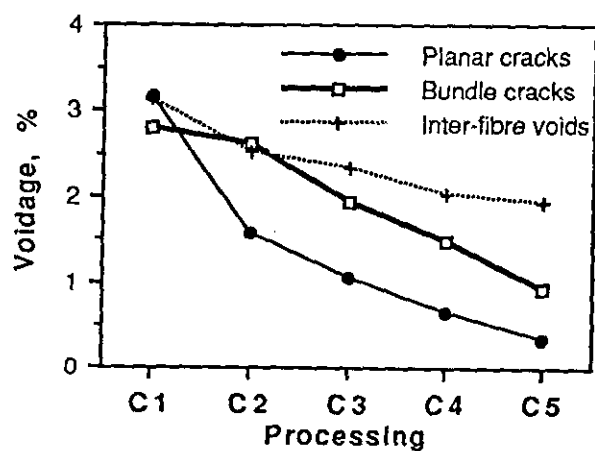


Figure 4.33 Variation of voidage in planar and bundle cracks and inter-fibre voids (pores and cracks) on multiple resin impregnation

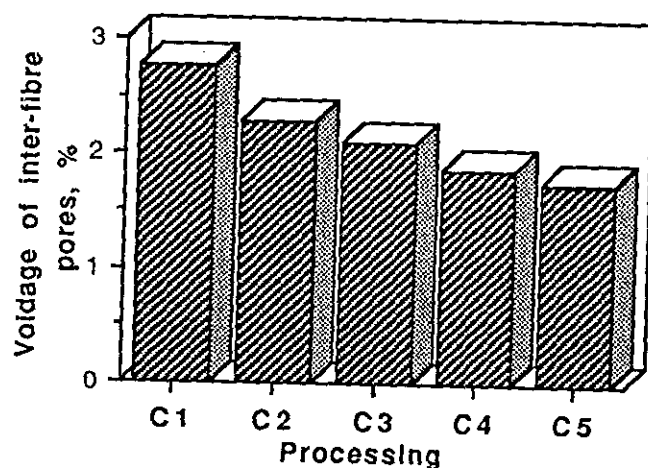


Figure 4.34 Variation of voidage in inter-fibre pores on multiple resin impregnation

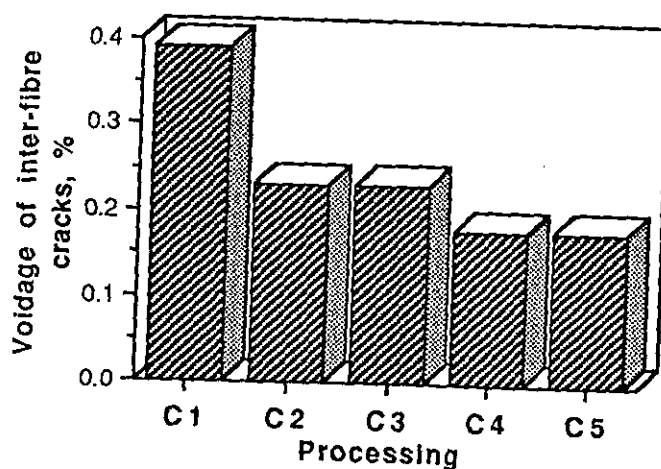


Figure 4.35 Variation of voidage in inter-fibre cracks on multiple resin impregnation

FIGURES

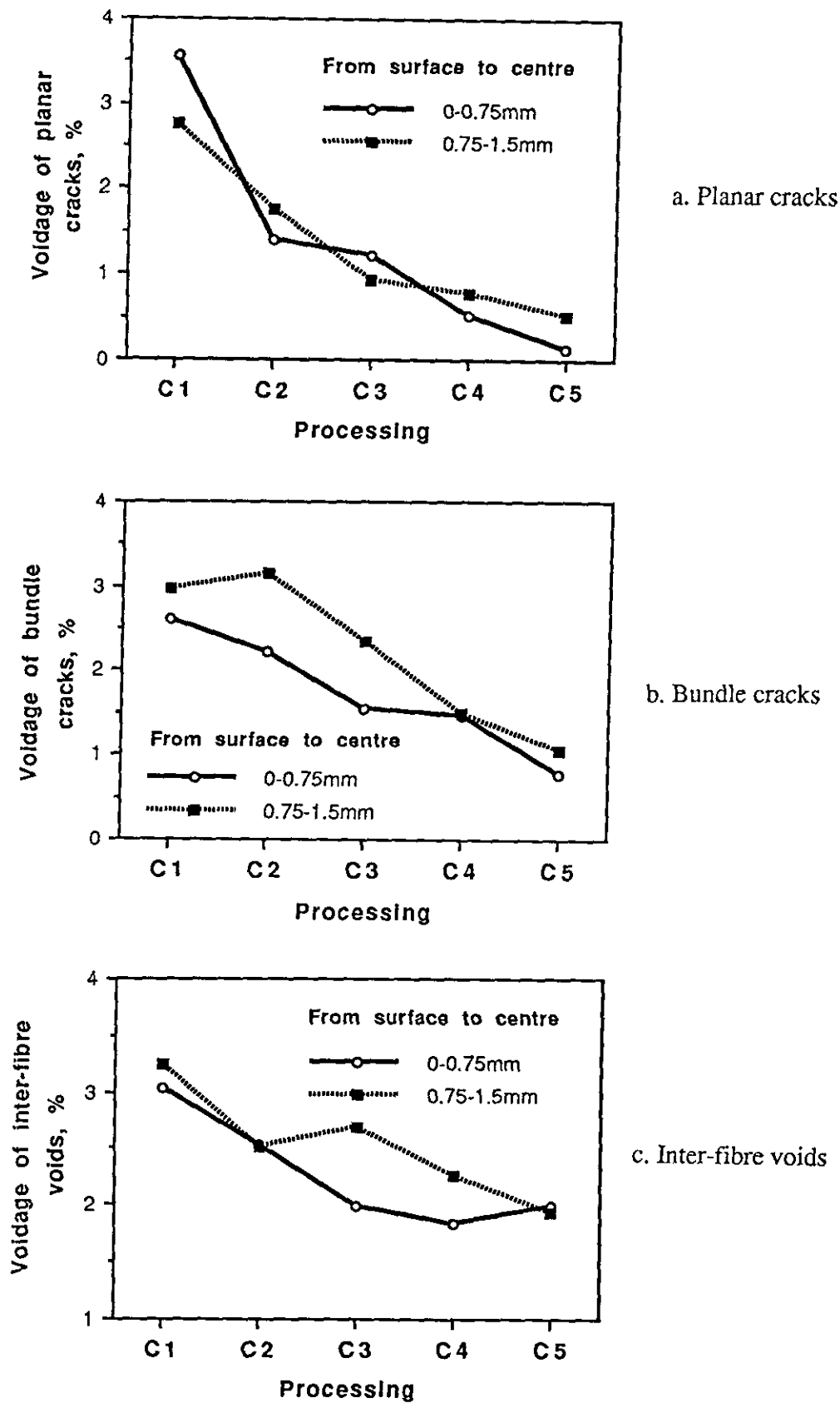


Figure 4.36 Voidage changes in the direction normal to the cloth layers on multiple resin impregnation

FIGURES

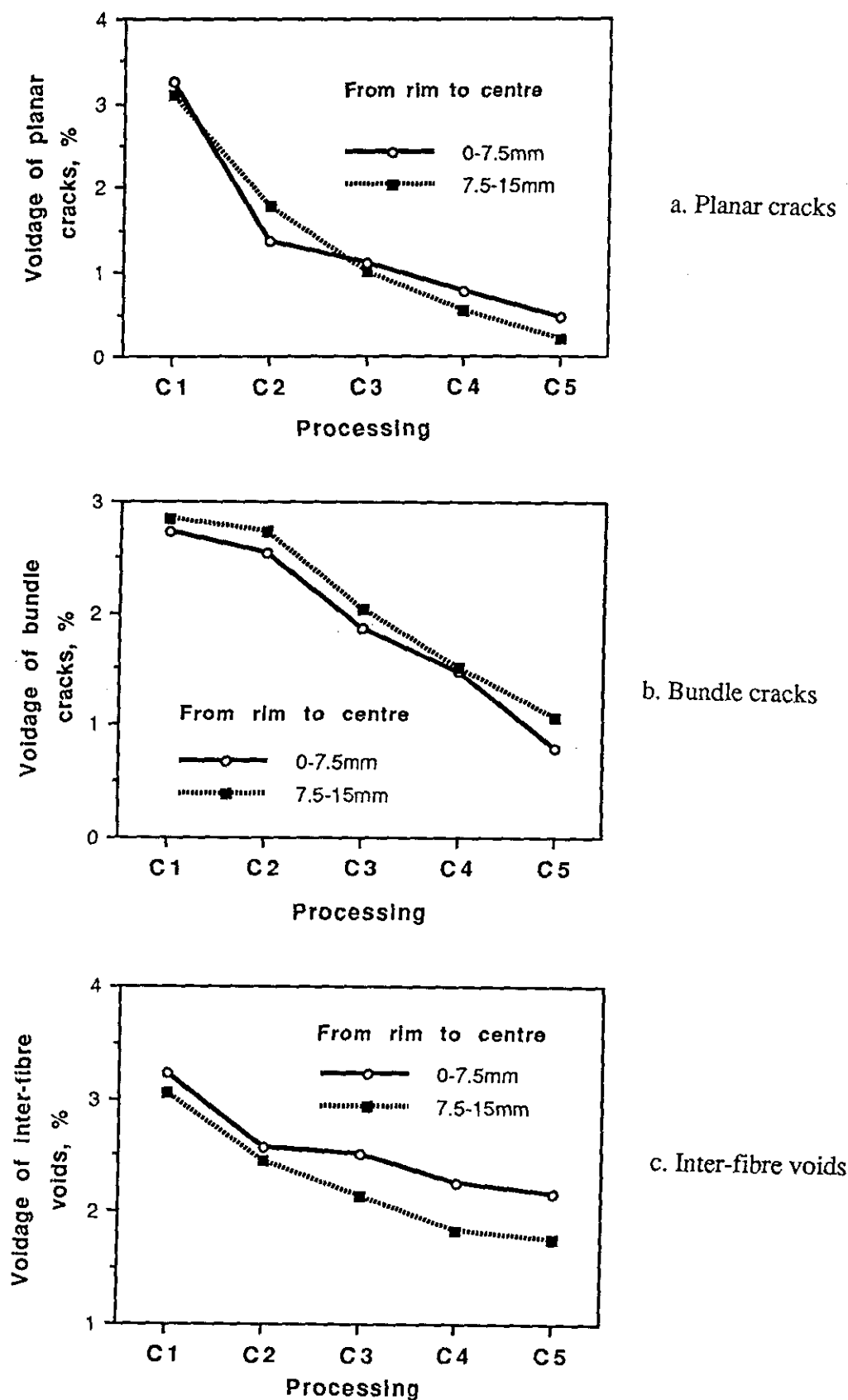
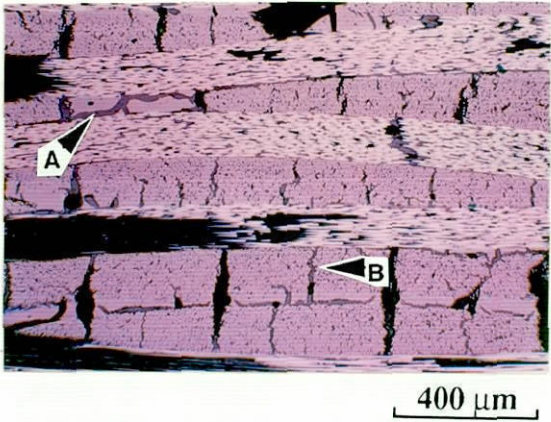
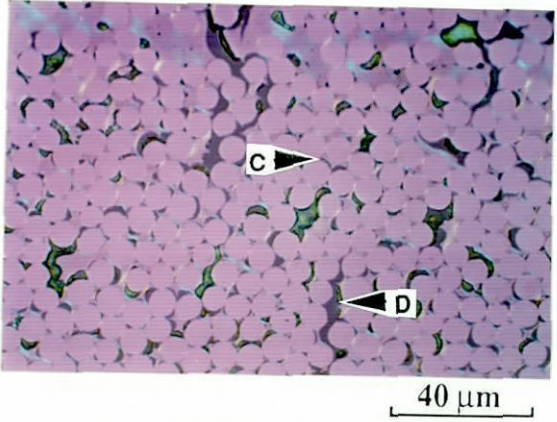


Figure 4.37 Voidage changes in the layer direction on multiple resin impregnation

FIGURES



a. New resin phase in planar and bundle cracks



b. New resin phase in inter-fibre pores and cracks

Figure 4.38 The uncarbonised composite after the first resin impregnation

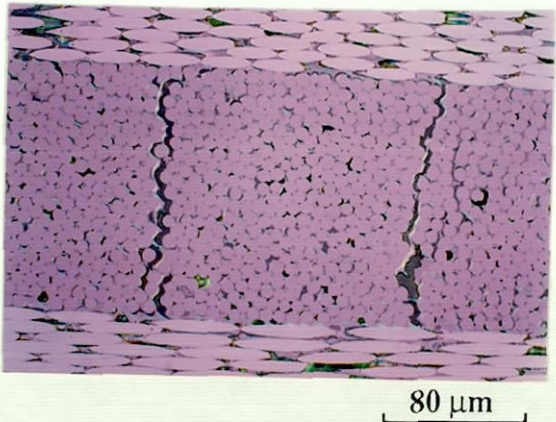


Figure 4.39 The carbonised composite after the first resin impregnation

FIGURES

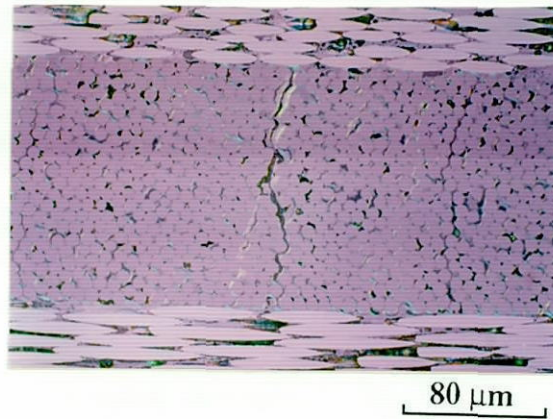


Figure 4.40 Impregnated carbon with multiple layers in narrow cracks after the second resin impregnation

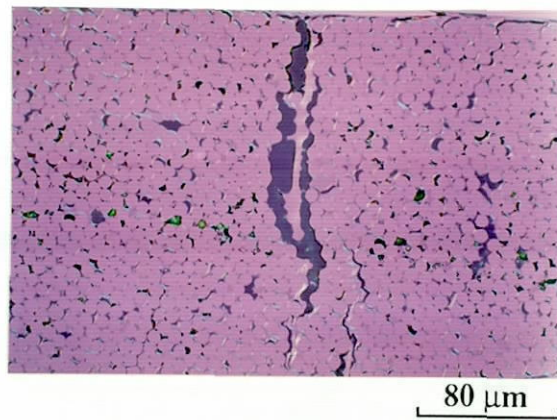


Figure 4.41 Impregnated carbon in a wide bundle crack after the second resin impregnation

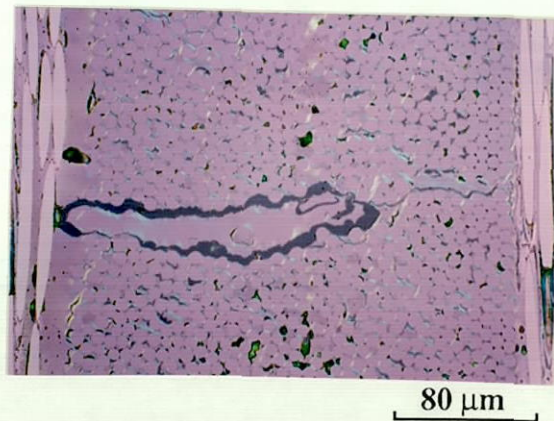
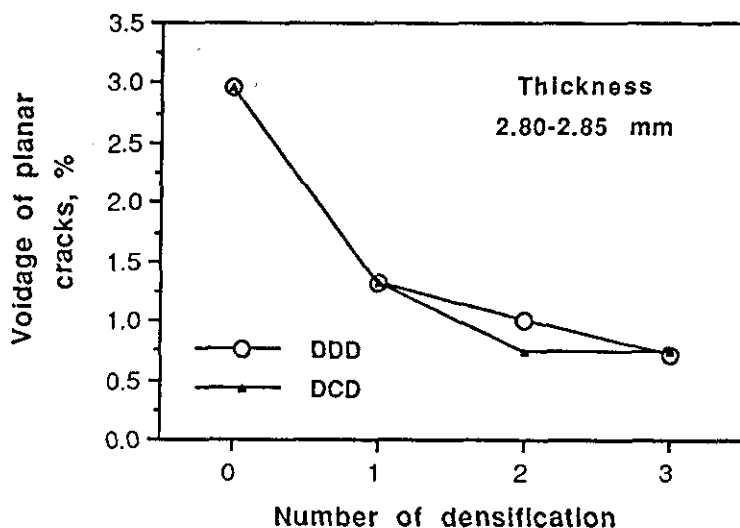
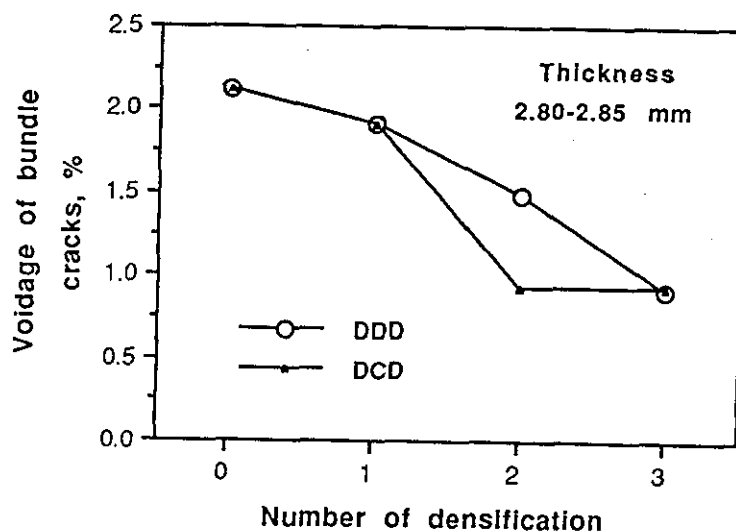


Figure 4.42 Impregnated carbon with multiple layers in a wide bundle crack, C5

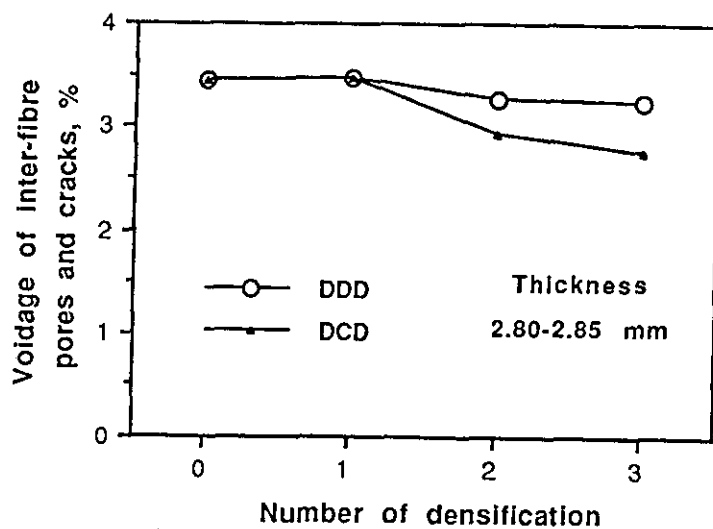
FIGURES



a. Planar cracks



b. Bundle cracks



c. Inter-fibre pores and cracks

Figure 4.43 Variation of voidage in the densification processes initiated by CVD

FIGURES

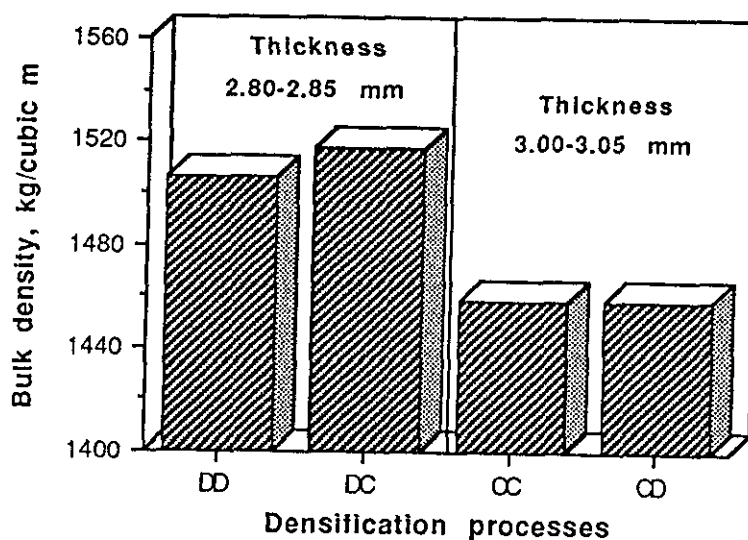


Figure 4.44 Bulk density of the composites processed by two densification cycles

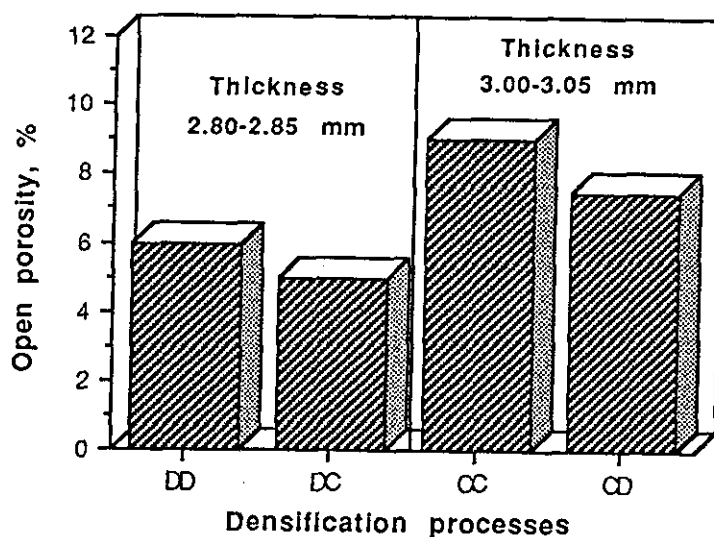


Figure 4.45 Open porosity of the composites processed by two densification cycles

FIGURES

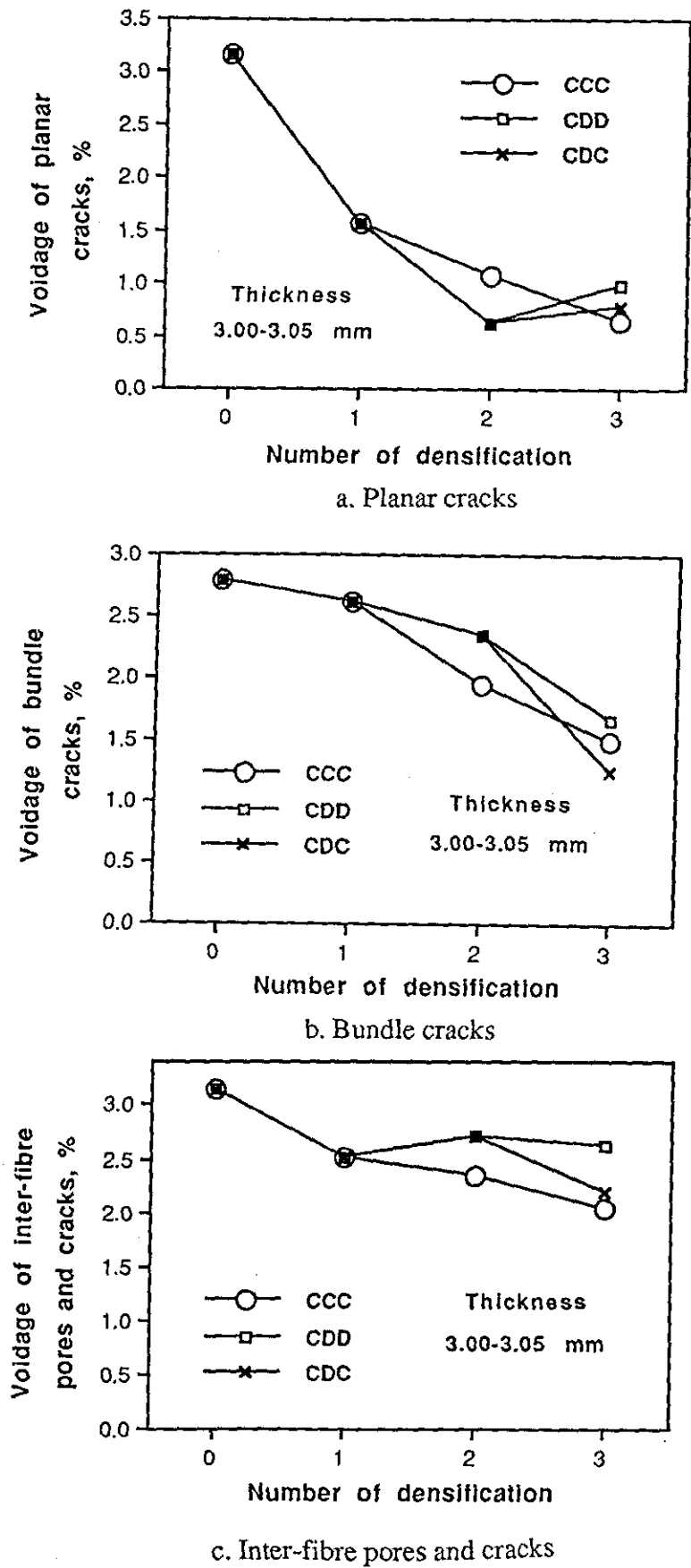


Figure 4.46 Variation of the voidage in the densification processes initiated by resin impregnation

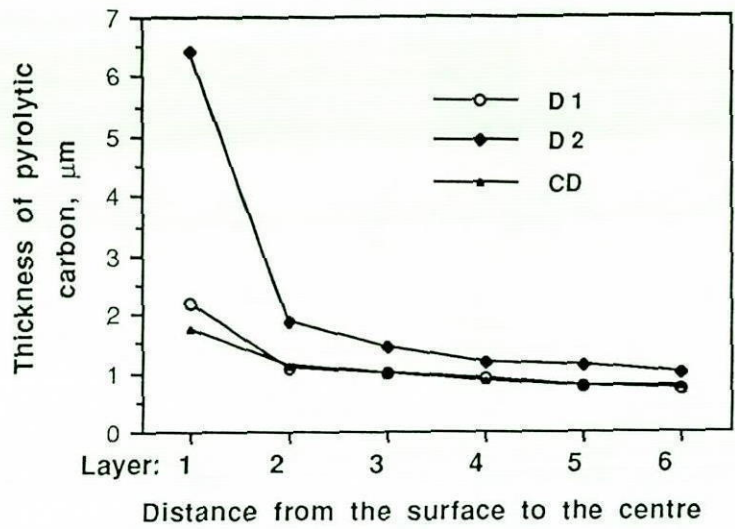


Figure 4.47 Thickness of pyrolytic carbon deposited in the composites densified by CD and the early two cycles of CVD.

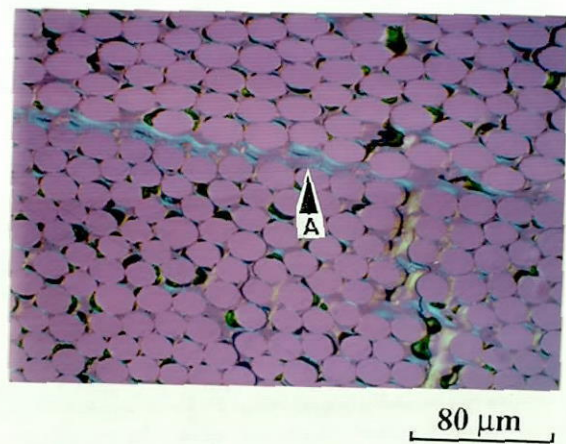


Figure 4.48 Pyrolytic carbon in the tributary channels of the planar cracks in the the composite densified by CD processing

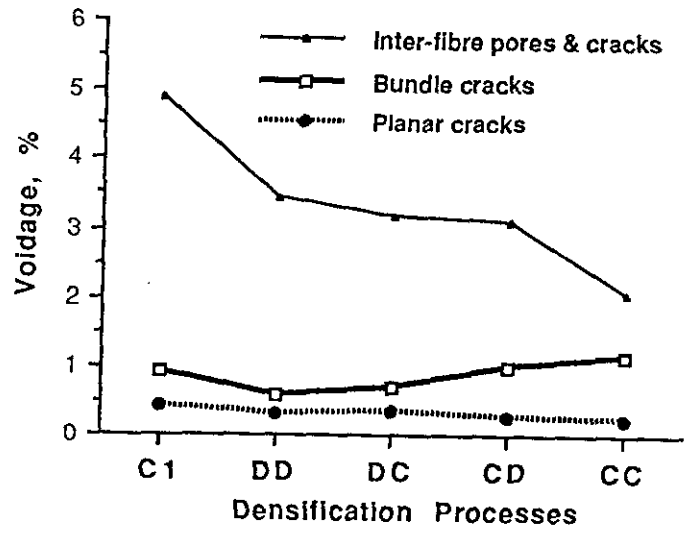


Figure 4.49 Voidage in the Pitch fibre reinforced composites processed by two cycles of densification

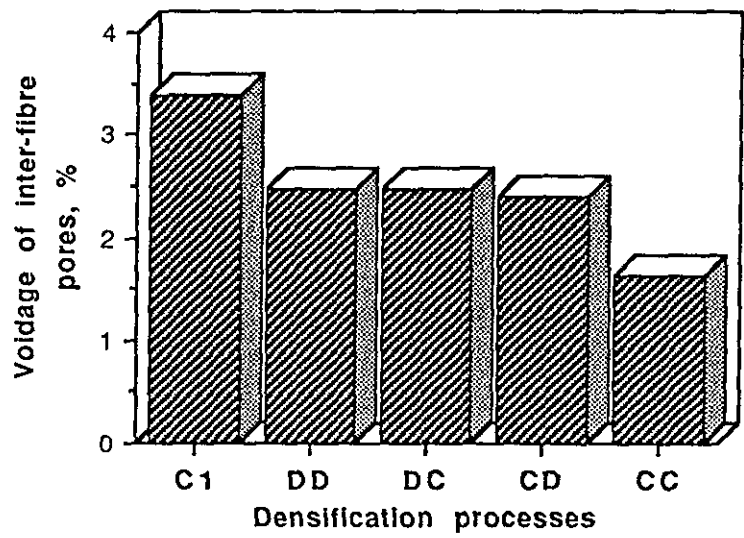


Figure 4.50 Voidage of inter-fibre pores in the pitch fibre reinforced composites processed by two cycles of densification

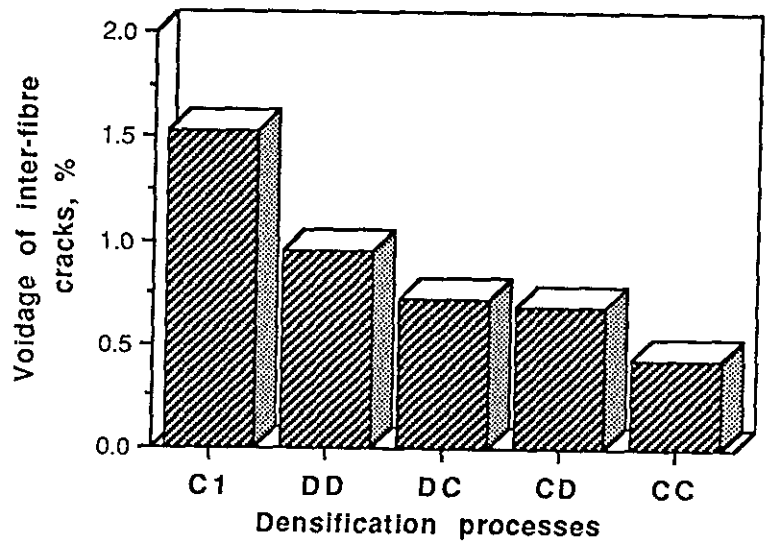


Figure 4.51 Voidage of inter-fibre cracks in the pitch fibre reinforced composites processed by two cycles of densification

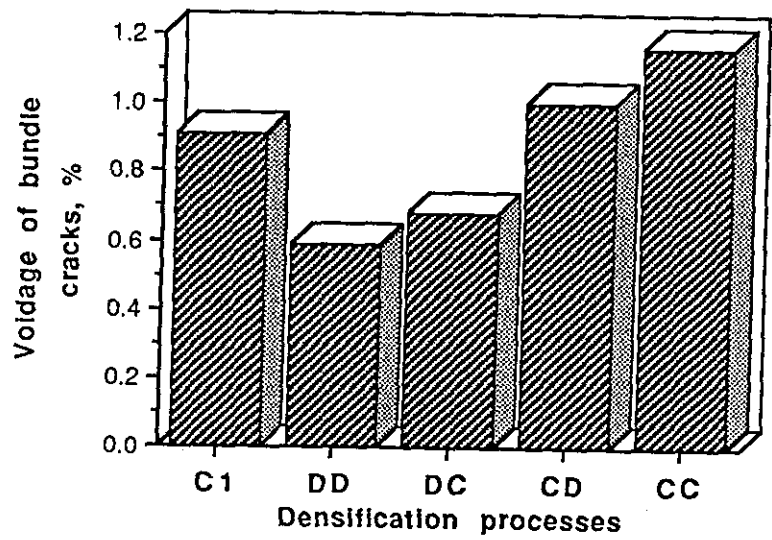


Figure 4.52 Voidage of bundle cracks in the pitch fibre reinforced composites processed by two cycles of densification

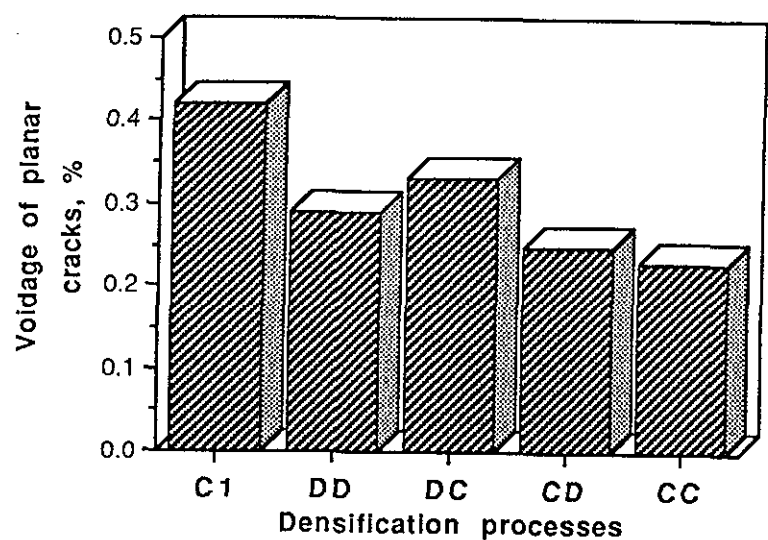


Figure 4.53 Voidage of planar cracks in the pitch fibre reinforced composites processed by two cycles of densification

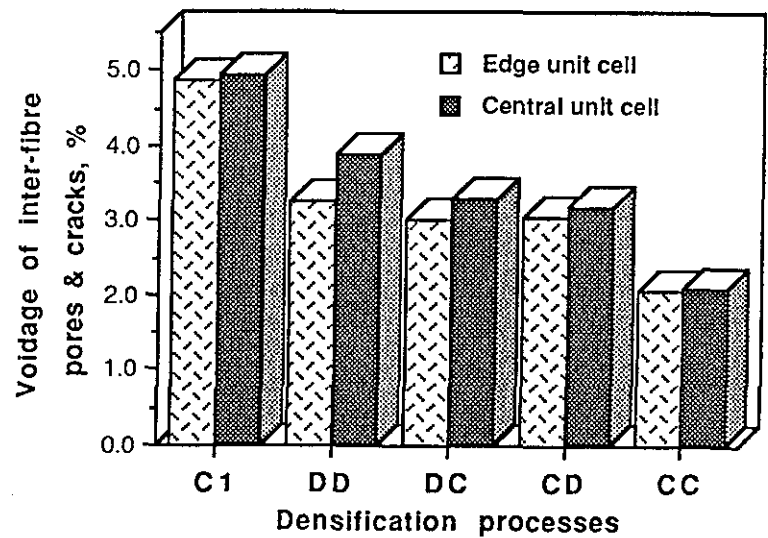


Figure 4.54 Changes of voidage of inter-fibre pores and cracks in the direction normal to the cloth layers for the pitch fibre reinforced composites processed by two cycles of densification

FIGURES

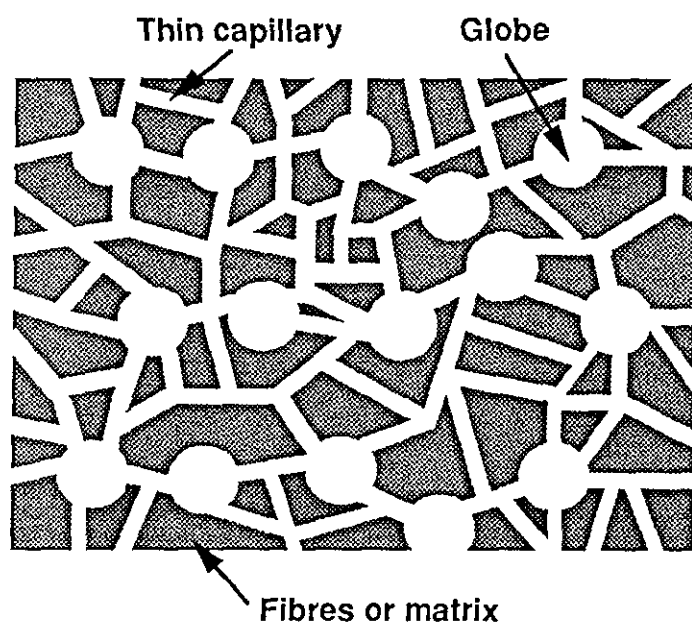


Figure 4.55 Schematic illustration of void model corresponding to behaviour of the densification for the pitch fibre reinforced composites

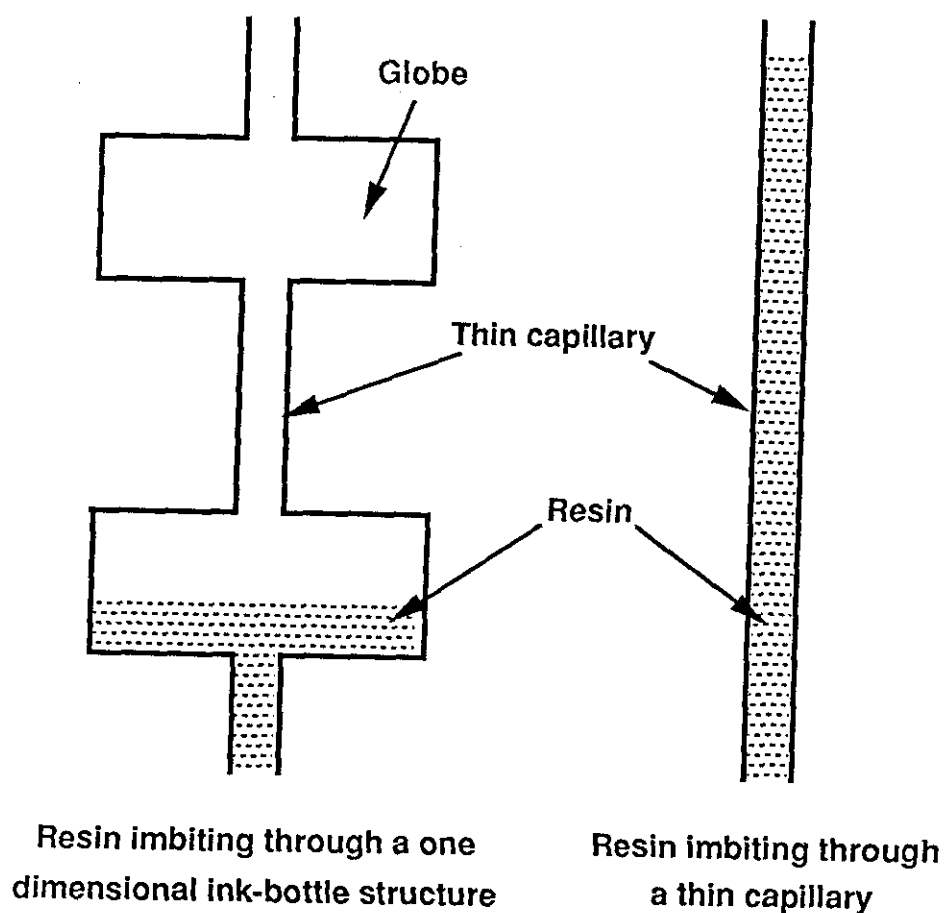


Figure 4.56 Ingression of resin could be hindered by one dimensional ink-bottle structure

FIGURES

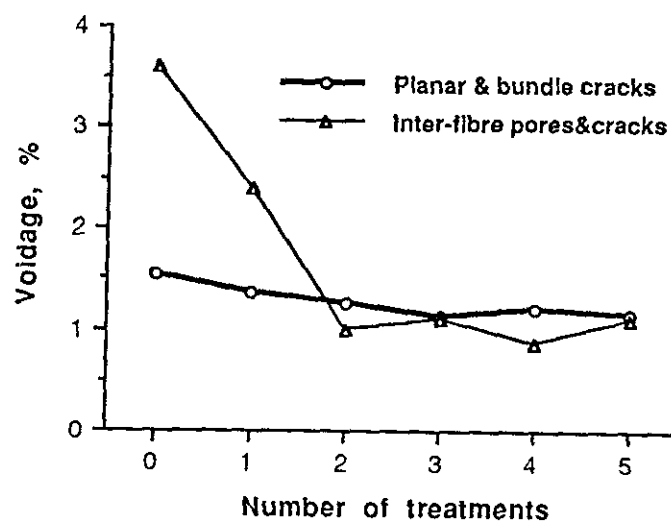
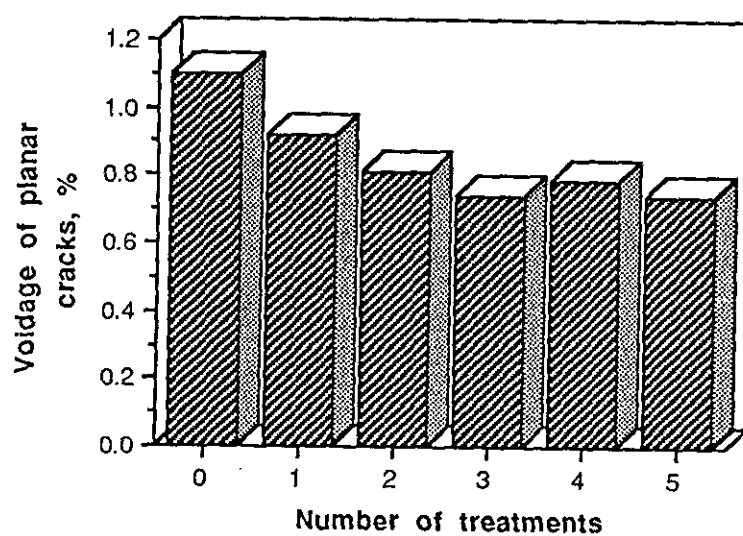
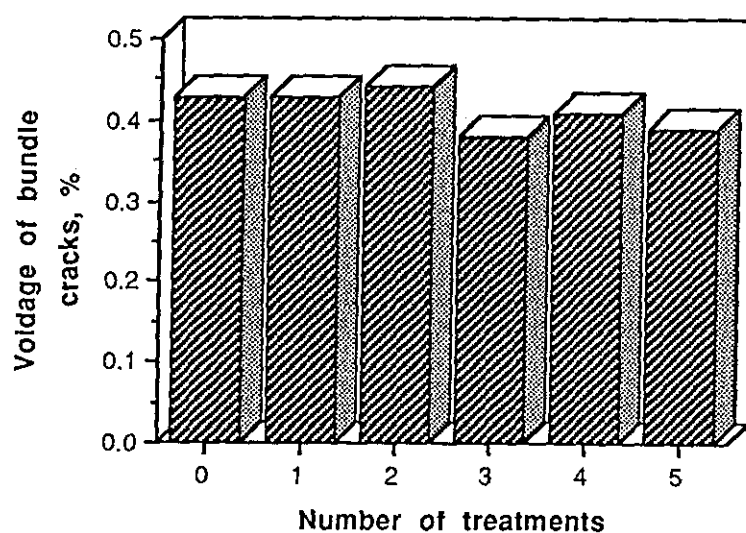


Figure 4.57 Variation of voidage in the rayon fibre reinforced composites during densification by DCDCD

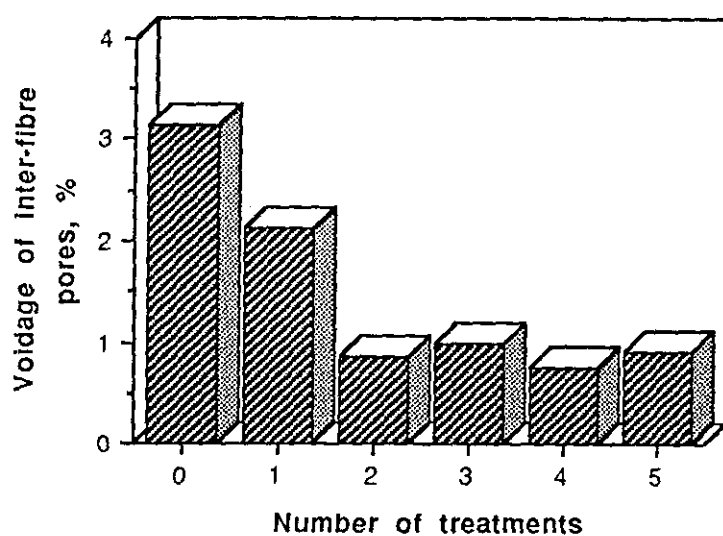


a. Planar cracks

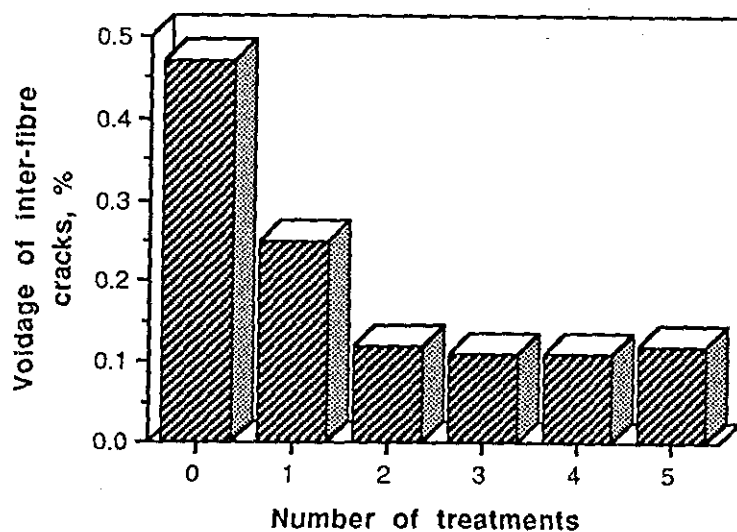


b. Bundle cracks

Figure 4.58 Variation of voidage of planar and bundle cracks in the rayon fibre reinforced composites during densification by DCDCD



a. Inter-fibre pores



b. Inter-fibre cracks

Figure 4.59 Variation of voidage of inter-fibre pores and cracks in the rayon fibre reinforced composites during densification by DCDCD

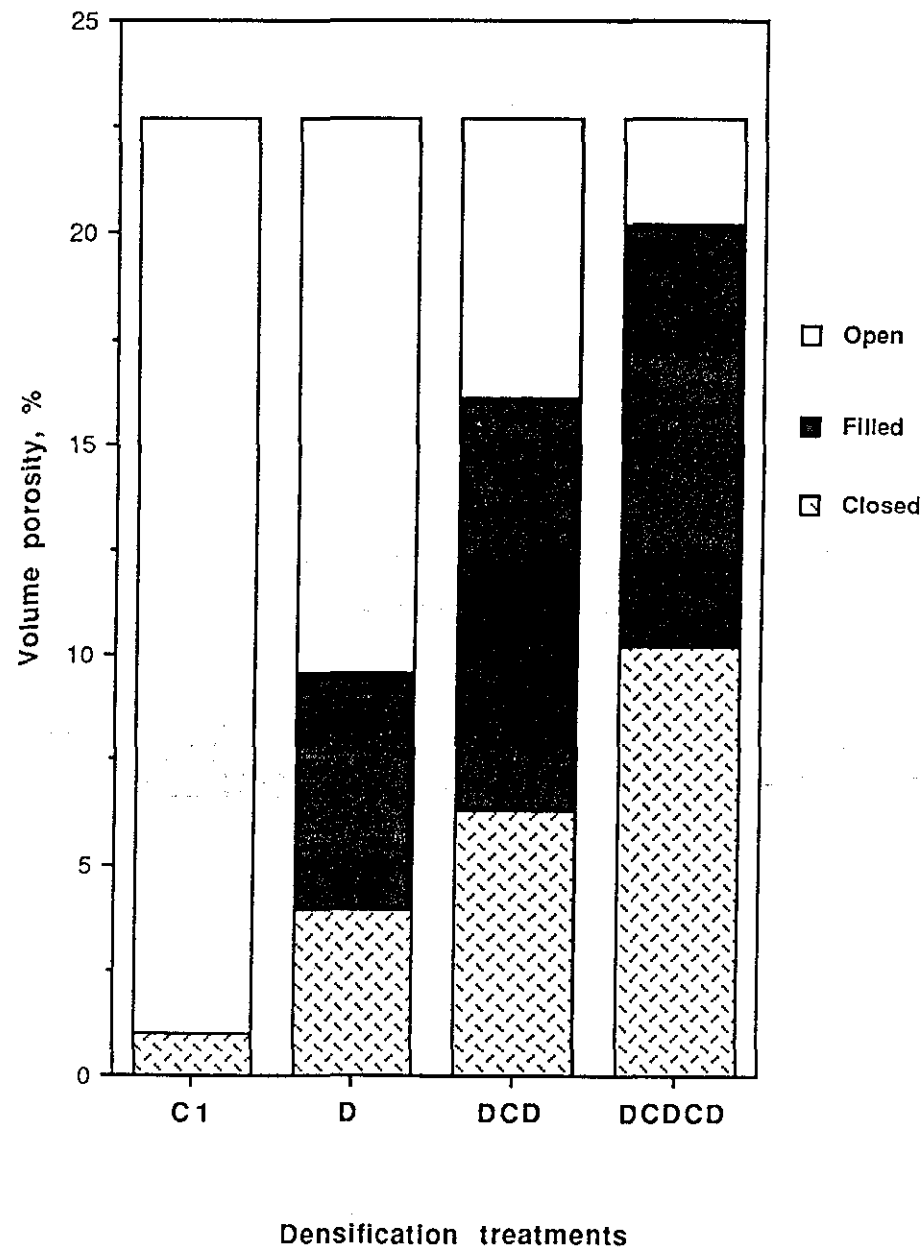


Figure 4.60 Variation of volume porosity in the rayon fibre reinforced composites during densification by DCDCD

AVERAGE BREADTH OF VOIDS IN CARBONISED PREFORMS, μm

Materials	Inter-fibre pores	Inter-fibre cracks	Planar cracks	Bundle cracks
Rayon-SR	4.4	18.8	19.7	28.0
Pitch-SR	5.0	19.3	18.5	28.7
PAN-SR	3.5	15.5	23.2	33.7

Densification behaviour in two cycles of densification processes:-

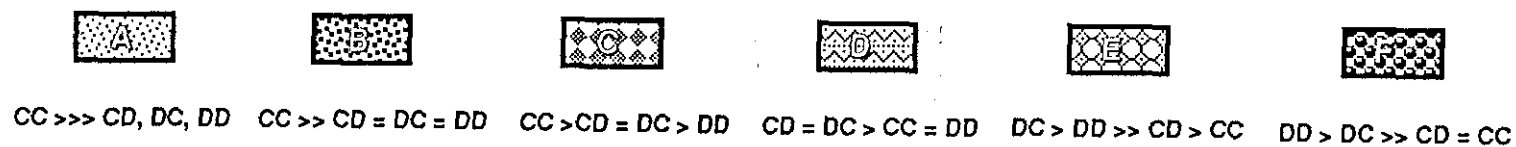


Figure 4.61 Relationship between void structure and densification behaviour in two cycles of densification treatments

FIGURES

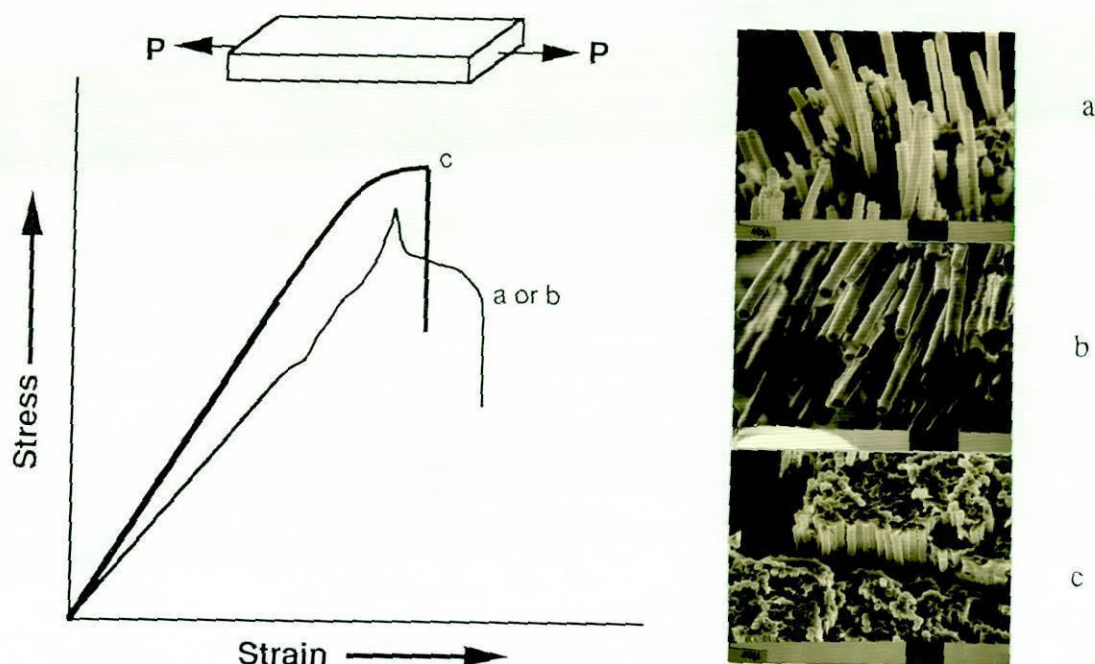


Figure 4.62 Stress-strain diagrams and SEM fractographs of the composites made with: a) rayon fibres, b) pitch fibres and c) PAN fibres, tensile strength test.

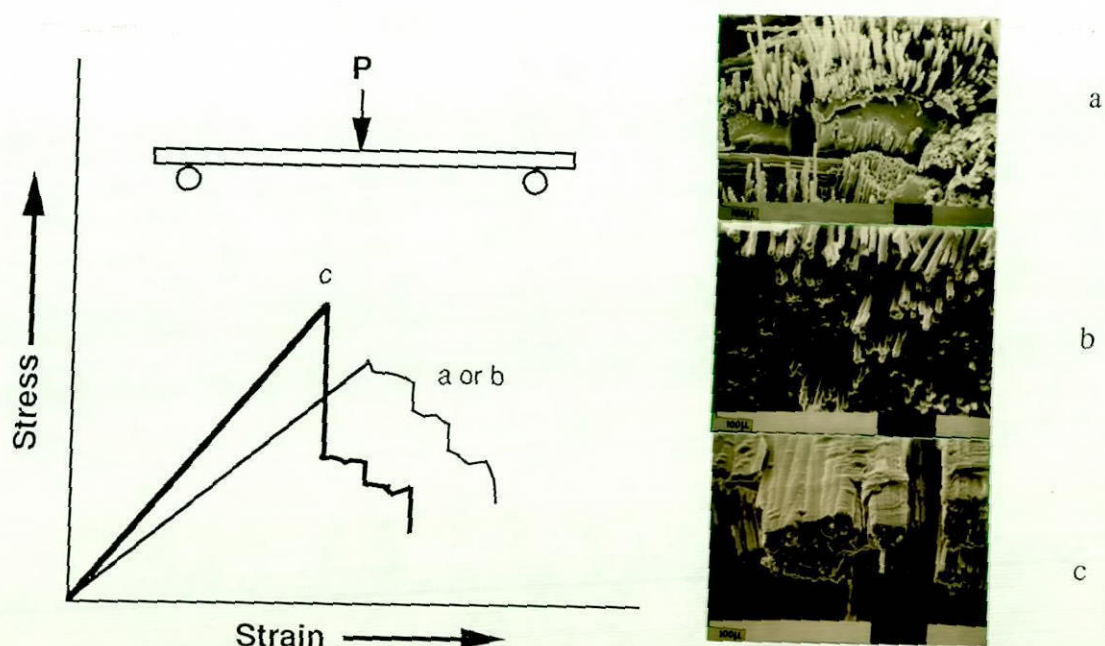


Figure 4.63 Stress-strain diagrams and SEM fractographs of the composites made with: a) rayon fibres, b) pitch fibres and c) PAN fibres, flexural strength test.

FIGURES

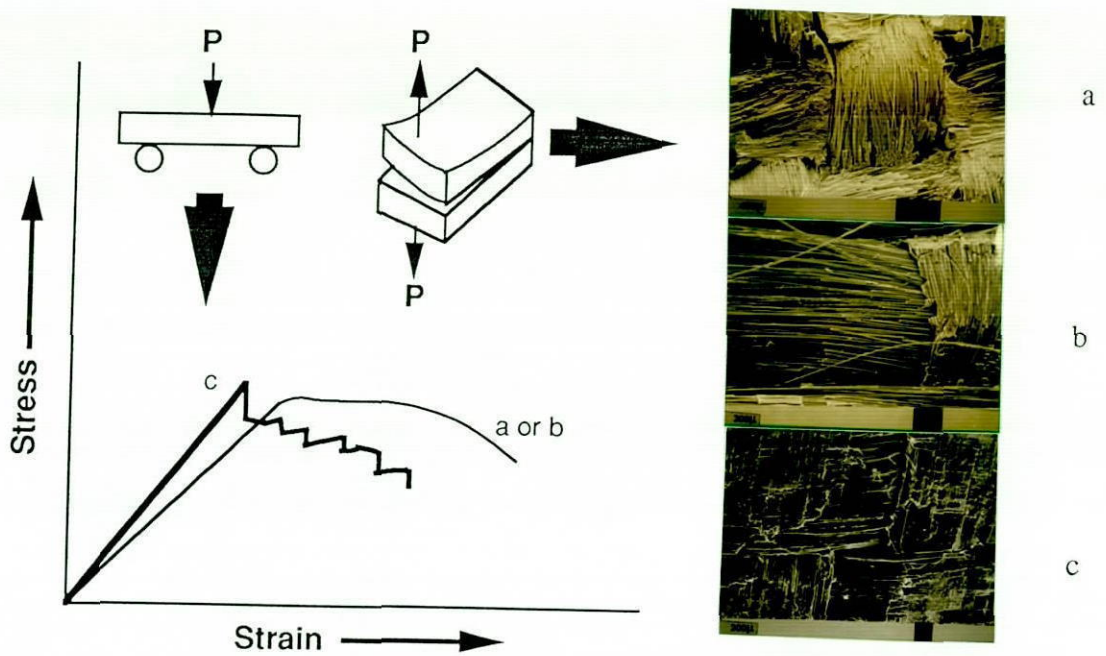


Figure 4.64 Stress-strain diagrams during ILSS test and SEM micrographs of cleavage fracture of the composites made with:
a) rayon fibres, b) pitch fibres and c) PAN fibres.

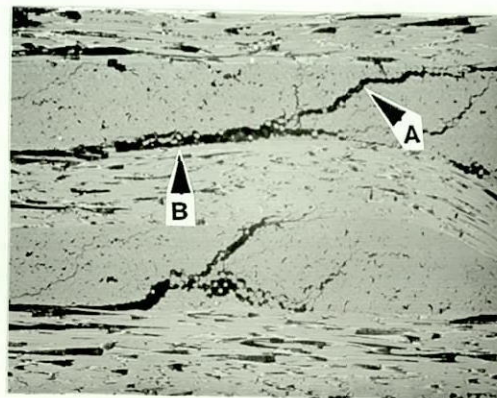


Figure 4.65 A composite with weak bonding at fibre/matrix interface involves both interlaminar and intra-laminar fracture in interlaminar shear strength test. The rayon fibre composite. A. Intra-laminar crack, B. Interlaminar crack.

FIGURES

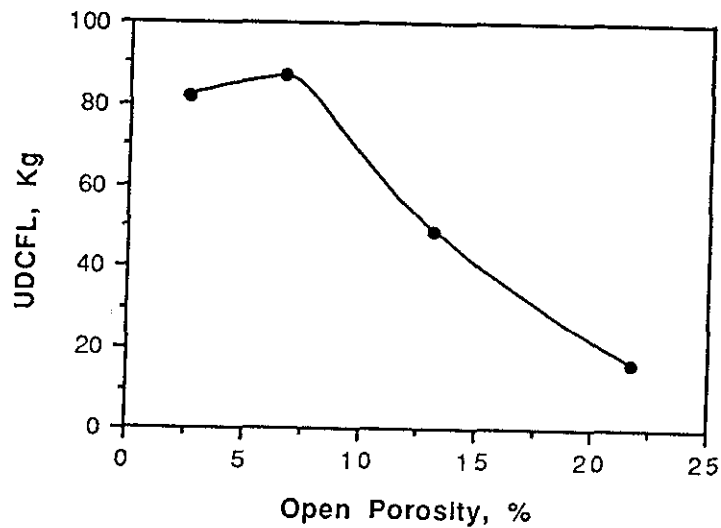


Figure 4.66 Relationship between open porosity and ultimate diametral compression-failure-load (UDCFL) for the composites from various stages of densification process, DCDCD.

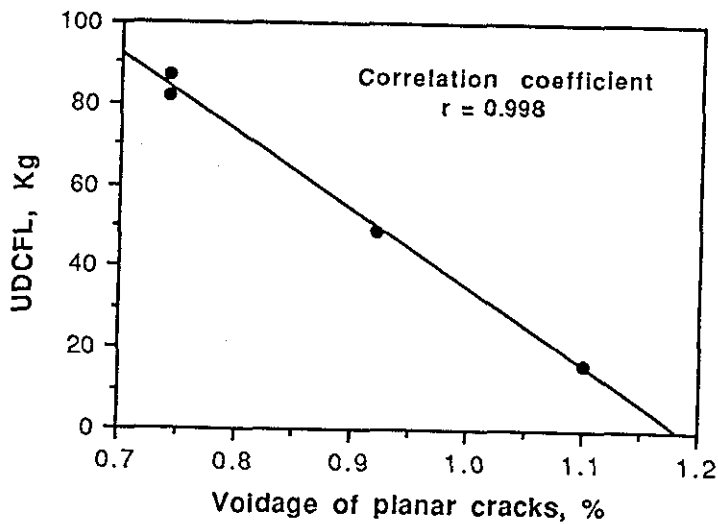


Figure 4.67 Relationship between voidage of planar cracks and ultimate diametral compression-failure-load for the composites from various stages of densification process, DCDCD.

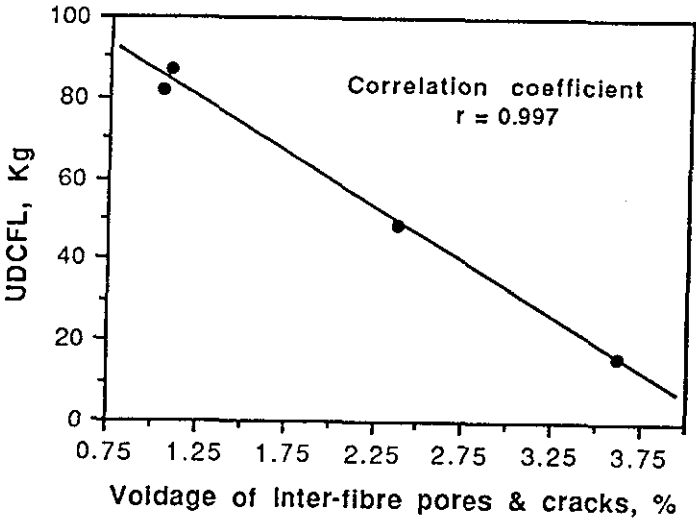


Figure 4.68 Relationship between voidage of inter-fibre pores and cracks and ultimate diametral compression-failure-load for the composites from various stages of densification process, DCDCD.

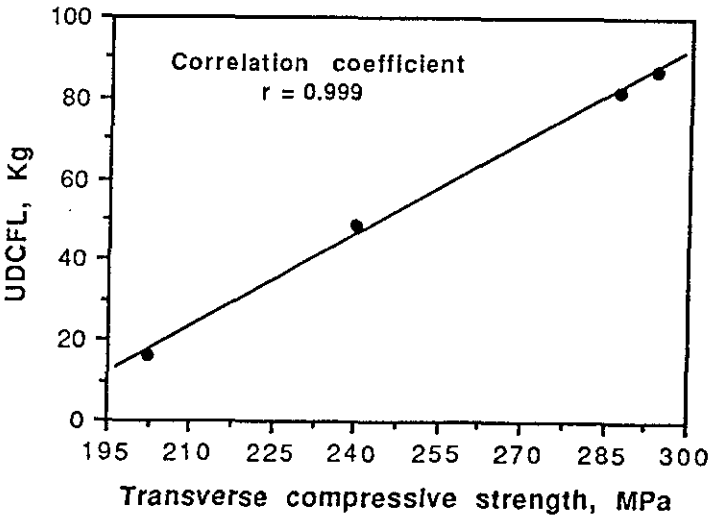


Figure 4.69 Relationship between transverse compressive strength and ultimate diametral compression-failure-load for the composites from various stages of densification process, DCDCD.

FIGURES

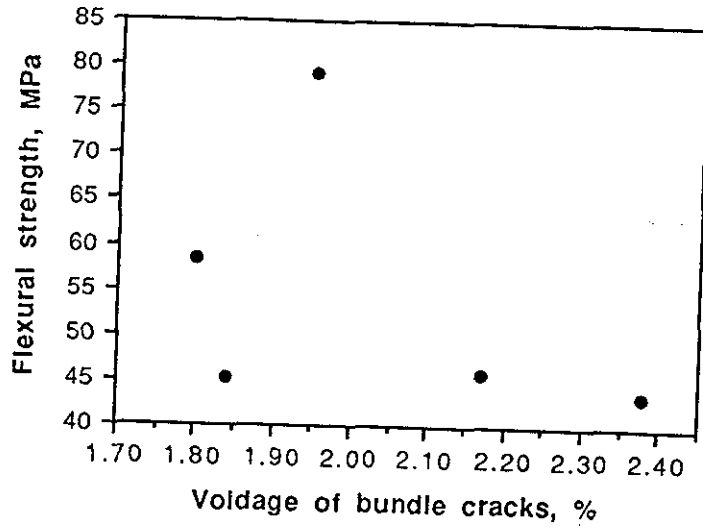


Figure 4.70 Relationship between flexural strength and voidage of bundle cracks for the PAN fibre based composites produced from constant thickness moulding

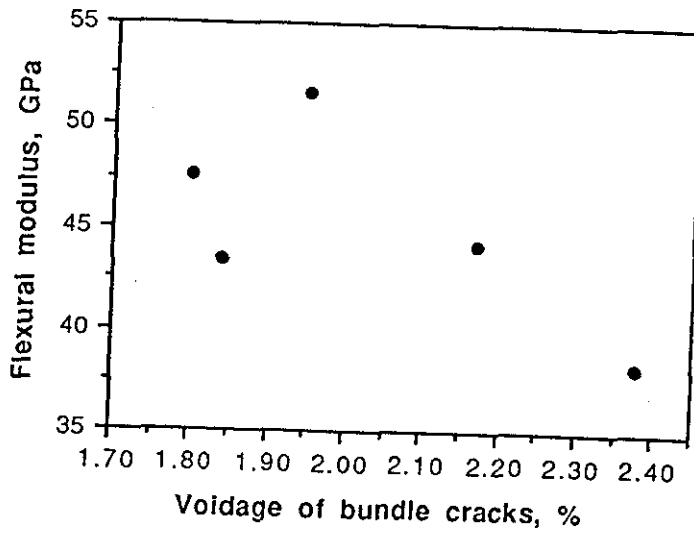


Figure 4.71 Relationship between flexural modulus and voidage of bundle cracks for the PAN fibre based composites produced from constant thickness moulding

FIGURES

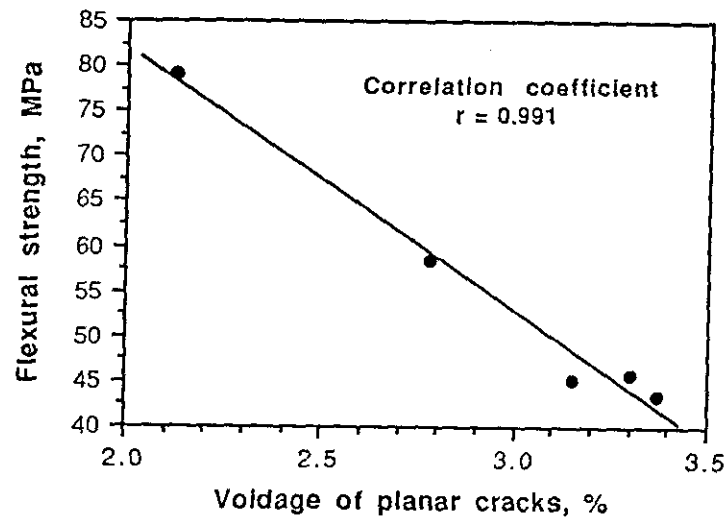


Figure 4.72 Relationship between flexural strength and voidage of planar cracks for the PAN fibre based composites produced from constant thickness moulding

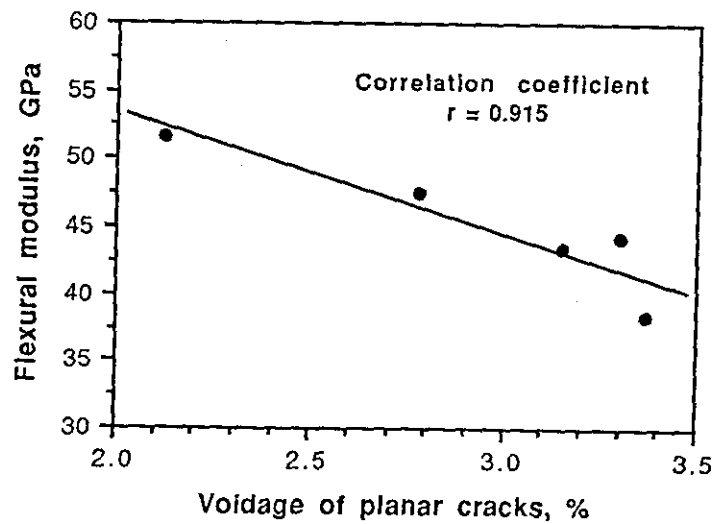
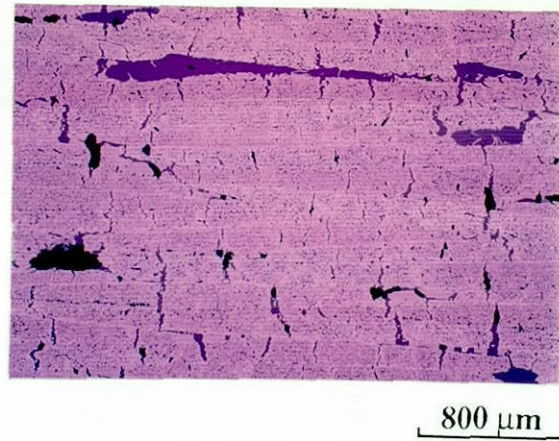
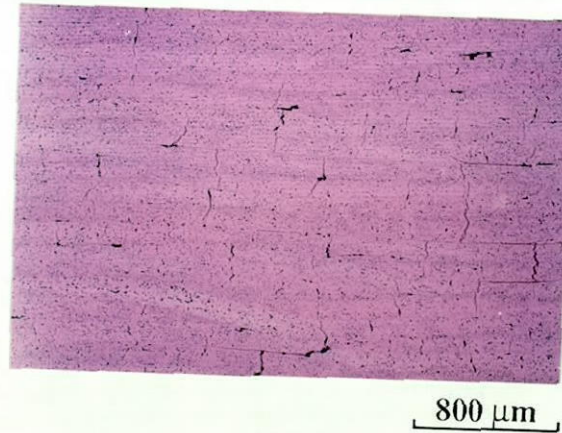


Figure 4.73 Relationship between flexural modulus and voidage of planar cracks for the PAN fibre based composites produced from constant thickness moulding

FIGURES



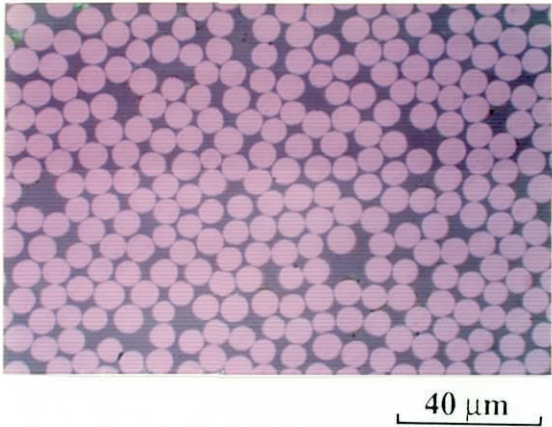
- a. Some planar cracks in a composite produced from constant thickness moulding have breadth similar to the length of the bundle cracks



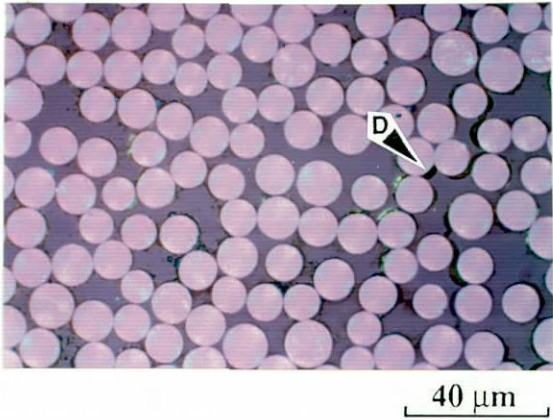
- b. A composite produced from constant pressure moulding does not include the thick planar cracks as shown in Figure 4.74 a.

Figure 4.74 Micrographs of the PAN fibre reinforced composites produced from different moulding techniques

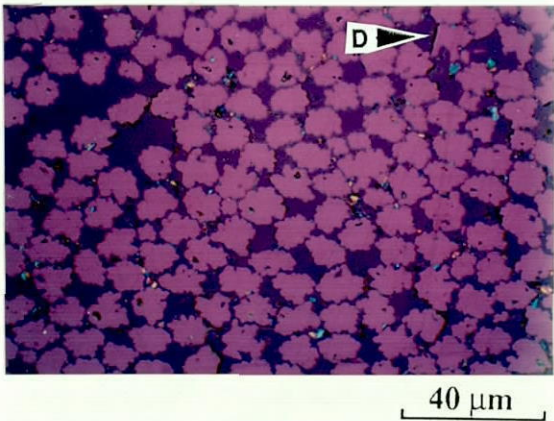
FIGURES



a. PAN-SR



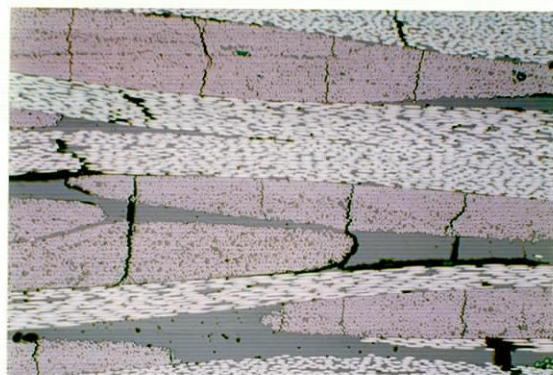
b. Pitch-SR



c. Rayon-SR

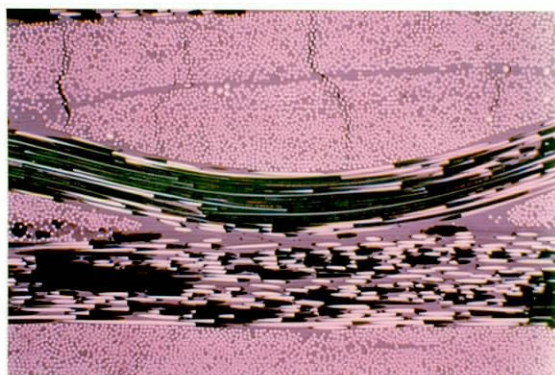
Figure 4.75 Micrographs of the moulded preforms observed in a high magnification

FIGURES



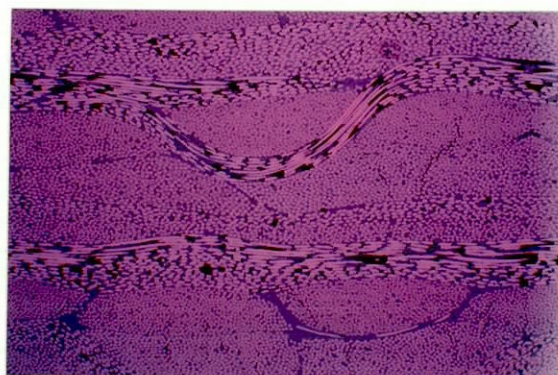
400 μm

a. PAN-SR



400 μm

b. Pitch-SR



400 μm

c. Rayon-SR

Figure 4.76 Micrographs of the moulded preforms observed in a low magnification

FIGURES

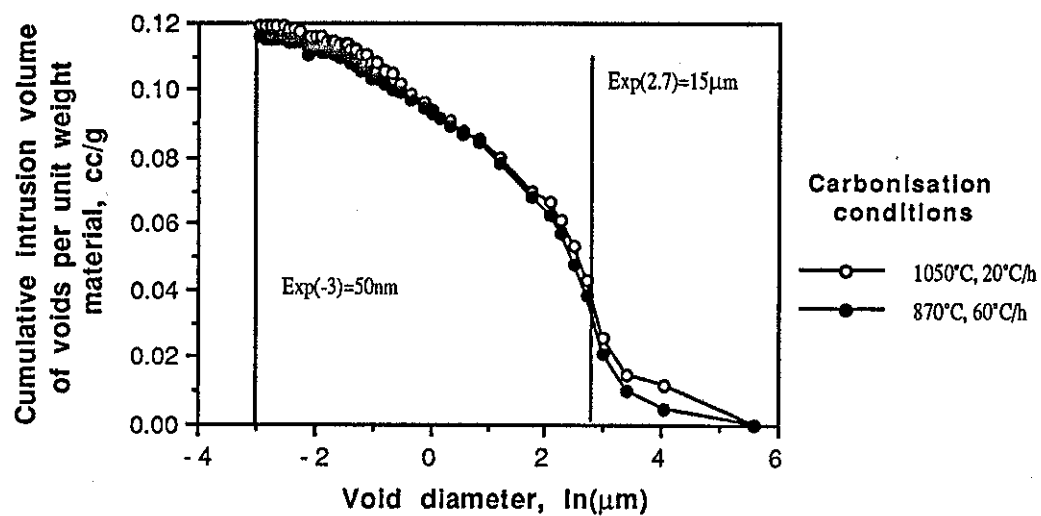


Figure 4.77 Void size distribution of the PAN fibre reinforced carbonised preforms carbonised at different conditions

